PARAMETRIC AND NONPARAMETRIC PI/PID CONTROLLER TUNING METHOD FOR INTEGRATING PROCESSES BASED ON MAGNITUDE OPTIMUM

Tomaž Kos

Doctoral Dissertation
Jožef Stefan International Postgraduate School
Ljubljana, Slovenia

Supervisor: Asst. Prof. Dr. Damir Vrančić,
Department of Systems and Control, Jožef Stefan Institute, Ljubljana, Slovenia

Evaluation Board:
Asst. Prof. Dr. Pavle Boškoski, Chair,
Department of Systems and Control, Jožef Stefan Institute, Ljubljana, Slovenia

Prof. Mikuláš Huba, Member,
Department of E-mobility, Automation and Drives, Institute of Automotive Mechatronics, Faculty of Electrical Engineering and Information Technology, Slovak University of Technology (STU), Slovakia

Assoc. Prof. José Paulo Barroso de Moura Oliveira, Member,
University of Tras-os-Montes e Alto Douro, Vila Real, Portugal

MEDNARODNA PODIPLOMSKA ŠOLA JOŽEFA STEFANA
JOŽEF STEFAN INTERNATIONAL POSTGRADUATE SCHOOL

Tomaž Kos

PARAMETRIC AND NONPARAMETRIC PI/PID CONTROLLER TUNING METHOD FOR INTEGRATING PROCESSES BASED ON MAGNITUDE OPTIMUM

Doctoral Dissertation

PARAMETRIČNA IN NEPARAMETRIČNA METODA ZA NASTAVLJANJE PARAMETROV PI/PID REGULATORJEV ZA INTEGRIRNE PROCESE NA PODLAGI AMPLITUDNEGA OPTIMUMA

Doktorska disertacija

Supervisor: Asst. Prof. Dr. Damir Vrančić

Ljubljana, Slovenia, April 2021

Acknowledgements

Throughout these four exciting, yet exhausting years, several people have helped me and thus contributed to the work presented in this dissertation. This page is dedicated to all of them. However, it is only an outline of acknowledgements, as true gratitude is difficult to express in writing.

First and foremost, my infinite gratitude goes to my doctoral supervisor Asst. Prof. Dr. Damir Vrančić, without whom all this would not have been possible. He provided me with an appropriate environment that nurtured and encouraged new scientific ideas. I am grateful for his support, enthusiasm, guidance, encouragement and freedom to conduct research during the last four and a half years. I am grateful for the opportunity to join the Department of Systems and Control of the Jožef Stefan Institute.

I would like to thank the members of the thesis committee for their quick review and constructive comments. Their efforts have improved the quality of this work.

Furthermore, I would like to thank my current and former colleagues at the Department of Systems and Control for providing me with a relaxed and productive work environment, for sharing their knowledge, thoughts, and ideas with me, and for the daily lunch breaks where laughter and fruitful discussions took place.

In addition, I would like to thank Prof. Dr. Tadej Rojac of the Electronic Ceramic Department, who introduced me to the world of research and science, for his enthusiasm, encouragement, and constant support since I started working at the Jožef Stefan Institute eight years ago. At the same time, I would like to thank Dr. Jurij Koruza and his research group for their financial support and for accepting me at TU Darmstadt.

I would like to acknowledge the support of the Young Researchers Programme grant no. PR-07603 and the Research Programme P2-0001 of the Slovenian Research Agency that funded my research. In addition, the Erasmus traineeship exchange programme is gratefully acknowledged.

Furthermore, I would like to thank all of my friends and classmates for the laughter and support that made the entire graduation process more enjoyable. I am grateful to my entire family for their support and encouraging words. Finally, but most importantly, I would like to thank my girlfriend Vanja Gruden for putting up with me and my occasional grumpiness, for her constant support, and her ability to make work-related problems disappear.

Abstract

Integrating systems are commonly found in power and paper mills, aerospace control systems, storage tanks, distillation columns, chemical reactors, and petroleum industries. Due to their open-loop instability resulting in an unconstrained output for a constrained input, efficient control of integrating processes is challenging. Control of integrating processes has attracted the interest of researchers for many decades, and several control structures and tuning methods have been developed so far. However, among the existing tuning methods, it is difficult to find one based on a relatively simple experiment and tuning procedure that leads to highly efficient tracking and disturbance rejection control, similar to the magnitude optimum multiple integration (MOMI) tuning method.

In this dissertation, an extension of the MOMI tuning method is proposed for integrating processes controlled by a two-degrees-of-freedom (2-DOF) proportional-integral (PI) and proportional-integral-derivative (PID) controller. The developed method is nonparametric, i.e., it does not require an explicit process model to compute the controller parameters. The controller parameters can be calculated either from measurements in the time-domain or from a process transfer function of arbitrary order with a time delay. Both approaches are exactly equivalent and do not introduce errors in the calculation of the controller parameters.

Furthermore, the developed extension of the tuning procedure provides an additional option to achieve the best overall closed-loop performance (optimal tracking and disturbance-rejection performance) by using the reference weighting parameter or two reference filter structures. Moreover, an additional parameter is provided to modify the speed of the closed-loop response by setting the average closed-loop residence time, i.e., a measure that defines the closed-loop time constant.

Additionally, the stability and robustness of the proposed tuning method to perturbations in the process parameters are studied. The robustness of the measured characteristic areas in a noisy environment is also investigated, and a new approach to reduce the sensitivity of the measured characteristic areas on high-frequency noise is proposed.

In addition to tuning, this thesis develops a method for identifying the lower-order process model either directly from the time-domain measurements or from an arbitrary-order process transfer function with a time delay.

The proposed controllers were also compared with other PI/PID tuning methods for integrating processes. The comparison showed superior control performance compared to the other tuning methods currently proposed. In addition, the proposed tuning method was tested on the following laboratory and industrial setups: a charge amplifier drift compensation system, a laboratory hydraulic system, an industrial autoclave, and a solid oxide fuel cell temperature control system. The closed-loop responses were fast and stable in all experiments.

Povzetek

Integrirni procesi se pojavljajo v različnih vejah industrije: najdemo jih v elektrarnah in papirnicah, letalsko-vesoljskih nadzornih sistemih, skladiščnih cisternah, destilacijskih kotlih, kemičnih reaktorjih in naftni industriji. Zaradi mejno nestabilne prenosne funkcije, ki povzroči neomejen izhod pri omejenem vhodu, je tako zahtevnejše tudi zaprtozančno vodenje integrirnih procesov. Vodenje integrirnih sistemov preučujejo že vrsto desetletij in do sedaj je bilo razvitih že veliko različnih metod nastavljanja parametrov regulatorjev. Med obstoječimi metodami pa težko najdemo takšno, ki omogoča enostavno nastavljanje parametrov regulatorja in hkrati zelo učinkovito regulacijsko in sledilno vodenje, kar je prednost MOMI (ang. *magnitude optimum multiple integration*) metode za stabilne procese.

Delo naslavlja razširitev MOMI metode za vodenje integrirnih procesov s proporcionalno-integrirnim (PI) in proporcionalno-integrirno-diferencirnim (PID) regulatorjem z dvema prostostnima stopnjama (ang. *2-DOF*). Razvita razširitev je neparametrična, kar pomeni, da za izračun parametrov regulatorja ne potrebuje modela procesa. Parametre regulatorja lahko izračunamo iz časovnega odziva procesa (časovna domena) ali pa neposredno iz prenosne funkcije procesa poljubnega reda z mrtvim časom (frekvenčna domena). Pri tem sta oba pristopa izračuna parametrov regulatorja popolnoma enakovredna.

Skupno optimalno regulacijsko in sledilno delovanje smo dosegli z utežitvijo signala reference (ang. *reference weighting*) ali s pomočjo filtriranja referenčnega signala. Hitrost zaprtozančnega odziva smo nastavili z dodatnim parametrom, ki določa zaprtozančno časovno konstanto (ang. *average closed-loop residence time*).

V delu smo preučevali tudi stabilnost in robustnost predlagane metode nastavljanja parametrov regulatorjev. Ravno tako smo analizirali robustnost izračuna karakterističnih površin (ang. *characteristic areas*) iz signalov procesa, ki vsebujejo merilni šum. V delu je predlagan nov način izračuna omenjenih površin s pomočjo filtriranja signalov.

Poleg nastavljanja parametrov regulatorjev delo obravnava tudi novo metodo za identifikacijo modela nižjega reda neposredno iz časovnega odziva (časovna domena) ali iz prenosne funkcije procesa poljubnega reda z mrtvim časom (frekvenčna domena).

Predlagano metodo nastavljanja parametrov PI/PID regulatorjev smo primerjali z nekaterimi drugimi metodami. Predlagana metoda je v veliki večini primerov dosegla bolj učinkovito zaprtozančno vodenje v primerjavi z ostalimi metodami. Na koncu dela smo predlagano metodo preizkusili tudi na naslednjih laboratorijskih in industrijskih sistemih: sistem za kompenzacijo lezenja napetosti ojačevalnika električnega naboja, laboratorijski hidravlični sistem, industrijski avtoklav in sistem za nadzor temperature trdo oksidnih gorivnih celic (ang. *SOFC*). Zaprtozančni odzivi so bili v vseh primerih hitri in stabilni.

Contents

List of Figures

List of Tables

Abbreviations

1-DOF	One-degree-of-freedom
2-DOF	Two-degrees-of-freedom
ABC	Artificial bee colony
ADC	Analogue-to-digital converter
ADRC	Active disturbance rejection control
Air HEX	Air heat exchanger
CI	Clegg integrator
CSTR	Continuous stirred tank reactor
DAQ	Data acquisition
DC	Direct current
DOB	Disturbance observer-based
DS	Direct synthesis
DTC	Dead-time compensator
ESO	Extended state observer
FO	Fractional-order
FPI	Filtered proportional–integral
FOTD	First-order plus time delay
GA	Genetic algorithm
GEVP	Generalized eigenvalue problem
HO-PID	Higher-order proportional-integrative-derivative
IAE	Integral of the absolute error
IAT^2E	Integral of the squared time absolute error
IFOTD	First-order integrating systems with/without delay
IMC	Internal model control
INPTD	Integrating process with an inverse response with a time delay
IP	Integrating process
I-PD	Integral–proportional derivative
IPs	Integrating processes
ISE	Integral of squared error
IST^2E	Integral of squared time squared error
IST^3E	Integral of cubed time squared error
ISTE	Integral of time squared error
ITD	Pure integrator plus time delay
LMI	Linear matrix inequality
LQR	Linear quadratic regulator
LTI	Linear time-invariant
MDPM	Multiple dominant pole method
MO	Magnitude optimum
MOMI	Magnitude optimum multiple integrations
MP	Method product
MPC	Model predictive control

Ms	... Maximum sensitivity
NG	... Natural gas
NI	... National instruments
NMP	... Non-minimum phase
PCCS	... Parallel cascade control strategy
PCS	... Parallel control structure
PD	... Proportional–derivative
PDO	... Predictive disturbance observer
PI	... Proportional–integral
PID	... Proportional–integral–derivative
PLC	... Programmable logic controller
PRBS	... Pseudorandom binary sequence
PSO	... Particle swarm optimisation
RHP	... Right half plane
SCADA	... Supervisory control and data acquisition
SCCS	... Series cascade control structure
SIMC	... Skogestad internal model control
SISO	... Single-input single-output
SNR	... Signal-to-noise ratio
SOFC	... Solid-oxide fuel cell
SOPDT	... Second-order plus dead time
USB	... Universal serial bus
WGC	... Weighted geometrical centre

Chapter 1

Introduction

A large part of this chapter was originally published in Kos, T. et al., Applied Sciences (2020), 10: 4, T. Kos et al., Applied Sciences (2020), 10: 17, and T. Kos et al., AIP Advances (2019), 9: 3.

We would like to point out to the reader that the MATLAB files used for the calculations of the parameters, the simulations and the plotting of the data in this work are available online [1].

1.1 Proportional–Integral–Derivative (PID) Controller

A proportional-integral-derivative (PID) controller is the most commonly used control algorithm in industry [2]–[4], although several more advanced control structures have been developed. It is used in a wide range of operating conditions in various processes due to its simple tuning, good closed-loop performance, low cost and robustness. In order to achieve the best cost-performance ratio in an industrial environment, satisfactory control performance must be achieved with a control structure that is as simple as possible. Industrial controllers are, therefore, in most cases simple PID controllers [5]. According to the survey [6], "*on over eleven thousand controllers in the refining, chemicals and pulp and paper industries, 97% of regulatory controllers utilise a PID feedback control algorithm*". In most cases, the derivative term is not used [7]. The design is usually based on simple time-delayed plant models [4, Ch. 1]. Another reason for the wide acceptance of PID controllers in industrial processes is an extensive range of tuning methods for controlling broad classes of process problems [4], [8]. Their functional simplicity allows engineers to operate them in a simple and straightforward manner [9]. According to [10], "*many strategies proposed can be easily eliminated if they are compared with well-tuned PID*". Moreover, as stated in [11]: "*the PID controllers still have significant importance due to their applicability in a wide range of processes with different characteristics*". Moreover, PID controller research is also expanding to the field of network control and telematics applications [12].

In [11], a study of PID, dead-time compensator (DTC) and model predictive control (MPC) strategies applied to single-input single-output (SISO) processes with time delay is presented with the aim of deciding whether to use classical PID controllers or advanced control strategies in typical process control problems. It has been shown that the choice depends on the quality of the process model, i.e. for an industrial environment where robust solutions are needed, a PID with anti-windup provides good or even better results than more complex strategies (DTC, MPC). Similar results were presented in [8], where it is shown that for a given robustness level of maximum sensitivity (Ms), the PID controller is generally better than the Smith predictor, which is specialized for controlling the processes

with large time delays. The study also showed that the Smith predictor is much more sensitive to the process time-delay errors.

A simple PID controller in a closed-loop configuration is shown in Figure 1.1. It consists of three parameters (K_P, K_I, K_D), each of which covers the transient and steady-state response. The disturbance-rejection and reference tracking performance depend on the tuning of these parameters. A poorly tuned controller may result in an oscillatory or unstable response. Although PID control has only three parameters, tuning is not a simple task. Despite the existence of self-tuning algorithms [13], [14], PID controllers are poorly tuned in practice due to a lack of expertise and time. According to [15], "*a visit to a process plant will usually show that a large number of the PID controllers are poorly tuned*". Furthermore, [16] states:"*... 25% of all PID controller loops use default factory settings, implying that they have not been tuned at all*".

Various tuning methods have been proposed in scientific works to date. The tuning rules first proposed by Ziegler and Nichols [17] were followed by many tuning techniques, such as Cohen-Coon, Chien-Hrones-Reswick and refined Ziegler-Nichols rules. In addition to these typical tuning rules, more advanced methods have also been proposed. The latter mostly use complex algorithms for process identification [16], [18]–[26]. According to the literature [16], the number of tuning rules for stable overdamped processes is much larger than that for integrating processes. This indicates that PID tuning for integrating processes is not an intensively studied area.

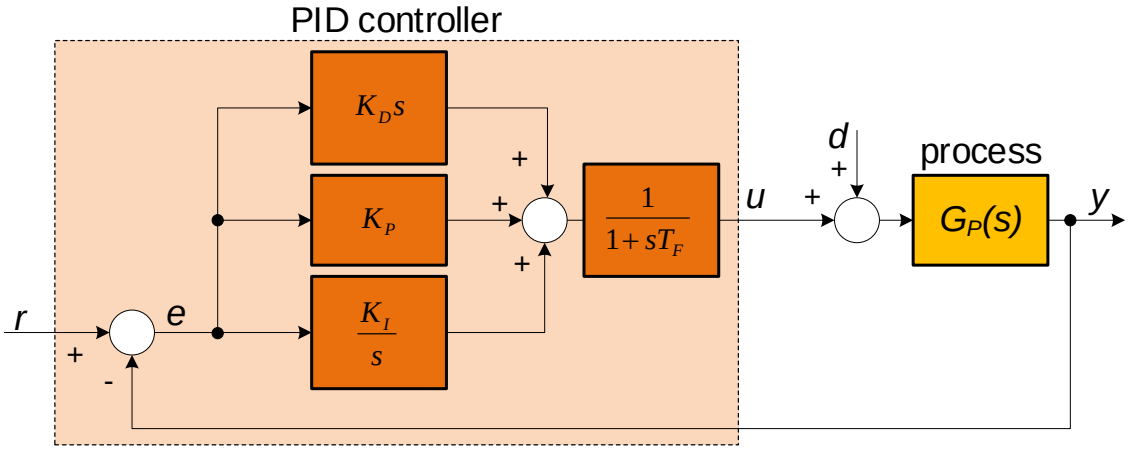

Figure 1.1: Proportional–Integral–Derivative (PID) controller. The closed-loop system with a PID controller.

1.2 Integrating Processes (IPs)

Integrating processes (IPs) contain at least one pole at their origin and are common in industry. The main feature of IPs is their open-loop instability, which leads to an unbound output for a bound input, i.e., when perturbed, the process output drifts to extreme values [27]. An example of the open-loop step response of a simple time-delayed IP is shown in Figure 1.2. Accordingly, the efficient control of IPs is a challenging task [28].

IPs are found in power and paper mills, aerospace control, and petroleum industries, and can be classified according to the process order. Typical representatives of the processes that employ pure integrator plus time delay (ITD) transfer function models are the oil-water-gas separators in the oil industry [28], the bottom-level control in a distillation column [29], the composition control loop of a high-purity distillation column [30], heat-

integrated distillation columns [31], isothermal continuous copolymerization reactors [32], storage tanks with an outlet pump [33], the roll angle control of an aircraft during vertical-takeoff [34], industrial injection moulding machines [35], pulp and paper plants [28], and the high-pressure steam flow to steam turbine generators in power plants [36].

Integrating first-order with/without time delay (IFOTD) systems can be encountered in liquid-storage tanks [37], jacketed continuous stirred tank reactors (CSTR) performing exothermic reactions [38], and paper drum dryers [39]. The most common examples of an IP with an inverse response with a time delay (INPTD) are a boiler steam drum [40], catalytic tube reactors with exothermic chemical reactions [27], and municipal solid waste incinerator temperature with inlet load rate changes. Examples of higher-order IPs include heat transfer and multiple liquid-storage tanks connected in series.

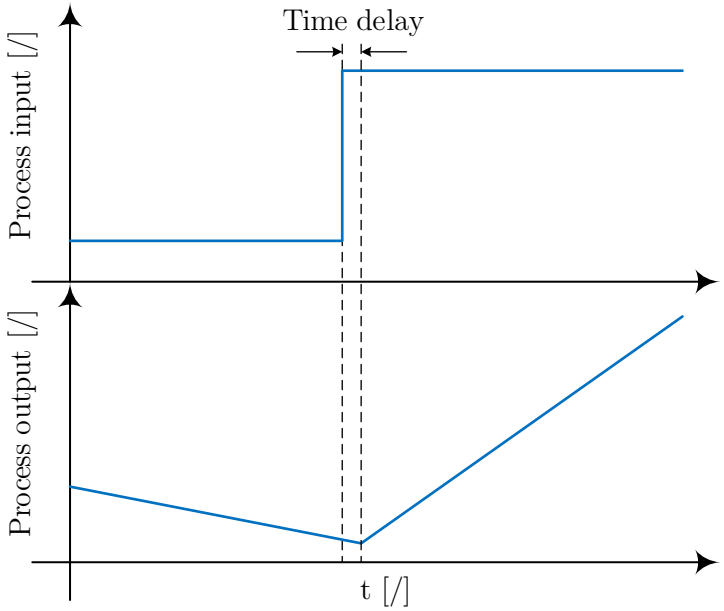

Figure 1.2: Simple time-delayed integrating process open-loop response.

IPs are also common in other applications, such as a charge amplifier, which is an electronic circuit that produces an output voltage proportional to the integral of the input current [41]. They are used to convert electric charges or electric currents into voltage signals and are mainly used to measure the response of various capacitive, piezoelectric and pyroelectric sensors, quantum detectors, photodiodes and other devices that generate very small charges [42]–[45]. The charge amplifiers are also used to measure the direct piezoelectric coefficient of piezoelectric samples [46]–[52], including the dynamic piezoelectric properties of bones [53], polarization measurement of dielectric samples [54]–[62], and in the development of various environmental sensors [63]–[66].

In addition, the open-loop response of various industrial processes, such as liquid storage tanks, boilers, liquid level systems with a pump at the outlet, and chemical batch reactors, is slow and has a large dominant time constant. Time-delay is present in process industries due to recycling loops, transport delays, composition analysis loops, etc. An IP model could be used when the required settling time is much shorter than the dominant time constant of a process, even for the first-order time-delay processes [25, p. 15]. As observed in [29], the controller design based on IPs could provide better closed-loop performance than designs based on the first-order process plus time delay.

IP models are also typically used in alternative closed-loop control structures [67], e.g., in a "model-free" approach named Active Disturbance Rejection Control (ADRC) [68]. As explained in [67], "*one of its main components may be denoted as an Extended State Observer (ESO) built upon integral plant models. Thereby, the modelling errors caused by the less detailed "ultra-local" integral models are merged with external disturbances*". Since only two identified process parameters are used, the main advantage of such an approach is its simplicity.

Due to the large dominant time constant, larger overshoots and closed-loop settling times may occur when controlling IPs. The problem is even more pronounced for larger time delays (dead times) [28], [69], [70]. Moreover, a balanced tracking and control performance is usually harder to achieve. Therefore, efficient control of IPs is challenging for both tracking and disturbance-rejection. Therefore, tuning of PID controllers requires special attention in terms of robustness, noise sensitivity, and closed-loop performance. Note that controllers designed for self-regulating processes perform poorly when applied to IPs, e.g., PID controllers are likely to generate larger overshoots or oscillations for IPs with dead time due to the presence of integral action [10].

1.3 Closed-Loop Control of Integrating Processes (IPs)

The controller design for integrating and unstable processes has been studied by several researchers. Some of the proposed solutions are based on the use of a single closed-loop controller, while others use complex control structures. Several IP tuning methods have been proposed so far [16], [71]. To simplify the presentation, the proposed methods are divided into classical closed-loop control structures and complex closed-loop control structures.

1.3.1 Classical closed-loop control structures

These techniques can be classified according to their IP model structure, i.e., tuning methods for ITD [5], [28], [72]–[96], for IFOTD [7], [15], [40], [71], [97]–[139], for higher-order IPs with time delay [140]–[147], and nonparametric tuning methods for IPs [148]–[150].

First, we present the tuning methods for ITD. The method of Mercader and Baños [91] for the PI controller considers process uncertainties. The design is based on optimising the disturbance-rejection performance with constraints on the magnitude of the sensitivity. Raza et al. [92] developed a tuning rule derived in terms of maximum sensitivity (Ms) based on pole-placement and frequency-response matching criteria. In [5], [28], Visioli proposed a PID controller and a three-state structure to achieve a time-optimal tracking response. Since this method uses an identification technique (least-squares-based) to compute the process model during steady-state changes, it is not necessary to know the process model in advance. Bagheri and Nemati [85] proposed an analytical tuning rule for the PI controller in a two-degrees-of-freedom (2-DOF) structure. The optimisation of the disturbance-rejection response was achieved by minimizing the Integral of the Absolute Error (IAE) criterion for a disturbance input step signal. Tracking performance was improved by using the set-point weighting parameter. Robustness to model uncertainties was achieved by minimising the maximum sensitivity function. Visioli [87] proposed analytical tuning formulas for the PID controller applied to the IPs obtained using genetic algorithms (GA) optimisation of the integral squared error performance criterion. Separate rules for optimal set-point tracking and disturbance-rejection were proposed.

Controller designs based on the Internal Model Control (IMC) tuning rules for PID controllers have been proposed by Grimholt and Skogestad [78], Yin et al. [73], and Vanavil et al. [96]. Grimholt and Skogestad [78] proposed the calculation of the PI and PID parameters depending on the minimum IAE on disturbances for a given robustness level, defined as the sensitivity peak (Ms). Yin et al. [73] proposed an IMC-based PID controller utilizing an optimal H_2 scheme to improve the disturbance rejection ability. The PID parameters are obtained using the Maclaurin series approximation approach. A trade-off between tracking and disturbance-rejection is achieved with a reference filter. Vanavil et al. [96] proposed an IMC-based method using the PID controller in series with a lead-lag compensator. The solution is based on the H_2 optimal closed-loop transfer function for tracking and disturbance-rejection. The proposed method has a user-defined tuning parameter λ to set the desired trade-off between the closed-loop performance and the robustness of the designed controller.

Controller designs based on the IMC tuning rules for PI controllers have been proposed by Dalen and Di Ruscio [79], Takeda and Yamashita [80], and Nath et al. [83]. Dalen and Di Ruscio [79] developed an IMC-based PI controller tuning rule, whose main feature is the method product (MP) parameter, i.e., the product of the PI controller proportional gain and the integral time constant, and the integrating plus time delay model gain. Unlike most PI controller tuning rules where the method product parameter is constant, the rule proposes an optimal MP parameter that ensures optimal closed-loop system robustness or performance, i.e., minimising the IAE or sensitivity index Ms. Takeda and Yamashita [80] developed a practical method to identify the IP with dead-time dynamics under continuous self-excited oscillation. The IMC filter parameter is then derived from the phase/gain margin and the process's dead-time. Nath et al. [83] proposed a graphical treatment for tuning the IMC-PI controller, based on the desired gain and phase margin specifications.

Integral–proportional derivative (I-PD) control strategies have been proposed by Chakraborty et al. [76] and Peker and Kaya [74]. Chakraborty et al. [76] proposed an I–PD control strategy (see Figure 1.3) for the IPs with time delay. The proposed scheme consists of an inner PD loop (controller G_{C2}) and an outer I-loop (controller G_{C1}). Proposed formulas for the PD controller setting are derived with gain-margin and phase-margin specifications, while the integral gain is obtained in terms of the critical gain of the inner-loop process.

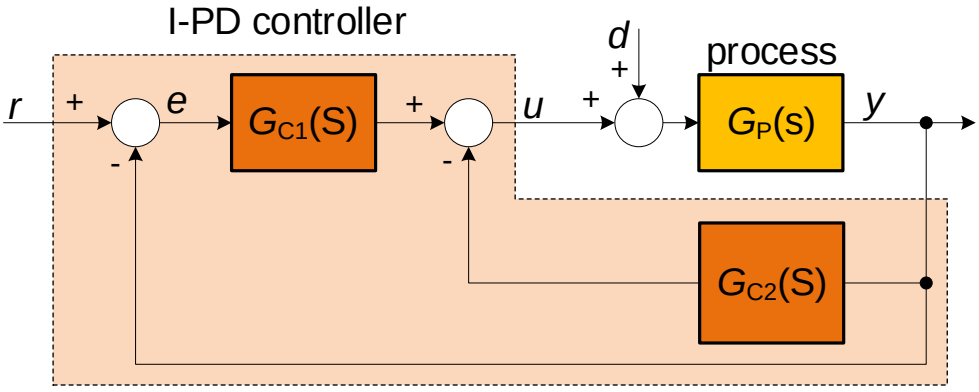

Figure 1.3: I-PD control structure. The solution was proposed by Chakraborty et al. [76]: $G_{C1}(s) = I$ and $G_{C2} = PD$.

Peker and Kaya [74] similarly proposed analytical tuning rules for the I-PD controller to control the IPs with time delay. To obtain the optimal controller parameters, the integral of cubed time squared error (IST^3E) performance criterion was minimized using particle

swarm optimisation (PSO), which is an evolutionary optimization method. PI-PD controller (see Figure 1.4) for the control of ITD was proposed by Kaya [89]. Analytical tuning rules were obtained with minimization of the closed-loop error based on the IST^{3}E criterion.

A two-degrees-of-freedom (2-DOF) PD-PI controller with nth order binominal filter and a second-order reference filter for improving tracking performance (see Figure 1.5) was proposed by Huba in [95]. The controller's performance is scalable by the multiple real dominant pole method that integrates the tuning of the parameters of the noise filter, the controller, and the reference filter.

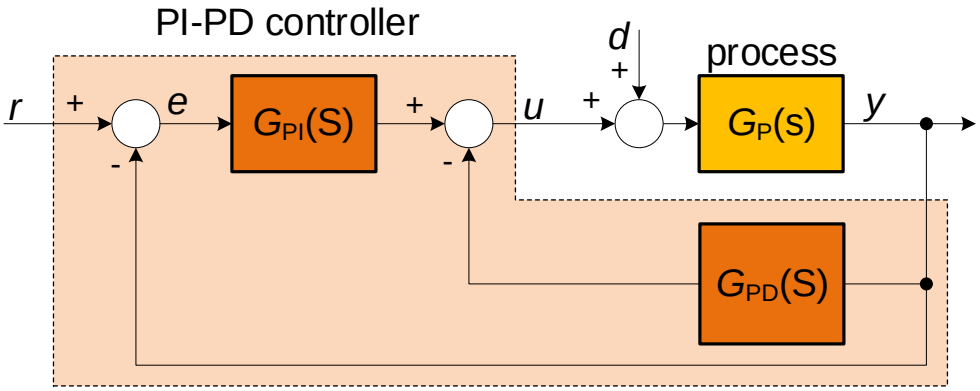

Figure 1.4: PI-PD control structure. The solution was proposed by Kaya [89]. G_{PI}, G_{PD}, and G_{P} are the PI controller, PD controller and the controlled process, respectively.

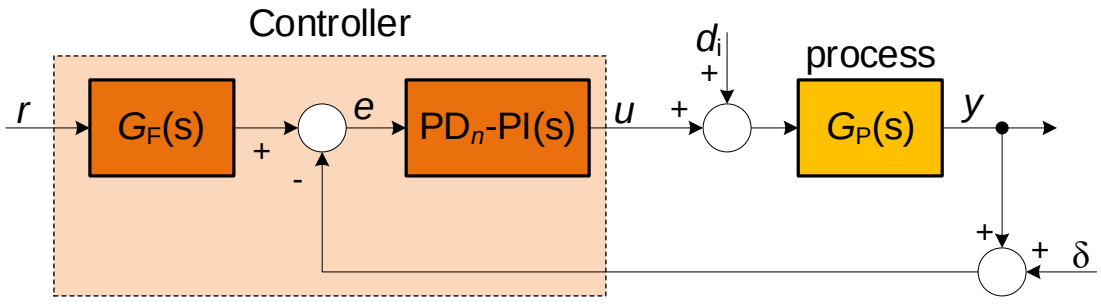

Figure 1.5: 2-DOF PD-PI controller with nth order binominal filter and a reference filter. The solution was proposed by Huba [95]. G_{P}, G_{F}, and δ are the controlled process, reference filter and the measurement noise, respectively.

A method for the auto-tuning of PID controllers based on closed-loop identification was proposed by Rene Pereira et al. [94]. This method consists of closed-loop identification of the model (after the reference or the disturbance step is changed), performance evaluation, and retuning of the PID controller. Siddiqui et al. [90] proposed a similar model-free PI/PID tuning method that uses a simple closed-loop reference step change (with proportional control gain only) to identify the process model. Based on the process overshoot, the process is approximated as a second-order plus dead time (SOPDT) transfer function. The controller parameters are calculated using a direct synthesis approach with an IMC tuning rule based on the obtained model. Similarly, in [93] Shamsuzzoha et al. proposed the PI controller tuning, which applies the closed-loop set-point change to obtain the controller parameters from an unidentified process. The PI-controller parameters are then obtained

directly from the response of the process: the overshoot, the time to the first peak, and the relative steady-state change.

In [75], a novel approach to tuning discrete-time PID controllers with higher-order derivatives with a special focus on noise attenuation filters was proposed by Huba and Vrančić. These controllers provide a third degree of freedom in the control design dedicated to attenuation of measurement noise. Huba [72] proposed two integrated tuning procedures for the joint design of a PID controller in series with an nth-order binomial low-pass filter. The proposed higher-order controller represents an intermediate step between integer and fractional-order PID controllers. Then, in [77], a derivation of higher-order PID controllers by generalising the Skogestad Internal Model Control (SIMC) method [15] was proposed by Huba for analytical model-based controller tuning. In [88], Huba et al. proposed a higher-order proportional-integrative-derivative (HO-PID) control. It consists of a traditional PI control with an mth-order derivative action and an $n > m$th order series binominal filter. In terms of simplicity, the tuning of the proposed controller is comparable to that of the PI controller.

Vítečková and Víteček [82] proposed robust and simple analytical 2-DOF PI/PID controller tuning rules based on the multiple dominant pole method (MDPM). The method allows the computation of controller parameters while maintaining non-oscillatory closed-loop responses without overshoots. A similar method was proposed by the same authors in [84].

Note that the tuning methods for ITD can also be used for other IP types if the process can be modelled by the ITD model. This can be achieved, for example, by using a relay feedback identification method [74], [79], [86], [89], [92], [94].

Next, the IFOTD tuning methods are presented. Some of the tuning methods do not use the integrating term of the controller (Eriksson et al. [120], Kuzishchin et al. [121]). Therefore, these methods are not suitable for rejecting the process input disturbances. Anil and Padma Sree [116] developed a PID controller tuning method for IFOTD processes with or without an additional process zero. The method is based on a pole-placement strategy, while the tuning parameter is the maximum sensitivity (Ms). This is similar to the method of Medarametla and Komanapalli [113]. In [114], Medarametla and Manimozhi similarly proposed an analytical PID tuning method. A second-order reference filter is used to reduce overshoot. The same authors proposed similar analytical PID controller tuning rules for various IPs in [104]. Overshoots are reduced by cancelling some controller zeros and using a fourth-order reference filtering. In [131], Zhang et al. proposed analytical tuning rules for a PID controller for IPs with time delay. The rules were obtained using direct synthesis and modified multiple dominant pole-placement methods. Taguchi and Araki [105] proposed analytical tuning rules for a 2-DOF PID controller, in which the optimal closed-loop response is achieved by two-step tuning of the closed-loop transfer function. Vítečková and Víteček [103] proposed analytical PI/PID controller tuning rules for ITD and IFOTD based on the MDPM. When the closed-loop tracking responses have higher overshoots, the method employs a 2-DOF PID controller. Vilanova et al. [98] proposed robust tuning of PI/PID controllers specifically tuned for load disturbance attenuation, i.e., the desired disturbance-rejection behaviour is specified in terms of a single free parameter that determines the closed-loop disturbance-rejection time constant. In [132], Darwish proposed a method to determine the PID controller gains by matching the frequency response of the closed-loop and reference model.

Controller designs based on IMC-PID tuning rules have been proposed by Kumar and Padma Sree [71], Jin and Liu [137], Skogestad [15], Panda [101], Ghousiya Begum et al. [127], Najafizadegan et al. [138], Ranganayakulu et al. [136], Goud and Rao [122], Shamsuzzoha and Lee [124], and Kaya [134]. The IMC filter time constant in the method of Kumar and Padma Sree [71] was chosen to set the trade-off between performance and

robustness of tracking and disturbance-rejection. Similarly, the IMC filter time constant was used to choose the robustness level in Jin and Liu [137] method. Skogestad [15] proposed simple analytical model reduction rules and improved IMC-PID tuning rules named Skogestad Internal Model Control (SIMC). In order to improve disturbance-rejection for IPs, the rule for the integral term was modified. The method proposed by Panda [101] derived controller parameters by equating the closed-loop response with a desired closed-loop response involving a user-defined tuning parameter λ. Laurent's series is used to deal with singularity problems with IPs. Ghousiya Begum et al. [127] calculated the PID controller parameters using IMC - H_2 minimization for integrating and double integrating time-delay processes with a right half plane (RHP) zeros. The method uses a single adjustable tuning parameter to set the desired trade-off between closed-loop performance and robustness of the designed controller. In [138], Najafizadegan et al. considered the design of IMC-PID controllers as an optimization problem by combining loop shaping and Linear Matrix Inequality (LMI) approaches. The parameters of the PID controller are computed in such a way that the crossover frequency of the gain, the phase margin, and the phase and amplitude of the open-loop system are separately set to the desired values at different frequencies. This loop shaping procedure is fully formulated as an LMI generalized eigenvalue problem (GEVP). Ranganayakulu et al. [136] proposed an IMC–PID controller using a higher-order fractional IMC filter to control IPs with time delay. The use of a higher-order fractional IMC filter structure eliminates the need to use a reference filter or set-point weighting. The higher-order Padé algorithm is used to approximate the process time delay. Optimal controller settings are identified using a systematic procedure that minimizes the IAE for a fixed maximum sensitivity Ms. In [135], Hemavathy et al. propose an IMC-PD controller with a fractional-order (FO) filter for IFOTD. The process time delay is approximated with a first-order Pade algorithm. Goud and Rao [122] proposed a second-order noise filter to reduce the noise effect on the PID controlled IPs. The value of the filter time constant is based on an iterative approach, i.e., function of the loop gain crossover frequency and the design parameter whose value is chosen as a tradeoff between robustness, performance, and measurement noise reduction. The controller parameters are calculated using the Optimal H_2 - IMC based technique. Shamsuzzoha and Lee [124] proposed a simple IMC-PID controller for IFOTD and ITD processes. Since the method is based on optimising the disturbance-rejection, a reference filter was proposed to improve the tracking performance. Kaya [134] proposed a 2-DOF IMC control structure for controlling IPs with time delay. The controllers are tuned according to the gain and phase margins specified by the user.

Tuning rules, obtained by optimisation, were proposed by Bingul and Karahan [139], Kaya and Cengiz [102], Irshad and Ali [100], Kaya [111], [115], [123], Kaya and Peker [125], and Ali and Majhi [97]. Bingul and Karahan [139] tuned a PID controller using particle swarm optimisation (PSO) and artificial bee colony (ABC) algorithms. For controlling IPs with an inverse response, Kaya and Cengiz [102] proposed analytical PI/PID tuning rules based on the integral performance criteria. To obtain relationships between the controller and the process models, repeated optimizations were performed on the error signal (to minimize it). Similarly, analytical tuning rules for PI/PID controllers were obtained by Irshad and Ali [100]. The integral of time squared error (ISTE), the integral of squared time squared error (IST^2E), and IST^3E were minimized with PSO to obtain optimal controller parameters. A reference filter is used to reduce overshoots in the tracking response. Kaya [115] proposed an I-PD controller for controlling the IPs. Analytical tuning expressions were derived by minimizing the error signal using weighted criteria of the ISTE and IST^2E. In [125], Kaya and Peker extended the previous tuning rules with an additional performance criterion (IST^3E) that improved the closed-loop responses. A similar I-PD controller was proposed in [111], [123], by the same author (Kaya), for control of the IPs

with an inverse response. Analytic tuning expressions were derived by minimizing the error signal using integral performance criteria (ISTE, IST^{2}E, and IST^{3}E). In [97], Ali and Majhi proposed tuning formulas for a class of IPs based on minimizing the Integral of Squared Error (ISE). To achieve optimal load disturbance-rejection for the IPs, the ISE criterion is minimized with the constraint that the Nyquist curve slope, at the gain transition frequency, has a specified inclination.

Atic and Kaya [117] proposed a tuning method for the PI controllers in which the obtained stability-boundary loci determine the controller parameters. A similar approach was used by Atic et al. [99] for the PID controllers. Alyoussef and Kaya [110] propose a new analytical approach to find the stability region centroid for PI controllers. The proposed method eliminates drawing of the stability region. In [108], Cokmez et al. obtained stability regions, satisfying the specified gain and phase margin on IPs with a time delay for a FO PI controller. Using a relay feedback identification method, the method was also tested on higher-order IP. Pai et al. [40] proposed analytical PI/PID controller tuning rules for IPs with an inverse response (non-minimum phase zeros). Based on the model and the minimal IAE criterion, the controller parameters were computed using the golden section search algorithm. Ozyetkin et al. [118] proposed a PID controller tuning for IPs with time delay and inverse response. First, the stability region in the PI controller parameters plane, corresponding to the derivative gain, is determined (stability boundary locus method), and then the weighted geometrical centre (WGC) of this region is found (geometrical center approach). Srivastava and Pandit [107] developed a PID controller with a unique reference filter that creates a 2-DOF control system. The controller tuning is based on a linear quadratic regulator (LQR) using a dominant pole-placement approach to achieve a good disturbance-rejection performance. A PID controller with set-point weighting in series with a lead/lag compensator for IPs with time delay was proposed by Seshagiri Rao et al. [109]. Analytical tuning rules are derived for a class of IPs based on the desired closed-loop transfer function (direct synthesis method).

Panda et al. [119] proposed a relay feedback approach to identify model parameters in a closed-loop for a class of IPs. The process parameters are calculated from an oscillatory process response obtained by the ideal relay experiment. The controller parameters are calculated with an IMC-PID tuning rule using a direct synthesis approach based on the obtained model. Similarly, Veronesi and Visioli [112] proposed a methodology for the closed-loop performance evaluation of a PID controller. First, the process is approximated as IFOTD from the closed-loop step response. The performance is then evaluated by comparing it with the performance provided by the SIMC [15] tuning rule. If the performance is not satisfactory, the PID controller is retuned using the same tuning rule. Shamsuzzoha and Skogestad [7] also proposed a similar tuning procedure. PI/PID controller tuning rules and a method to identify IPs with a time delay and inverse response from an open-loop step response were proposed by Luyben [106]. The process is approximated as IFOTD with an inverse response.

Irshad and Ali [128] proposed a parallel control structure (PCS) for a class of IPs that acts as a 2-DOF controller (see Figure 1.6). For tracking and disturbance-rejection, PD controller G_{C1} and PID controller G_{C2} are proposed, respectively. PSO minimised the integral performance criteria (ISTE, IST^{2}E and IST^{3}E) to obtain optimal controllers' parameters. Ajmeri and Ali [126] also proposed an identical controller structure. The controllers' parameters are obtained using the direct synthesis approach, i.e., the desired closed-loop transfer functions for tracking and disturbance-rejection are specified separately. The tuning parameters are defined by the Ms value.

Ozyetkin et al. [129] proposed the PI-PD controller (see Figure 1.4) tuning method to control the time-delayed systems. The method is based on the computation of controller parameters regions using the stability boundary locus and the computation of the WGC of

the plotted regions. A similar solution was proposed by Raja and Ali [133] for unstable and IPs with time delay and inverse response. PD and PI controller parameters are determined by defined Ms value, Routh–Hurwitz stability criteria and by comparing the first and the second derivatives of the expected and the actual closed-loop transfer functions. Similarly, Ozyetkin [130] proposed a fractional order PI-PD controller to control the time-delay processes. The proposed method uses an identical procedure to obtain the controller parameters. A significant advantage of the proposed methods is the calculation of the controller parameters without complex solutions and proven stability.

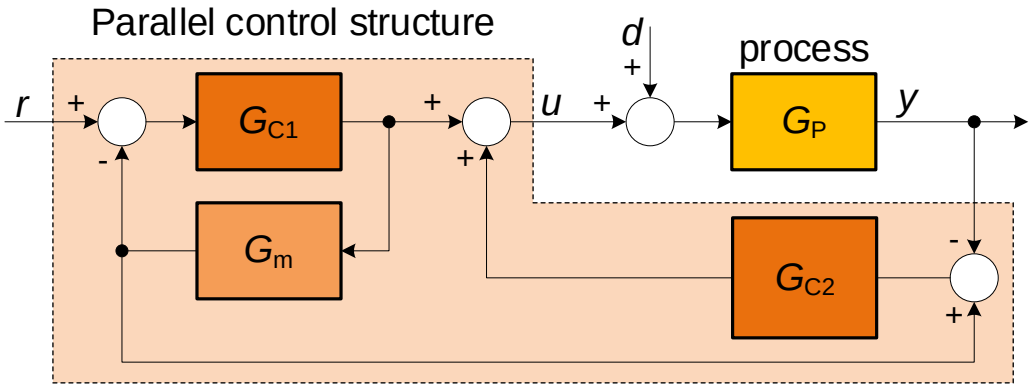

Figure 1.6: Parallel control structure (PCS). Irshad and Ali [128] proposed the solution. G_{C1}, G_{C2}, G_P and G_m are PD controller, PID controller, the controlled process and the nominal model, respectively.

Note that most tuning methods for IFOTD can be applied to other types of IPs if the process can be modelled by the IFOTD model [7], [15], [99], [100], [102], [104], [106], [108]–[119], [123], [125], [127], [128], [131], [134], [137], [138].

Next, tuning methods for general (higher-order) IPs with time delay have been reviewed. Papadopoulos [144] proposed the tuning of PID controllers for general IPs using the symmetrical-optimum method. The method is useful for disturbance-rejection but leads to higher overshoots of the process output during setpoint changes. A PID controller with an additional zero for controlling second-order IPs was proposed by Papadopoulos et al. [141]. The controller tuning rules also included the sampling time Ts of the controller. Meena and Devanshu [145] proposed tuning of the PID controller using a genetic algorithm optimisation. In [142], Šekara and Mataušek proposed a new classification for a large class of stable, oscillatory, integrating, and unstable processes with or without time delay. This was done using the proposed ρ–φ parameter plane, defined by the normalised gain, ρ, and the angle of the Nyquist curve slope φ at the process' ultimate frequency. Formulas are then proposed for tuning the PID controller to achieve the desired trade-off between performance and robustness in the selected region of the ρ–φ parameter plane.

Hamamci and Koksal [143] proposed a simple and effective stabilisation method for IPs with time delay using FO PD controllers. The proposed method is based on finding the stability regions according to the fractional orders of the derivative elements. Siddiqui et al. [146] proposed PID controllers with filter in the parallel control structure (PCS) for the IPs with time delay and inverse response (see Figure 1.6). The controllers are tuned by frequency response matching with the DS (direct synthesis) controller, making the method applicable to the higher-order process. In addition, a derivative filter is included as an integral part of the design of the controllers.

Anwar and Pan [147] proposed two controller design approaches for the IPs with time delay, based on frequency response matching. In the first approach, a cascade feedback

loop is proposed. The inner loop consists of a proportional (P) controller. The parameters of the PID controller in the outer loop are obtained by frequency response matching using a reference model with the desired specifications. In the second approach, the design is based on a desired disturbance-rejection model of the system. Although the proposed solution was tested on the third-order IP, the closed-loop disturbance-rejection model was of the second-order. Similarly, Raza and Anwar [140] proposed two control structures to control IPs with time delay. The control structures are identical to those described in the previous method. However, the disturbance-rejection closed-loop system was of the third-order.

Nonparametric tuning methods are data-based, i.e., they directly exploit the closed- or the open-loop process datasets without requiring an explicit process model. This is an attractive approach for alleviating the drawbacks of the process–model mismatches. Jeng [149] proposed a PI/PID controller tuning method that enables the specification of the desired closed-loop transfer function for disturbance-rejection, while tracking can be improved using PID controllers independently with set-point weighting. In [150], Dey, Mudi, and Simhachalam developed an auto-tuning PD controller (see Figure 1.7) that adjusts the proportional and derivative gains to improve the overall performance (set-point tracking and process output disturbance-rejection). However, due to the lack of an integrator, the proposed method is not suitable for rejecting process input disturbances.

Mataušek and Šekara [148] proposed the PI and the PID tuning rules based on an extended Ziegler–Nichols experiment (in addition to the ultimate gain and frequency, the steady-state gain and the tangent to the process Nyquist curve at the ultimate frequency should also be determined). The controller parameters are calculated by optimisation (solution of two nonlinear algebraic equations).

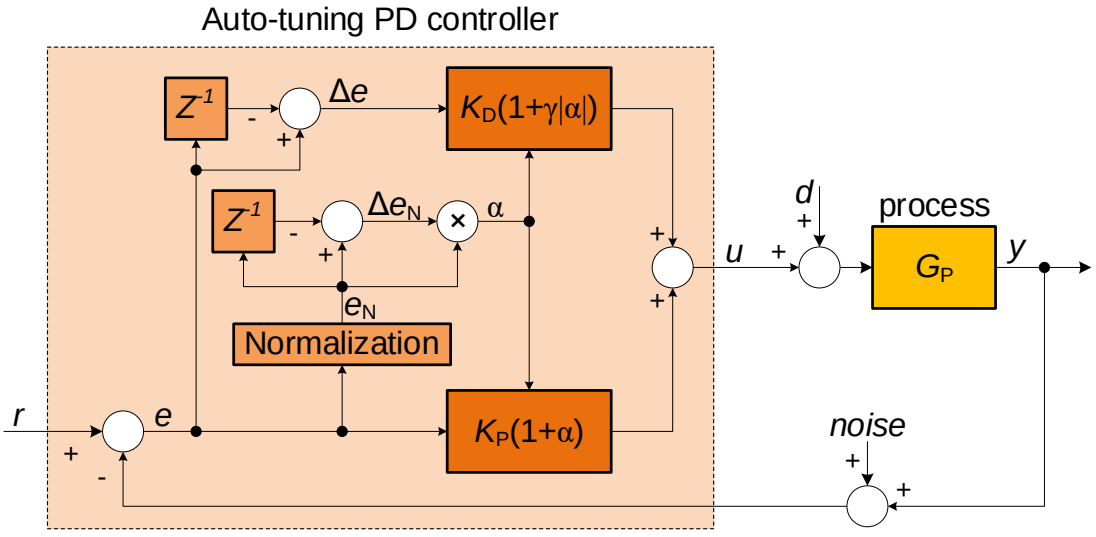

Figure 1.7: Block diagram of the auto-tuning PD controller. The solution was proposed by Dey, Mudi, and Simhachalam [150].

1.3.2 Complex closed-loop control structures

Zhang et al. [151] proposed a modified Smith predictor with a pre-filter for the first-order stable and time-delayed IPs. The proposed tuning rule allows tuning of the controllers based on the time-domain properties, such as desired overshoot and rise time, or on frequency-domain criteria, such as stability margin and bandwidth. Similarly, a modified

Smith predictor (see Figure 1.8) was proposed by Mataušek and Ribić in [152] for the control of stable, integrating, and unstable processes, consisting of a 2-DOF PID controller in series with a second-order filter, defined by the dead-time and an adjustable parameter. Optimal parameters were determined using PSO. The performance indices are the IAE and the maximum sensitivity to measurement noise M_n, while the robustness indices are the maximum sensitivity Ms and the maximum complementary sensitivity Mp.

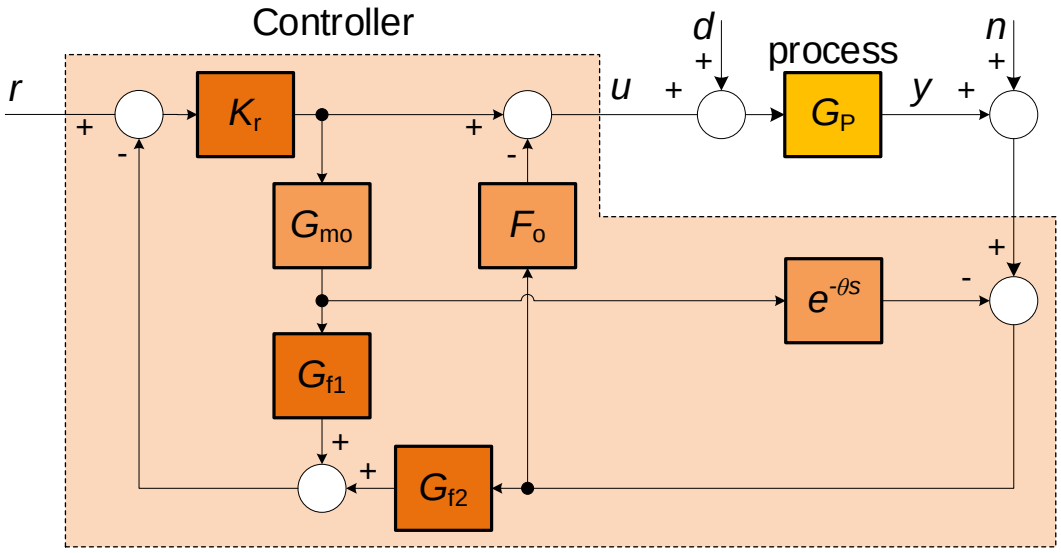

Figure 1.8: Modified Smith predictor. The solution was proposed by Mataušek and Ribić [152]: $G_{mo}(s) = K_P/s$, $F_o(s) = K_o(T_o s+1)/(T_f s+1)$.

In [153], Zhang and Sun extended the Smith predictor to the IPs. The proposed solution has two adjustable parameters for shaping the tracking and disturbance-rejection responses. Chakraborty et al. [154] proposed an all-PD control structure based on the Smith predictor scheme with gain- and phase-margin specifications for ITD processes. Padhan and Majhi [155] proposed a modified parallel cascade control scheme (see Figure 1.9) for stable, unstable and IPs with time delay. The proposed scheme consists of two PID controllers (G_{cd1} and G_{cd2}), a reference filter G_{cs}, and a modified Smith predictor in the primary loop to improve the closed-loop performance. The design of the controllers and the reference filter is based on loop shaping and ISE performance measures, respectively.

A control scheme based on a dead-time compensator for stable and IPs was proposed by García and Albertos [156]. The predictor provides an estimate of the non-delayed process output based on a discrete-time representation of the continuous-time model. Any classical tuning approach for processes without time delay can be used to tune the controllers.

Davó and Baños [157] proposed a proportional-integral compensator plus a Clegg integrator (PI+CI) to control the ITD processes (see Figure 1.10). The proposed solution is equipped with a variable band reset block that reduces the effect of time delay.

Huba [158] analysed the optimal tuning of a predictive disturbance observer (PDO)-based filtered PI (FPI) controller applied to the first-order plus time delay (FOTD) and ITD processes. The performance is then compared with that obtained using traditional 2-DOF PI control. Both controllers were tuned using the multiple real dominant pole method.

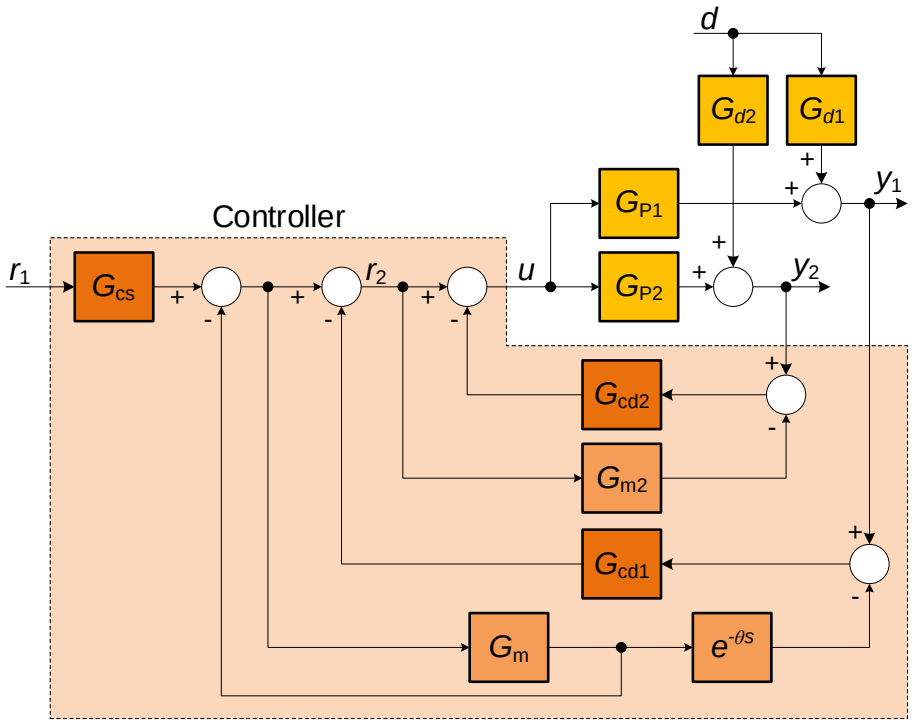

Figure 1.9: Modified cascade control scheme. The solution was proposed by Padhan and Majhi [155]. G_{P1} and G_{P2} are outer and inner loop processes, G_m and G_{m2} corresponding process models without time delay, G_{d1} and G_{d2} transfer functions of the processes disturbances, G_{cd1} and G_{cd2} are the PID controllers, and G_{cs} is the reference filter.

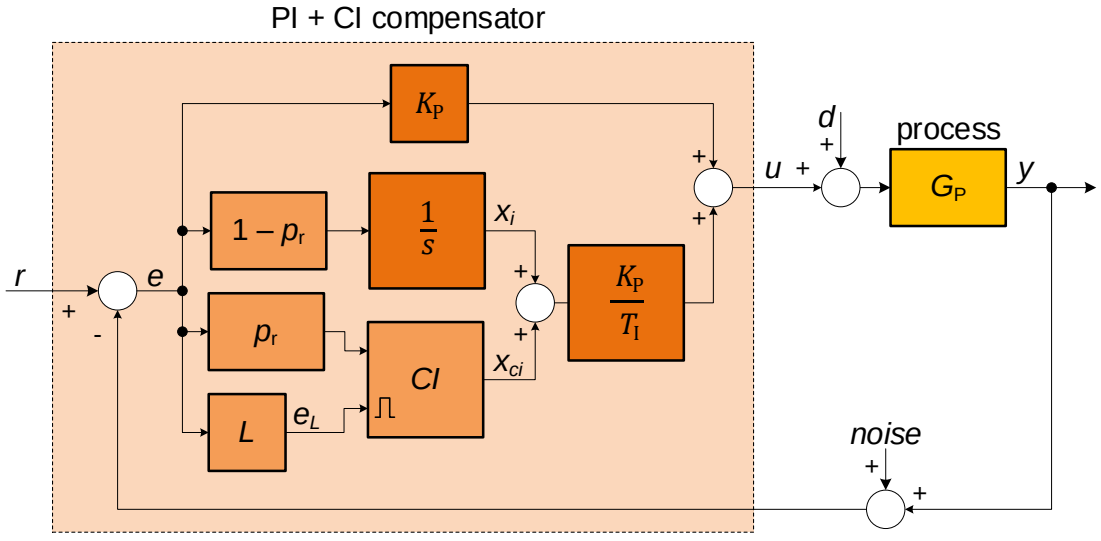

Figure 1.10: PI+CI compensator structure. Davó and Baños [157] proposed the solution.

In [159], Liu and Gao propose a modified IMC design based on a 2-DOF control structure (see Figure 1.11), which allows separate optimisation of tracking and disturbance-rejection performance. Two IMC control designs are proposed based on different disturbance types, i.e., step and ramp disturbance. The method uses a single adjustable tuning parameter corresponding to the time constant of the closed-loop transfer function,

which sets the desired tradeoff between disturbance-rejection performance and the closed-loop robustness. Jin et al. [160] proposed a 2-DOF control scheme based on the IMC structure, which allows separate optimisation of the disturbance-rejection and tracking responses. The design of the controllers for tracking and disturbance-rejection is based on a process model without time delay.

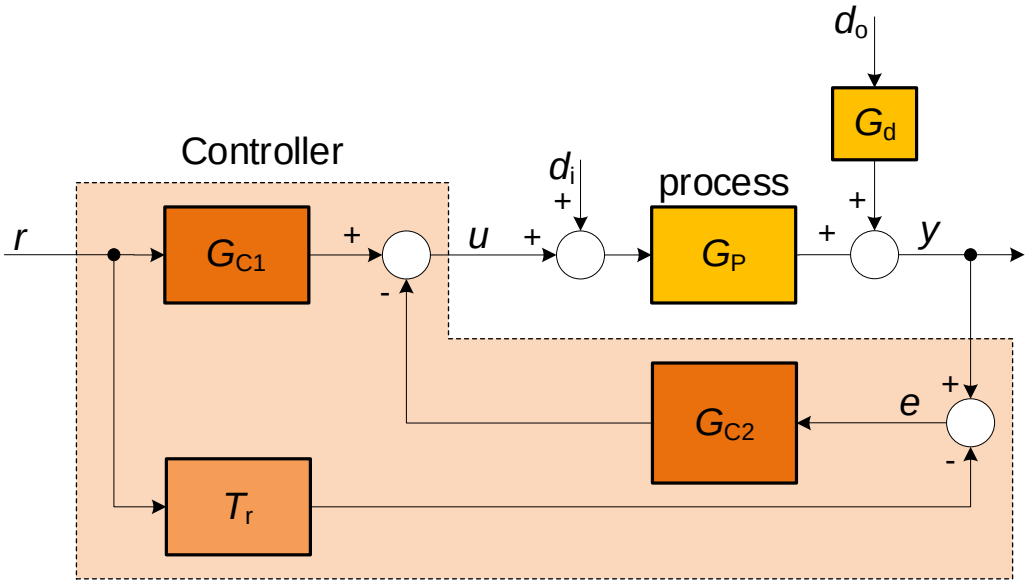

Figure 1.11: 2-DOF control structure. Liu and Gao [159] proposed the solution. G_P, G_{C1}, G_{C2}, T_r and G_d denotes the process, the tracking controller, the disturbance-rejection controller, the desired transfer function for tracking and the process disturbance transfer function, respectively.

Modified Smith predictor in a cascade structure (see Figure 1.12), consisting of three controllers, was proposed by Uma et al. [161] for IPs with time delay and with/without positive zero. The primary loop has a tracking PID controller with filter (G_{cs}) and a disturbance PD controller with lead-lag filter (G_{cd}), while the secondary loop has an IMC controller G_{c2} that stabilizes the process. The primary loop controllers are derived based on the process type and the desired closed-loop transfer function (direct synthesis method). Analytical tuning expressions for a class of the IPs are proposed. In [162], the same authors propose a modified Smith predictor design for non-minimum-phase IPs. The method uses a similar (non-cascaded) controller structure as the one proposed in [158]. The design of all controllers is based on the direct synthesis approach. In order to reduce unwanted overshoots in tracking, an additional degree-of-freedom is proposed in the form of a set-point weighting.

A predictor-based 2-DOF control design was proposed by Wang et al. [163]. The proposed control design was based on using a dead-time compensator (DTC) to predict the non-minimum-phase (NMP) dynamics. In [164], Zhang et al. proposed a disturbance observer-based (DOB) control scheme for controlling non-minimum phase IPs with time delay. Set-point tracking and the disturbance-rejection can be individually adjusted by the controller and the DOB filter. By optimising the disturbance-rejection criterion, the optimal DOB filter can be designed systematically.

Controller parameters for IFOTD or first- and second-order unstable processes with time delay in a discrete domain were developed by Wang et al. [165]. The solution is based on a 2-DOF control structure. The first controller is designed analytically with respect to

the specification of the H_2 optimal control performance specification for tracking. The second controller is derived according to the desired closed-loop transfer function for load disturbance-rejection.

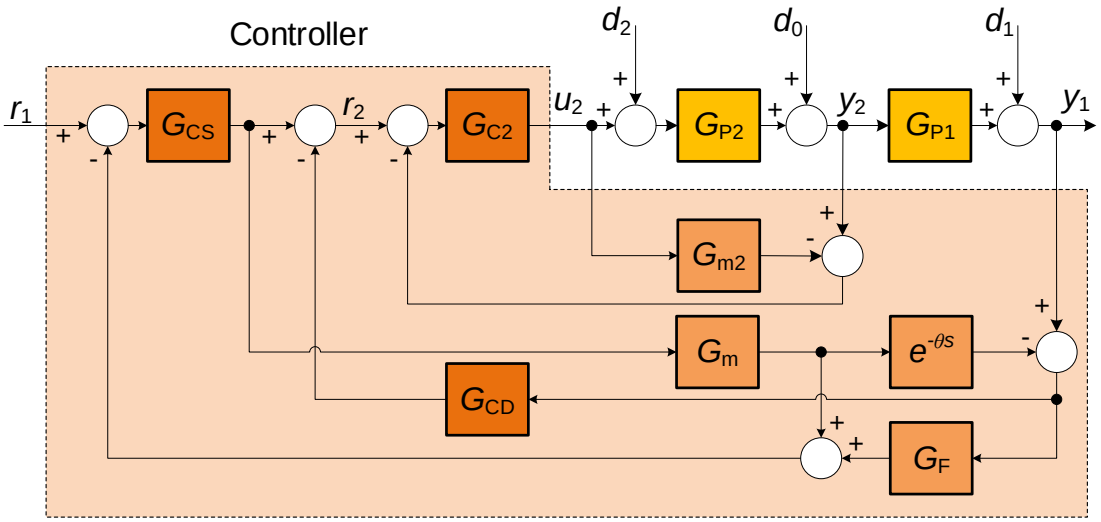

Figure 1.12: Series cascade control strategy with Smith predictor. The controller was proposed by Uma et al. [161]. G_{CS}, G_{CD} and G_{C2} are the primary tracking, primary disturbance-rejection and the secondary loop controller, respectively. G_{P2}, G_{P1}, G_{m2} and G_m are the secondary process's transfer functions, primary process, secondary process model, and overall process transfer function without delay, respectively. G_F is the first-order filter.

Raja and Ali [166] proposed a modified parallel cascade control strategy (PCCS) for a class of stable and unstable time-delayed IPs. The solution consists of three controllers: the primary PI controller for tracking, the PD controller for stabilizing the unstable/integrating primary process model, and the secondary loop controller for disturbance-rejection, obtained using the IMC approach. The proposed control strategy requires tuning of four to six controller parameters. In [167], the previous solution for IP models with a large time delay was extended by including the Smith predictor in the outer loop (see Figure 1.13). The extended PCCS also consists of three controllers: the primary controller G_{c1} for the tracking, the primary stabilizing controller G_{cd1}, and the secondary controller G_{cd2} for disturbance-rejection. The controller settings are determined by equating the first and the second derivatives of the desired and the actual closed-loop transfer functions about the origin of an s-plane using the Routh–Hurwitz stability criterion, and the IMC approach, respectively.

Similarly, a parallel cascade control strategy using FO controllers in combination with a Smith predictor was proposed by Pashaei and Bagheri [168] to control stable, unstable and IPs with a large time delay. The proposed solution also consists of three controllers: the primary FO controller for tracking, the primary PD controller for stabilizing, and the secondary FO controller for disturbance-rejection. The FO controller settings are determined using the FO-IMC approach, and the design of the stabilizing controller is based on the Routh-Hurwitz-stability criterion. Uma and Rao [169] proposed a modified Smith predictor design to control non-minimum phase unstable processes with/without zero. The proposed solution includes two controllers: PID in series with a lag filter for tracking and PID in series with a lead/lag filter for disturbance-rejection. A set-point weighting is proposed to minimise the overshoots.

Raja and Ali [170] proposed a modified serial cascade control structure (SCCS) with two PI and a P controller for a class of IP models with/without positive zero (see Figure 1.14). The parameters of the PI (G_{C1} and G_{C2}) and the P (G_{CD1}) controller are determined using the method of moments and the Routh–Hurwitz stability criterion, respectively. In [171], the same authors propose SCCS with a Smith predictor. The controller parameters are determined by moment matching, i.e., by equating the Maclaurin series of the expected and the actual closed-loop transfer functions. The tuning of the controller involves the adjustment of three to six parameters (depending on the plant model). In [172], Rodríguez et al. propose a modified feedforward compensator for the IPs. To achieve a good tracking performance, the controller with a reference filter is proposed. The proposed tuning rule for the compensator allows a trade-off between the overshoot and settling time.

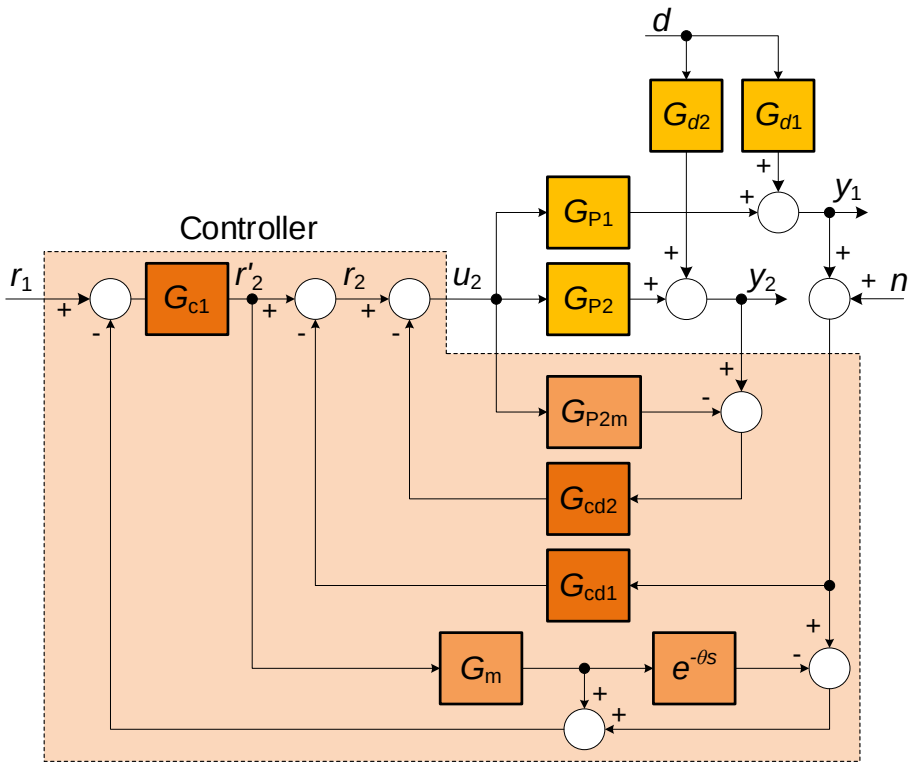

Figure 1.13: Parallel cascade control strategy with Smith predictor. Raja and Ali [167] proposed the solution. G_{c1} and G_{cd1} are the tracking and stabilizing controller, G_{cd2} denotes the disturbance-rejection controller, G_{P1} and G_{P2} are the primary and the secondary process models. G_{P2m} and G_m represent the secondary process model's transfer functions and the overall process model without time delay.

SCCS (see Figure 1.15), consisting of two controllers and a reference filter, is proposed by Padhan and Majhi [173] for a class of IPs with time delay. The controller G_{C2} in the inner loop, based on the IMC approach, rejects the disturbances entering the inner loop. The controller G_{C3} in the outer loop, which consists of a PID controller in series with a lead/lag compensator, rejects outer loop disturbances and stabilizes the IPs with time delay. The reference filter G_{C1} is used to improve the tracking performance. The proposed structure has been tested on the second-order integrating model with time delay.

Zhong and Normey-Rico [174] proposed a disturbance observer-based 2-DOF control structure for controlling IPs with dead-time. It requires the model of the controlled system.

Once the model is identified, only two tuning parameters are required: the set-point and the disturbance-response time constants.

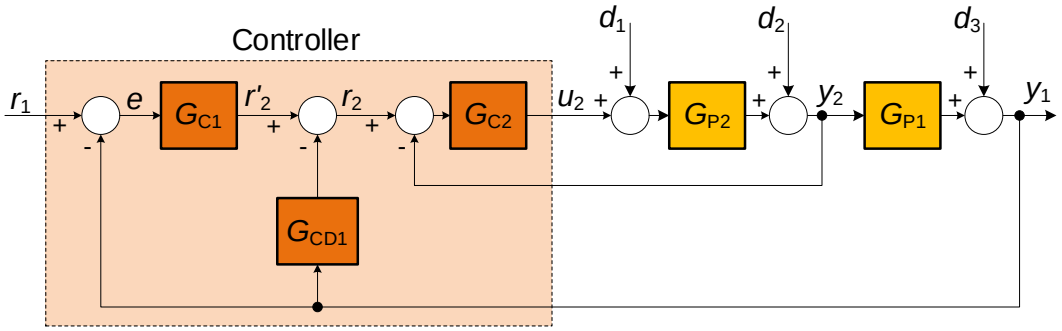

Figure 1.14: Series cascade control strategy. Raja and Ali [170] proposed the solution. G_{C1} and G_{C2} are PI controllers, and G_{CD1} is a P controller. G_{P1} and G_{P2} denote the primary and secondary process model.

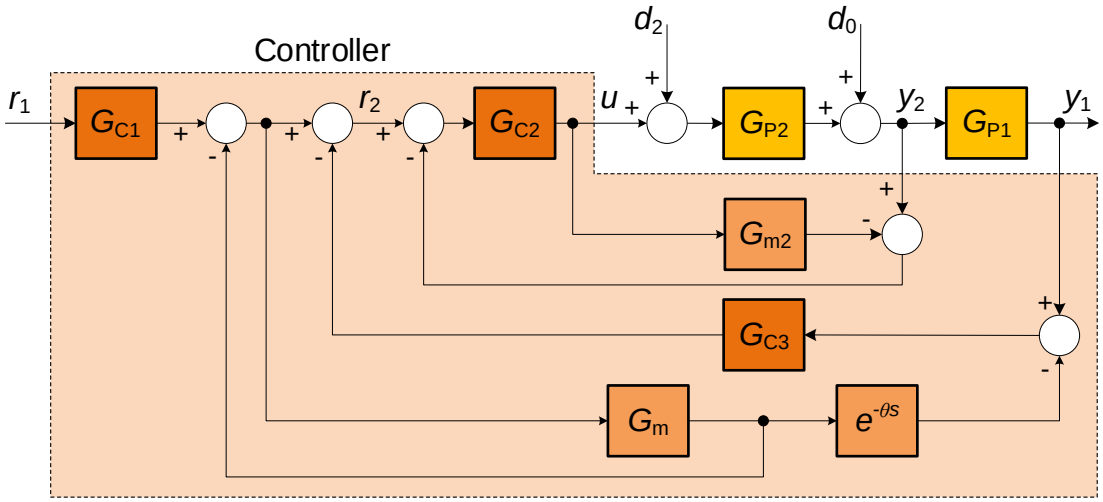

Figure 1.15: Series cascade control structure. The solution was proposed by Padhan and Majhi [173]. G_{c1}, G_{c2}, and G_{c3} are the reference filter, inner loop controller, and outer loop disturbance-rejection controller, respectively. G_{P1}, G_{P2}, G_m, and G_{m2} denote transfer functions of the primary process, secondary process, delay-free model of the overall process, and model of G_{P2}.

1.4 Purpose of the Dissertation

There are many PI and PID controller tuning methods for the IPs that have been developed in the last few decades. However, most of the existing tuning methods either require an accurate IP model, work on a limited range of IP models, or require additional optimization of the controller parameters. Moreover, the closed-loop efficiency and robustness of some of the methods are questionable. On the other hand, there is an obvious need in practice for a tuning method for IPs that is easy to implement, leads to efficient closed-loop control, and does not require sophisticated identification of the process.

The Magnitude Optimum (MO) is a controller tuning rule based on the closed-loop optimal frequency response [175]–[177]. The closed-loop performance for tracking and disturbance-rejection is usually fast and oscillation-free [178]. By using a nonparametric time-domain approach with multiple integrations of the process signals, the applicability of the MO method has been significantly extended. This extension is called the Magnitude Optimum Multiple Integration method (MOMI) [178]–[180] and retains all the advantages of the MO method. The extension provides using either the identified process model or the measurements of the process input and output signals for the calculation of the controller parameters [178], [179]. Therefore, this can be an attractive approach to mitigate the disadvantages of process model mismatch.

Since the original method MO was developed for stable (non-integrating) processes, the MOMI method cannot be directly applied for IPs. Namely, if the 1-DOF controller structure is used, the MO criteria will result in zero integrating gain of the PI/PID controller. Since the resulting P/PD controller cannot reject input disturbances, the original MOMI tuning method cannot be used for IPs.

The main goal of the dissertation is to extend the MOMI tuning method to IPs, by using several different controller structures and to analyse the performance, stability and robustness of the above method. The developed method remains nonparametric, i.e., it does not require an explicit process model to compute the controller parameters. This is an attractive approach since an intermediate step to compute the process model, which could be affected by a possible process model mismatch, can be eliminated. The controller parameters can be calculated from the so-called characteristic areas (process moments) [25], which can be obtained from the process closed- or open-loop time responses or from the arbitrary process transfer function with time delay. Moreover, the approaches are equivalent in the frequency and time domains (according to the MO criteria) without introducing errors in calculating the controller and reference filter parameters.

In practice, there is often a requirement to optimise either the reference tracking speed, disturbance rejection performance, or both. Therefore, the developed extension of the tuning procedure provides an additional possibility to emphasize either the disturbance rejection or the tracking performance via the reference weighting parameter. In addition, two reference filter structures have been developed to achieve the best overall closed-loop performance (optimal tracking and disturbance-rejection performance). The main advantage of using a reference filter is that such a filter can significantly improve the tracking performance without degrading the disturbance-rejection performance. The parameters of the reference filter are also calculated using the characteristic areas, so the process model is not needed.

In some cases, the calculated closed-loop speed might be too high. In this case, the controller parameters should be detuned. The detuning factor which is easily understood by the operators is the speed of the closed-loop control. Therefore, in this work, an additional measure is provided to change the closed-loop speed, which is the average closed-loop residence time [25]. The advantage of this measure is that it defines the tracking and disturbance-rejection speed of the control loop. Based on the mentioned measure, the user has the ability to recalculate the controller parameters and speed up or slow down the closed-loop response. It is worth mentioning that the mentioned additional speed parameter can also be calculated from the characteristic areas.

Tuning the controller without considering the stability or robustness limitations can lead to oscillatory or unstable closed-loop control even with minor changes of the actual process parameters. Therefore, the stability and robustness properties of the proposed tuning method have also been investigated. Furthermore, the robustness of the calculated characteristic areas from noisy process measurements is also investigated. Namely, by using

a suitable filter, the accuracy of the measured process moments can be significantly improved.

In practice, the process model is often needed for better optimisation of the closed-loop responses. Therefore, in this thesis, an analytical method is proposed to identify the lower-order process model (second-order process with zero and time delay) directly from the characteristic areas, i.e., from the process' closed- or open-loop time responses (in the time-domain) or from the higher-order transfer function with time delay (in the frequency-domain). The advantage of such an approach is that the lower-order model can also be obtained from an infinite order model (e.g. heat transfer) or from the process model containing the sum of the process models with different time delays.

1.5 Aims and Hypotheses

The main objectives of this work are as follows:

- enhancement of the MOMI tuning method to integrating processes using different 2-DOF PI/PID control structures,
- development of the reference filter whose parameters are calculated using the characteristic areas (explicit process model is not required),
- estimation of integrating processes models from the characteristic areas,
- analysis of the average closed-loop residence time,
- calculation of the controller parameters as a function of the desired speed of the closed-loop (i.e. the desired average closed-loop residence time),
- stability, robustness and noise sensitivity analysis of the developed tuning method,
- performance comparison with other tuning methods,
- development of practical performance criteria, and
- testing of the method on some laboratory and industrial plants.

The main hypotheses proposed, investigated and confirmed in this thesis are as follows:

- The PI/PID controller parameters can be computed from the parametric and nonparametric description of the process (e.g., by using the characteristic areas).
- The reference filter can be calculated from the parametric and nonparametric description of the process and can significantly improve the tracking performance without degrading the disturbance-rejection performance (i.e., achieving the optimal tracking and disturbance-rejection).
- From the parametric and nonparametric description of the process, controller parameters can be calculated according to the specified average closed-loop residence time and the desired disturbance-rejection performance.
- The second-order process model with zero and time delay can be reliably computed from the parametric or nonparametric description of the actual process (e.g. by using the characteristic areas).

1.6 Scientific Contributions

The main advantage over the currently proposed tuning methods for the integrating processes is that the computation of all parameters (controllers and reference filters) is based on either a nonparametric or parametric process description, i.e., the computations do not require an explicit process model. More precisely,

- the controller parameters with the reference filter are calculated analytically from the time response of the process or from the transfer function of a general order with time delay (both approaches are equivalent),
- the optimisation of disturbance-rejection and/or reference tracking is achieved by the reference filter or the reference weighting parameters,
- the controller parameters are calculated according to the desired speed of the closed-loop response,
- the calculation of the parameters of the PI/PID controller and the reference filter is based on simple algebraic expressions, which makes the proposed method suitable for implementation in less demanding hardware, such as slower PLC controllers,
- the derivation of an analytical method for identifying the lower-order process model (the second-order process with zero and time-delay) directly from the characteristic areas, and
- the calculation of the characteristic areas (process moments) from the process signals in noisy environments is significantly improved.

1.7 Structure of the Dissertation

The remainder of the thesis is organised as follows.

Chapter 2 introduces the magnitude optimum (MO) and magnitude optimum multiple integration (MOMI) methods including a 2-DOF controller in a closed-loop configuration with a process.

Chapter 3 derives the estimated low-order integrating process models directly from the characteristic areas measured from the process response.

Chapters 4 and 5 present the extension of the MOMI tuning method for integrating processes to 2-DOF PI/PID control structures. In addition, the optimal reference weighting parameters and the reference filters are derived here, as well as the calculation of the controller parameters as a function of the desired average closed-loop residence time.

In Chapter 6, the stability, robustness and noise sensitivity analysis of the proposed tuning method are investigated. In addition, a new approach is proposed to reduce the high-frequency noise sensitivity in the calculation of the characteristic areas.

Chapter 7 compares the performance of the proposed method with some other tuning methods for integrating processes. In addition, some novel practical performance criteria are developed.

Real-time experiments on some laboratory and industrial systems are outlined in Chapter 8.

Finally, Chapter 9 concludes the thesis and provides directions for future work.

Chapter 2

MO and MOMI for Integrating Processes

A large part of this chapter was originally published in T. Kos et al., Applied Sciences (2020), 10: 17.

In this chapter, we present a method for nonparametric identification of the process using so-called characteristic areas (process moments) [25]. These areas can be identified from the time response of a closed or open loop (in the time domain) or directly from an arbitrary rational transfer function with a pure time delay (in the frequency domain). It should be noted that both approaches (time domain and frequency domain) are equivalent. The characteristic areas are later used for the calculation of the parameters of the controller and the reference filters, as well as for the process model fitting.

Figure 2.1 shows a 2-DOF controller in a closed-loop configuration with a process. Signals u, d, y, and r represent the process output, the input disturbance, the controller output, and the controller reference, respectively.

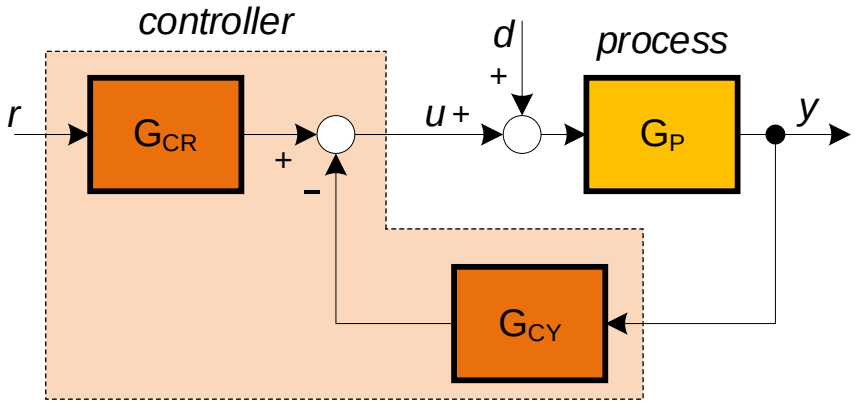

Figure 2.1: Universal closed-loop control scheme using the 2-DOF controller.

The process is defined by the stable transfer function:

$$G_{\mathrm{P}}(s) = \frac{K_{\mathrm{PR}}}{s} \frac{1 + b_1 s + b_2 s^2 + \cdots + b_{\mathrm{m}} s^m}{1 + a_1 s + a_2 s^2 + \cdots + a_{\mathrm{n}} s^n} e^{-sT_{\mathrm{delay}}}, \tag{2.1}$$

where T_{delay} represents the process time delay. As stated in [176], "*one possible design aim is to maintain the closed-loop magnitude response curve as flat and as close to unity for*

as large bandwidth as possible" (see Figure 2.2). Thus, the goal is to find a controller whose low-frequency closed-loop response is as close to unity as possible [178].

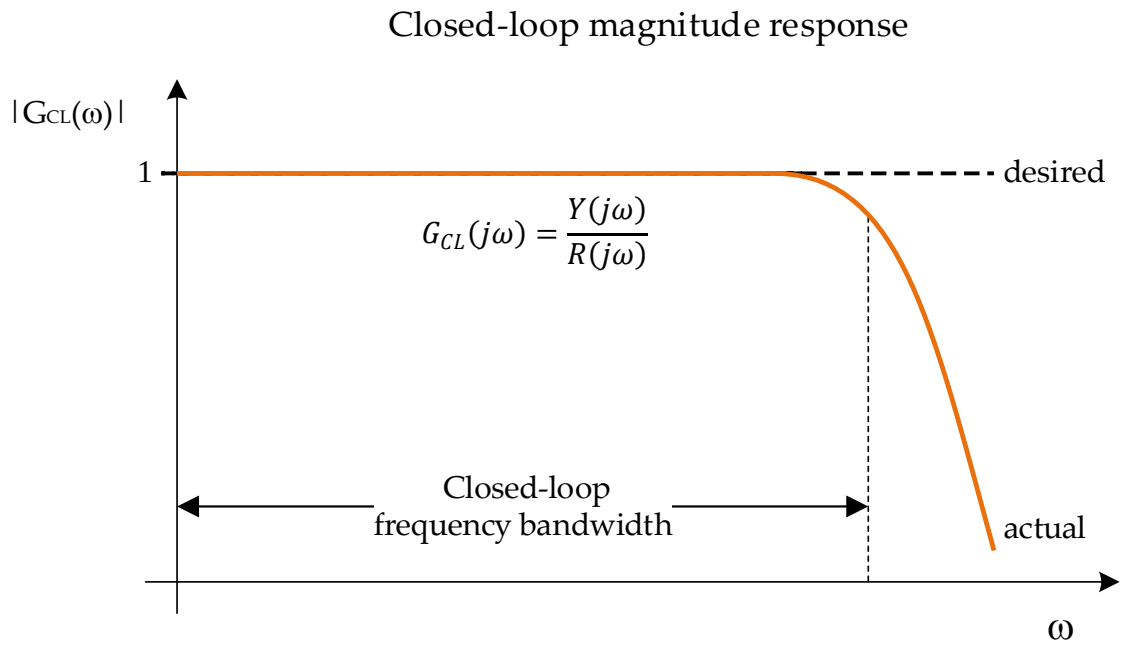

Figure 2.2: The closed-loop magnitude frequency response according to the magnitude optimum (MO) method.

This approach is referred to as modulus optimum, Betragsoptimum, or magnitude optimum (MO) and leads to relatively optimal closed-loop time response for most process models when considering the speed of its response and robustness [178].

With a 2-DOF controller (shown in Figure 2.1), the closed-loop transfer function becomes:

$$G_{CL}(s) = \frac{Y(s)}{R(s)} = \frac{G_{\mathrm{P}}(s)G_{\mathrm{CR}}(s)}{1 + G_{\mathrm{P}}(s)G_{\mathrm{CY}}(s)}. \tag{2.2}$$

The controller is configured so that

$$G_{\mathrm{CL}}(0) = 1, \tag{2.3}$$

$$\lim_{\omega \to 0}\left[\frac{d^{2k}|G_{\mathrm{CL}}(j\omega)|^2}{d\omega^{2k}}\right] = 0; k = 1,2,\cdots,k_{\max} \tag{2.4}$$

is fulfilled for as many k as possible [176], [179]. Equation (2.3) is thus easily satisfied. If the controller structure contains an integral term, and the closed-loop response is stable, the steady-state control error is zero; thus, Equation (2.3) is satisfied. The number of satisfied conditions in Equation (2.4) is correlated with the number of controller parameters (controller order). For the PI controller $k_{\max} = 2$, and the PID controller $k_{\max} = 3$.

Let us define the closed-loop transfer function by the following equation:

$$G_{\mathrm{CL}}(s) = \frac{f_0 + f_1 s + f_2 s^2 + \cdots}{e_0 + e_1 s + e_2 s^2 + \cdots}. \tag{2.5}$$

Then, the following conditions must be satisfied to fulfil Expression (2.4) [178]:

$$\sum_{i=0}^{2n} (-1)^{i+n} \left(f_i f_{2n-i} {e_0}^2 - e_i e_{2n-i} {f_0}^2 \right) = 0; n = 1,2, ... \tag{2.6}$$

The first two equations in Condition (2.6) should be satisfied to calculate the PI controller parameters. The first three equations in Condition (2.6) should be satisfied to calculate the PID controller parameters.

To simplify further derivations, process (2.1) is developed into an infinite Taylor series [179]:

$$G_{\mathrm{P}}(s) = \frac{G_{\mathrm{P1}}}{s} = \frac{A_0 - A_1 s + A_2 s^2 - A_3 s^3 + \cdots}{s}, \tag{2.7}$$

where A_{i} represents the "characteristic areas" of the process [178], which can be expressed by process parameters (2.1) [176]:

$$\begin{gathered}
A_0 = K_{\mathrm{PR}} \\
A_1 = K_{\mathrm{PR}} \left(a_1 - b_1 + T_{\mathrm{delay}} \right) \\
A_2 = K_{\mathrm{PR}} \left(b_2 - a_2 - T_{\mathrm{delay}} b_1 + \frac{{T_{\mathrm{delay}}}^2}{2!} \right) + A_1 a_1 \\
A_3 = K_{\mathrm{PR}} \left(a_3 - b_3 + T_{\mathrm{delay}} b_2 - \frac{{T_{\mathrm{delay}}}^2 b_1}{2!} + \frac{{T_{\mathrm{delay}}}^3}{3!} \right) + A_2 a_1 - A_1 a_2 \ . \\
A_4 = K_{\mathrm{PR}} \left(-a_4 + b_4 - T_{\mathrm{delay}} b_3 + \frac{{T_{\mathrm{delay}}}^2 b_2}{2!} - \frac{{T_{\mathrm{delay}}}^3 b_1}{3!} + \frac{{T_{\mathrm{delay}}}^4}{4!} \right) + \\
+ A_3 a_1 - A_2 a_2 + A_1 a_3 \\
\vdots \\
A_{\mathrm{k}} = K_{\mathrm{PR}} \left((-1)^{k+1} (a_{\mathrm{k}} - b_{\mathrm{k}}) + \sum_{i=1}^{k} (-1)^{k+i} \frac{{T_{\mathrm{delay}}}^i b_{\mathrm{k}-i}}{i!} \right) + \\
+ \sum_{i=1}^{k-1} (-1)^{k+i-1} A_{\mathrm{i}} a_{\mathrm{k}-i}
\end{gathered} \tag{2.8}$$

This means that the characteristic areas can be obtained directly from the process transfer function. Moreover, the characteristic areas can also be calculated in the time domain, i.e., from the time response of the process. For this purpose, the steady-state of the process should first be changed.

Then, the multiple integrations of the process input ($u(t)$) and output ($y(t)$) signals can be calculated [176], [179]:

$$\begin{aligned} u_0 &= \frac{u(t)-u(0)}{\Delta U} \\ I_{U1}(t) &= \int_0^t u_0(\tau)d\tau \qquad\qquad I_{Y1}(t) = \frac{y(t)-y(0)-\dot{y}(0)\cdot t}{\Delta U} \\ I_{U2}(t) &= \int_0^t I_{U1}(\tau)d\tau \qquad\qquad I_{Y2}(t) = \int_0^t I_{Y1}(\tau)d\tau \\ &\vdots \qquad\qquad\qquad\qquad \vdots \end{aligned} \tag{2.9}$$

where u_0 represents the normalised process input signal, and

$$\Delta U = u(\infty) - u(0). \tag{2.10}$$

The characteristic areas are expressed as follows:

$$\begin{aligned} &A_0 = y_0(\infty);\ y_1 = A_0 I_{U1}(t) - I_{Y1}(t) \\ &A_1 = y_1(\infty);\ y_2 = A_1 I_{U1}(t) - A_0 I_{U2}(t) + I_{Y2}(t) \\ &A_2 = y_2(\infty);\ y_3 = A_2 I_{U1}(t) - A_1 I_{U2}(t) + A_0 I_{U3}(t) - I_{Y3}(t) \\ &\quad\vdots \end{aligned} \tag{2.11}$$

Note that $\ddot{y}(0) = \dddot{y}(0) = \cdots = 0$ and that A_0 is equal to the steady-state gain of the process, K_{PR}. In practice, the integration in Expression (2.9) may end when the process signals settle. Therefore, Expression (2.9) can be recursively and simply calculated, therefore the process model (2.1) is not needed. Therefore, the process can be easily parameterized by using the characteristic areas from any change in the process steady-state [178].

For clarity, a graphical representation of the characteristic area A_1 is shown in Figure 2.3. Signals u_0 and y_0 represent the responses of the process input and the process output, respectively [178].

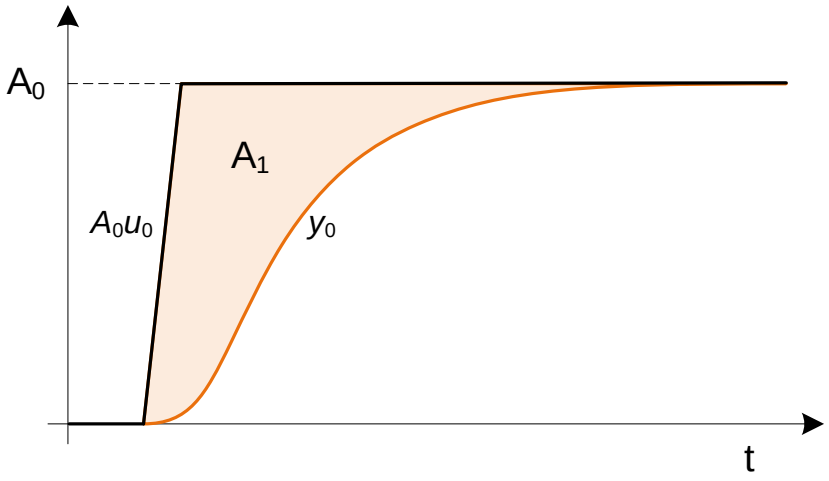

Figure 2.3: Graphical representation of characteristic area A_1. This area was measured after the change of the process steady state.

In practice, certain rules must be followed to accurately calculate characteristic areas from the process response corrupted by noise. Some practical guidelines for calculating characteristic areas from process time responses in practice, including high-frequency process noise, can be found in [181]. In Chapter 6.3, an additional in-depth noise analysis was performed. As shown in Chapter 8, the method was also tested on a real process with present noise. In all the mentioned tests, it was found that the calculated areas and, hence, the controller parameters were not significantly sensitive to the high-frequency process noise.

Chapter 3

Process Model Estimation

The goal of a control system is to force a dynamic process into the desired behaviour. The success of this goal is often conditioned by the existence of an accurate mathematical model of the process [27], [35], [182]. According to [183], "*the primary goal of system or process identification is to determine a model that will match the performance of the system or process to be identified*". Models are used for simulation purposes, quality control, fault detection, and control design [37], [182]. According to [37], "*Models can be used to simulate expected process behaviour with a proposed control system. Also, models are often "embedded" in the controller itself; in effect, the controller can use a process model to anticipate the effect of control action*". They also play a vital role when real-time system experiments are dangerous or costly [37], [182]. In this chapter, we focus on Linear Time-Invariant (LTI) single-input-single-output (SISO) processes.

Model parameters are identified by feeding a set of input signals into the system. Then, the response of the system is collected by taking measurements with appropriate sensors, which are affected by the measurement noise [35], [37], [182], [183]. Various input data signals can be used, such as step, pulse, a square wave, sine, and pseudorandom binary sequences (PRBS). To prevent the process output from drifting too far from the set-point, process identification can also be performed in a closed-loop configuration, although this is not possible in all cases. According to [184], "*for safety and economic reasons, many industrial processes of the type integrating and unstable processes are not permitted to run in an open-loop manner*".

Based on the information obtained, identification methods can be divided into time-domain and frequency-domain methods [35], [183]. A comprehensive survey of identification methods was presented in [184], [185].

Some of the less used methods in the frequency-domain are using sinusoidal or impulse process input signals. The sinusoidal test is usually time-consuming, and the impulse test is not suitable for nonlinear systems [184]. Frequency identification methods, based on the process input step response, usually apply a two-step identification procedure: estimation of the process response in two frequency regions [186]. A more common frequency-domain identification method is a relay feedback identification method [2], [187], [188]. Several variants of relay identification methods have been proposed in the literature [2], [119], [189]–[202]. According to [184] and [185], they can be categorised into three main groups: describing function method, curve fitting approach and frequency response estimation for model fitting. The advantage of the relay feedback methods is the process identification in the closed-loop configuration. Moreover, the relay identification solution proposed by Šekara and Mataušek [199] "*is implemented without breaking the loop with the controller in operation*". Relay identification is widely used for controller auto-tuning [2], [119], [191], [195], [201]. According to [200], "*the success of relay feedback auto-tunes lies in the fact*

that it identifies one important point on the Nyquist curve: the point at the crossover frequency (ultimate frequency)". Moreover, relay identification has been improved with a shifting method [189]–[191], [194], [202], which is still based on biased relay feedback. The shifting method can find up to three points on the frequency characteristics [194].

The step test is the most commonly used method in the time domain because of its simplicity. It can be further divided into the model-fitting approach and the time integral approach [184], [186]. Model fitting techniques roughly estimate the process model, such as the first-order plus dead time (FOTD) model and the second-order plus dead time (SOPDT) model, based on two-point fitting [25], [203], [204]. According to [25], [27], for the purpose of controller tuning, the lower-order model effectively describes the higher-order (HO) linear process. Later, three-point fitting was proposed [205]–[208], as well as a method for obtaining the HO model with dead time [209] for stable processes with underdamped responses. To improve the identification accuracy and robustness to high-frequency noise, the time integral approach was proposed [25], [210]–[212]. In [211], benchmark examples were used to show that the time integral algorithm improves the identification accuracy and robustness to high-frequency noise compared to other step identification methods.

Another method for process identification in the time-domain is the Method of Moments [213]–[215]. The method uses subsequent (multiple) integrations of the input and output-time responses of the process ([214]) to obtain so-called Moments or "characteristic areas" of the process. Note that characteristic areas are a nonparametric description of the process. As explained in Chapter 2, characteristic areas can be obtained from the closed-loop or open-loop time response of a process (in the time-domain) or from the general-order transfer function with a time delay (in the frequency-domain). This means that the method can also be used to reduce existing HO models. Moreover, the characteristic areas can also be obtained from integrating processes (see Chapter 2). Vrečko et al. [216] have shown that SOPDT (four-parameter model) can be calculated analytically from the characteristic areas. Since the model does not contain a zero, it is not suitable for certain applications; see, e.g., a calculation of higher-order reference filter parameters in Chapter 5.4.2.

This chapter proposes a method for identifying the five-parameter model from characteristic areas: the second-order process with zero plus dead time. The method can also be used to reduce the HO process model, to obtain the process model from the original infinite-order model (e.g. heat transfer), or to obtain the process model containing the sum of the various process delays.

3.1 Identification Algorithm

In [25], it was shown that even higher-order systems could be successfully approximated by the second-order process model with time delay (four-parameter model):

$$G_{\mathrm{M}}(s) = \frac{K_{\mathrm{M}} e^{-T_{\mathrm{dm}} s}}{s(1 + a_{1\mathrm{m}} s + a_{2\mathrm{m}} s^2)}, \tag{3.1}$$

where T_{dm} and K_{M} represent the process time delay and steady-state gain, respectively. $a_{1\mathrm{m}}$ and $a_{2\mathrm{m}}$ are the corresponding dynamic parameters. Vrečko et al. [216] have shown that all parameters of the process model (3.1) can be calculated analytically from Expressions (2.8). Therefore, the process model can be obtained directly from the characteristic areas.

As explained, a model without zero is not suitable for certain applications. Therefore, the modelling method proposed by Vrečko et al. [216] is extended.

The chosen process model is a second-order process with a zero and pure time delay

$$G_{\mathrm{M}}(s) = \frac{K_{\mathrm{M}}(1 + b_{1\mathrm{m}}s)e^{-T_{\mathrm{dm}}s}}{s(1 + a_{1\mathrm{m}}s + a_{2\mathrm{m}}s^2)}, \tag{3.2}$$

where $b_{1\mathrm{m}}$ represents the process zero.

In order to express the parameters of the model (3.2) in terms of the characteristic areas A_0–A_4, Expression (3.2) is inserted in Expressions (2.8). The following result is obtained:

$$\begin{aligned}
A_0 &= K_{\mathrm{M}} \\
A_1 &= K_{\mathrm{M}}(a_1 - b_1 + T_{\mathrm{dm}}) \\
A_2 &= K_{\mathrm{M}}\left(-a_2 - T_{\mathrm{dm}}b_1 + \frac{{T_{\mathrm{dm}}}^2}{2!}\right) + A_1a_1\,. \\
A_3 &= K_{\mathrm{M}}\left(-\frac{{T_{\mathrm{dm}}}^2 b_1}{2!} + \frac{{T_{\mathrm{dm}}}^3}{3!}\right) + A_2a_1 - A_1a_2 \\
A_4 &= K_{\mathrm{M}}\left(-\frac{{T_{\mathrm{dm}}}^3 b_1}{3!} + \frac{{T_{\mathrm{dm}}}^4}{4!}\right) + A_3a_1 - A_2a_2
\end{aligned} \tag{3.3}$$

As can be seen from Expressions (3.3), characteristic area A_0 is equal to the process steady-state gain. The remaining process model parameters can be calculated directly from Expressions (3.3). The time delay can be calculated from the following sixth-order polynomial:

$$\alpha {T_{\mathrm{dm}}}^6 + \beta {T_{\mathrm{dm}}}^5 + \gamma {T_{\mathrm{dm}}}^4 + \delta {T_{\mathrm{dm}}}^3 + \varepsilon {T_{\mathrm{dm}}}^2 + \vartheta T_{\mathrm{dm}} + \rho = 0, \tag{3.4}$$

where

$$\begin{aligned}
\alpha &= {A_0}^3, \\
\beta &= -6A_1{A_0}^2, \\
\gamma &= 6\big(-A_2{A_0}^2 + 3{A_1}^2A_0\big), \\
\delta &= 24\big(A_3{A_0}^2 - {A_1}^3\big), \\
\varepsilon &= 72\big(A_4{A_0}^2 + A_2{A_1}^2 - 2A_3A_1A_0\big), \\
\vartheta &= 144\big(A_3{A_1}^2 - {A_2}^2A_1 - A_4A_1A_0 + A_3A_2A_0\big), \\
\rho &= 144\big(A_4{A_1}^2 + {A_3}^2A_0 + {A_2}^3 - A_4A_2A_0 - 2A_3A_2A_1\big).
\end{aligned} \tag{3.5}$$

Expression (3.4) has six solutions for T_{dm}, which may be real or complex. The zero of the process model can be calculated from the following expression:

$$b_{1\mathrm{m}} = \frac{{A_0}^3{T_{\mathrm{dm}}}^3 - 3A_1{A_0}^2{T_{\mathrm{dm}}}^2 - 6A_2{A_0}^2T_{\mathrm{dm}} - 6A_3{A_0}^2 + 6{A_1}^2A_0T_{\mathrm{dm}} + 12A_2A_1A_0 - 6{A_1}^3}{3({A_0}^3{T_{\mathrm{dm}}}^2 - 2A_1{A_0}^2T_{\mathrm{dm}} - 2A_2{A_0}^2 + 2{A_1}^2A_0)}\,, \tag{3.6}$$

and parameters $a_{1\mathrm{m}}$ and $a_{2\mathrm{m}}$ can be calculated from the following expressions:

$$\begin{aligned} a_{1\mathrm{m}} &= \frac{A_1}{A_0} + b_{1\mathrm{m}} - T_{\mathrm{dm}}, \\ a_{2\mathrm{m}} &= -\frac{A_2}{A_0} + \frac{{T_{\mathrm{dm}}}^2}{2} - b_{1\mathrm{m}} T_{\mathrm{dm}} + \frac{A_1(A_1 + A_0 b_{1\mathrm{m}} - A_0 T_{\mathrm{dm}})}{{A_0}^2}. \end{aligned} \tag{3.7}$$

The flowchart of the proposed model-fitting method is shown in Figure 3.1. In the beginning, time delay T_{dm0} (model zero $b_{1\mathrm{m}} = 0$) is determined by blocks A–D. This variable is used for decision-making. T_{dm0} is calculated by block A from the following third-order polynomial:

$$\frac{{T_{d\mathrm{m0}}}^3}{6} - \frac{{T_{d\mathrm{m0}}}^2 A_1}{2A_0} + T_{\mathrm{dm0}} \left(\frac{{A_1}^2}{{A_0}^2} - \frac{A_2}{A_0} \right) - \frac{{A_1}^3}{{A_0}^3} + \frac{2A_1 A_2}{{A_0}^2} + \frac{A_3}{A_0} = 0. \tag{3.8}$$

Expression (3.8) has three solutions for T_{dm0}, which may be real or complex. The time delay must be real and non-negative to represent a feasible solution. These constraints can be expressed as follows:

$$\begin{aligned} \Im(T_{\mathrm{dm0}}) &= 0 \\ \Re(T_{\mathrm{dm0}}) &\geq 0 \end{aligned}. \tag{3.9}$$

The correct result is the smallest positive real number obtained by blocks B and C. Condition D checks if the solution exists, otherwise, T_{dm0} is set to 0.

Next, block E computes time delay T_{dm} from Expressions (3.4) and (3.5). The time delay must be real and non-negative to represent a feasible solution. These constraints (block F) can be expressed as follows:

$$\begin{aligned} \Im(T_{\mathrm{dm}}) &= 0 \\ \Re(T_{\mathrm{dm}}) &\geq 0 \end{aligned}. \tag{3.10}$$

Condition G checks if the feasible solution(s) exists, otherwise $T_{\mathrm{dm}} = T_{\mathrm{dm0}}$ (time delay at $b_{1\mathrm{m}} = 0$). Model parameters $b_{1\mathrm{m}}$, $a_{1\mathrm{m}}$ and $a_{2\mathrm{m}}$ are calculated according to Expressions (3.6) and (3.7), as shown in block H.

The process model must be stable, i.e., $a_{1\mathrm{m}}$ and $a_{2\mathrm{m}}$ must be non-negative. These boundary conditions (block I) can be expressed as follows:

$$\begin{aligned} a_{1\mathrm{m}} &\geq 0 \\ a_{2\mathrm{m}} &\geq 0 \end{aligned}. \tag{3.11}$$

If there are multiple solutions (block J), the appropriate solution is selected according to the process type (block K), i.e., for a minimum phase or non-minimum phase process. Note that the process type must be specified by the user. In the case of a minimum phase process, the correct solution is the one with $T_{\mathrm{dm}} \geq T_{\mathrm{dm0}}$ and *vice versa*. These constraints can be expressed as follows:

$$\begin{aligned} T_{\mathrm{dm}} &\geq T_{\mathrm{dm0}} \quad \text{process} = \text{minimum phase} \\ T_{\mathrm{dm}} &< T_{\mathrm{dm0}} \quad \text{process} = \text{non-minimum phase} \end{aligned}. \tag{3.12}$$

The final condition (block L) checks whether there is a matching solution. If the condition is satisfied, the loop is terminated. Otherwise, the algorithm sets $T_{\mathrm{dm}} = T_{\mathrm{dm0}}$

(time delay at $b_{1m} = 0$) and then blocks H–K are called again. Note that block L is called only once to avoid unwanted code loops.

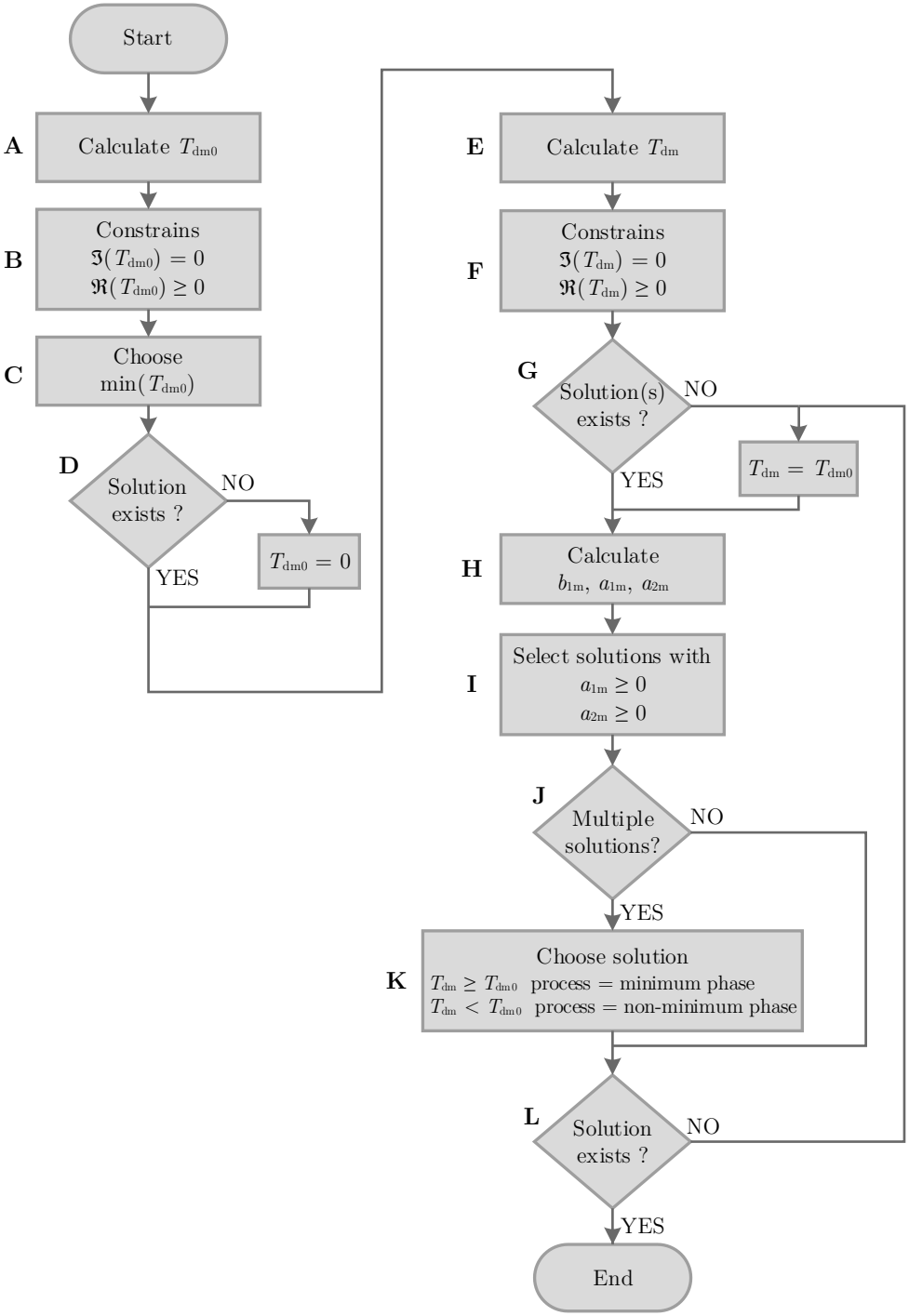

Figure 3.1: Flowchart of the proposed model-fitting method.

As has been shown, the second-order process model (3.2) can be estimated from the characteristic areas, and the only parameter required by the user is the type of process (minimum phase or non-minimum phase process), which in practice can be easily obtained from the process time-response. To save the reader effort and time, all MATLAB files

required to implement the proposed identification method and calculate the process model parameters from the characteristic areas are available online [1].

3.2 Illustrative Example

The proposed model-fitting method was tested on the following family of process models:

$$G_{\mathrm{P1}}(s) = \frac{(1+bs)e^{-T_{\mathrm{delay}}s}}{s(1+Ts)^n}, \tag{3.13}$$

where b, T_{delay}, T, and n represent the process numerator time constant, the time delay, the time constant, and the process-order, respectively. The test experiments were performed for different values of all four parameters of the process (3.13). Time constant T was always calculated from the selected process order and time delay as follows:

$$T \times n + T_{delay} = 1. \tag{3.14}$$

The fitting of the identified second-order process model (3.2) to the actual process (3.13) was evaluated using the following time-domain criterion:

$$\mathrm{IAE} = \frac{\int_0^\infty |e|(t)dt}{\left|\max(y_{G_{\mathrm{P1}}}) - \min(y_{G_{\mathrm{P1}}})\right|}, \tag{3.15}$$

where e is the open-loop step-response difference between the actual process (3.13) (y_{GP1}) and the identified process model (3.2) output signal (y_{GM}):

$$e = y_{G_{\mathrm{P1}}} - y_{G_{\mathrm{M}}}. \tag{3.16}$$

Expression (2.8) was used to calculate the characteristic areas from the transfer function of the process (3.13). Then, the parameters of the process model (3.2) were calculated from the characteristic areas, according to the flowchart shown in Figure 3.1.

The actual flow of the algorithm in Figure 3.1 depends on the selection of the parameters of the process (3.13). The results of all the conditions (rhomboid-shaped blocks in Figure 3.1) for a different selection of the process parameters (process zero, time delay, time constant, and process order) are shown in Figure 3.2. The conditions shown represent all the decisions made by the algorithm. For example, D = NO means that the answer of block D in Figure 3.1 is NO (there is no real positive solution for the process model time delay T_{dm0}), G = NO means that there is no real positive solution for the process model time delay T_{dm}, J = YES means that there are multiple solutions for computing the dynamic process parameters $a_{1\mathrm{m}}$ and $a_{2\mathrm{m}}$, and L = NO indicates that there are no solutions for the model parameters when T_{dm} is used, so in the next iteration $T_{\mathrm{dm}} = T_{\mathrm{dm0}}$. Note that for each process, only one of the conditions shown in the figure is met, so there is no overlap.

Calculated process model (3.2) parameters $b_{1\mathrm{m}}$ and T_{dm} for the selected process G_{P1} parameters are shown in Figures 3.3 and 3.4, respectively. As can be seen from Figures 3.3 and 3.4, calculated process model parameters $b_{1\mathrm{m}}$ and T_{dm} for lower-order processes ($n = 1$, 2) are identical to actual process parameters b and T_{delay}. For higher-order processes ($n = 3$–8), calculated $b_{1\mathrm{m}}$ deviates from b and becomes zero for a wider set of actual process parameters, while parameter T_{dm} becomes higher than T_{delay}, as expected.

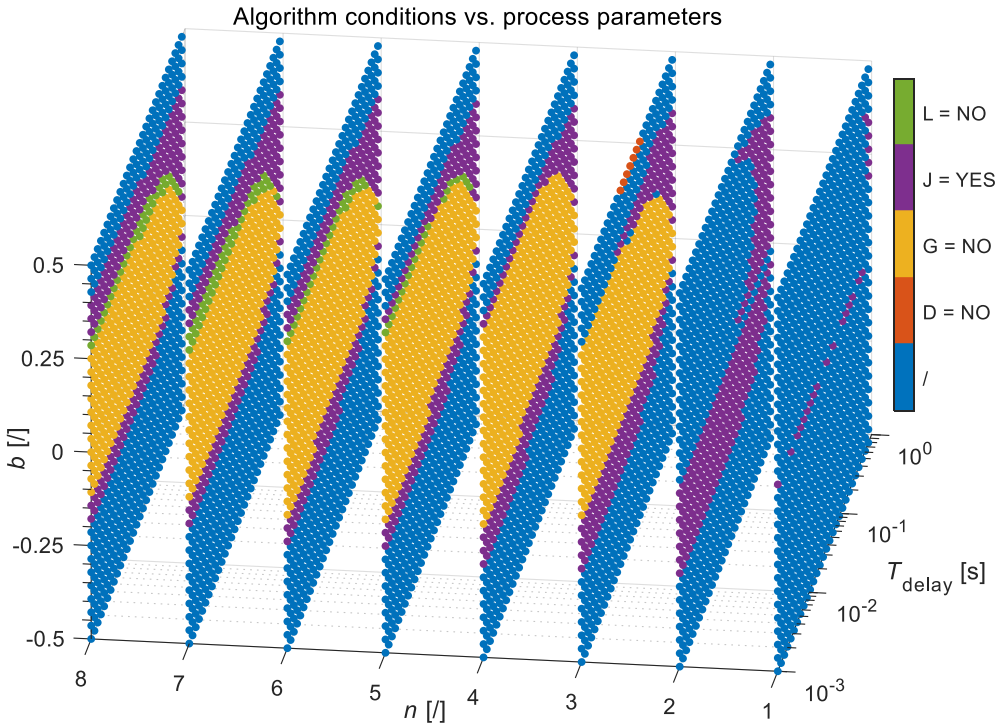

Figure 3.2: The results of the algorithm conditions for process $G_{\mathrm{P1}}(\mathrm{s})$ parameters perturbation.

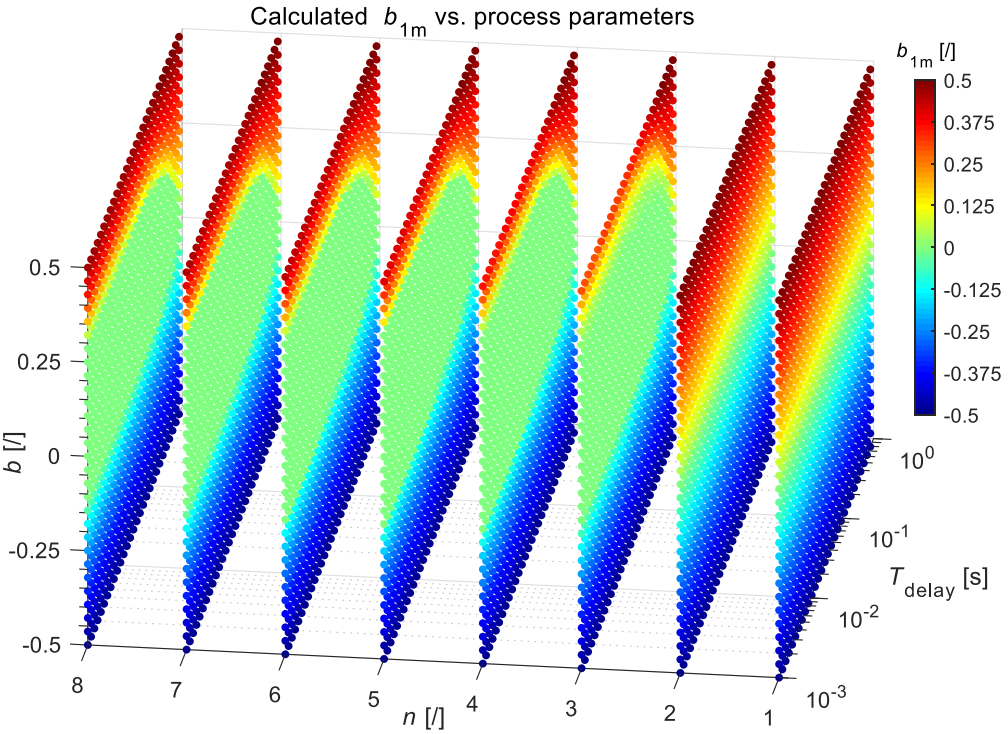

Figure 3.3: Calculated zeroes $b_{1\mathrm{m}}$ for process $G_{\mathrm{P1}}(\mathrm{s})$ parameters perturbation.

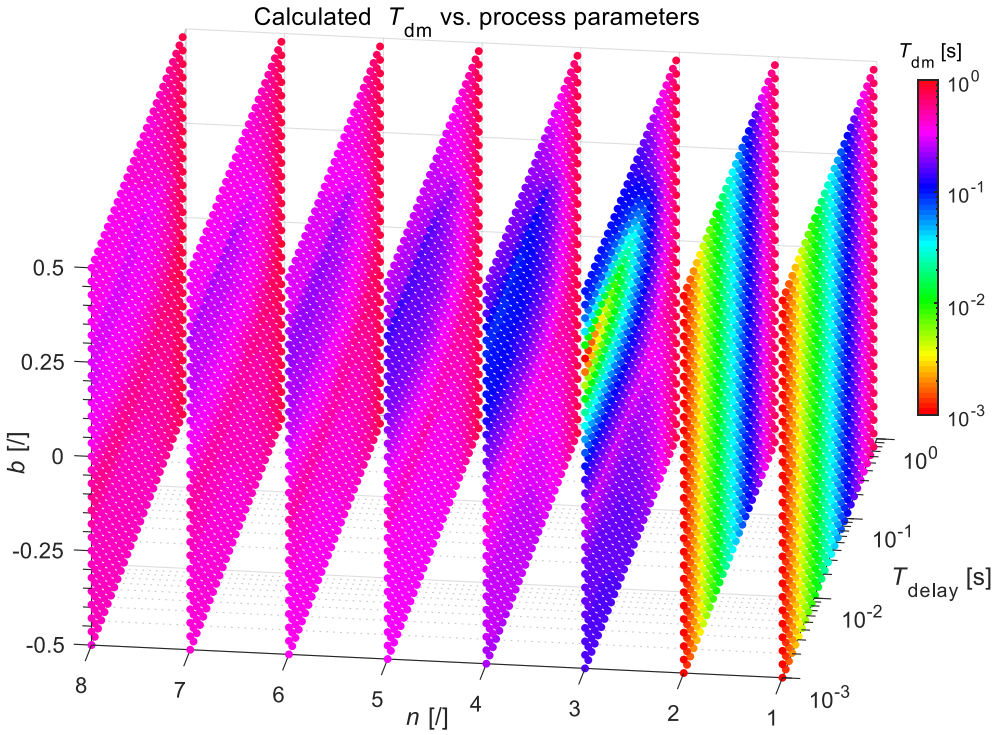

Figure 3.4: Calculated time delays T_{dm} for process $G_{\mathrm{P1}}(\mathrm{s})$ parameters perturbation.

The IAE criterion values for process G_{P1} are shown in Figure 3.5. The IAE criterion is 0 for the first- and second-order processes (perfect fit) and increases as the process order and numerator time constant b increase. However, the maximum value of IAE is still relatively low (0.068).

Next, the proposed model identification method was compared with that of Vrečko et al. [216] (the method with fixed b_{lm}=0). For this purpose, the absolute difference of IAE criteria was calculated by the following expression:

$$\mathrm{IAE}_{\Delta} = \mathrm{IAE}_{\mathrm{Vrecko}} - \mathrm{IAE}_{\mathrm{proposed}}. \tag{3.17}$$

If the performance of both methods is identical, the calculated criterion difference will be 0, otherwise the value will be larger.

The absolute difference of the IAE criterion for process G_{P1} is shown in Figure 3.6. As expected, the IAE values of both methods are identical in the cases where $b_{\mathrm{lm}} = 0$. However, in other cases, the difference of IAE criteria confirms the superiority of the proposed model identification method. Note that the maximum difference of the IAE_{Δ} criterion is 0.67.

In practice, certain rules must be followed to accurately calculate the areas from the process response corrupted by noise. Some practical guidelines for computing characteristic areas from process time responses in practice, including high-frequency process noise, can be found in [181]. Additional in-depth noise analysis was performed in Chapter 6.3.

All MATLAB files used to present the results are available online [1]. Note that the above reference also includes the MATLAB files used in all other examples in this paper.

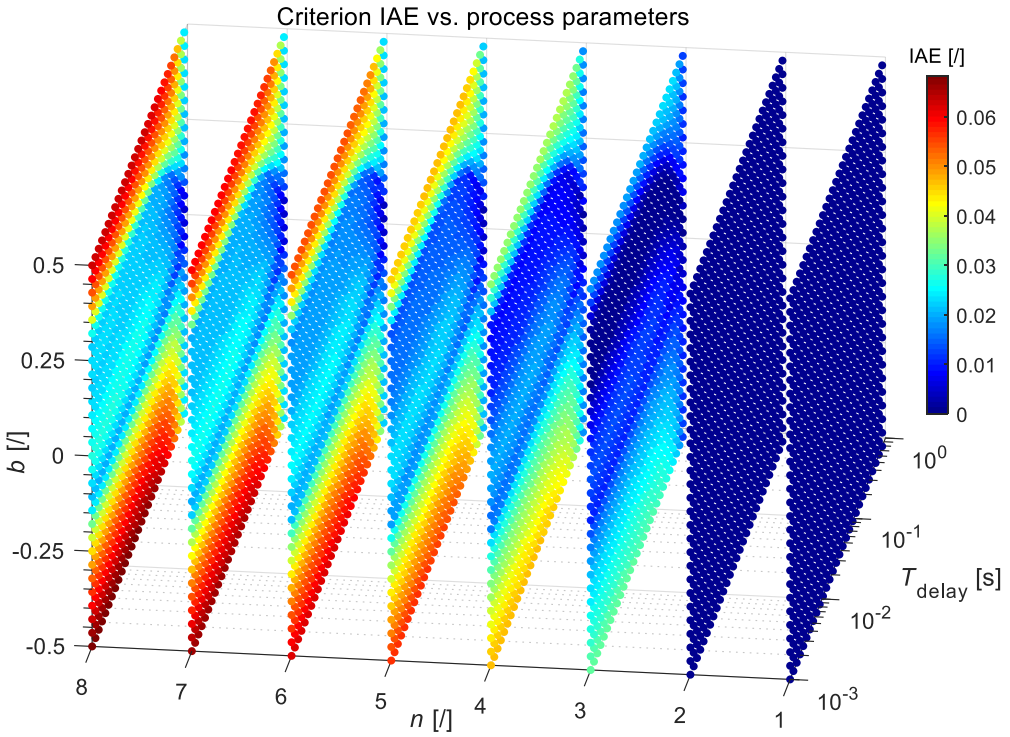

Figure 3.5: The IAE criterion values for process $G_{\mathrm{P1}}(\mathrm{s})$ parameters perturbation.

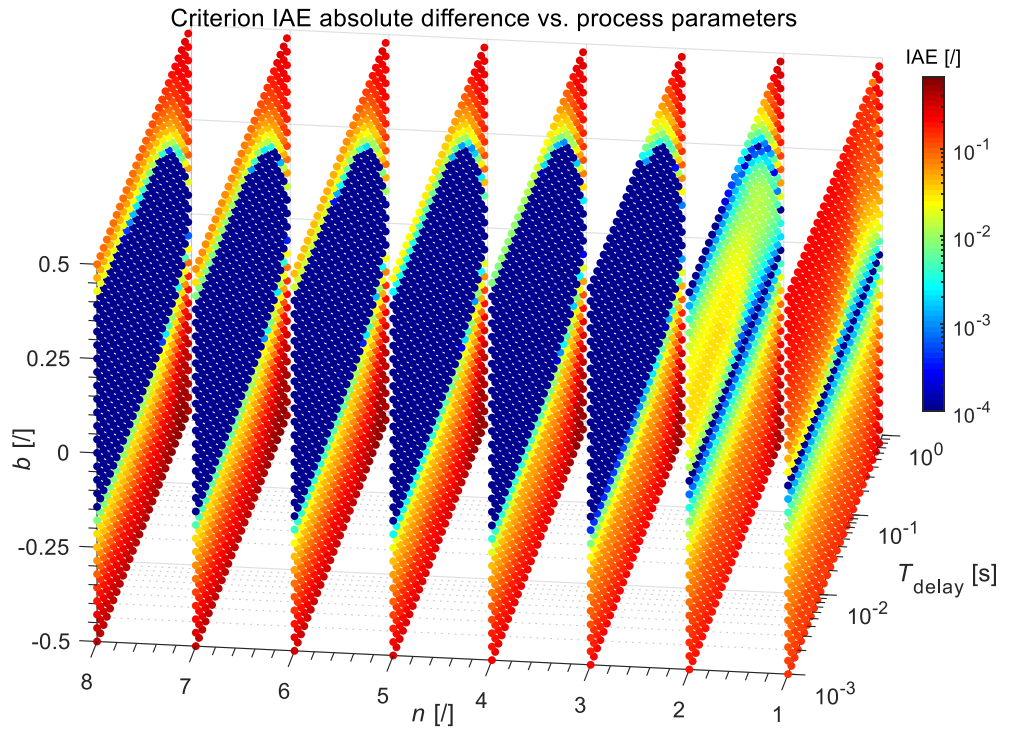

Figure 3.6: The absolute difference of the IAE criteria for process $G_{\mathrm{P1}}(\mathrm{s})$ parameters perturbation. Values are calculated from the IAE criterion of the method proposed by Vrečko et al. [216] and the IAE criterion of the proposed model-fitting method.

Chapter 4

PI Controller for the Integrating Processes

A large part of this chapter was originally published in Kos, T. et al., Applied Sciences (2020), 10: 4.

The process in a closed-loop configuration with a 2-DOF PI controller is shown in Figure 4.1. Signals d, y, r, and u represent the input disturbance, the process output, the controller reference, and the controller output, respectively. Parameter b is the proportional weighting factor, while K_P and K_I represent the proportional and integral gains, respectively.

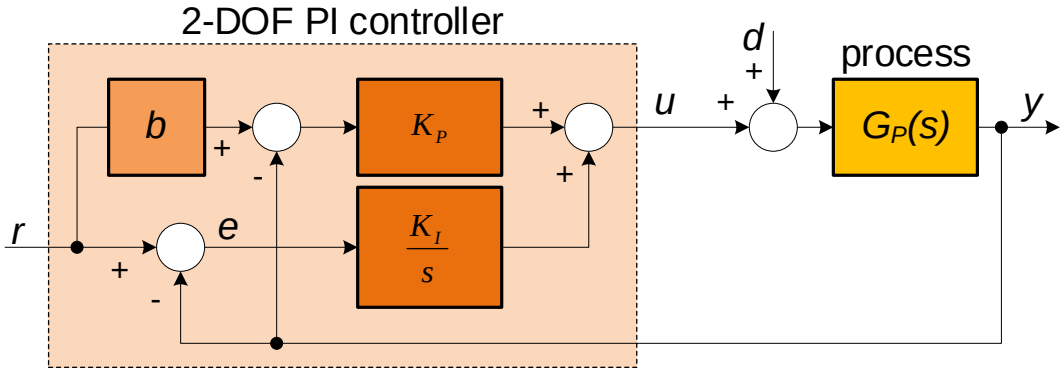

Figure 4.1: General closed-loop scheme with a 2-DOF PI controller.

The IP was modelled with the rational transfer function (2.1). In order to simplify subsequent derivations, the process (2.1) was developed into an infinite Taylor series (2.7). In addition, the closed-loop transfer function is represented by expression (2.2).

The next step is to calculate the parameters of the 2-DOF PI controller. A controller can be defined by the next transfer functions:

$$\begin{aligned} G_{\mathrm{CR}}(s) &= bK_\mathrm{P} + \frac{K_\mathrm{I}}{s}, \\ G_{\mathrm{CY}}(s) &= K_\mathrm{P} + \frac{K_\mathrm{I}}{s}, \end{aligned} \tag{4.1}$$

where b, K_P, and K_I are the reference weighting factor, proportional gain, and integral gain, respectively.

By applying the controller and process transfer functions (Expressions (4.1) and (2.7), respectively) to the closed-loop transfer function (Expression (2.2)), the following closed-loop transfer function parameters (2.5) are obtained:

$$\begin{aligned} e_0 &= A_0 K_{\mathrm{I}} \\ e_1 &= -A_1 K_{\mathrm{I}} + A_0 K_{\mathrm{P}} \\ e_2 &= A_2 K_{\mathrm{I}} - A_1 K_{\mathrm{P}} + 1 \\ e_3 &= -A_3 K_{\mathrm{I}} + A_2 K_{\mathrm{P}} \\ e_4 &= A_4 K_{\mathrm{I}} - A_3 K_{\mathrm{P}} \\ &\vdots \end{aligned} \tag{4.2}$$

$$\begin{aligned} f_0 &= A_0 K_{\mathrm{I}} \\ f_1 &= -A_1 K_{\mathrm{I}} + A_0 b K_{\mathrm{P}} \\ f_2 &= A_2 K_{\mathrm{I}} - A_1 b K_{\mathrm{P}} \\ f_3 &= -A_3 K_{\mathrm{I}} + A_2 b K_{\mathrm{P}} \\ &\vdots \end{aligned} \tag{4.3}$$

To compute two PI controller parameters, the first two equations in Conditions (2.6) must be satisfied [217]. The first condition in (2.6) gives the following result:

$$K_{\mathrm{I}} = 0.5 A_0 \big(1 - b^2\big) {K_{\mathrm{P}}}^2, \tag{4.4}$$

and the second condition in (2.6) results in

$$K_{\mathrm{I}} = \frac{\big(A_0 A_2 - 0.5 {A_1}^2\big)\big(1 - b^2\big){K_{\mathrm{P}}}^2 \; + \; A_1 K_{\mathrm{P}} - 0.5}{A_2}. \tag{4.5}$$

The controller gain (K_{P}) can be calculated by equating Expressions (4.4) and (4.5):

$$K_{\mathrm{P}} = \frac{-A_1 + \sqrt{{A_1}^2 + \xi}}{\xi}, \tag{4.6}$$

where

$$\xi = (1 - b^2)\big(A_0 A_2 - {A_1}^2\big). \tag{4.7}$$

To facilitate the implementation of the proposed tuning method and to save the reader's time and effort, all MATLAB files used to calculate the PI parameters are available online [1].

Remark 4.1. *Suppose that the value of ξ in Equation (4.7) approaches zero (if the reference weighting factor b is close to or equal to one, or the difference of the characteristic areas in the brackets is close to zero). In this case, proportional gain K_{P} can be calculated by developing the expression under the square root in Equation (4.6) into a Taylor series. In this case, the proportional gain becomes*

$$K_{\mathrm{P}} = \frac{0.5}{A_1}. \tag{4.8}$$

However, when b = 1 (1-DOF PI controller), the Integral gain (4.4) becomes $K_I = 0$, and we obtain a proportional (P) controller. Therefore, the disturbance-rejection performance deteriorates when the value of factor b is increased. The influence of factor b on the tracking and the disturbance-rejection performance is shown by an illustrative example in Chapter 4.1.

Remark 4.2. *While Expressions (4.6) and (4.4) lead to stable and fast closed-loop responses for a large majority of IP models, closed-loop stability is still not guaranteed for an arbitrary process model. Closed-loop stability and robustness are discussed in detail in Chapter 6.*

As explained in Chapter 2, characteristic areas A_0 to A_4 can be obtained directly from the process transfer function or calculated from the time response of the process as the steady-state of the process changes. The steps for the PI controller tuning are presented in Table 4.1.

Table 4.1: The instruction for the PI controller tuning.

Step	Description
1	Determine the characteristic areas from Expression (2.8) if the process model is known. Otherwise, modify the process steady-state. Perform sampling of the controller and process output signals during the process transient. Areas A_0 to A_2 are calculated from Expressions (2.9)–(2.11). The initial values of the process input and output signals can be estimated by averaging before changing the controller output signal.
2	Select a suitable reference weighting factor $0 \leq b < 1$.
3	Calculate the controller parameters according to Equations (4.6) and (4.4).

Remark 4.3. *Proportional gain K_P for a second-order IP ($b_m = 0$, a_3–$a_n = 0$) can be calculated by the following expression:*

$$K_P = \frac{-K_{PR}\left(a_1 + T_{delay}\right)\sqrt{{K_{PR}}^2\left(a_1 + T_{delay}\right)^2 + \xi}}{\xi}, \tag{4.9}$$

where

$$\xi = \frac{{K_{PR}}^2}{2}(b^2 - 1)({T_{delay}}^2 + 2a_1 T_{delay} + 2a_2). \tag{4.10}$$

Integral gain K_I can be calculated from Expression (4.4) considering that A_0 equals K_{PR}:

$$K_I = 0.5 K_{PR}\left(1 - b^2\right){K_P}^2. \tag{4.11}$$

When calculating the PI controller parameters for a first-order process, a_2 is replaced by 0 in Expression (4.10).

4.1 Illustrative Example

For the illustrative example, a second-order IP was selected:

$$G_{\mathrm{P}}(s) = \frac{1}{s(1+s)^2}. \tag{4.12}$$

Characteristic areas were calculated from Expression (2.8):

$$A_0 = 1, A_1 = 2, A_2 = 3. \tag{4.13}$$

The parameters of the PI controller, shown in Table 4.2, were calculated from Expressions (4.9) and (4.11). The parameters were calculated for different values of reference weighting factor b. The closed-loop responses for the input disturbance and the reference change when applying a 2-DOF PI controller are shown in Figure 4.2.

Table 4.2: The PI controller parameters.

b	K_{I}	K_{P}
0	0.0359	0.2679
0.2	0.0343	0.2671
0.5	0.0259	0.2630
0.7	0.0170	0.2585
0.9	0.0061	0.2530

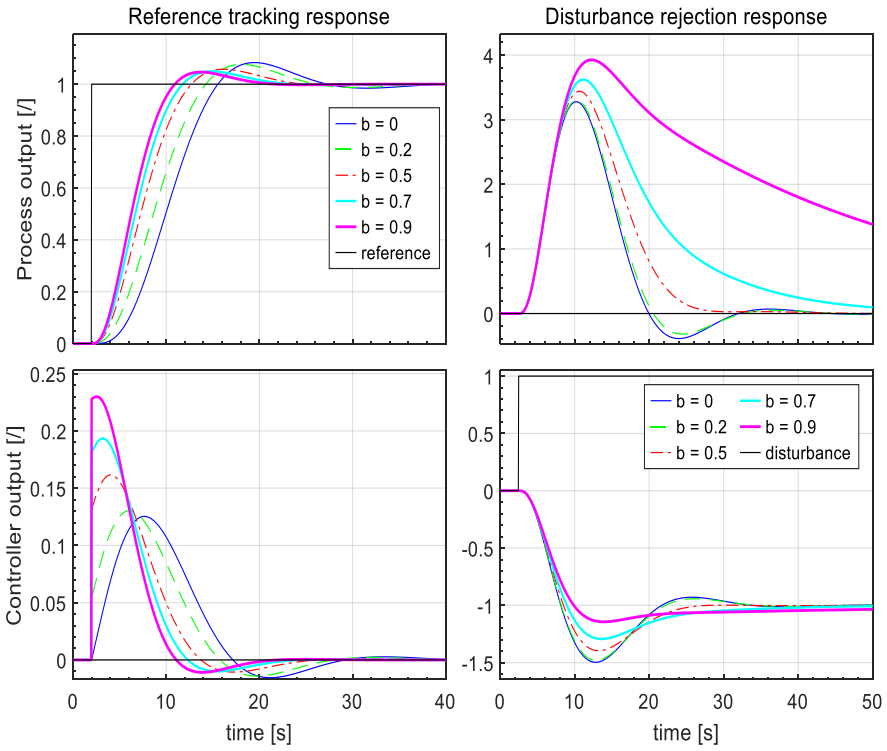

Figure 4.2: Process G_{P} closed-loop responses. Comparison between different values of b.

As can be seen in Figure 4.2, tracking and disturbance-rejection performance are correlated with factor b. The tracking performance increases as factor b increases. Thus, if tracking performance is the most important, choose a value of $b \geq 0.7$. On the other hand, the best disturbance-rejection performance is achieved with $b \leq 0.2$. A good compromise between tracking and disturbance-rejection performance is $b = 0.5$.

Remark 4.4. *The best overall performance (optimal tracking and disturbance-rejection) could be achieved by using a higher-order reference pre-filter instead of reference weighting factor b, similar to the proposed solution for non-integrating processes* [218]. *In this case, the controller parameters should be the same as those calculated with $b = 0$, while pre-filter parameters should be adjusted to achieve the optimal tracking response. However, such a solution would require a more complex controller implementation, which is in contrast with the simplicity of the presented tuning method. Nevertheless, a reference filter structure for a PID controller is presented in Chapter 5.4.*

4.2 Reference Weighting and Reference Filtering Equivalence

In addition to the set-point weighting [25], [219], a 2-DOF controller can also be realized using the reference filtering [219], [220]. The filter (G_F) in the closed-loop configuration with the controller (G_C) and the process (G_P) is shown in Figure 4.3.

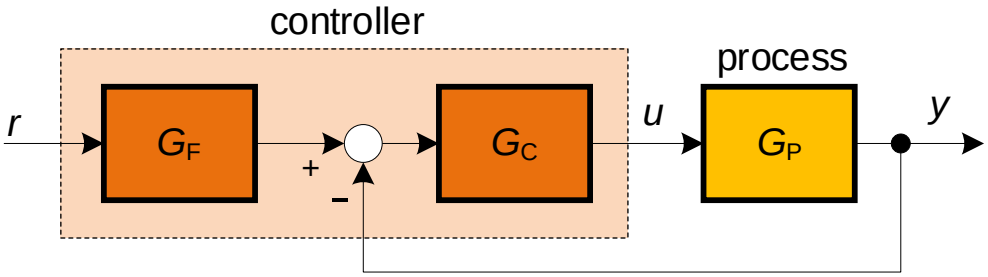

Figure 4.3: Reference filter G_F with controller G_C and process G_P.

Closed-loop transfer function G_{CL1} from reference r to process output y is the following:

$$G_{\mathrm{CL1}}(s) = \frac{Y(s)}{R(s)} = \frac{G_\mathrm{F} G_\mathrm{P} G_\mathrm{C}}{1 + G_\mathrm{P} G_\mathrm{C}}. \tag{4.14}$$

When applying the 1-DOF PI controller transfer functions:

$$G_\mathrm{C}(s) = K_\mathrm{P} + \frac{K_\mathrm{I}}{s}, \tag{4.15}$$

to the (4.14), the following transfer function (1-DOF PI controller) is obtained:

$$G_{\mathrm{CL1}}(s) = \frac{G_\mathrm{F}(K_\mathrm{I} + K_\mathrm{P} s) G_\mathrm{P}}{s + (K_\mathrm{I} + K_\mathrm{P} s) G_\mathrm{P}}. \tag{4.16}$$

The transfer function of the 2-DOF PI controller using set-point weighting is obtained by applying the controller transfer functions (4.1) to the closed-loop transfer function (2.2):

$$G_{\mathrm{CL}}(s) = \frac{(K_{\mathrm{I}} + bK_{\mathrm{P}}s)G_{\mathrm{P}}}{s + (K_{\mathrm{I}} + K_{\mathrm{P}}s)G_{\mathrm{P}}}. \tag{4.17}$$

The purpose of reference filter G_{F} is to make transfer function $G_{\mathrm{CL1}}(\mathrm{s})$ (4.16) equal to $G_{\mathrm{CL}}(\mathrm{s})$ (4.17). Equating (4.16) and (4.17) gives the following first-order reference filter transfer function:

$$G_{\mathrm{F}}(s) = \frac{1 + b\dfrac{K_{\mathrm{P}}}{K_{\mathrm{I}}}s}{1 + \dfrac{K_{\mathrm{P}}}{K_{\mathrm{I}}}s} = \frac{1 + bT_{\mathrm{I}}s}{1 + T_{\mathrm{I}}s}. \tag{4.18}$$

In the case that reference weighting factor $b > 0$, the reference filter also contains zero.

4.3 Average Closed-Loop Residence Time

The average closed-loop residence time T_{CL} [25] is related to the closed-loop time constant. According to [25, p. 27], it can be calculated as follows:

$$T_{\mathrm{CL}} = \frac{\int_0^\infty \big(y(\infty) - y(t)\big)dt}{y(\infty)}, \tag{4.19}$$

where y is the response of the process output to the reference step-like change, where $y(0) = 0$. Since T_{CL} is directly related to the time constant of the closed-loop and thus to the speed of the closed-loop control, it can be used as an additional user-defined tuning parameter. However, it should be noted that T_{CL} does not provide a good estimate of the closed-loop speeds on closed-loop responses with significant overshoots due to the integration of the process response (4.19).

In the following derivation, the average closed-loop residence time T_{CL} will be calculated. The IP model was chosen according to Expression (2.7). The closed-loop transfer function (2.2) was calculated from the 2-DOF PI controller (4.1) and the IP model (2.7). The following parameters of the closed-loop transfer function (2.5) are then obtained (after dividing the numerator and denominator by A_0K_{I}):

$$\begin{aligned} e_0 &= 1 \\ e_1 &= \frac{-A_1K_{\mathrm{I}} + A_0K_{\mathrm{P}}}{A_0K_{\mathrm{I}}} \\ &\vdots \end{aligned} \tag{4.20}$$

$$\begin{aligned} f_0 &= 1 \\ f_1 &= \frac{-A_1K_{\mathrm{I}} + A_0bK_{\mathrm{P}}}{A_0K_{\mathrm{I}}} \\ &\vdots \end{aligned} \tag{4.21}$$

The average closed-loop residence time T_{CL} (4.19) can then be calculated simply by applying the final value theorem [221] to the Expression (4.19).

The result is the following:

$$T_{\mathrm{CL}} = e_1 - f_1. \tag{4.22}$$

After inserting Expressions (4.20) and (4.21) into Expression (4.22), the final expression for T_{CL} is obtained:

$$T_{\mathrm{CL}} = \frac{K_{\mathrm{P}} - bK_{\mathrm{P}}}{K_{\mathrm{I}}} = (1-b)T_{\mathrm{I}}, \tag{4.23}$$

where T_{I} is the integral time constant of the controller. As can be seen from Expression (4.23), the average closed-loop residence time correlates with the integral time constant and the proportional weighting factor. T_{CL} decreases (the speed of the closed-loop response increases) by decreasing T_{I} and increasing b.

Note that Expression (4.23) applies only to cases where $b < 1$. As explained in Remark 4.1, when $b = 1$, we obtain the proportional controller (P) instead of the PI controller. In this case, the average closed-loop residence time can be calculated in a similar way as before from the following expression:

$$T_{\mathrm{CL}} = \frac{1}{A_0 K_{\mathrm{P}}}. \tag{4.24}$$

When taking into account the Expression (4.8), it also follows that:

$$T_{\mathrm{CL}} = \frac{2A_1}{A_0}. \tag{4.25}$$

To change the speed of the closed-loop response (the closed-loop time constant), the PI controller parameters can be recalculated, accordingly. The proportional gain (K_{P}) of the controller can be obtained by equating the first condition of the magnitude optimum (4.4) and Expression (4.23):

$$K_{\mathrm{P}} = \frac{1}{T_{\mathrm{CLD}}} \frac{2}{A_0(1+b)}, \tag{4.26}$$

where T_{CLD} is the desired average closed-loop residence time, which can be defined by the following expression:

$$T_{\mathrm{CLD}} = T_{\mathrm{CL}} \times K_{\mathrm{CL}}, \tag{4.27}$$

where K_{CL} is the time factor of the closed-loop. Note that if $K_{\mathrm{CL}} > 1$, the desired closed-loop residence time increases (the desired closed-loop speed decreases).

In case $b = 1$, the P controller parameter can be calculated from the following expression:

$$K_{\mathrm{P}} = \frac{1}{A_0 T_{\mathrm{CLD}}}. \tag{4.28}$$

The steps for the re-tuning of the PI controller are presented in Table 4.3.

To facilitate the calculation of the average closed-loop residence time and save the reader's time and effort, all MATLAB files are available online [1].

Table 4.3: The instruction for the re-tuning of the PI controller.

Step	Description
1	Calculate the PI controller parameters according to the instructions in Table 4.1.
2	Determine the current average closed-loop residence time T_{CL} from Expression (4.23) if $b < 1$, and from Expression (4.24) or (4.25) if $b = 1$.
3	Select the desired average closed-loop residence time T_{CLD} using Expression (4.27). To slow down the desired closed-loop speed by a factor of 2, select $K_{CL} = 2$.
4	If $b < 1$, recalculate the proportional (K_P) and integral (K_I) gain of the controller according to Equations (4.26) and (4.4), respectively. Otherwise, use Equation (4.28).

4.3.1 Illustrative example

The calculation of the controller parameters, according to the desired time factor of the closed-loop K_{CL}, is presented below. The chosen process is second-order IP (4.12). Characteristic areas A_0–A_3 are given by Expression (4.13). The parameters of the PI controller for $b = 0.5$ for different closed-loop time factors K_{CL} are given in Table 4.4. The table also contains the desired average closed-loop residence times T_{CLD} (according to selected K_{CL}). The closed-loop responses using a 2-DOF PI $b = 0.5$ controller for different K_{CL} for input disturbance ($d = 1$) and setpoint change ($r = 1$) are shown in Figure 4.4. It can be seen that the tracking and disturbance-rejection performance is closely correlated with the closed-loop time factor K_{CL}. The closed-loop performance increases when factor K_{CL} decreases. However, if K_{CL} is lower than 1, oscillatory closed-loop responses occur (see, for example, response for $K_{CL} = 0.5$). In general, therefore, K_{CL} should not be much lower than 1. Note that the K_{CL} factor influences both the tracking and the disturbance-rejection performance.

Table 4.4: The PI controller parameters for different K_{CL} and $b = 0.5$.

K_{CL}	K_P	K_I	T_{CLD}
0.5	0.52593	0.10373	2.5352
0.75	0.35062	0.04610	3.8028
1	0.26297	0.02593	5.0704
2	0.13148	0.00648	10.1407
3	0.08766	0.00288	15.2111

As has been shown, the closed-loop performance correlates with the average closed-loop residence time T_{CL}. If the user finds the closed-loop response too fast, it can be slowed down by increasing the T_{CLD} accordingly (by increasing factor K_{CL}). The advantage of using a T_{CLD} (or factor K_{CL}) is an accurate prediction of the closed-loop time constant. Consequently, when T_{CLD} is changed, the user can predict the speed of the closed-loop response.

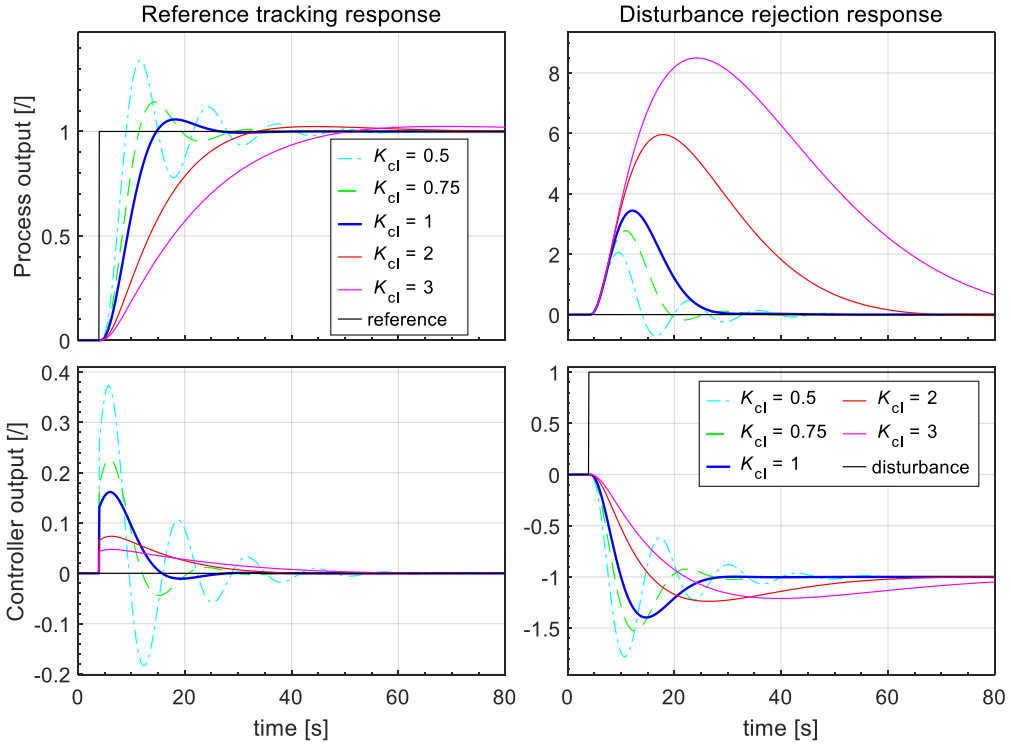

Figure 4.4: Closed-loop responses for the second-order IP (4.12) for different values of K_{CL}.

In future work, we will strive to find common tuning parameters that include both the average closed-loop residence time and the high-frequency noise attenuation of the controller.

4.4 Examples on Some Process Models

The proposed MOMI extension for the PI controller applied to the IPs was tested on four process models. The following second-order, delayed, fourth-order and non-minimum phase IPs were selected:

$$\begin{aligned} G_{\mathrm{P1}}(s) &= \frac{1}{s(1+s)(1+0.2s)}, \\ G_{\mathrm{P2}}(s) &= \frac{e^{-s}}{s}, \\ G_{\mathrm{P3}}(s) &= \frac{1}{s(1+s)^4}, \\ G_{\mathrm{P4}}(s) &= \frac{1-2s}{s(1+s)^2}. \end{aligned} \tag{4.29}$$

The calculated areas, according to Expression (2.8), are given in Table 4.5. The PI controller parameters for all four process models, for the reference weighting factors $b = 0$, $b = 0.5$, and $b = 0.9$, were calculated from Equations (4.4) and (4.6) and are shown in Table 4.6.

The closed-loop responses when applying a 2-DOF PI controller with three values of b for input disturbance ($d = 1$) and reference change ($r = 1$) are shown in Figures 4.5–4.8. The experiment results for all four process models showed that the proposed tuning method

yielded relatively fast and highly damped responses with slight overshoots, in accordance with the magnitude optimum criterion. An exception was $b = 0.9$, where slow disturbance-rejection responses were observed (see illustrative example in Chapter 4.1).

The closed-loop amplitude response (between reference and process output) is shown in Figure 4.9. It can be seen that all four processes, at different selections of parameter b, gave a flat amplitude response at lower frequencies, all according to the MO criterion (see Figure 2.2).

Table 4.5: The calculated characteristic areas for process models.

Process	A_0	A_1	A_2
G_{P1}	1	1.2	1.24
G_{P2}	1	1	0.5
G_{P3}	1	4	10
G_{P4}	1	4	7

Table 4.6: The PI controller parameters for different IP models and parameter b.

	$b = 0$		$b = 0.5$		$b = 0.9$	
Process	K_I	K_P	K_I	K_P	K_I	K_P
G_{P1}	0.093	0.432	0.069	0.428	0.017	0.419
G_{P2}	0.172	0.586	0.117	0.559	0.025	0.512
G_{P3}	0.0097	0.140	0.0069	0.135	0.0015	0.127
G_{P4}	0.0113	0.151	0.0076	0.142	0.0016	0.128

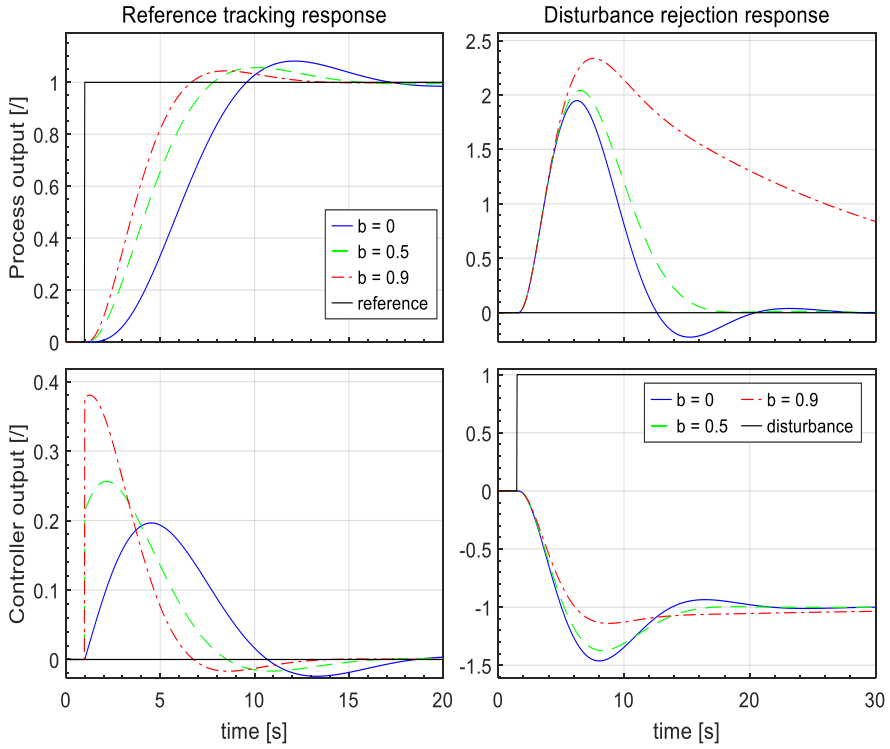

Figure 4.5: The process G_{P1} closed-loop responses for different values of b.

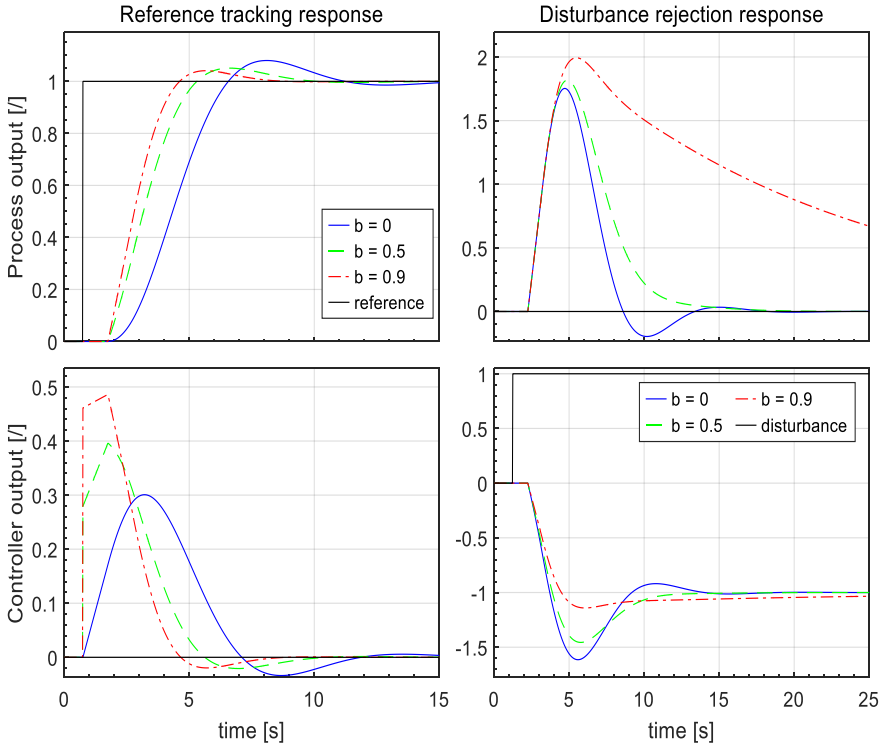

Figure 4.6: The process G_{P2} closed-loop responses for different values of b.

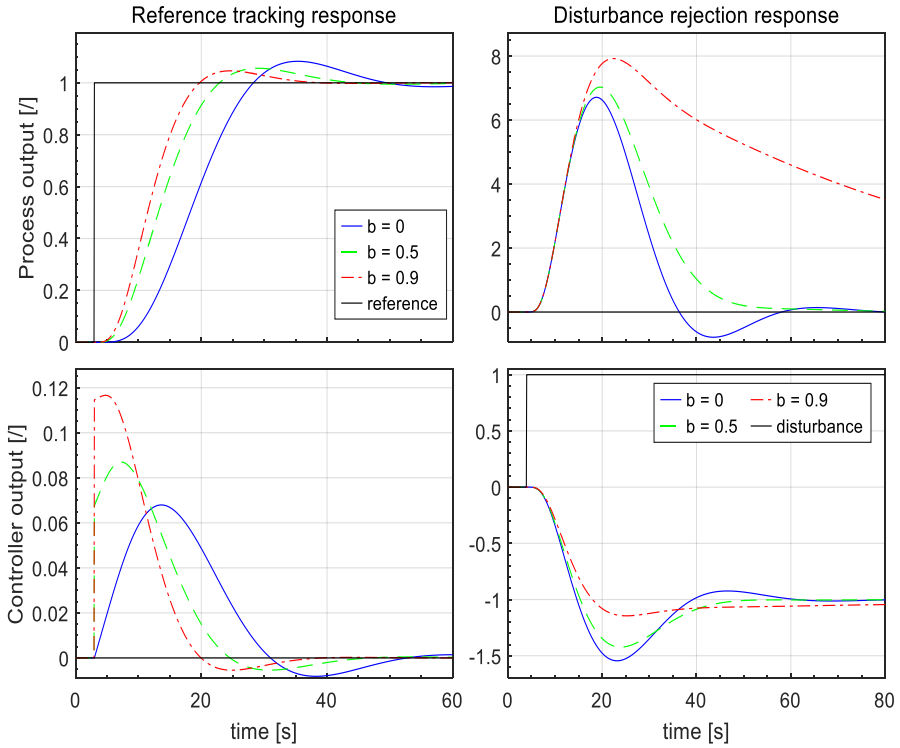

Figure 4.7: The process G_{P3} closed-loop responses for different values of b.

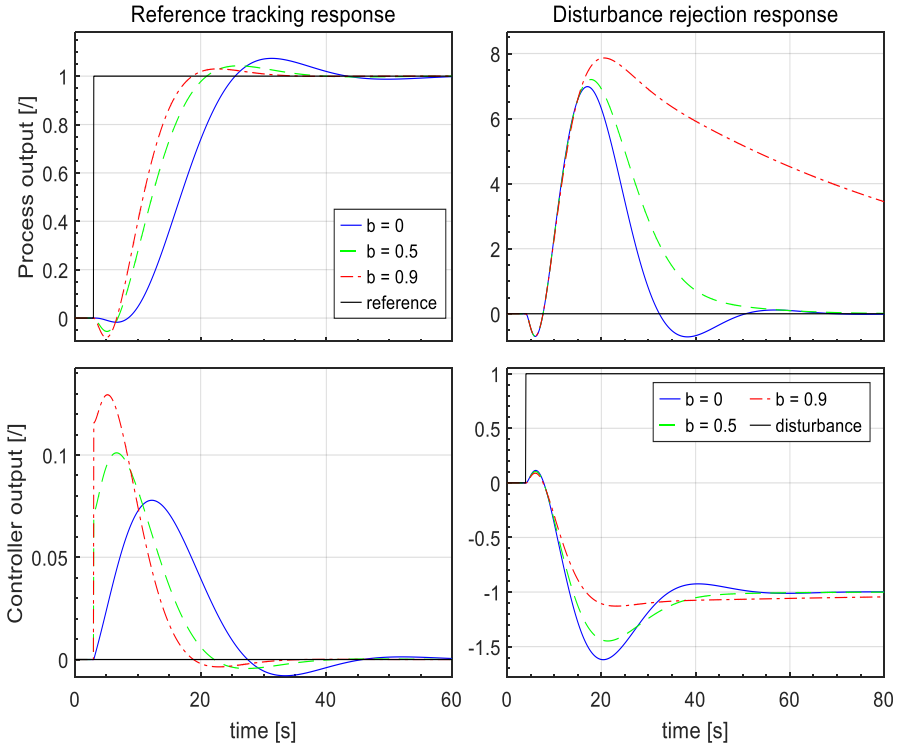

Figure 4.8: The process G_{P4} closed-loop responses for different values of b.

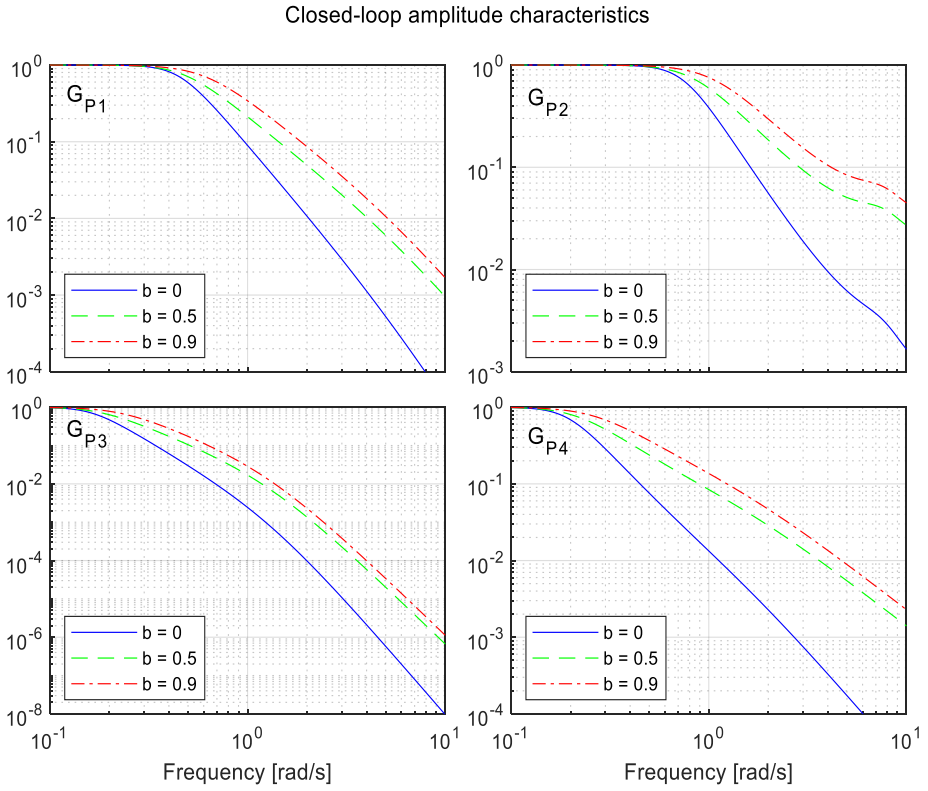

Figure 4.9: Bode plots (for a different value of b) for all tested processes.

Chapter 5

PID Controller for the Integrating Processes

A large part of this chapter was originally published in T. Kos et al., Applied Sciences (2020), 10: 17.

Figure 5.1 shows the closed-loop system with a 2-DOF PID controller. Signals y, d, u, and r represent the process output, disturbance, controller output, and controller reference, respectively. Parameters b and c are the proportional and derivative weighting factors, while K_{D}, K_{P}, K_{I}, and T_{F} represent the derivative gain, proportional gain, integral gain, and filter time constant, respectively.

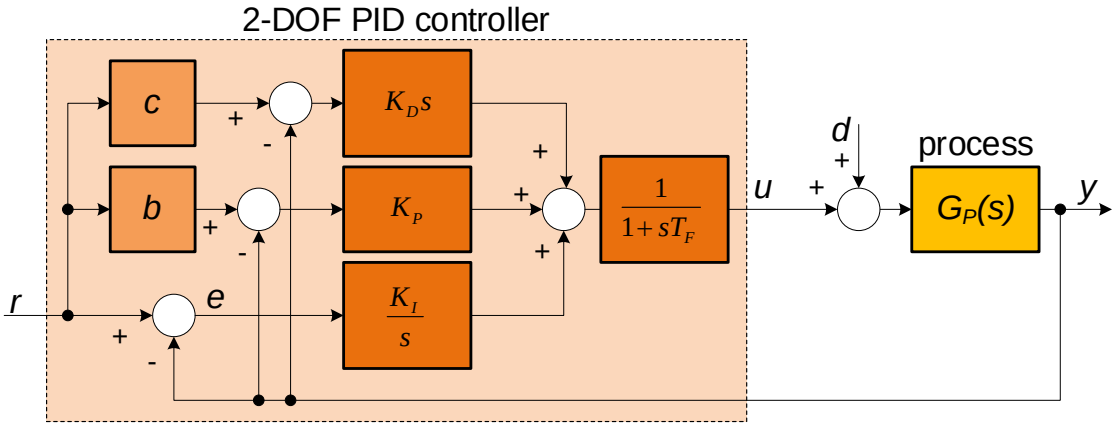

Figure 5.1: The closed-loop system with a 2-DOF PID controller.

The controller shown in Figure 5.1 is defined by the following transfer functions:

$$\begin{aligned} G_{\mathrm{CR}}(s) &= \frac{bK_{\mathrm{D}}s^2 + bK_{\mathrm{P}}s + K_{\mathrm{I}}}{s(1+sT_{\mathrm{F}})}, \\ G_{\mathrm{CY}}(s) &= \frac{K_{\mathrm{D}}s^2 + K_{\mathrm{P}}s + K_{\mathrm{I}}}{s(1+sT_{\mathrm{F}})}. \end{aligned} \tag{5.1}$$

To simplify the derivations, $c = b$ is chosen. Thereafter, this controller will be referred to as $\mathrm{PID}_{\mathrm{b}}$. While the controller filter

$$G_{\mathrm{F}} = \frac{1}{1+sT_{\mathrm{F}}} \tag{5.2}$$

is part of the transfer function of the PID_b controller. In order to simplify the derivation of the parameters of the PID_b controller, the controller filter is considered part of the process (2.1). Therefore, the aforementioned filter must be added to Expression (2.1) each time the PID_b controller parameters are calculated using the final formula.

The controller filter is used to reduce the high-frequency output noise of the controller. The controller's high-frequency gain equals $K_{HF} = K_D \div T_F$ [25]. In addition to specifying the controller filter time constant, it can also be calculated based on the desired high-frequency gain as follows:

$$T_\text{F} = \frac{K_\text{D}}{K_\text{HF}}. \tag{5.3}$$

First, the controller parameters (including the derivative gain K_D) should be calculated with $T_\text{F} = 0$. Then, the controller parameters can be recalculated using Equation (5.3). The procedure can be repeated until the T_F value settles. In practice, up to three iterations are usually sufficient.

In the following derivation, the parameters of the PID_b controller are calculated. The IP has been modelled by the transfer function (2.1). To simplify subsequent derivations, the process (2.1) has been developed into an infinite Taylor series (2.7). Then, the transfer functions of the process (2.7) and the controller (5.1) are inserted into a closed-loop transfer function (2.2). In this way, the following closed-loop transfer function (2.5) parameters are obtained:

$$\begin{aligned}
e_0 &= A_0 K_\text{I} \\
e_1 &= -A_1 K_\text{I} + A_0 K_\text{P} \\
e_2 &= A_2 K_\text{I} - A_1 K_\text{P} + A_0 K_\text{D} + 1 \\
e_3 &= -A_3 K_\text{I} + A_2 K_\text{P} - A_1 K_\text{D} \\
e_4 &= A_4 K_\text{I} - A_3 K_\text{P} + A_2 K_\text{D} \\
&\vdots
\end{aligned} \tag{5.4}$$

$$\begin{aligned}
f_0 &= A_0 K_\text{I} \\
f_1 &= -A_1 K_\text{I} + A_0 b K_\text{P} \\
f_2 &= A_2 K_\text{I} - A_1 b K_\text{P} + A_0 b K_\text{D} \\
f_3 &= -A_3 K_\text{I} + A_2 b K_\text{P} - A_1 b K_\text{D} \\
f_4 &= A_4 K_\text{I} - A_3 b K_\text{P} + A_2 b K_\text{D} \\
&\vdots
\end{aligned} \tag{5.5}$$

To simplify the PID_b controller parameters' derivation, in the next step, all closed-loop transfer function parameters, represented by Expressions (5.4) and (5.5), are divided by $A_0 K_\text{I}$. Consequently, the following closed-loop transfer function parameters (2.5) are obtained:

$$\begin{aligned}
e_0 &= 1 \\
e_1 &= G_{10} + T_\text{I} \\
e_2 &= G_{20} + G_{10} T_\text{I} + K_\text{DI} + G_{00} K_\text{I1} \\
e_3 &= G_{30} + G_{20} T_\text{I} + G_{10} K_\text{DI} \\
e_4 &= G_{40} + G_{30} T_\text{I} + G_{20} K_\text{DI} \\
&\vdots
\end{aligned} \tag{5.6}$$

$$\begin{aligned} f_0 &= 1 \\ f_1 &= G_{10} + bT_{\mathrm{I}} \\ f_2 &= G_{20} + G_{10}bT_{\mathrm{I}} + bK_{\mathrm{DI}} \\ f_3 &= G_{30} + G_{20}bT_{\mathrm{I}} + G_{10}bK_{\mathrm{DI}} \\ f_4 &= G_{40} + G_{30}bT_{\mathrm{I}} + G_{20}bK_{\mathrm{DI}}, \\ &\vdots \end{aligned} \tag{5.7}$$

where

$$\begin{gathered} T_{\mathrm{I}} = \frac{K_{\mathrm{P}}}{K_{\mathrm{I}}}, K_{\mathrm{I1}} = \frac{1}{K_{\mathrm{I}}}, K_{\mathrm{DI}} = \frac{K_{\mathrm{D}}}{K_{\mathrm{I}}}, \\ G_{00} = \frac{1}{A_0}, G_{10} = -\frac{A_1}{A_0}, G_{20} = \frac{A_2}{A_0}, G_{30} = -\frac{A_3}{A_0}, G_{40} = \frac{A_4}{A_0}. \end{gathered} \tag{5.8}$$

For calculating the three PID$_{\mathrm{b}}$ controller parameters, the first three equations in Condition (2.6) should be solved [222]. The first condition of Expression (2.6) gives the following result:

$$K_{\mathrm{DI}} = \frac{0.5(1-b^2){T_{\mathrm{I}}}^2 - \frac{G_{00}}{K_{\mathrm{I}}}}{(1-b)}, \tag{5.9}$$

and the second condition in Expression (2.6) provides the following result:

$$K_{\mathrm{I}} = -\frac{G_{00}(b-1)^2\left(-2{G_{10}}^2 - 2G_{10}T_{\mathrm{I}} + 2G_{20} + b{T_{\mathrm{I}}}^2(1+b)\right)}{0.25(b^2-1)^3{T_{\mathrm{I}}}^4}. \tag{5.10}$$

The third condition of Expression (2.6) gives the following fourth-order polynomial:

$$\alpha{T_{\mathrm{I}}}^4 + \beta{T_{\mathrm{I}}}^3 + (\gamma_1+\gamma_2){T_{\mathrm{I}}}^2 + (\delta_1+\delta_2)T_{\mathrm{I}} + (\varepsilon_1+\varepsilon_2) = 0, \tag{5.11}$$

where

$$\begin{aligned} \alpha &= (1-b)(1+b)^2({G_{10}}^2(1-b) + 2bG_{20}), \\ \beta &= 8\left((1-b^2){G_{10}}^3 + (2b^2+b-1)G_{10}G_{20} - b(1+b)G_{30}\right), \\ \gamma_1 &= 8(-(b^2-3){G_{10}}^4 + (3b^2+b-6){G_{10}}^2G_{20} - 2(b^2+b-1)G_{10}G_{30}), \\ \gamma_2 &= 8\left((1-b^2){G_{20}}^2 + b(1+b)G_{40}\right), \\ \delta_1 &= 16\left(2{G_{10}}^5 - 6{G_{10}}^3G_{20} + 3({G_{10}}^2G_{30} + G_{10}{G_{20}}^2)\right), \\ \delta_2 &= 16(-G_{10}G_{40} - G_{20}G_{30}), \\ \varepsilon_1 &= 16({G_{10}}^6 - 4{G_{10}}^4G_{20} + 2{G_{10}}^3G_{30} + 4{G_{10}}^2{G_{20}}^2), \\ \varepsilon_2 &= 16(-{G_{10}}^2G_{40} - 2G_{10}G_{20}G_{30} - {G_{20}}^3 + G_{20}G_{40}). \end{aligned} \tag{5.12}$$

To calculate the PID$_{\mathrm{b}}$ parameters, the integral time constant T_{I}, represented by Expressions (5.11) and (5.12), should be solved first. The correct result is the highest positive real number. In the next step, the integral gain, K_{I}, should be calculated using Equation (5.10).

In the last step, the proportional K_{P} and derivative K_{D} gains can be calculated using the following expression:

$$\begin{aligned} K_{\mathrm{P}} &= K_{\mathrm{I}} T_{\mathrm{I}}, \\ K_{\mathrm{D}} &= \frac{0.5(1-b^2){T_{\mathrm{I}}}^2 K_{\mathrm{I}} - G_{00}}{(1-b)}. \end{aligned} \tag{5.13}$$

Since the computation of the $\mathrm{PID_b}$ controller's parameters requires solving the fourth-order polynomial, the final derivation of the tuning formula is not presented. Regardless, the tuning formula remains analytical. To facilitate the implementation of the proposed tuning method and save the reader's time and effort, all the MATLAB files used to calculate the $\mathrm{PID_b}$ parameters are available online [1].

Remark 5.1. *The weighting factor b influences disturbance-rejection and tracking performance. When b approaches 1, the integral gain K_I (5.10) approaches 0* [223]*. For $b = 1$, we obtain the following PID controller:*

$$\begin{aligned} K_{\mathrm{P}} &= \frac{K_{\mathrm{D}} A_0 + 0.5}{A_1}, \\ K_{\mathrm{I}} &= 0, \\ K_{\mathrm{D}} &= \frac{A_3}{2(A_1 A_2 - A_0 A_3)}. \end{aligned} \tag{5.14}$$

Thus, we get a PD controller that cannot reject the input disturbances of the process. For this reason, the performance of the disturbance rejection deteriorates when the value of the weighting factor b is increased. In practice, the value of b should be limited within the interval $0 \leq b < 0.9$ [223]*. An illustrative example of the tracking and the disturbance-rejection performance and its relationship with factor b is shown in Chapter 5.1.*

Remark 5.2. *The $\mathrm{PID_b}$ controller parameters calculated using Expressions (5.10) and (5.13) result in stable and fast closed-loop responses for most IP models. However, closed-loop stability is not guaranteed for every process model. Chapter 6 provides additional information on closed-loop stability and robustness.*

Remark 5.3. *To obtain the a-priori selected high-frequency controller gain K_{HF}, the exact value of T_F can be calculated using the procedure described below Equation (5.3).*

As explained in Chapter 2, characteristic areas A_0 to A_4 can be obtained directly from the process transfer function or calculated from the process time response when changing the process steady-state. The steps for the $\mathrm{PID_b}$ controller tuning are presented in Table 5.1.

Table 5.1: The instruction for the PID_b controller tuning.

Step	Description
1	Select the appropriate filter time constant T_F of the PID_b controller.
2	Determine characteristic areas A_0–A_4. If the process is given in a Laplace form, use Expression (2.8) (frequency-domain). Otherwise, change the steady-state of the process, capture the controller and process output signals, and calculate the characteristic areas using Expressions (2.9)–(2.11) (time-domain). The controller's initial values and the process output signals (before the first change of the process input signal) can be approximated from the measurements. Remember to add the filter time constant, T_F, to the process transfer function (2.1) before calculating the areas. When using the time-domain approach, use the first-order filter with a time constant equal to T_F to filter the process output signal.
3	Choose the reference weighting factor b. As seen in Remark 5.1, the recommended values are $0 \leq b < 0.9$.
4	Use Expressions (5.10) and (5.13) to compute the PID_b parameters K_P, K_I, and K_D.

5.1 Illustrative Example

The following second-order delayed IP is chosen to illustrate the proper design:

$$G_\text{P}(s) = \frac{e^{-0.2s}}{s(1+s)^2}. \tag{5.15}$$

First, the PID_b controller filter time constant $T_\text{F} = 0.01$ s is added to the process (5.15). Using Expression (2.8), the following characteristic areas are calculated from the transfer function of the process (5.15) with a filter:

$$A_{0\text{F}} = 1, A_{1\text{F}} = 2.21, A_{2\text{F}} = 3.4421, A_{3\text{F}} = 4.6758, A_{4\text{F}} = 5.9095. \tag{5.16}$$

In the next step, Expressions (5.10) and (5.13) are used to compute the parameters of the PID_b controller for different values of reference weighting factor b. The calculated parameters presented in Table 5.2 are applied to the PID_b controller. The closed-loop responses (reference step change $r = 1$ and input disturbance step change $d = 1$) are shown in Figure 5.2.

As can be seen in Figure 5.2, the reference weighting factor b has a significant effect on the closed-loop responses. Tracking (reference-following) performance is improved at higher values of b. Therefore, in cases where good tracking is desired, select a value of $b \geq 0.5$. However, high values of b degrade the disturbance-rejection performance, i.e., the disturbance-rejection becomes significantly worse at $b > 0.7$. The most effective disturbance-rejection is achieved with $b \leq 0.5$. An acceptable compromise between both tracking and disturbance-rejection seems to be $b = 0.5$.

Table 5.2: The PID_b controller parameters.

b	K_P	K_I	K_D
0	0.93011	0.23327	0.85427
0.2	0.93383	0.2486	0.85466
0.5	0.85191	0.19158	0.84114
0.7	0.75396	0.11619	0.8251
0.9	0.64303	0.03635	0.80683

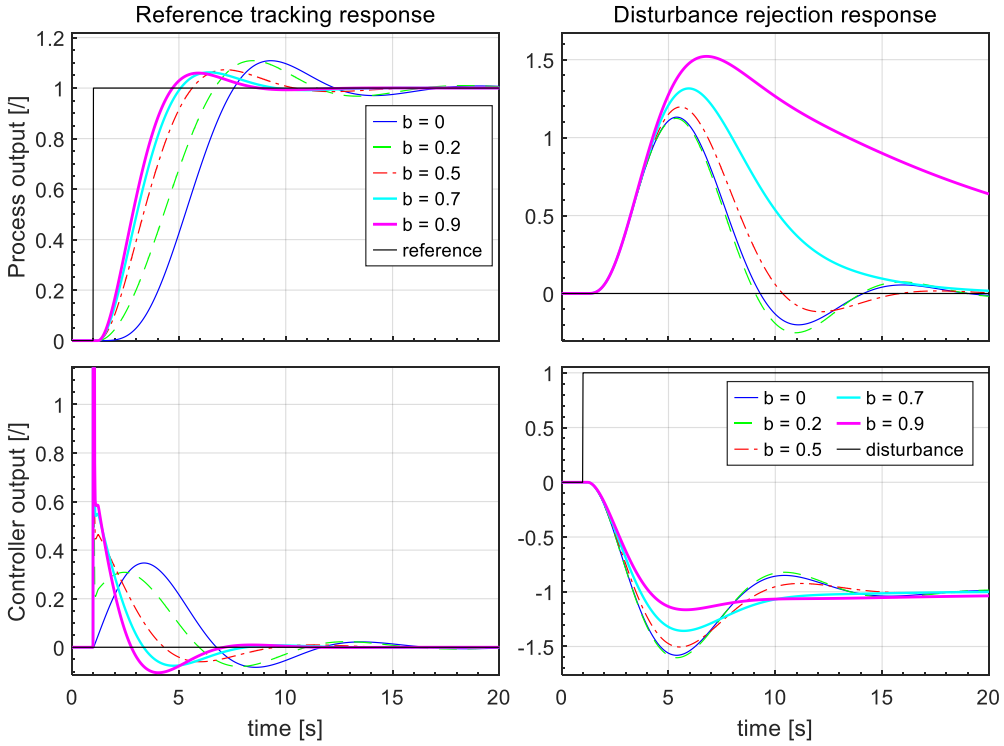

Figure 5.2: Closed-loop responses for the second-order delayed IP G_P (see Expression (5.15)). Note that, for clarity, the controller output response is zoomed in for the reference step change.

5.2 Reference Weighting and Reference Filtering Equivalence

As shown in Chapter 4.2, in addition to using set-point weighting [25], [219], the 2-DOF controller can also be realized with reference filtering [219], [220] (see Figure 4.3).

The closed-loop transfer function when using the 1-DOF PID controller with a reference filter is as follows:

$$G_{\text{CL1}}(s) = \frac{Y(s)}{R(s)} = \frac{G_\text{F} G_\text{P} G_\text{C}}{1 + G_\text{P} G_\text{C}}, \tag{5.17}$$

where

$$G_{\mathrm{C}}(s) = \frac{K_{\mathrm{I}} + K_{\mathrm{P}} s + K_{\mathrm{D}} s^2}{s(1 + sT_{\mathrm{F}})}. \tag{5.18}$$

The purpose of the reference filter G_{F} is to make the transfer function G_{CL1}(s) (5.17) equal to the closed-loop transfer function using the set-point weighting. To this end, the transfer functions of the PID$_{\mathrm{b}}$ controller (5.1) are inserted into a closed-loop transfer function (2.2), which is then equated to (5.17). The result is the following second-order reference filter transfer function:

$$G_{\mathrm{F}}(s) = \frac{1 + b\frac{K_{\mathrm{P}}}{K_{\mathrm{I}}} s + b\frac{K_{\mathrm{D}}}{K_{\mathrm{I}}} s^2}{1 + \frac{K_{\mathrm{P}}}{K_{\mathrm{I}}} s + \frac{K_{\mathrm{D}}}{K_{\mathrm{I}}} s^2} = \frac{1 + bT_{\mathrm{I}} s + bT_{\mathrm{I}} T_{\mathrm{D}} s^2}{1 + T_{\mathrm{I}} s + T_{\mathrm{I}} T_{\mathrm{D}} s^2}. \tag{5.19}$$

In the case when reference weighting factor $b > 0$, the reference filter contains zero. Note that if $b = 1$, the filter becomes static gain $G_{\mathrm{F}} = 1$.

5.3 Average Closed-Loop Residence Time

As shown in Chapter 4.3, the desired average closed-loop residence time T_{CLD} [25] is related to the closed-loop time constant. Based on this measure, the parameters of the controller can be recalculated, which in turn speeds up or slows down the closed-loop response.

In the following derivation, the average closed-loop residence time T_{CL} will be calculated. The IP model was chosen according to Expression (2.7). The closed-loop transfer function (2.2) was calculated from the PID$_{\mathrm{b}}$ controller (5.1) and the IP model (2.7). The following parameters of the closed-loop transfer function (2.5) are then obtained (after dividing the numerator and denominator by $A_0 K_{\mathrm{I}}$):

$$\begin{aligned} e_0 &= 1 \\ e_1 &= \frac{-A_1 K_{\mathrm{I}} + A_0 K_{\mathrm{P}}}{A_0 K_{\mathrm{I}}} \\ &\vdots \end{aligned} \tag{5.20}$$

$$\begin{aligned} f_0 &= 1 \\ f_1 &= \frac{-A_1 K_{\mathrm{I}} + A_0 b K_{\mathrm{P}}}{A_0 K_{\mathrm{I}}} \\ &\vdots \end{aligned} \tag{5.21}$$

Note that the parameters of the closed-loop transfer function are identical to those in (4.20) and (4.21). Thus, the average closed-loop residence time T_{CL} (for both cases: $b < 1$ and $b = 1$) is identical to that calculated for the PI controller ((4.23) and (4.24)).

To change the speed of the closed-loop response (the desired closed-loop time constant), the parameters of the PID$_{\mathrm{b}}$ controller can be recalculated accordingly. First, the expressions for the case when $b < 1$ are presented. The average closed-loop residence time T_{CL} can be calculated from Expression (4.23). The desired average closed-loop residence time T_{CLD} is defined in Expression (4.27). Unlike the PI controller, T_{CLD} has an upper limit, i.e., the value when the derivative gain $K_{\mathrm{D}} = 0$.

This maximum average closed-loop residence time $T_{\mathrm{CL(MAX)}}$ (for $K_{\mathrm{D}} = 0$) can be obtained by inserting Expressions (5.10) and (5.13) into Expression (4.23):

$$T_{\mathrm{CL(MAX)}} = \frac{A_1 + \sqrt{{A_1}^2 b^2 + A_0 A_2 (1 - b^2)}}{0.5 A_0 (1 + b)}. \tag{5.22}$$

In the case when $T_{\mathrm{CLD}} < T_{\mathrm{CL(MAX)}}$, the $\mathrm{PID_b}$ controller can be used. Otherwise, the proposed PI controller should be selected, as will be explained later on.

The expression for recalculating the integral time constant T_{I} of the controller can be obtained from Expression (4.23):

$$T_{\mathrm{I}} = \frac{T_{\mathrm{CLD}}}{(1 - b)}. \tag{5.23}$$

Controller's integral gain (K_{I}) can be recalculated according to Equation (5.10), and the proportional (K_{P}) and derivative (K_{D}) gains can be recalculated according to the Expressions (5.13).

In the case where $T_{\mathrm{CLD}} \geq T_{\mathrm{CL(MAX)}}$, the $\mathrm{PID_b}$ controller should be replaced by the proposed PI controller. In this case, the K_{P} and K_{I} parameters of the controller can be calculated according to Equations (4.26) and (4.4) (see Chapter 4.3).

As explained in Remark 5.1, when $b = 1$, the proportional-derivative (PD) controller is applied instead of the PID controller. In this case, T_{CL} can be computed from Expression (4.24). From Expression (5.14), it follows that:

$$T_{\mathrm{CL}} = \frac{A_1 A_2 - A_0 A_3}{0.5 A_0 A_2}. \tag{5.24}$$

Again, there is an upper limit to the desired average closed-loop residence time T_{CLD}. This maximum average closed-loop residence time $T_{\mathrm{CL(MAX)}}$ (when $K_{\mathrm{D}} = 0$) can be obtained by inserting Expression (5.14) into (4.24):

$$T_{\mathrm{CL(MAX)}} = \frac{2 A_1}{A_0}. \tag{5.25}$$

In the case where $T_{\mathrm{CLD}} < T_{\mathrm{CL(MAX)}}$, the PD controller can be used. Otherwise, the P controller is applied, as will be explained later on.

The recalculated proportional gain (K_{P}) of the controller, corresponding to the selected T_{CLD}, can be obtained from Expression (4.24):

$$K_{\mathrm{P}} = \frac{1}{A_0 T_{\mathrm{CLD}}}, \tag{5.26}$$

and the expression for the derivative gain (K_{D}) can be obtained from Expression (5.14):

$$K_{\mathrm{D}} = \frac{A_1 K_{\mathrm{P}} - 0.5}{A_0}. \tag{5.27}$$

In the case where $T_{\mathrm{CLD}} \geq T_{\mathrm{CL(MAX)}}$, the PD controller should be replaced by the P. In this case, controller parameter K_{P} can be calculated according to Equation (5.26).

The steps for the re-tuning of the $\mathrm{PID_b}$ controller if $b < 1$ are presented in Table 5.3. If $b = 1$, the steps for the re-tuning of the PD controller are presented in Table 5.4.

Table 5.3: The instruction for the re-tuning of the PID_b controller if $b < 1$.

Step	Description
1	Calculate the controller parameters according to the instructions in Table 5.1.
2	Determine the average closed-loop residence time T_{CL} from Expression (4.23).
3	Determine the maximum average closed-loop residence time $T_{\text{CL(MAX)}}$ from Expression (5.22).
4	Select the desired average closed-loop residence time T_{CLD} according to Expression (4.27). To slow down the desired closed-loop speed by a factor of 2, select $K_{\text{CL}} = 2$.
5	If $T_{\text{CLD}} < T_{\text{CL(MAX)}}$, the PID_b controller can be used. Therefore, recalculate the controller parameters according to Expressions (5.23), (5.10), and (5.13). If $T_{\text{CLD}} \geq T_{\text{CL(MAX)}}$, the proposed PI controller should be used instead. In this case, the K_{P} and K_{I} parameters can be calculated according to Equations (4.26) and (4.4).

Table 5.4: The instruction for the re-tuning of the PD controller if $b = 1$.

Step	Description
1	Calculate the controller parameters according to the instructions in Table 5.1.
2	Determine the average closed-loop residence time T_{CL} from Expression (4.24) or (5.24).
3	Determine the maximum average closed-loop residence time $T_{\text{CL(MAX)}}$ from Expression (5.25).
4	Select the desired average closed-loop residence time T_{CLD} according to Expression (4.27). To slow down the desired closed-loop speed by a factor of 2, select $K_{\text{CL}} = 2$.
5	If $T_{\text{CLD}} < T_{\text{CL(MAX)}}$, the PD controller can be used. Therefore, recalculate the controller parameters according to Expressions (5.26) and (5.27). If $T_{\text{CLD}} \geq T_{\text{CL(MAX)}}$, the P controller should be used, instead. In this case, controller parameter K_{P} can be recalculated according to Equation (5.26).

To facilitate the calculation of the average closed-loop residence time and save the reader's time and effort, all MATLAB files are available online [1].

5.3.1 Illustrative example

The calculation of the controller parameters, according to the desired time factor of the closed-loop K_{CL}, is presented below. The chosen process is second-order IP (5.15). The controller filter time constant is set to $T_{\text{F}} = 0.01$ s. Characteristic areas $A_{0\text{F}}$–$A_{4\text{F}}$ (including filter time constant) are given by Expression (5.16). The parameters of the PID_b controller, for $b = 0.5$ and for different closed-loop time factors K_{CL}, are given in Table 5.5. The table also contains the desired average closed-loop residence times T_{CLD} (depending on the selected K_{CL}). The calculated maximum average closed-loop residence time $T_{\text{CL(MAX)}} = 5.5467$ (5.22). Note that the PI controller was used for $K_{\text{CL}} = 3$ (see Table 5.5), since $T_{\text{CLD}} \geq T_{\text{CL(MAX)}}$.

Table 5.5: The PID_b controller parameters for different K_{CL} and $b = 0.5$. The calculated $T_{CL(MAX)} = 5.5467$.

K_{CL}	K_P	K_I	K_D	T_{CLD}
0.5	2.297	1.0331	1.8304	1.1117
0.75	1.2907	0.38703	1.2285	1.6675
1	0.85191	0.19158	0.84114	2.2233
2	0.32265	0.036279	0.15206	4.4467
3	0.1999	0.014985	0	6.67

The closed-loop responses on setpoint change ($r = 1$) and input disturbance ($d = 1$), using a PID_b controller with $b = 0.5$, for different K_{CL} are shown in Figure 5.3. It can be seen that the tracking and disturbance-rejection performance is closely correlated with the closed-loop time factor K_{CL}. The closed-loop performance increases when factor K_{CL} decreases. However, if K_{CL} is lower than 1, oscillatory closed-loop responses occur (see, for example, response for $K_{CL} = 0.5$). In general, therefore, K_{CL} should not be much lower than 1. Note that factor K_{CL} influences both the tracking and the disturbance-rejection performance.

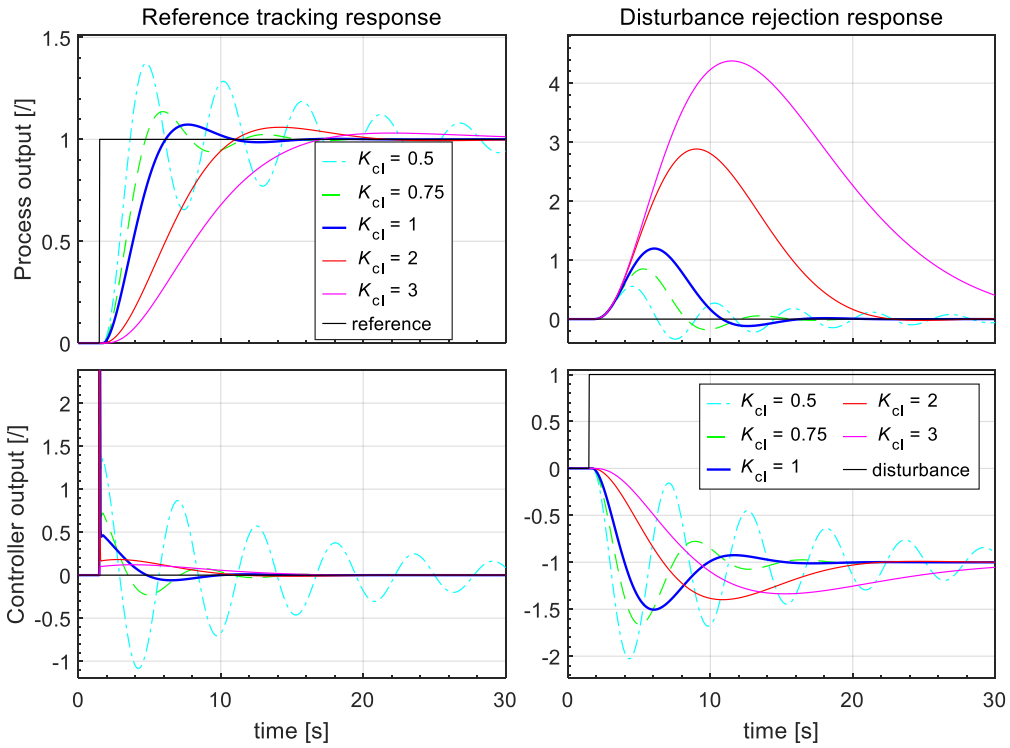

Figure 5.3: Closed-loop responses for the second-order delayed IP (5.15) for different values of K_{CL}. Note that, for clarity, the controller output response is zoomed in for the reference step change.

As has been shown, the closed-loop performance correlates with the average closed-loop residence time T_{CL}. If the user finds the closed-loop response too fast, it can be slowed down by increasing the T_{CLD} accordingly (by increasing factor K_{CL}). The advantage of using a T_{CLD} (or factor K_{CL}) is an accurate prediction of the closed-loop time constant.

Consequently, when T_{CLD} is changed, the user can predict the speed of the closed-loop response.

In future work, we will strive to find common tuning parameters that include both the average closed-loop residence time and the high-frequency noise attenuation of the controller.

5.4 Optimal Tracking and Disturbance-Rejection

In addition to using the reference-weighting parameter b (note that $c = b$), closed-loop tracking can be improved by applying a reference filter. The main advantage of using a reference filter is that such a filter can significantly improve the tracking response without degrading disturbance-rejection response (the optimal one, as calculated with $b = 0$). In this way, the best overall response can be achieved. A similar approach was proposed in [218] for non-integrating processes. Filter (G_{F}) in the closed-loop configuration with PID controller (G_{C}) and process (G_{P}) is shown in Figure 4.3. For the proposed tuning method with a reference filter, the controller parameters are calculated for weighting factor $b = 0$ to retain the good disturbance-rejection properties, while the controller structure is a 1-DOF PID ($b = 1$).

Here, two controller structures with reference filters are proposed according to the following filter order: the PID controller with the second-order filter ($\mathrm{PID}_{\mathrm{f2}}$) and the higher-order filter ($\mathrm{PID}_{\mathrm{fh}}$).

5.4.1 The second-order filter

The closed-loop transfer function G_{CL} from the reference to the process output is the following:

$$G_{\mathrm{CL}}(s) = \frac{G_{\mathrm{F}}(K_{\mathrm{I}} + K_{\mathrm{P}}s + K_{\mathrm{D}}s^2)G_{\mathrm{P}}}{s + (K_{\mathrm{I}} + K_{\mathrm{P}}s + K_{\mathrm{D}}s^2)G_{\mathrm{P}}}. \tag{5.28}$$

The purpose of reference filter G_{F} is to make the reference following transfer Function (5.28) as closely as possible to the desired function with the PD controller ($b = 1$):

$$G_{\mathrm{CL1}}(s) = \frac{(K_{\mathrm{P1}} + K_{\mathrm{D1}}s)G_{\mathrm{P}}}{s + (K_{\mathrm{P1}} + K_{\mathrm{D1}}s)G_{\mathrm{P}}}, \tag{5.29}$$

where K_{P1} and K_{D1} represent the parameters (5.14) of the PD controller. The structure of reference filter G_{F} is chosen as follows:

$$G_{\mathrm{F}}(s) = \frac{1 + b_{\mathrm{F1}}s + b_{\mathrm{F2}}s^2}{\left(1 + \frac{K_{\mathrm{P}}}{K_{\mathrm{I}}}s + \frac{K_{\mathrm{D}}}{K_{\mathrm{I}}}s^2\right)}. \tag{5.30}$$

The denominator of the filter (5.30) is chosen to cancel the zeros of the controller in the closed-loop transfer function (5.28), similar to the approach proposed by Medarametla and Manimozhi [104]. The numerator of the filter (parameters b_{F1} and b_{F2}) is then calculated by equating the first two characteristic areas (A_0 and A_1) of the closed-loop transfer function (5.28) (using Expression (2.8) with G_{CL} instead of G_{P1} in Expression (2.7)) with the equivalent areas of the desired closed-loop transfer function G_{CL1} when using the PD controller (5.29).

Thus, the following filter parameters are obtained:

$$\begin{aligned} b_{\mathrm{F1}} &= \tfrac{K_{\mathrm{P}}}{K_{\mathrm{I}}} - \tfrac{1}{A_0 K_{\mathrm{P1}}}, \\ b_{\mathrm{F2}} &= \frac{{A_0}^2 K_{\mathrm{D}} {K_{\mathrm{P1}}}^2 + A_0 {K_{\mathrm{P1}}}^2 - A_0 K_{\mathrm{P}} K_{\mathrm{P1}} + A_0 K_{\mathrm{I}} K_{\mathrm{D1}} - A_1 K_{\mathrm{I}} K_{\mathrm{P1}} + K_{\mathrm{I}}}{{A_0}^2 K_{\mathrm{I}} {K_{\mathrm{P1}}}^2}. \end{aligned} \tag{5.31}$$

5.4.2 The higher-order filter

To achieve even faster tracking than with the PD controller (5.14), a higher-order filter can be used. Here, the calculation of the filter parameters is based on the process model. However, this does not mean that the main advantage of the proposed tuning method is lost (note that the process model is not required to calculate the controller parameters). Instead, the process model is estimated from the characteristic areas. The only parameter required by the user is the estimated process time delay, which can be easily obtained from the process time-response in practice. The chosen process model is a second-order process with zero and the estimated pure time delay

$$G_{\mathrm{M}}(s) = \frac{K_{\mathrm{M}}(1 + b_{1\mathrm{m}} s) e^{-T_{\mathrm{dm}} s}}{s(1 + a_{1\mathrm{m}} s + a_{2\mathrm{m}} s^2)}, \tag{5.32}$$

where T_{dm} and K_{M} represent the process time delay and steady-state gain, respectively. Note that the model parameters (except for the estimated time delay, T_{dm}) can be calculated directly from the equations for characteristic areas A_0 to A_3 (2.8):

$$\begin{aligned} K_{\mathrm{M}} &= A_0, \\ a_{1\mathrm{m}} &= \tfrac{2A_1\left(A_2 - \frac{A_0 T_{\mathrm{dm}}^2}{2}\right) - 2A_0\left(A_3 - \frac{A_0 T_{\mathrm{dm}}^3}{6}\right)}{A_0^2 T_{\mathrm{dm}}^2 - 2A_0 A_1 T_{\mathrm{dm}} - 2A_0 A_2 + 2A_1^2} + \tfrac{(A_1 - A_0 T_{\mathrm{dm}})(A_0 T_{\mathrm{dm}}^2 - 2A_1 T_{\mathrm{dm}})}{A_0^2 T_{\mathrm{dm}}^2 - 2A_0 A_1 T_{\mathrm{dm}} - 2A_0 A_2 + 2A_1^2}, \\ a_{2\mathrm{m}} &= \tfrac{\left(A_2 - \frac{A_0 T_{\mathrm{dm}}^2}{2}\right)(2A_2 - A_0 T_{\mathrm{dm}}^2) - 2(A_1 - A_0 T_{\mathrm{dm}})\left(A_3 - \frac{A_0\, T_{\mathrm{dm}}^3}{6}\right)}{A_0^2 T_{\mathrm{dm}}^2 - 2A_0 A_1 T_{\mathrm{dm}} - 2A_0 A_2 + 2A_1^2} + \\ &\quad + \tfrac{(A_1 - A_0 T_{\mathrm{dm}})(A_1 T_{\mathrm{dm}}^2 - 2A_2 T_{\mathrm{dm}})}{A_0^2 T_{\mathrm{dm}}^2 - 2A_0 A_1 T_{\mathrm{dm}} - 2A_0 A_2 + 2A_1^2}, \\ b_{1\mathrm{m}} &= \tfrac{2A_1\left(A_2 - \frac{A_0 T_{\mathrm{dm}}^2}{2}\right) - 2A_0\left(A_3 - \frac{A_0 T_{\mathrm{dm}}^3}{6}\right) - 2\left(\frac{A_1}{A0} - T_{\mathrm{dm}}\right)(A_1^2 - A_0 A_2)}{A_0^2 T_{\mathrm{dm}}^2 - 2A_0 A_1 T_{\mathrm{dm}} - 2A_0 A_2 + 2A_1^2}. \end{aligned} \tag{5.33}$$

For minimum-phase processes, the model transfer function can be simplified by setting $b_{1\mathrm{m}} = 0$, which simplifies the identification procedure.

Namely, all the process model parameters, including the process time delay T_{dm}, can be calculated analytically [216] from Expression (2.8):

$$K_{\mathrm{M}} = A_0,$$

$$\frac{T_{\mathrm{dm}}^3}{6} - \frac{T_{\mathrm{dm}}^2 A_1}{2A_0} + T_{\mathrm{dm}}\left(\frac{A_1^2}{A_0^2} - \frac{A_2}{A_0}\right) - \frac{A_1^3}{A_0^3} + \frac{2A_1A_2}{A_0^2} + \frac{A_3}{A_0} = 0,$$

$$a_{1\mathrm{m}} = \frac{A_1}{A_0} - T_{\mathrm{dm}}, \tag{5.34}$$

$$a_{2\mathrm{m}} = -\frac{A_2 + A_1 a_{1\mathrm{m}}}{A_0} + \frac{T_{\mathrm{dm}}^2}{2},$$

$$b_{1\mathrm{m}} = 0.$$

where T_{dm} is calculated from the third-order equation above. The result (among the three solutions) is the smallest positive real number. All the parameters of the process model (5.32) can also be calculated using the model estimation method described in Chapter 3.

The closed-loop transfer function from the reference to the process output, when process G_{P} is replaced by process model G_{M}, is as follows:

$$G_{\mathrm{CL}}(s) = \frac{G_{\mathrm{F}}K_{\mathrm{M}}(K_{\mathrm{D}}s^2+K_{\mathrm{P}}s+K_{\mathrm{I}})(1+b_{1\mathrm{m}}s)e^{-T_{\mathrm{dm}}s}}{(1+a_{1\mathrm{m}}s+a_{2\mathrm{m}}s^2)s^2+K_{\mathrm{M}}(K_{\mathrm{D}}s^2+K_{\mathrm{P}}s+K_{\mathrm{I}})(1+b_{1\mathrm{m}}s)e^{-T_{\mathrm{dm}}s}}. \tag{5.35}$$

We can now define the desired closed-loop transfer function as follows:

$$G_{\mathrm{CLD}}(s) = \frac{e^{-T_{\mathrm{dm}}s}}{\left(1 + \frac{T_{\mathrm{CL}}}{n}s\right)^n}, \tag{5.36}$$

where

$$\begin{array}{ll} n = 2 & T_{\mathrm{dm}} > 0 \\ n = 3 & T_{\mathrm{dm}} = 0 \end{array}. \tag{5.37}$$

T_{CL} is the desired average closed-loop residence time (see Chapters 4.3 and 5.3). Note that parameter T_{CL} is related to the speed of the PD controller response; therefore, it is calculated automatically, and no user input is required. Let us define the average closed-loop residence time T_{CL0} equal to the integral of the control error at the unit stepwise reference change [25]:

$$T_{\mathrm{CL0}} = \int_{t=0}^{t=\infty} e(t)dt = \frac{1}{A_0 K_{\mathrm{P1}}}, \tag{5.38}$$

where K_{P1} is the proportional gain of the PD controller. The desired average closed-loop residence time T_{CL} is then defined as follows:

$$T_{\mathrm{CL}} = \frac{T_{\mathrm{CL0}}}{K_{\mathrm{CL}}} = \frac{1}{A_0 K_{\mathrm{P1}} K_{\mathrm{CL}}}, \tag{5.39}$$

where parameter K_{CL} defines the speed-up coefficient of the average closed-loop residence time in relation to that obtained with the PD controller. According to the results of the

experiments using different process models, parameter $K_{\mathrm{CL}} = 3$ has proved to be a good compromise between tracking speed and robustness.

To equate Expressions (5.35) and (5.36), the time delay in the denominator of (5.35) is expressed by the second Pade's approximant:

$$e^{-T_{\mathrm{dm}}s} \approx \frac{1 - \frac{T_{\mathrm{dm}}}{2}s + \frac{T_{\mathrm{dm}}^2}{12}s^2}{1 + \frac{T_{\mathrm{dm}}}{2}s + \frac{T_{\mathrm{dm}}^2}{12}s^2}. \tag{5.40}$$

Using Equations (5.35) and (5.36), and considering (5.40) in the denominator of (5.35), the following reference filter transfer function is obtained:

$$G_{\mathrm{F}} = \frac{1 + b_{\mathrm{F1}}s + b_{\mathrm{F2}}s^2 + b_{\mathrm{F3}}s^3 + b_{\mathrm{F4}}s^4 + b_{\mathrm{F5}}s^5}{\left(1 + \frac{K_{\mathrm{P}}}{K_{\mathrm{I}}}s + \frac{K_{\mathrm{D}}}{K_{\mathrm{I}}}s^2\right)\left(1 + \frac{T_{\mathrm{dm}}}{2}s + \frac{T_{\mathrm{dm}}^2}{12}s^2\right)\left(1 + \frac{T_{\mathrm{CL}}}{n}s\right)^n}, \tag{5.41}$$

where n is calculated from Expression (5.37).

Parameters b_{F1} to b_{F5} in the numerator are calculated from the denominator of the closed-loop transfer function (5.35) without reference filter G_{F}:

$$\begin{aligned} den_{\mathrm{CL}} = {} & \frac{1}{A_0 K_{\mathrm{I}}}(1 + a_{1\mathrm{m}}s + a_{2\mathrm{m}}s^2)\left(1 + \frac{T_{\mathrm{dm}}}{2}s + \frac{T_{\mathrm{dm}}^2}{12}s^2\right)s^2 + \\ & + \left(1 + \frac{K_{\mathrm{P}}}{K_{\mathrm{I}}}s + \frac{K_{\mathrm{D}}}{K_{\mathrm{I}}}s^2\right) \times (1 + b_{1\mathrm{m}}s)\left(1 - \frac{T_{\mathrm{dm}}}{2}s + \frac{T_{\mathrm{dm}}^2}{12}s^2\right). \end{aligned} \tag{5.42}$$

by equating the terms with the same power of the Laplace variable s. The resulting parameters are the following:

$$\begin{aligned} b_{\mathrm{F1}} &= b_{1\mathrm{m}} - \tfrac{T_{\mathrm{dm}}}{2} + \tfrac{K_{\mathrm{P}}}{K_{\mathrm{I}}}, \\ b_{\mathrm{F2}} &= \tfrac{T_{\mathrm{dm}}(T_{\mathrm{dm}} - 6b_{1\mathrm{m}})}{12} + \tfrac{\left(A_0 K_{\mathrm{D}} - \frac{A_0 K_{\mathrm{P}} T_{\mathrm{dm}}}{2} + A_0 K_{\mathrm{P}} b_{1\mathrm{m}} + 1\right)}{A_0 K_I}, \\ b_{\mathrm{F3}} &= \tfrac{K_{\mathrm{D}} b_{1\mathrm{m}} - \frac{T_{\mathrm{dm}}(K_{\mathrm{D}} + K_{\mathrm{P}} b_{1\mathrm{m}})}{2} + \frac{T_{\mathrm{dm}}^2(K_{\mathrm{P}} + K_{\mathrm{I}} b_{1\mathrm{m}})}{12}}{K_{\mathrm{I}}} + \tfrac{\frac{T_{\mathrm{dm}}}{2} + T_{\mathrm{F}} + a_{1\mathrm{m}}}{A_0 K_{\mathrm{I}}}, \\ b_{\mathrm{F4}} &= \tfrac{\frac{T_{\mathrm{dm}}^2(K_{\mathrm{D}} + K_{\mathrm{P}} b_{1\mathrm{m}})}{12} - \frac{(K_{\mathrm{D}} T_{\mathrm{dm}} b_{1\mathrm{m}})}{2}}{K_I} + \tfrac{a_{2\mathrm{m}} + T_{\mathrm{F}} a_{1\mathrm{m}} + \frac{T_{\mathrm{dm}}(T_{\mathrm{F}} + a_{1\mathrm{m}})}{2} + \frac{T_{\mathrm{dm}}^2}{12}}{A_0 K_{\mathrm{I}}}, \\ b_{\mathrm{F5}} &= \tfrac{\frac{T_{\mathrm{dm}}^2(T_{\mathrm{F}} + a_{1\mathrm{m}})}{12} + \frac{T_{\mathrm{dm}}(a_{2\mathrm{m}} + T_{\mathrm{F}} a_{1\mathrm{m}})}{2} + T_{\mathrm{F}} a_{2\mathrm{m}}}{A_0 K_{\mathrm{I}}} + \tfrac{K_{\mathrm{D}} T_{\mathrm{dm}}^2 b_{1\mathrm{m}}}{12 K_{\mathrm{I}}}, \end{aligned} \tag{5.43}$$

where T_{F} is the controller filter time constant.

Remark 5.4. *For the calculation of the reference filters (second-order and higher-order) and the* process model *parameters (K_M, a_{1m}, a_{2m}, b_{1m}), characteristic areas without added controller filter time constant T_{F} must be used.*

Remark 5.5. *The reference filter is not in the feedback part of the closed-loop system transfer function. Therefore, as long as the reference filter is stable, it does not change the stability of the entire closed-loop system. By observing the higher-order reference filter Denominator (5.41), it can be seen that the majority of the filter poles are located on the*

left-hand side of the complex plane. The only part of the denominator filter that could become unstable is the following term:

$$\left(1+\frac{K_{\mathrm{P}}}{K_{\mathrm{I}}}s+\frac{K_{\mathrm{D}}}{K_{\mathrm{I}}}s^2\right). \tag{5.44}$$

Using a simple derivation, it can be shown that the above term (5.44) is stable when all controller gains have the same sign. The same applies to the second-order reference filter (5.30), which also contains the same term (5.44).

To facilitate the implementation of the proposed reference filters and save the reader's time and effort, all MATLAB files for computing the second- and higher-order filter parameters are available online [1]. As with the MOMI tuning method, the reference filter parameters can be calculated from the measured characteristic areas, which can be obtained from the steady-state time response of the process.

5.5 Examples on Some Process Models

In this chapter, the proposed method without reference filter ($\mathrm{PID_b}$ controller) was tested on some common process models. The chosen IPs were a delayed second-order process, a pure integrator plus time-delay process, a fourth-order process, and a non-minimum phase process. The following transfer functions represent these processes:

$$\begin{aligned}
G_{\mathrm{P1}}(s) &= \frac{e^{-0.2s}}{s(1+s)(1+0.2s)},\\
G_{\mathrm{P2}}(s) &= \frac{e^{-s}}{s},\\
G_{\mathrm{P3}}(s) &= \frac{1}{s(1+s)^4},\\
G_{\mathrm{P4}}(s) &= \frac{1-2s}{s(1+s)^2}.
\end{aligned} \tag{5.45}$$

Calculated characteristic areas A_0–A_4, according to Expression (2.8), are given in Table 5.6.

Table 5.6: The calculated characteristic areas for the IP models.

Process	A_0	A_1	A_2	A_3	A_4
G_{P1}	1	1.4	1.5	1.5213	1.5257
G_{P2}	1	1	0.5	0.16667	0.041667
G_{P3}	1	4	10	20	35
G_{P4}	1	4	7	10	13

Next, the a-priori chosen PID controller filter time constant $T_{\mathrm{F}} = 0.01$ s was added to the processes (5.45). Then, using Expression (2.8), characteristic areas $A_{0\mathrm{F}}$–$A_{4\mathrm{F}}$ were calculated. The values are shown in Table 5.7.

The parameters of the $\mathrm{PID_b}$ controller for different values of b ($b = 0$, $b = 0.5$, and $b = 0.7$) were calculated from Equations (5.10) and (5.13) using the calculated characteristic areas from Table 5.7. The calculated parameters for all selected IP models are shown in Table 5.8.

Table 5.7: The calculated characteristic areas for the IP models. Areas were calculated with the additional filter time constant $T_F = 0.01$ s.

Process	A_{0F}	A_{1F}	A_{2F}	A_{3F}	A_{4F}
G_{P1}	1	1.41	1.5141	1.5365	1.541
G_{P2}	1	1.01	0.5101	0.17177	0.04338
G_{P3}	1	4.01	10.0401	20.1004	35.201
G_{P4}	1	4.01	7.0401	10.0704	13.1007

Table 5.8: The PID_b controller parameters for different IP models and parameter b.

	$b = 0$			$b = 0.5$			$b = 0.7$		
	K_P	K_I	K_D	K_P	K_I	K_D	K_P	K_I	K_D
G_{P1}	2.6269	1.3991	1.4661	2.2778	1.1385	1.418	1.8731	0.63473	1.365
G_{P2}	1.128	0.47494	0.33942	1.0017	0.3258	0.30958	0.89095	0.18652	0.28414
G_{P3}	0.37914	0.04554	0.57814	0.3454	0.03499	0.55729	0.30728	0.02075	0.53411
G_{P4}	0.33133	0.03935	0.39492	0.2785	0.02479	0.34757	0.24024	0.01344	0.31634

The calculated controller parameters were applied to a PID_b controller. Figures 5.4–5.7 show the closed-loop responses for the input disturbance step change ($d = 1$) and the reference step change ($r = 1$). From the experimental results, it can be seen that the proposed tuning method provides relatively fast and stable closed-loop responses. Moreover, all responses were highly damped and exhibited only minor overshoots. The closed-loop responses are in accordance with the magnitude optimum criterion. Exceptions include the sluggish disturbance-rejection responses at $b = 0.7$. As expected, the best tracking performance was achieved with $b = 0.7$, and the best disturbance-rejection performance was achieved with $b = 0$ (see also the illustrative example in Chapter 5.1).

The Bode plots of the closed-loop amplitude gains (between the reference and the process output) are shown in Figure 5.8. This figure shows that all processes have a flat amplitude response in the lower frequency range, which is in accordance with the MO criterion (see Figure 2.2). Moreover, reference weighting factor b affects the closed-loop bandwidth, i.e., the closed-loop bandwidth decreases as factor b decreases. Therefore, the tracking performance improves with increasing factor b, which is consistent with the findings from Chapter 5.1 (illustrative example).

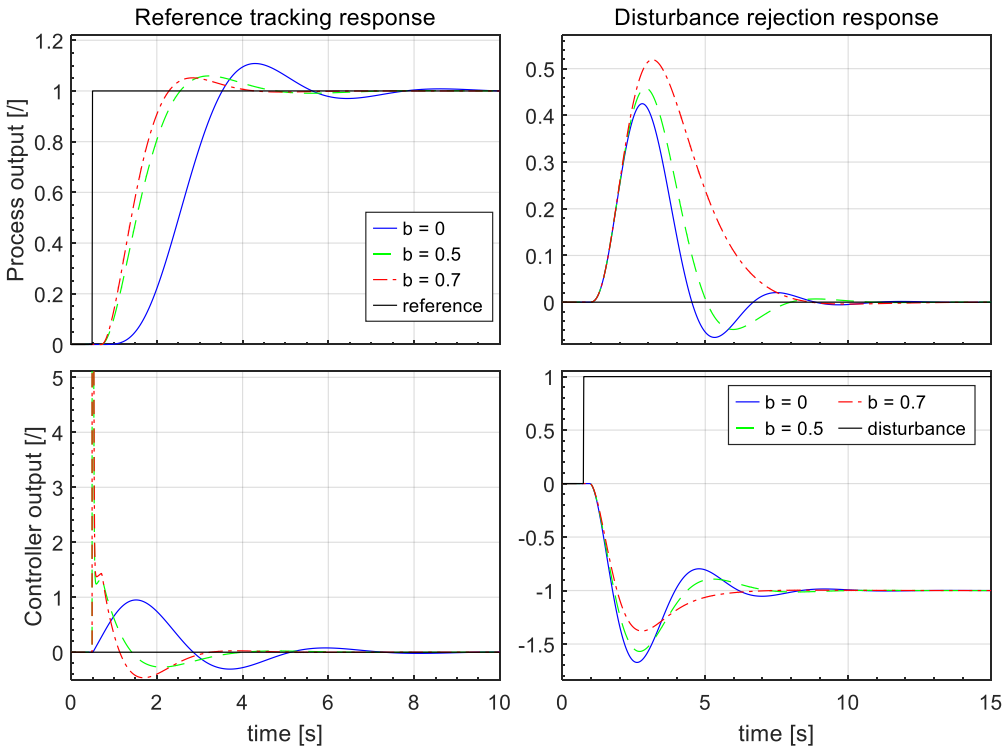

Figure 5.4: The process G_{P1} closed-loop responses for different values of b. Note that, for clarity, the controller output response is zoomed in for the reference step change.

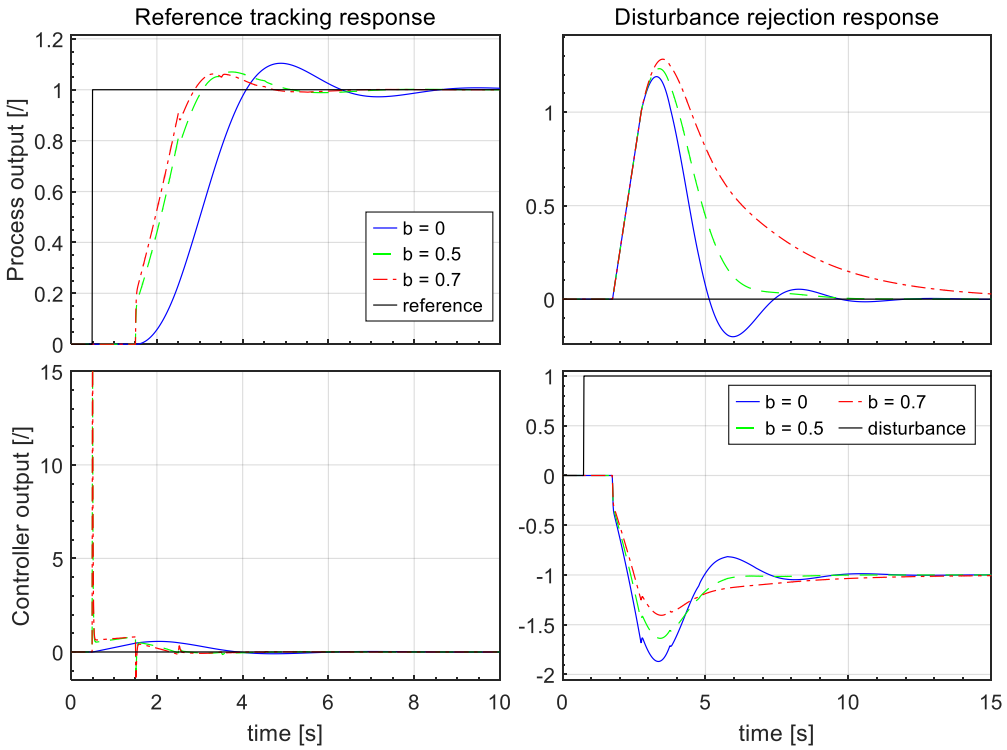

Figure 5.5: The process G_{P2} closed-loop responses for different values of b. Note that, for clarity, the controller output response is zoomed in for the reference step change.

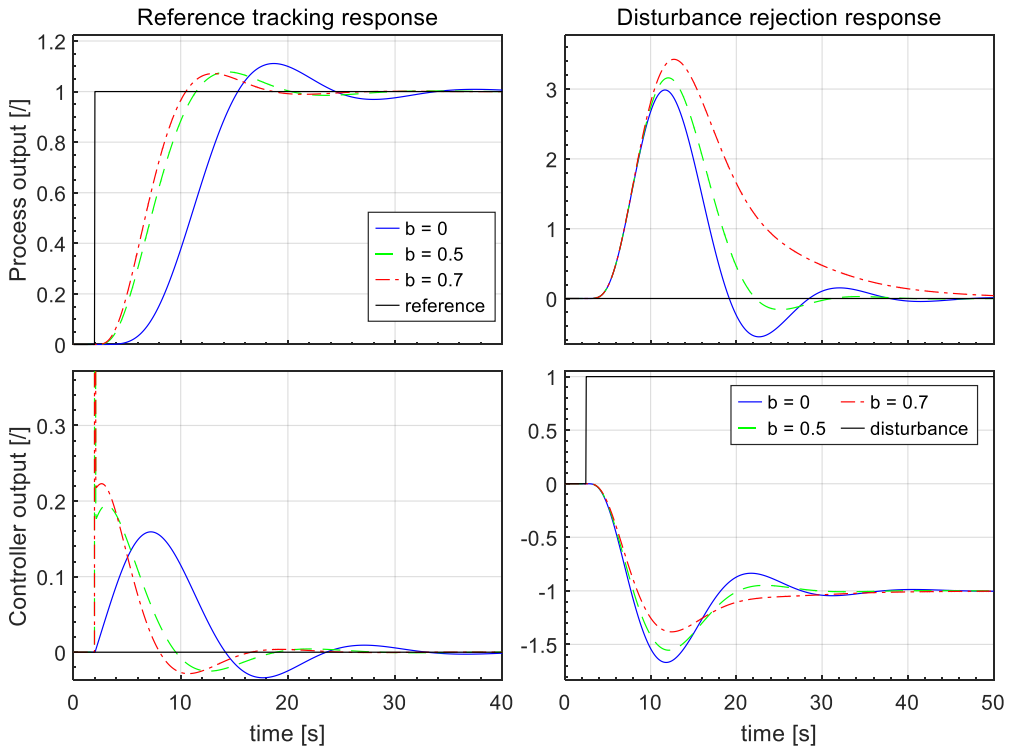

Figure 5.6: The process G_{P3} closed-loop responses for different values of b. Note that, for clarity, the controller output response is zoomed in for the reference step change.

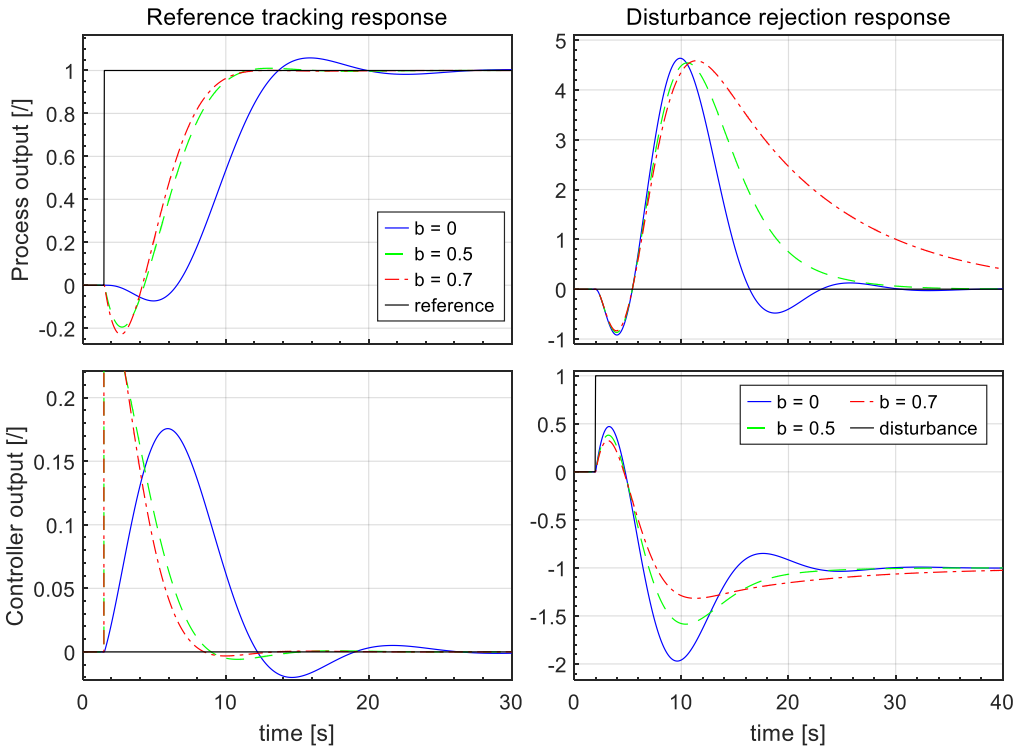

Figure 5.7: The process G_{P4} closed-loop responses for different values of b. Note that, for clarity, the controller output response is zoomed in for the reference step change.

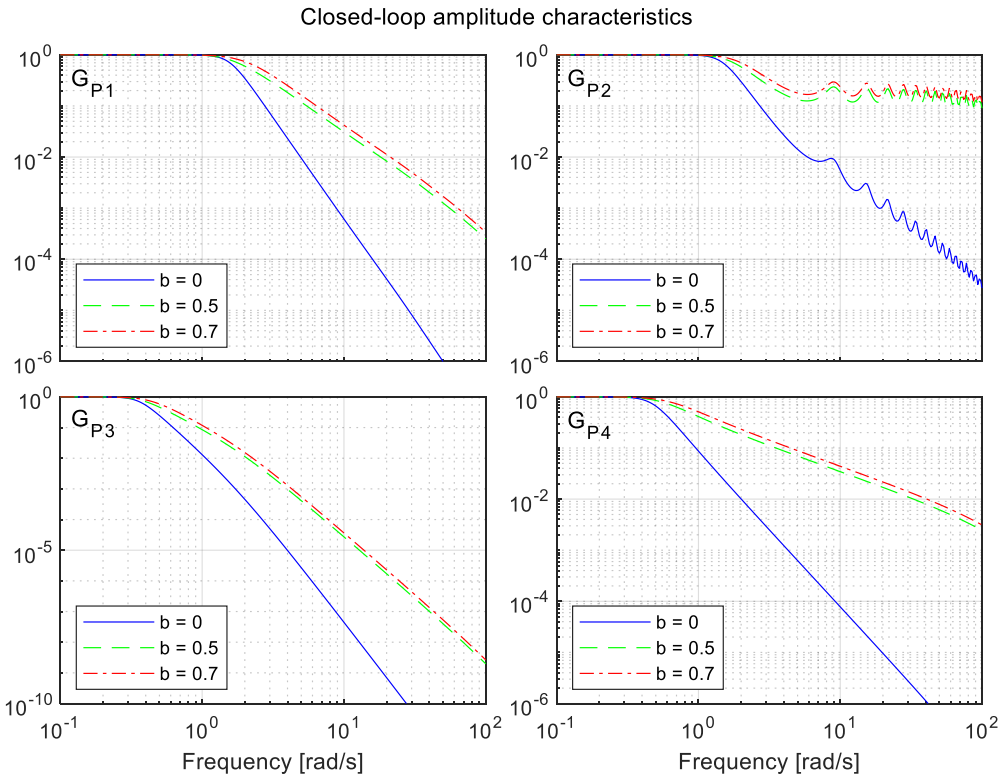

Figure 5.8: Bode plots (for a different value of b) for all tested processes.

5.6 Comparison of PI and PID$_b$ Performance

The performance of the proposed MOMI PID$_b$ method was compared with the MOMI PI method for IPs on four process models. Note that this PI controller also includes the reference weighting factor b on the proportional term. The following IPs were selected:

$$\begin{aligned} G_{\mathrm{P1}}(s) &= \frac{e^{-0.5s}}{s(1+4s)}, \\ G_{\mathrm{P2}}(s) &= \frac{e^{-0.5s}}{s(1+2s)^2}, \\ G_{\mathrm{P3}}(s) &= \frac{e^{-0.5s}}{s(1+s)^4}, \\ G_{\mathrm{P4}}(s) &= \frac{e^{-4s}}{s(1+0.5s)}. \end{aligned} \tag{5.46}$$

First, the parameters for the PI controller were determined. For this purpose, characteristic areas A_0–A_2, shown in Table 5.9, were calculated. The PI controller parameters for two different values of b ($b = 0$ and $b = 0.5$) were then calculated via Equations (4.9) and (4.11) using the calculated characteristic areas from Table 5.9. The calculated PI controller parameters for all four IP models are shown in Table 5.10.

Next, the parameters for the PID$_b$ controller were calculated. Note that the a priori chosen PID$_b$ controller filter time constant $T_F = 0.01$ s (5.2) was added to processes (5.46). Then, Expression (2.8) was used to calculate characteristic areas A_{0F}–A_{4F}, shown in Table 5.11. The parameters of the PID$_b$ controller for different values of b ($b = 0$ and $b = 0.5$)

were calculated from Equations (5.10) and (5.13) using the calculated characteristic areas from Table 5.11. The calculated PID_b controller parameters for all four IP models are shown in Table 5.12.

Table 5.9: The calculated characteristic areas for the IP models.

Process	A_0	A_1	A_2
G_{P1}	1	4.5	18.125
G_{P2}	1	4.5	14.125
G_{P3}	1	4.5	12.125
G_{P4}	1	4.5	10.25

Table 5.10: The PI controller parameters for different IP models and parameter b.

	$b = 0$		$b = 0.5$	
Process	K_I	K_P	K_I	K_P
G_{P1}	0.0065	0.1142	0.0048	0.1134
G_{P2}	0.0073	0.1211	0.0052	0.1182
G_{P3}	0.0078	0.1253	0.0055	0.121
G_{P4}	0.0084	0.1298	0.0058	0.1239

Table 5.11: The calculated characteristic areas for the IP models. Areas were calculated with the additional filter time constant $T_\text{F} = 0.01$ s.

Process	$A_{0\text{F}}$	$A_{1\text{F}}$	$A_{2\text{F}}$	$A_{3\text{F}}$	$A_{4\text{F}}$
G_{P1}	1	4.51	18.170	72.703	290.813
G_{P2}	1	4.51	14.170	38.663	97.973
G_{P3}	1	4.51	12.170	25.643	46.592
G_{P4}	1	4.51	10.295	15.895	18.721

Table 5.12: The PID_b controller parameters for different IP models and parameter b.

	$b = 0$			$b = 0.5$		
Process	K_P	K_I	K_D	K_P	K_I	K_D
G_{P1}	4.4939	1.7606	4.7353	3.4387	1.3668	4.4883
G_{P2}	0.44499	0.054126	0.82917	0.40688	0.044121	0.81421
G_{P3}	0.31757	0.033077	0.52446	0.28765	0.024817	0.50058
G_{P4}	0.25619	0.024309	0.34998	0.22777	0.01677	0.32033

The calculated controller parameters from Tables 5.10 and 5.12 were applied to the PI and PID_b controllers. Figures 5.9–5.12 show the compared closed-loop responses for the input disturbance step change ($d = 1$) and the reference step change ($r = 1$). This comparison shows the superior performance of the PID_b controller in tracking and disturbance-rejection.

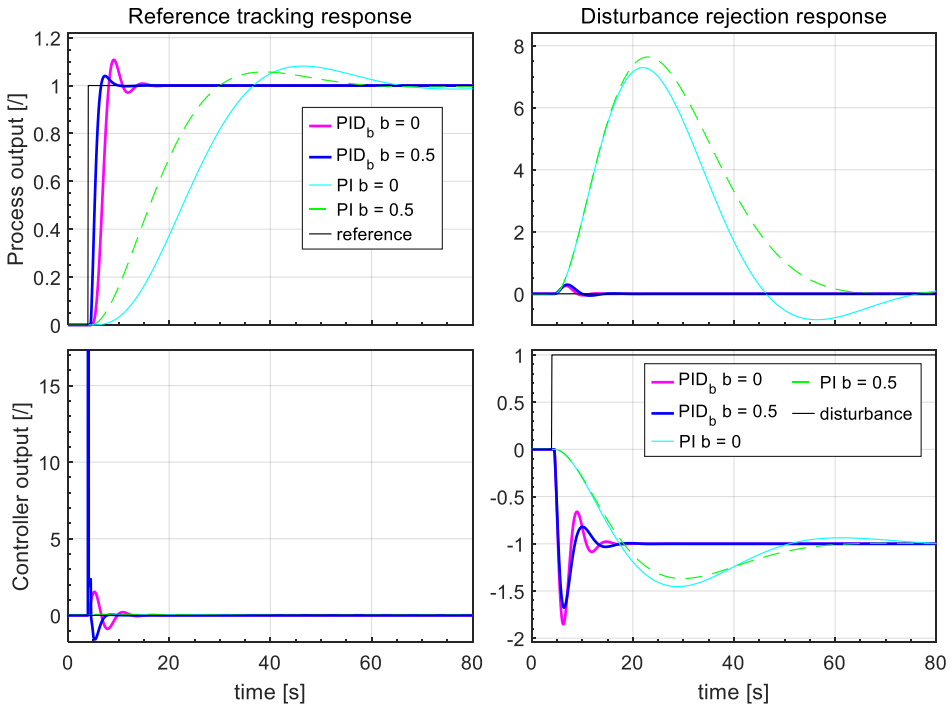

Figure 5.9: The PI and the PID_b controller closed-loop responses for process G_{P1}. Note that, for clarity, the controller output response is zoomed in for the reference step change.

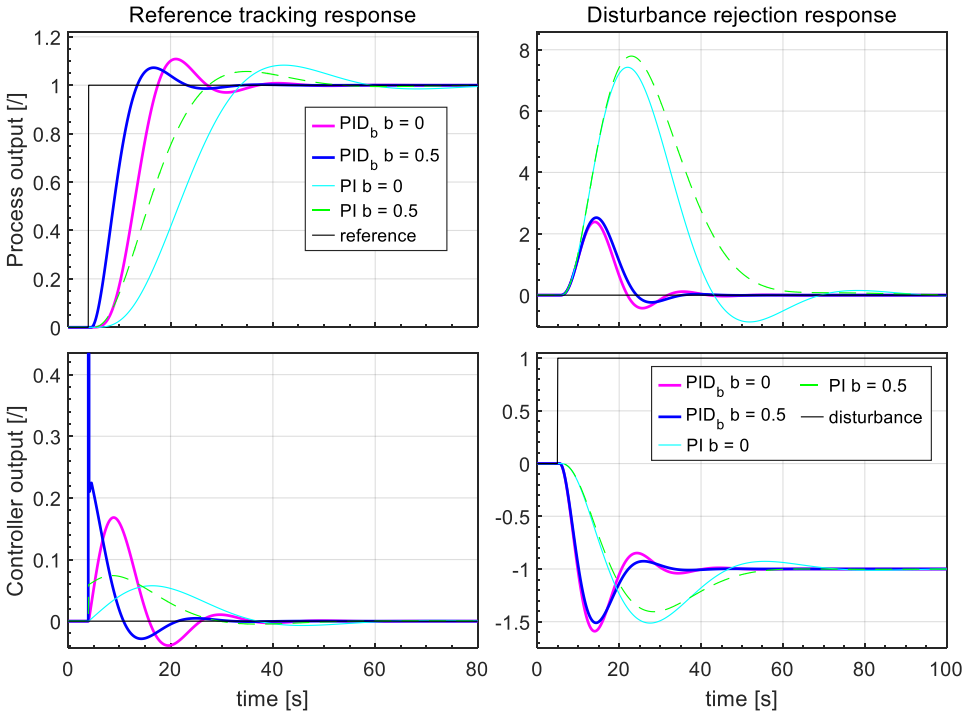

Figure 5.10: The PI and the PID_b controller closed-loop responses for process G_{P2}. Note that, for clarity, the controller output response is zoomed in for the reference step change.

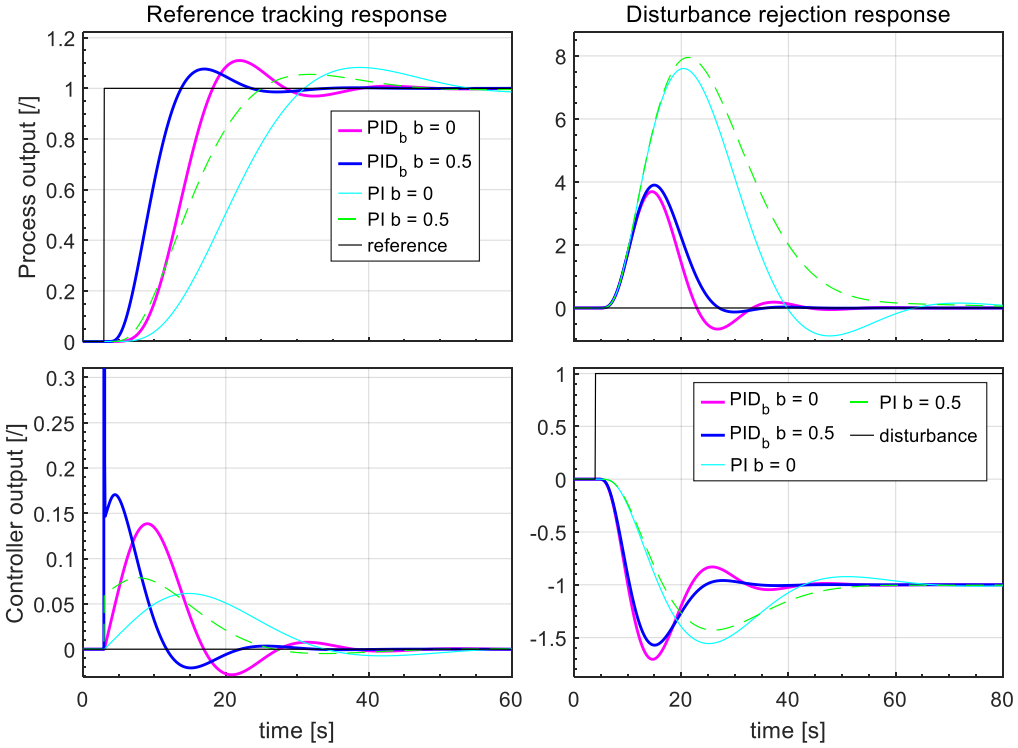

Figure 5.11: The PI and the PID_b controller closed-loop responses for process G_{P3}. Note that, for clarity, the controller output response is zoomed in for the reference step change.

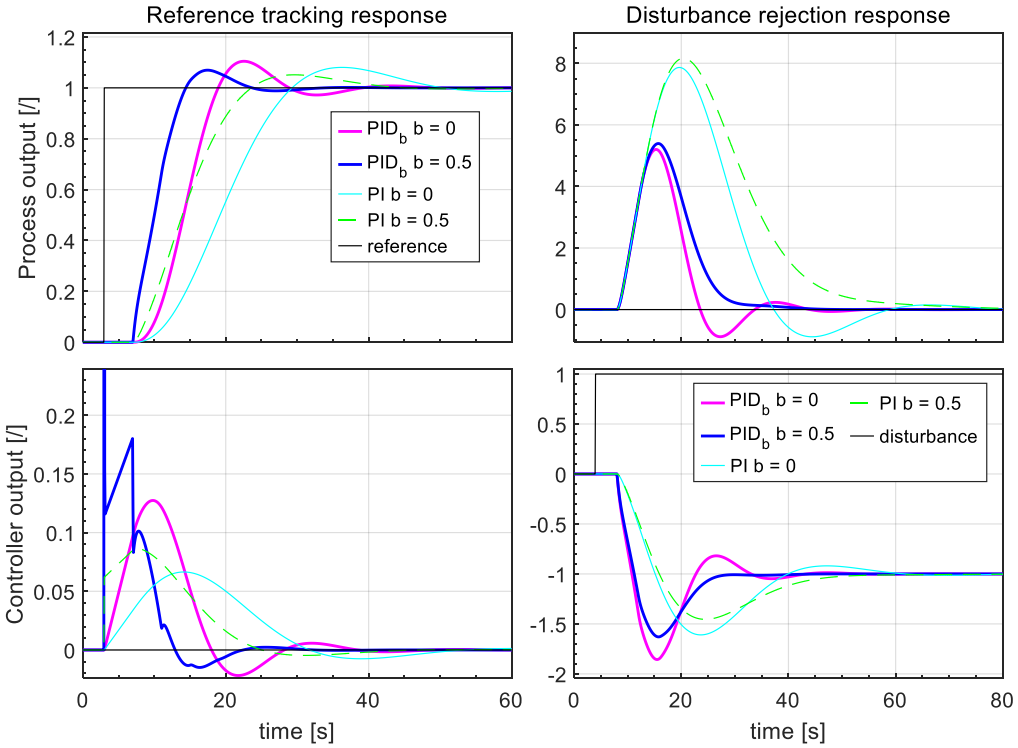

Figure 5.12: The PI and the PID_b controller closed-loop responses for process G_{P4}. Note that, for clarity, the controller output response is zoomed in for the reference step change.

5.7 Comparison of PID_f and PID_b Performance

Besides using reference weighting factor b, the 2-DOF controller can also be implemented using a PID with an additional reference filter (see Chapter 5.4).

Here, the proposed PID_b controller is compared with the proposed PID_{f2} and PID_{fh} controllers. The same process models, as in Chapter 5.5 (5.45), are used for this purpose.

The selected controller filter time constant was the same as before ($T_F = 0.01$ s). Characteristic areas A_{0F}–A_{4F} (with filter time constant) are given in Table 5.7. The PID_b controller parameters calculated with different values of b are given in Table 5.8. Note that for the PID_{f2} and PID_{fh} controllers, the proportional, integral, and derivative gains for PID_b with $b = 0$ were used.

The reference filter parameters for the PID_{f2} and PID_{fh} controllers were calculated from Equation (5.31) (PID_{f2} controller) and Equation (5.43) (PID_{fh} controller) using calculated characteristic areas A_0–A_4 (without filter time constant) from Table 5.6 and the calculated PID_b controller parameters ($b = 0$) from Table 5.8. The values of the PD controller parameters, the estimated second-order process model parameters, and the selected speed-up coefficients are shown in Table 5.13. The calculated reference filter parameters for the PID_{f2} and PID_{fh} controllers are given in Tables 5.14 and 5.15, respectively.

Table 5.13: The intermediate calculated parameters for the reference filters calculations.

Process	K_{P1}	K_{D1}	K_M	b_{1m}	T_{dm}	a_{1m}	a_{2m}	K_{CL}
G_{P1}	1.2651	1.2838	1	0	0.2	1.2	0.2	3
G_{P2}	0.74265	0.25007	1	0	1	0.0101	0	3
G_{P3}	0.249005	0.498512	1	0	0.935822	3.06418	2.69459	3
G_{P4}	0.193831	0.277263	1	−1.99879	0.011	1.99021	0.982906	3

Table 5.14: The PID_{f2} controller reference filter parameters.

Process	b_{F2}	b_{F1}
G_{P1}	0.59091	1.0871
G_{P2}	0.52881	1.0284
G_{P3}	9.2833	4.3089
G_{P4}	5.3174	3.2611

Table 5.15: The PID_{fh} controller reference filter parameters.

Process	b_{F5}	b_{F4}	b_{F3}	b_{F2}	b_{F1}	T_{dm}	T_{CL}	n
G_{P1}	0.019465	0.24389	0.83779	1.5782	1.7776	0.2	0.26348	2
G_{P2}	0.0036331	0.25639	0.93567	1.716	1.8749	1	0.44884	2
G_{P3}	33.5171	93.952	72.4423	30.8295	7.85696	0.935822	1.33866	2
G_{P4}	0.390273	25.8753	30.9495	18.5847	6.41596	0.011	1.71971	2

Figures 5.13–5.16 show a comparison of the closed-loop responses for the input disturbance step change ($d = 1$) and the reference step change ($r = 1$).

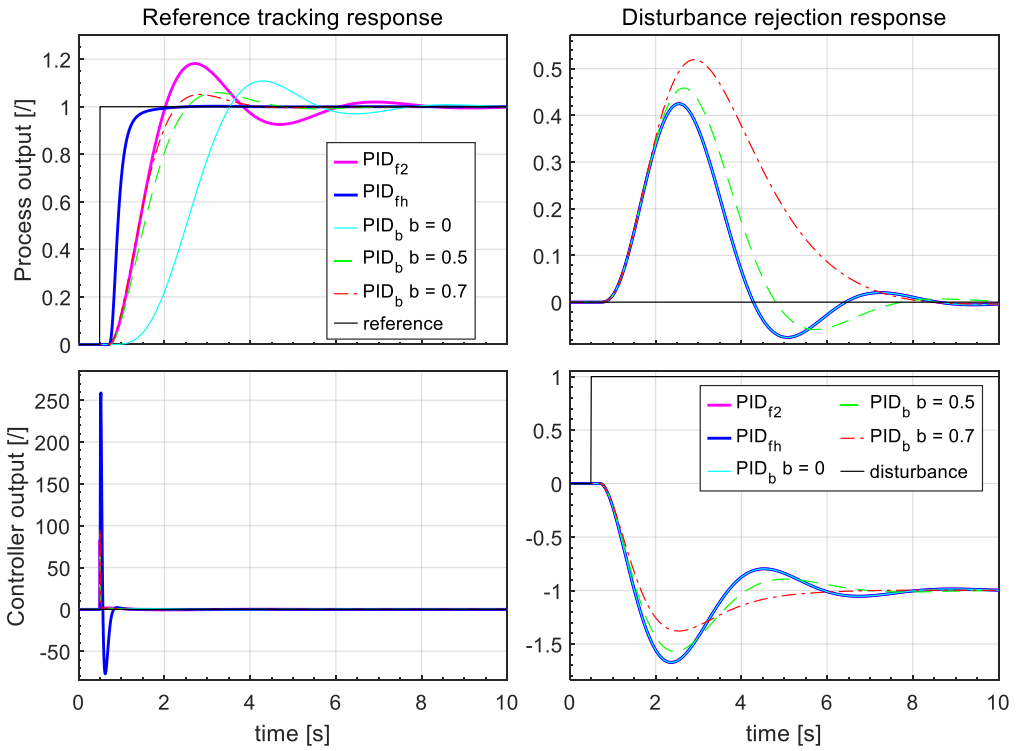

Figure 5.13: The PID_{b}, PID_{f2}, and PID_{fh} controllers closed-loop responses for process G_{P1}.

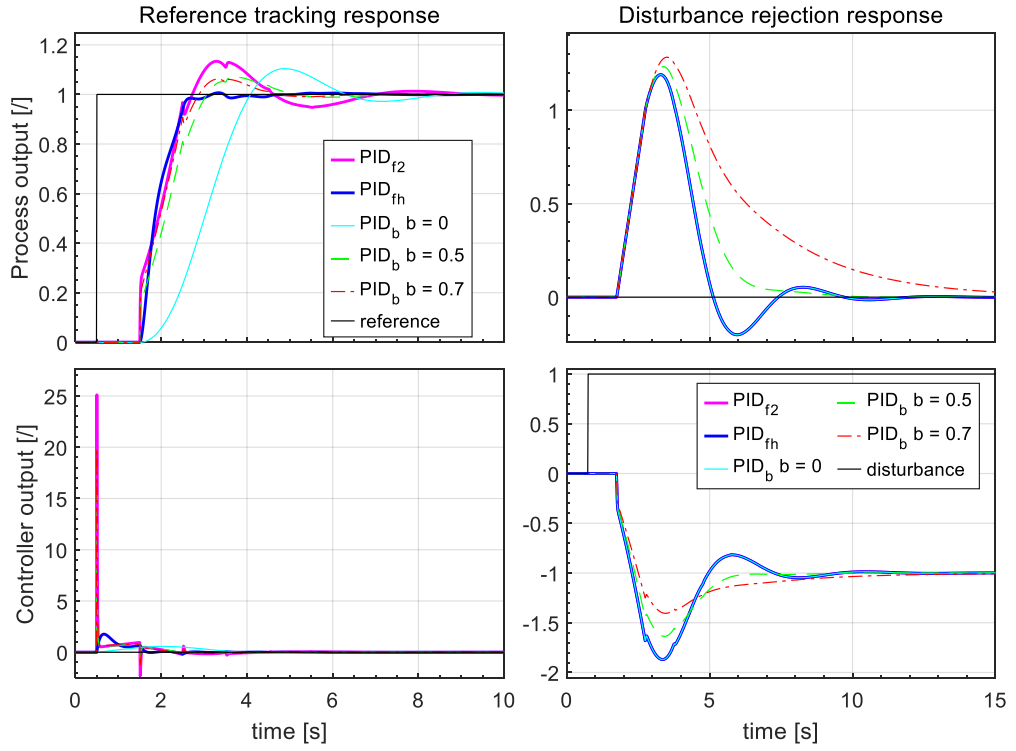

Figure 5.14: The PID_{b}, PID_{f2}, and PID_{fh} controllers closed-loop responses for process G_{P2}.

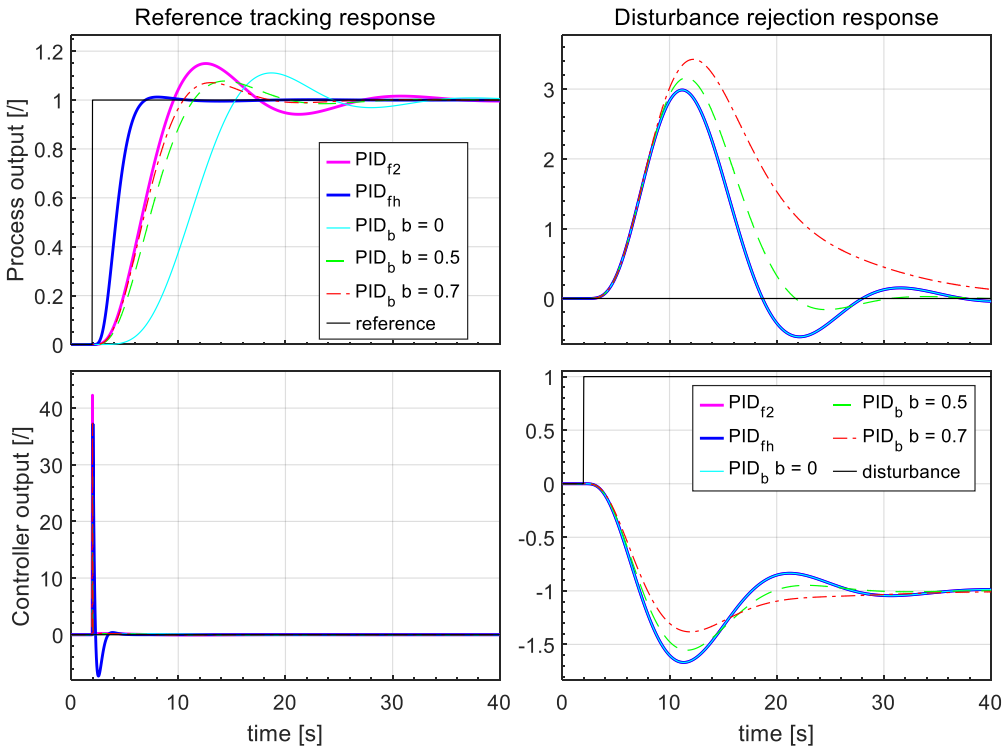

Figure 5.15: The PID_b, PID_{f2}, and PID_{fh} controllers closed-loop responses for process G_{P3}.

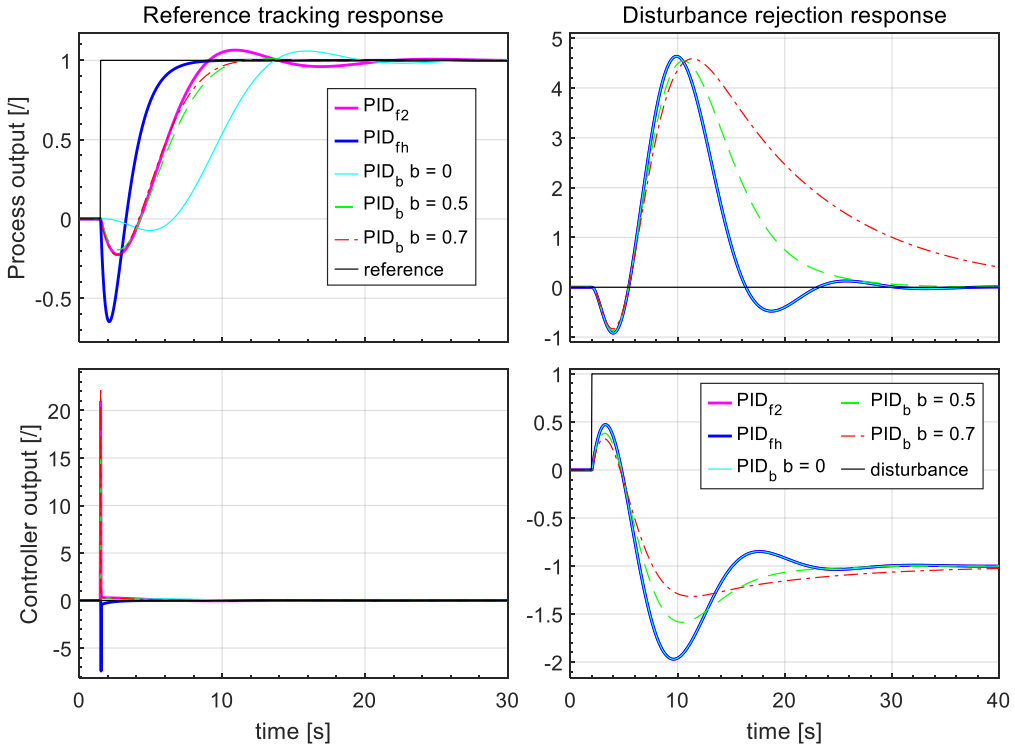

Figure 5.16: The PID_b, PID_{f2}, and PID_{fh} controllers closed-loop responses for process G_{P4}.

The comparison shows the superior tracking abilities of the PID_{f2} and PID_{fh} controllers. The tracking speed of the PID_{fh} controller is significantly larger than that of the other methods. Note that the disturbance rejection of the PID_{f2} and PID_{fh} controllers is equivalent to that of the PID_{b} controller with $b = 0$. Therefore, it can be concluded that the proposed tuning method for the PID_{f2} and PID_{fh} controller gives the best overall performance (optimal tracking and disturbance-rejection).

Chapter 6

Stability, Robustness and Noise Sensitivity

Part of this chapter was originally published in Kos, T. et al., Applied Sciences (2020), 10: 4, and T. Kos et al., Applied Sciences (2020), 10: 17.

In this chapter, the stability, robustness and noise sensitivity of the proposed tuning methods are investigated. First, the stability of the proposed tuning method is analysed. As shown, areas can be identified from a closed-loop or open-loop time response (in the time-domain) or directly from an arbitrary rational transfer function with a pure time delay (in the frequency domain). Therefore, robustness (frequency-domain) and noise sensitivity (time-domain) are investigated next.

6.1 Stability

In general, the stability of the closed-loop system can be calculated from the roots of the denominator (den_{CL}) of the closed-loop transfer function:

$$G_{\mathrm{CL}} = \frac{G_{\mathrm{P}} G_{\mathrm{CR}}}{1 + G_{\mathrm{P}} G_{\mathrm{CY}}} = \frac{num_{\mathrm{CL}}}{den_{\mathrm{CL}}}, \tag{6.1}$$

where

$$\begin{gathered} den_{\mathrm{CL}} = s(1 + a_1 s + a_2 s^2 + \cdots)(1 + sT_{\mathrm{F}})e^{sT_{\mathrm{delay}}} + \\ +(1 + b_1 s + b_2 s^2 + \cdots)(K_{\mathrm{D}} s^2 + K_{\mathrm{P}} s + K_{\mathrm{I}}) \end{gathered} \tag{6.2}$$

for the PID controller, and

$$den_{\mathrm{CL}} = s(1 + a_1 s + a_2 s^2 + \cdots)e^{sT_{\mathrm{delay}}} + (1 + b_1 s + b_2 s^2 + \cdots)(K_{\mathrm{P}} s + K_{\mathrm{I}}) \tag{6.3}$$

for the PI controller.

As can be seen, the denominator consists of a pure time delay, which complicates the stability analysis. The time delay in den_{CL} (6.2) and (6.3) can be developed into an infinite-order Taylor or Padé series. However, the analysis of the infinite-order series, e.g., using the Routh–Hurwitz stability criterion, is far from straightforward and beyond our research scope.

However, the stability and robustness of the closed-loop systems can be tested on process models covering most IPs in different industries.

One such process model is the second-order IP with a time delay:

$$G_{\mathrm{P}}(s) = \frac{K_{\mathrm{PR}} e^{-T_{\mathrm{delay}} s}}{s(1 + a_1 s + \alpha a_1^2 s^2)}. \tag{6.4}$$

Note that process $G_{\mathrm{P}}(s)$ (6.4) also covers pure time delay and pure first-order IPs. The stability and robustness of the closed-loop system are tested with different ratios of T_{delay}/a_1 and factor α. Note that this process has real poles only when $\alpha \leq 0.25$.

The closed-loop system's robustness was tested by measuring the maximum sensitivity function, Ms [18], [223], [224]. A higher value of Ms indicates a lower robustness of the system, since open-loop transfer function $G_{\mathrm{P}} G_{\mathrm{CY}}$ is closer to the critical point $(-1 + 0\mathrm{i})$. The most common values of Ms for IPs are usually higher than those for non-integrating processes [18] and typically range from 1.7 to 3.

The stability regions for the PI controller are shown in Figure 6.1. The system is stable for all processes with real process poles for $b = 0$, $b = 0.5$, and $b = 0.9$. Increasing factor b has a positive effect on system stability. This system is stable for any time delay when $\alpha \leq 0.88$ for $b = 0$, when $\alpha \leq 1.08$ for $b = 0.5$, and $\alpha \leq 1.73$ with $b = 0.9$. The overall stability improves by increasing the time delay or increasing b and decreasing factor α.

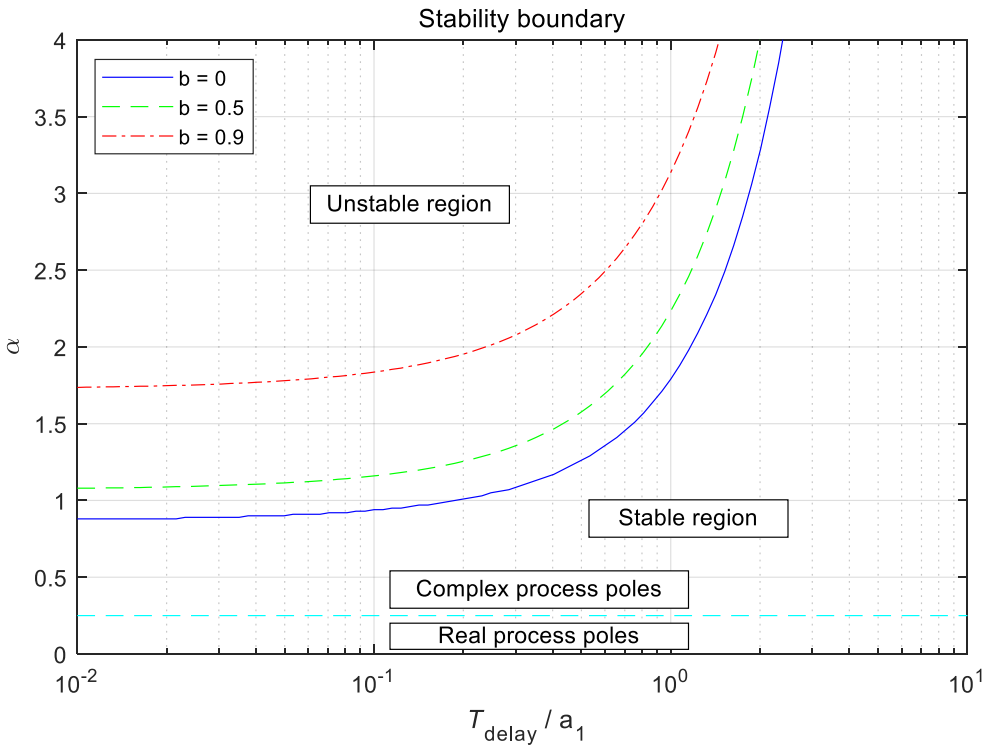

Figure 6.1: Stability region for process $G_{\mathrm{P}}(s)$ at different values of T_{delay}/a_1, α, and reference weighting factor b.

The maximum sensitivity functions are calculated for different values of b (0, 0.5, and 0.9) and are shown in Figures 6.2–6.4. Note that the Ms values for processes with real poles are below 2.4 for $b = 0$, below 2 for $b = 0.5$, and below 1.7 for $b = 0.9$. Thus, the expected robustness of the closed-loop is satisfactory and relatively high for the processes with real poles. Processes with complex poles lead to lower robustness, which is to be expected.

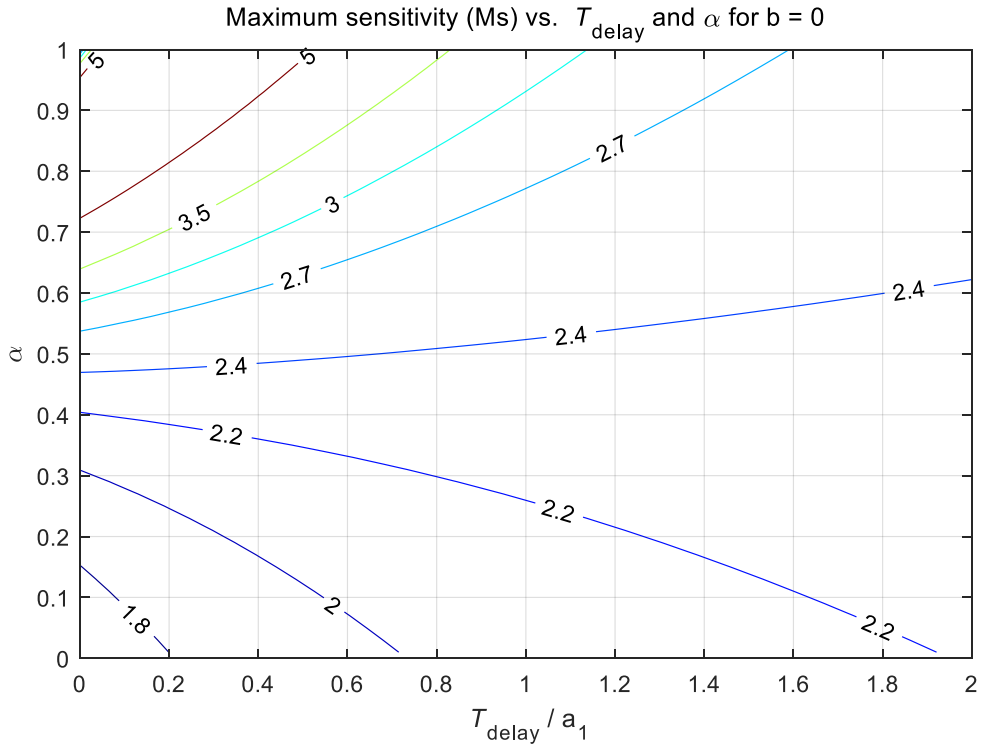

Figure 6.2: The values of Ms for $G_{\mathrm{P}}(s)$ and PI controller parameter $b = 0$ at different values of T_{delay} and α.

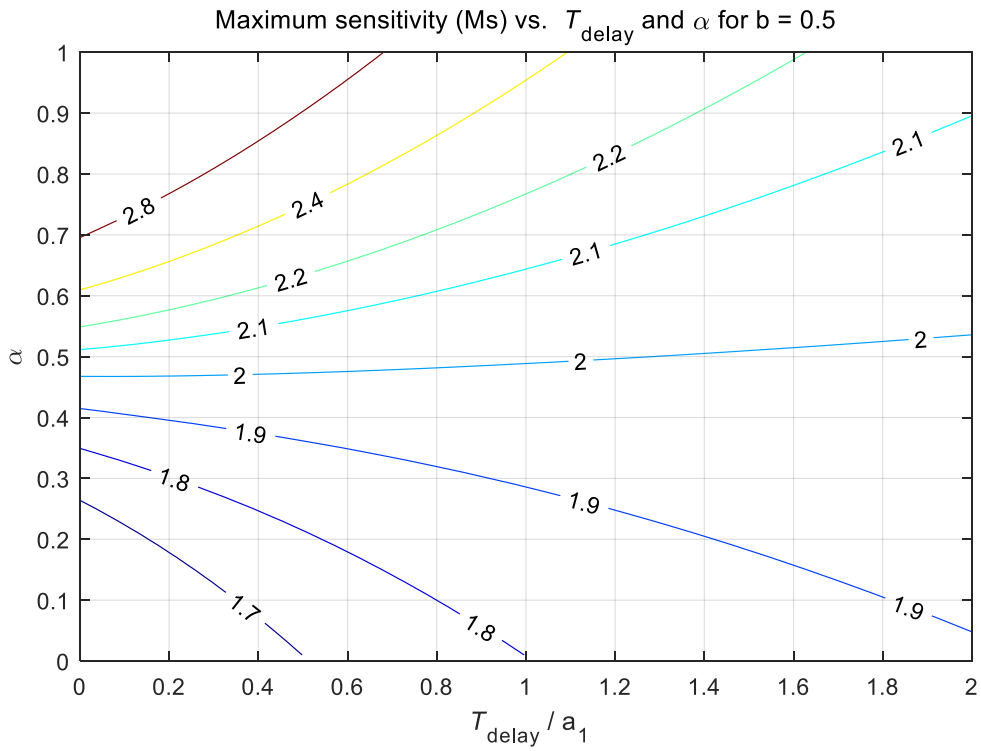

Figure 6.3: The values of Ms for $G_{\mathrm{P}}(s)$ and PI controller parameter $b = 0.5$ at different values of T_{delay} and α.

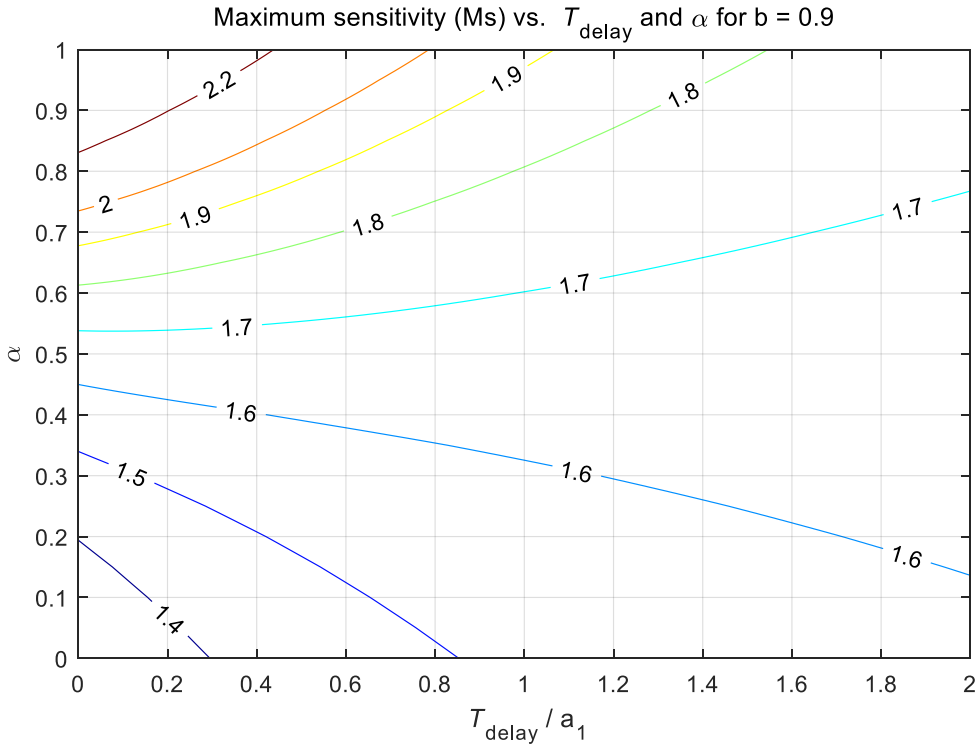

Figure 6.4: The values of Ms for $G_P(s)$ and PI controller parameter $b = 0.9$ at different values of T_{delay} and α.

The closed-loop stability, when using the PID controllers, is somehow changed. When the PID_b controller reference weighting factor is $b = 0$, the closed-loop system is stable for all positive values of α and T_{delay}. The system is also stable for all processes with real process poles for any b ($b = 0$, 0.5 and 0.9). As shown in Figure 6.5, increasing factor b has a negative effect on the system stability. The system is stable for any time delay with $b = 0.5$ when $\alpha \leq 1.5$, and $\alpha \leq 1.05$ when using $b = 0.9$. The overall stability improves by increasing the time delay or decreasing b and factor α.

The maximum sensitivity functions are calculated for different values of b (0, 0.5, and 0.9) and are shown in Figures 6.6–6.8. Note that the Ms values for processes with real poles are below 3.15 for $b = 0$, below 2.45 for $b = 0.5$, and below 1.85 for $b = 0.9$. Thus, the expected robustness of the closed-loop system is satisfactory and relatively high for the processes with real poles. As expected, the processes with complex poles lead to lower robustness.

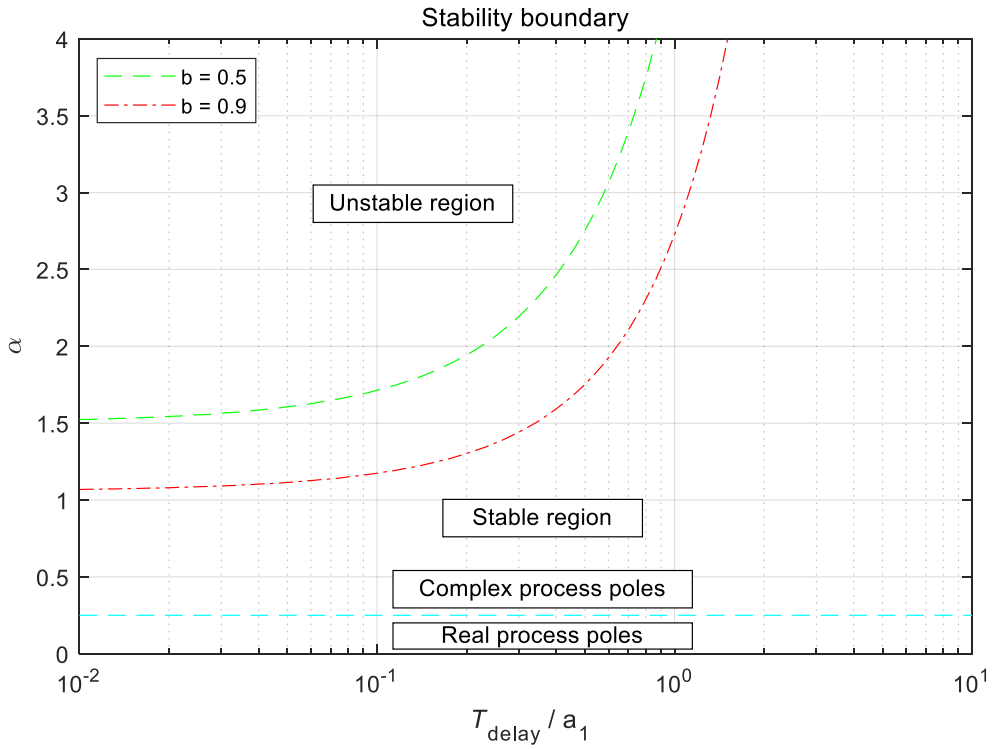

Figure 6.5: Stability region for process $G_{\mathrm{P}}(s)$ at different values of T_{delay}/a_1, α, and reference weighting factor b. Note that the system is stable when $b = 0$.

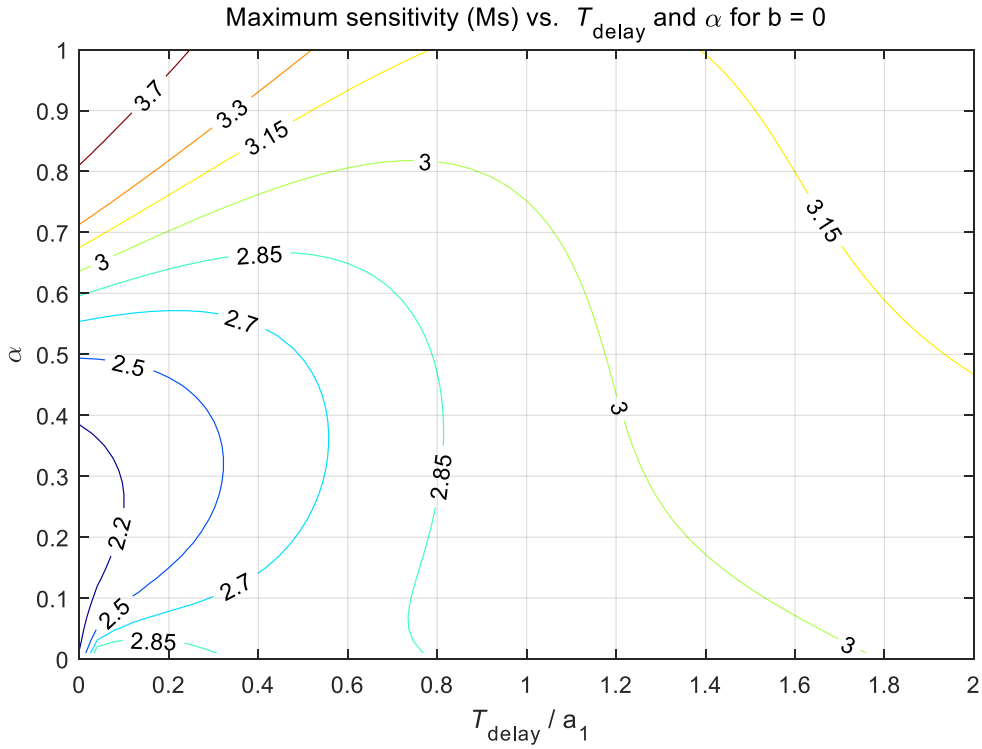

Figure 6.6: The values of Ms for $G_{\mathrm{P}}(s)$ and $\mathrm{PID_b}$ controller parameter $b = 0$ at different values of T_{delay} and α.

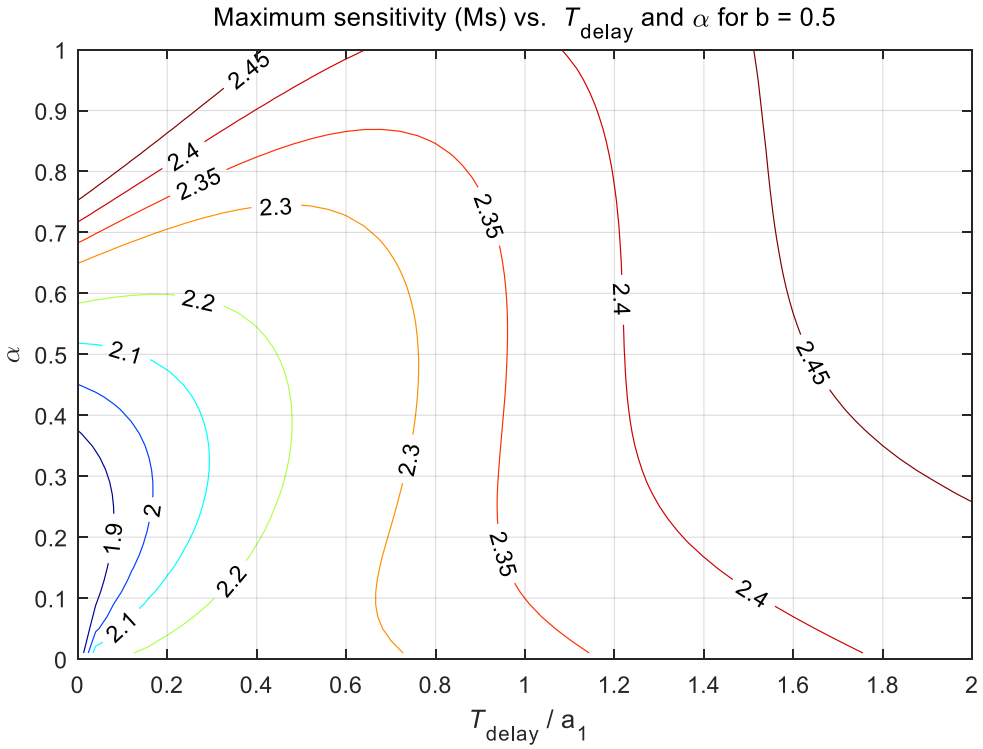

Figure 6.7: The values of Ms for $G_{\mathrm{P}}(s)$ and $\mathrm{PID_b}$ controller parameter $b = 0.5$ at different values of T_{delay} and α.

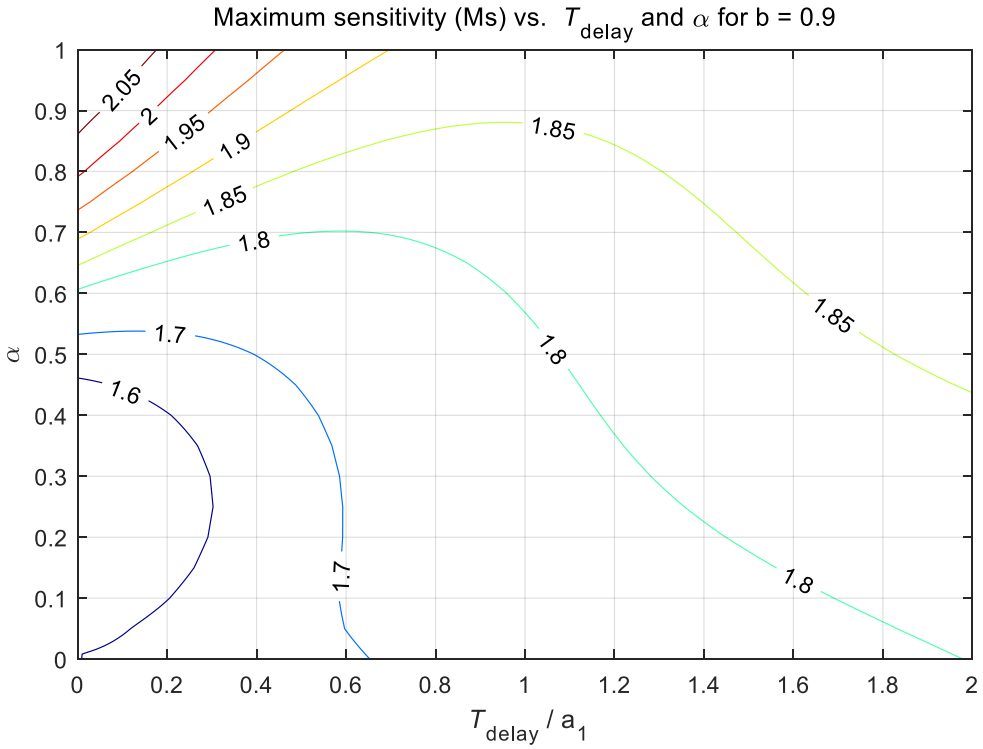

Figure 6.8: The values of Ms for $G_{\mathrm{P}}(s)$ and $\mathrm{PID_b}$ controller parameter $b = 0.9$ at different values of T_{delay} and α.

6.2 Robustness

This subchapter analyses the robustness of the proposed tuning method to the changes of the process steady-state gain, time-constant, and time delay. First, the effect of ± 10% change of the process steady-state gain and time delay on the closed-loop performance was investigated. Then, the maximum sensitivity Ms was measured for ± 20% changes of the process steady-state gain, time-constant, and time delay.

The robustness tests were performed for the following process model:

$$G_{\mathrm{P1}}(s) = \frac{e^{-s}}{s(1+s)^2}. \tag{6.5}$$

Next, PID controller filter time constant $T_{\mathrm{F}} = 0.01$ s was added to the process (6.5). Using Expression (2.8), the following characteristic areas (with and without filter time constant T_{F}) were calculated from the process (6.5) transfer function:

$$A_0 = 1, A_1 = 3, A_2 = 5.5, A_3 = 8.16667, A_4 = 10.875, \tag{6.6}$$

$$A_{0\mathrm{F}} = 1, A_{1\mathrm{F}} = 3.01, A_{2\mathrm{F}} = 5.5301, A_{3\mathrm{F}} = 8.22197, A_{4\mathrm{F}} = 10.9572. \tag{6.7}$$

First, the robustness of the proposed PI tuning method for the process model (6.5) is investigated. For this purpose, the PI controller parameters for reference weighting factors $b = 0.5$ and $b = 0$ were calculated using Expressions (4.4) and (4.6), as well as characteristic areas A_0–A_2(6.6):

$$\begin{aligned} &b = 0, K_{\mathrm{P}} = 0.18708, K_{\mathrm{I}} = 0.0175, \\ &b = 0.5, K_{\mathrm{P}} = 0.181, K_{\mathrm{I}} = 0.012285. \end{aligned} \tag{6.8}$$

The calculated parameters were applied to the PI controller. Robustness was examined by assuming a ± 10% change of the process steady-state gain and time delay (6.5). Figures 6.9 and 6.10 show the responses on the input disturbance step change ($d = 1$) and the reference step change ($r = 1$) for the PI controller with $b = 0$ and $b = 0.5$, respectively.

As can be seen from the process output responses, a change in the process gain or time delay has no significant influence on the tracking and disturbance-rejection performance. Nevertheless, the controller is slightly more sensitive to process gain perturbations.

Next, the closed-loop system robustness was tested by measuring the maximum sensitivity Ms for the perturbated process model (6.5). The calculated parameters (6.8) were applied to the PI controller. Then, the maximum sensitivity Ms was measured for a ± 20% change of the process steady-state gain, time-constant, and time delay. Figures 6.11 and 6.12 show the corresponding Ms values for the PI controller with $b = 0$ and $b = 0.5$, respectively. As can be seen from the figures, the closed-loop robustness deteriorates with positive process parameters change, i.e., Ms is the highest when the corresponding process parameters change for + 20%. The phenomenon is more pronounced for the PI controller with $b = 0$.

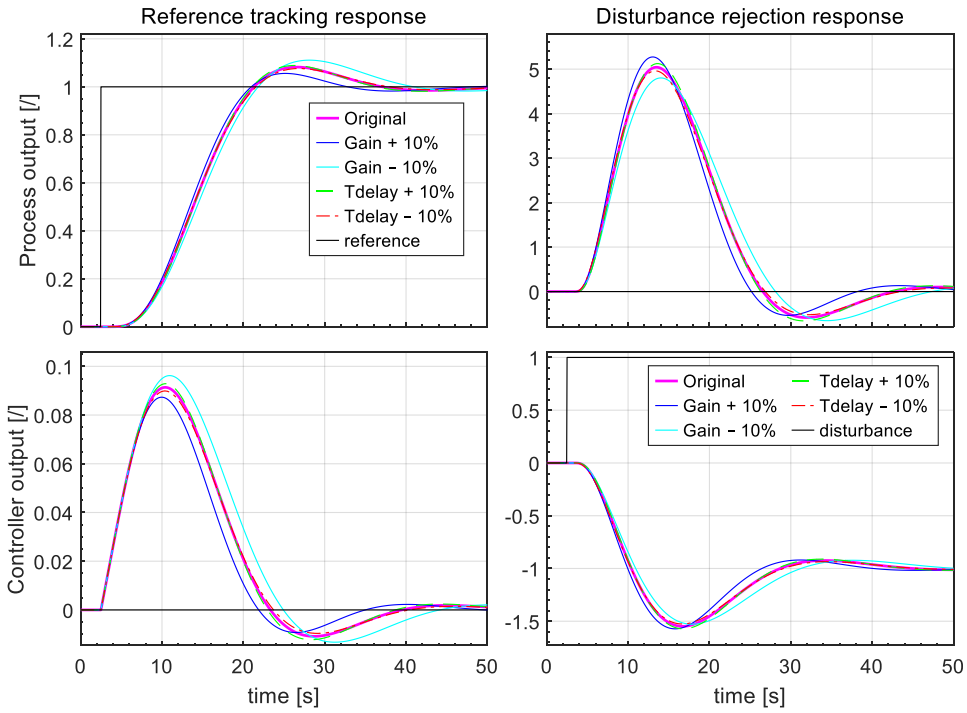

Figure 6.9: The frequency-domain robustness test for the PI controller with $b = 0$. The responses are for a process steady-state gain and time-delay parameter perturbation of $\pm$ 10%.

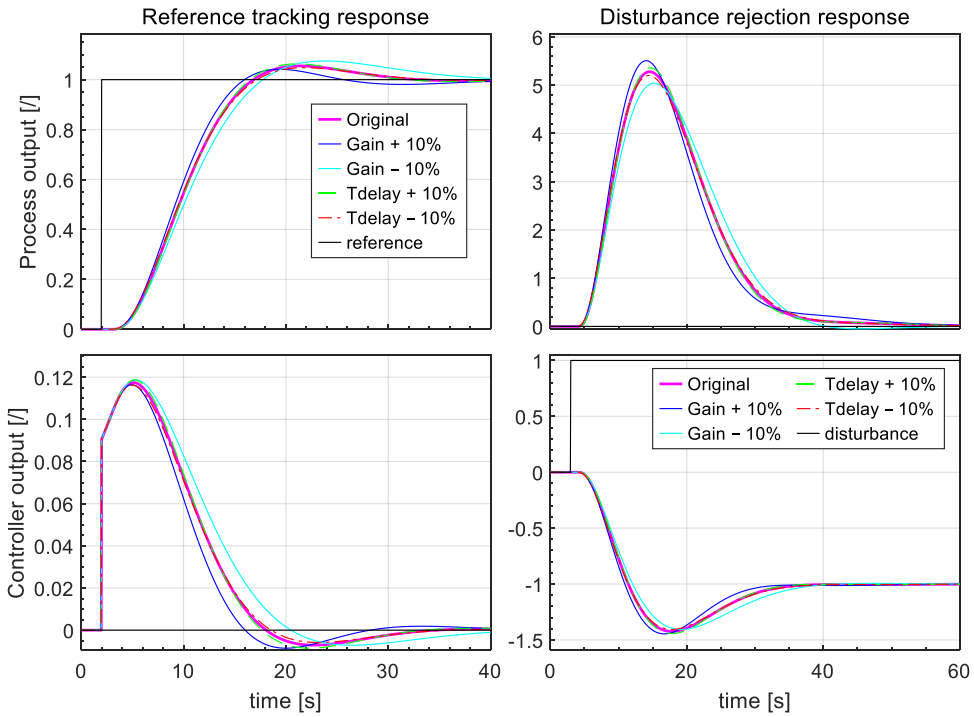

Figure 6.10: The frequency-domain robustness test for the PI controller with $b = 0.5$. The responses are for a process steady-state gain and time-delay parameter perturbation of $\pm$ 10%.

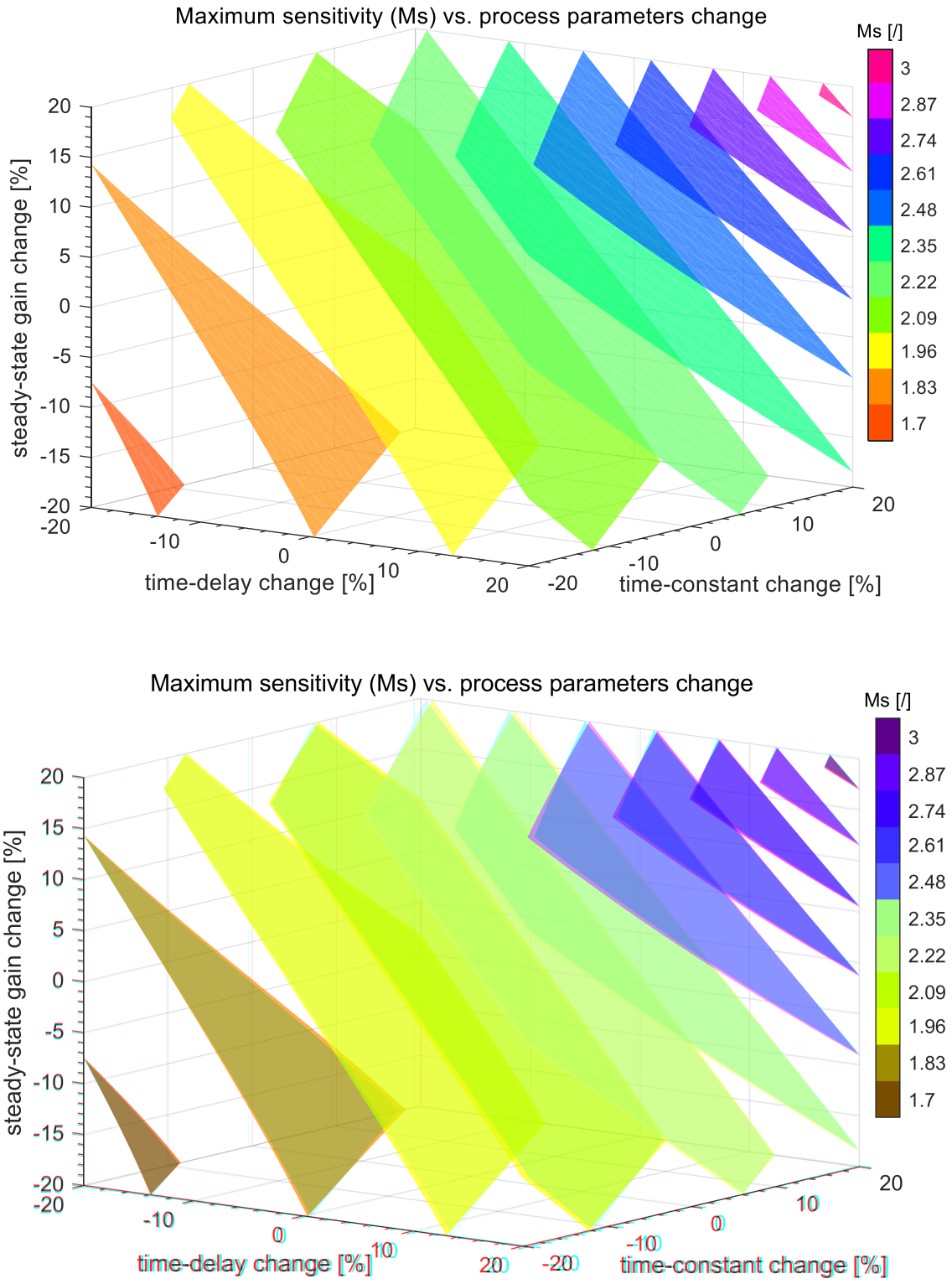

Figure 6.11: Contour plots of Ms for $G_{\mathrm{PI}}(\mathrm{s})$ and PI controller parameter $b = 0$. Values are for the process parameters perturbation of $\pm$ 20%. Nominal Ms = 2.1014. The lower figure shows an anaglyph (3D) representation of the upper figure (can be seen with red-cyan glasses).

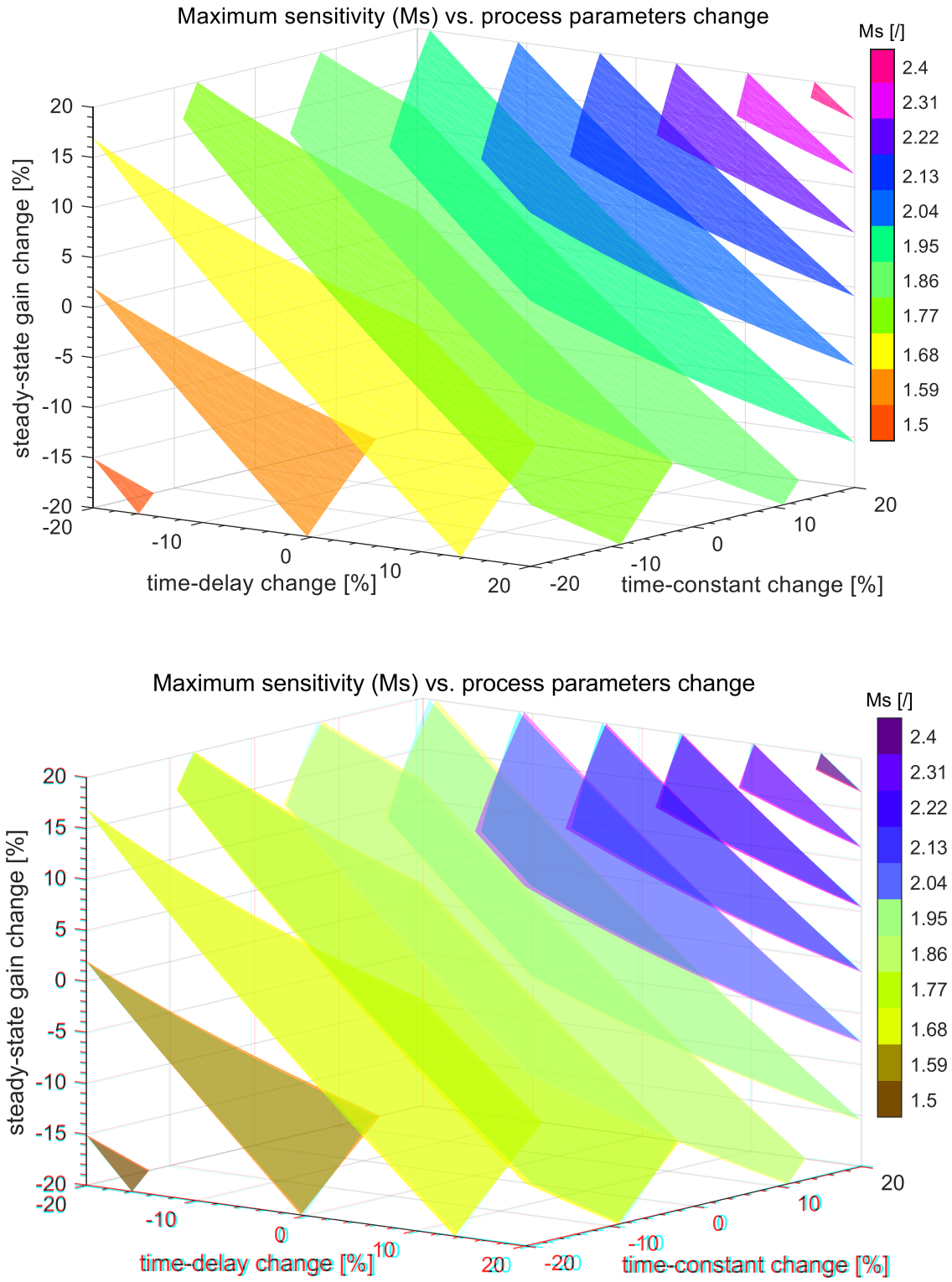

Figure 6.12: Contour plots of Ms for $G_{P1}(s)$ and PI controller parameter $b = 0.5$. Values are for the process parameters perturbation of $\pm$ 20%. Nominal Ms = 1.8215. The lower figure shows an anaglyph (3D) representation of the upper figure (can be seen with red-cyan glasses).

Next, the robustness of the proposed PID tuning method (PID_b and PID_fh controllers) is investigated for the process model (6.5). For this purpose, the parameters of the PID_b controller for $b = 0.5$ and $b = 0$ were calculated by using Expressions (5.10), (5.13) and (6.7):

$$\begin{array}{c} b = 0.5, K_\text{P} = 0.46336, K_\text{I} = 0.062992, K_\text{D} = 0.5563, \\ b = 0, K_\text{P} = 0.51394, K_\text{I} = 0.083446, K_\text{D} = 0.58265. \end{array} \tag{6.9}$$

In addition, the parameters of the PID_fh controller reference filter were calculated using Expression (5.43) (for chosen $K_\text{CL} = 3$) and characteristic areas A_0–A_4 (6.6):

$$\begin{array}{c} b_{\text{F5}} = 8.2389, b_{\text{F4}} = 25.8477, b_{\text{F3}} = 27.1014, b_{\text{F2}} = 15.97, b_{\text{F1}} = 5.6589, \\ T_\text{dm} = 1, T_\text{CL} = 1.0155, n = 2. \end{array} \tag{6.10}$$

The calculated parameters were applied to the PID_b and PID_fh controllers. Robustness was examined by assuming a ± 10% change in the steady-state gain and time delay of the process (6.5). Figures 6.13 and 6.14 show the corresponding responses on the reference step change ($r = 1$) and the input disturbance step change ($d = 1$) for the PID_b controller with $b = 0.5$ and the PID_fh controller, respectively.

As can be seen from the process output responses, a change in the process gain or time delay has no significant influence on tracking or disturbance-rejection performance. Nevertheless, the PID_fh controller appears to be somewhat more sensitive to process perturbations (especially to increased process gain).

Next, the robustness of the system closed-loop was checked by measuring the maximum sensitivity Ms for the process model (6.5). The calculated parameters (6.9) were applied to the PID_b controller. Then, the maximum sensitivity Ms was measured for ± 20% changes of the process steady-state gain, time-constant, and time delay. Figures 6.15 and 6.16 show the corresponding Ms values for the PID_b controller with $b = 0$ and $b = 0.5$, respectively. As shown in the figures, the closed-loop robustness deteriorates with positive process parameters change, i.e., Ms is the highest when the corresponding process parameters change for + 20%. The phenomenon is more pronounced for PID_b controller with $b = 0$.

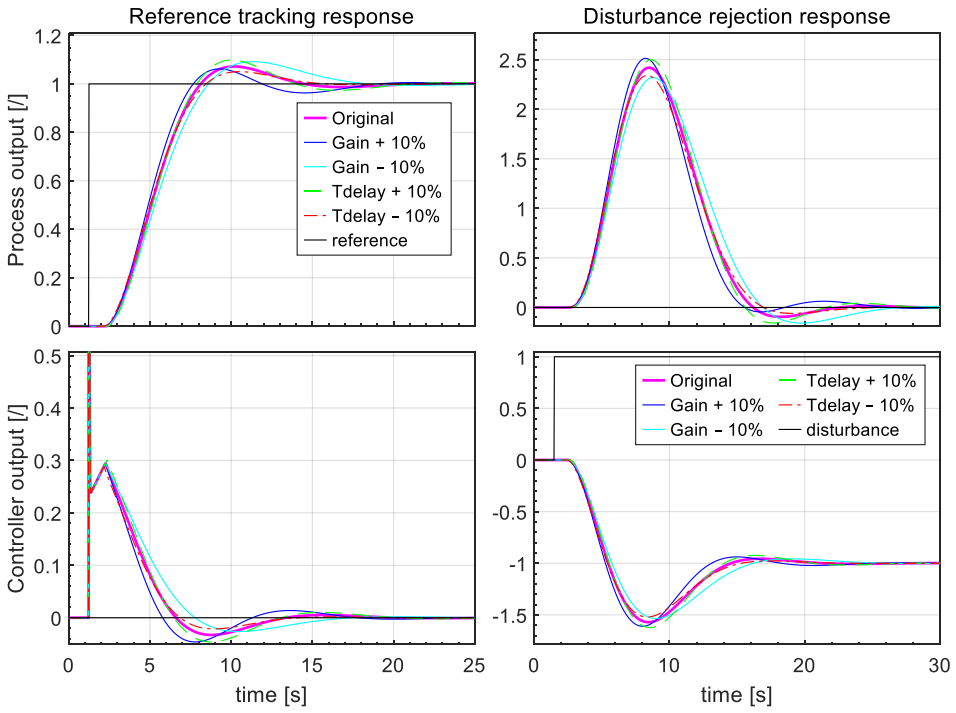

Figure 6.13: The frequency-domain robustness test for the PID_b controller with $b = 0.5$. The responses are for a process steady-state gain and time-delay parameter perturbation of $\pm$ 10%. Note that, for clarity, the controller output response is zoomed in for the reference step change.

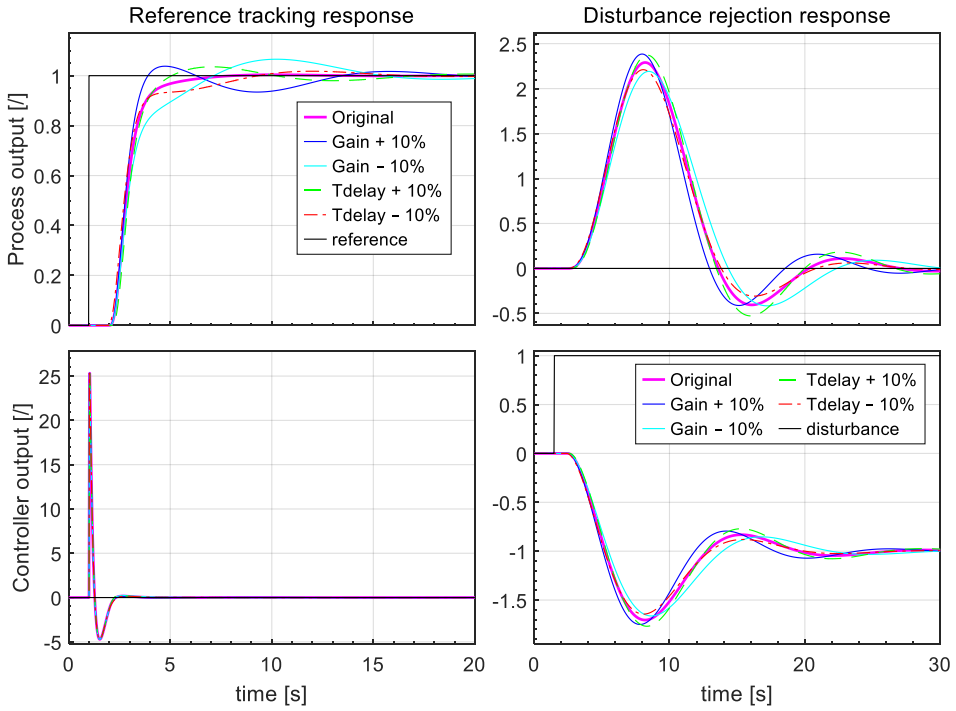

Figure 6.14: The frequency-domain robustness test for the PID_fh controller. The responses are for a process steady-state gain and time-delay parameter perturbation of $\pm$ 10%.

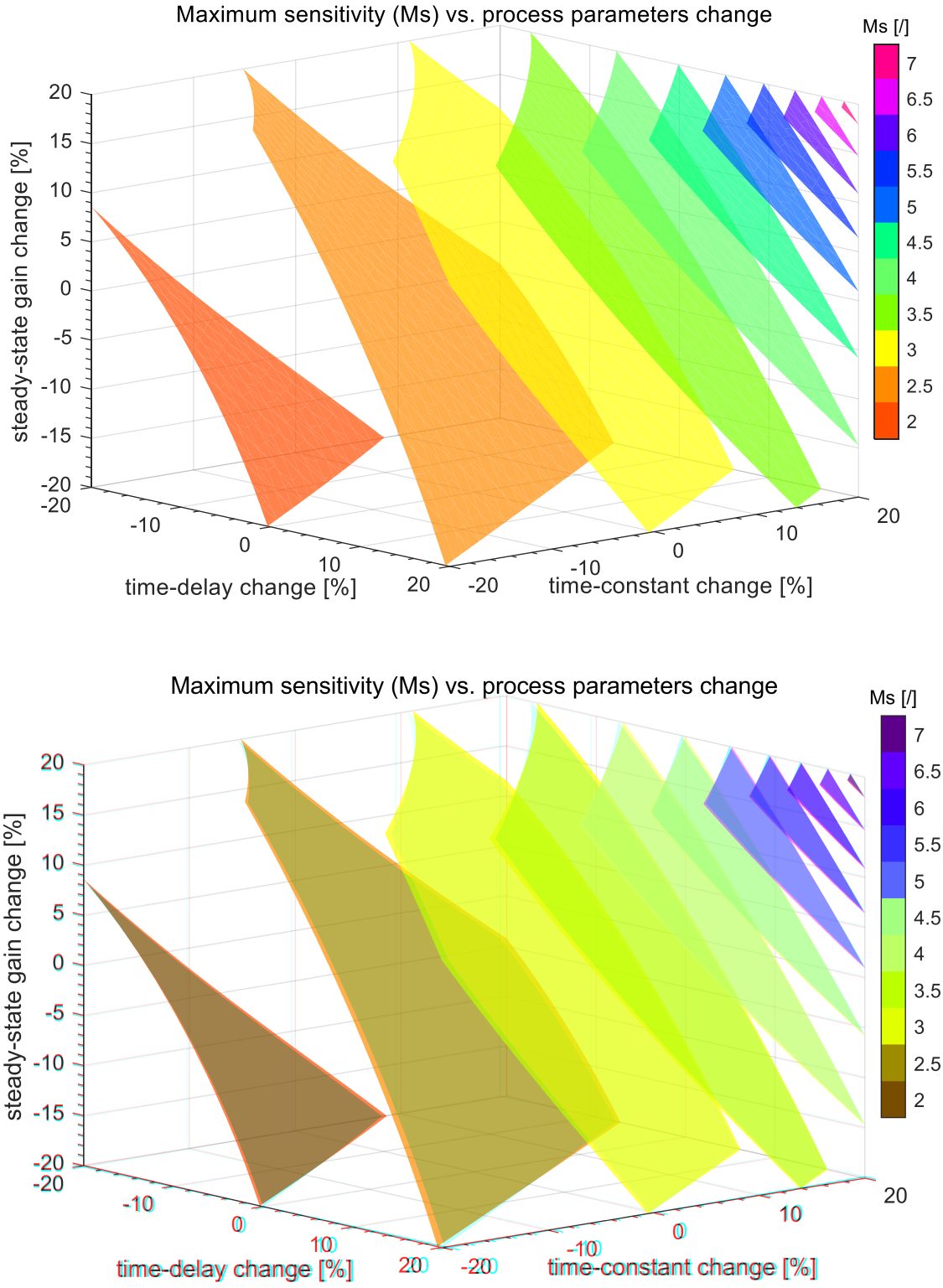

Figure 6.15: Contour plots of Ms for $G_{P1}(s)$ and PID_b controller parameter $b = 0$. Values are for the process parameters perturbation of $\pm$ 20%. Nominal Ms = 2.6858. The lower figure shows an anaglyph (3D) representation of the upper figure (can be seen with red-cyan glasses).

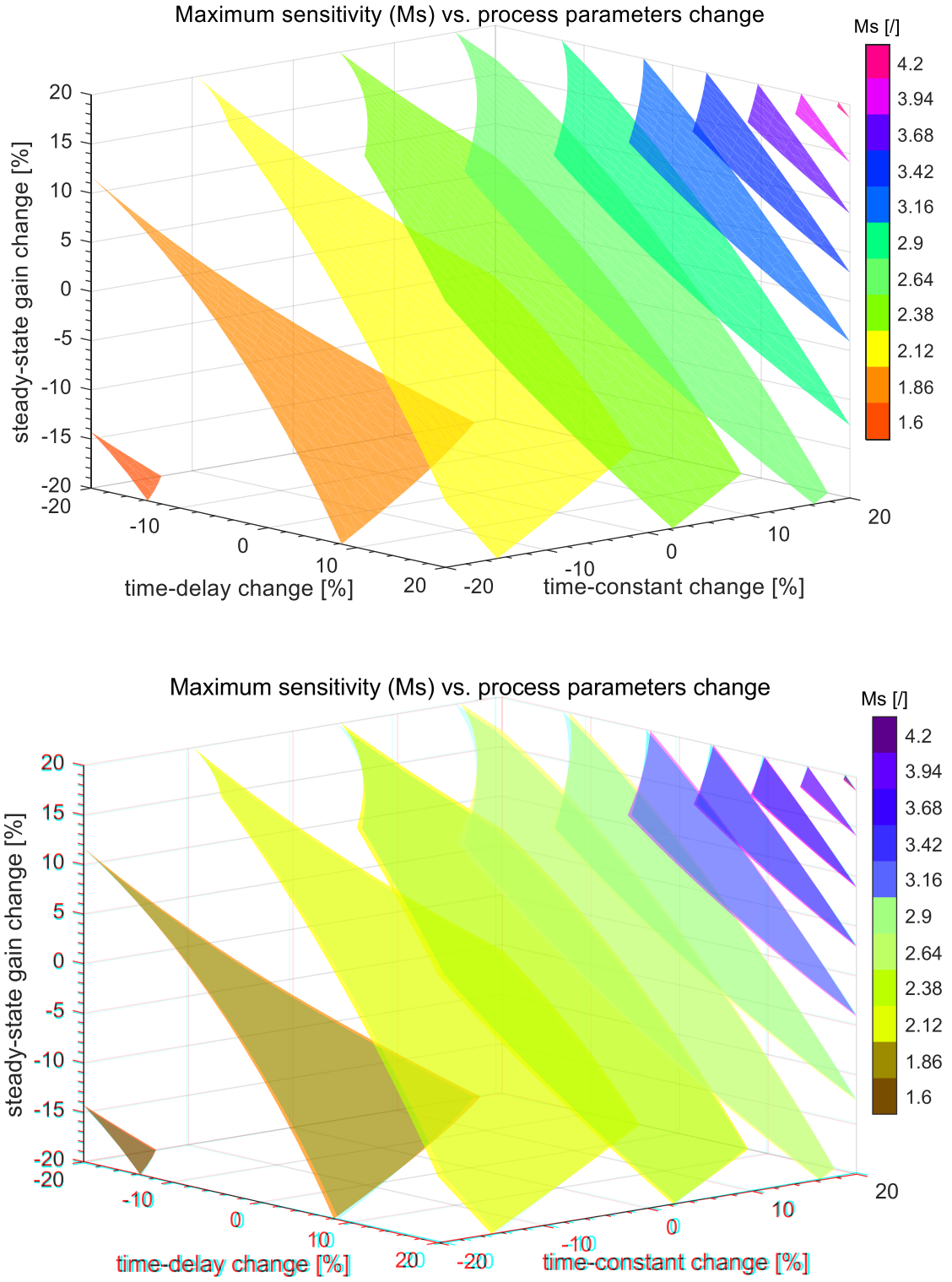

Figure 6.16: Contour plots of Ms for $G_{P1}(s)$ and PID_b controller parameter $b = 0.5$. Values are for the process parameters perturbation of $\pm$ 20%. Nominal Ms = 2.2288. The lower figure shows an anaglyph (3D) representation of the upper figure (can be seen with red-cyan glasses).

6.3 Noise Sensitivity

In this subchapter, the noise sensitivity of the calculated characteristic areas from the open-loop time-responses on the process is analysed. The robustness tests were performed on the process model (6.5). Nominal characteristic areas A_0–A_4, calculated with Expression (2.8), are given in (6.6).

First, the influence of high-frequency noise on the computation of the characteristic areas was investigated. The process time response with normally distributed random noise (MATLAB function randn) with an amplitude level of 0.1 is shown in Figure 6.17. Note that times t_0–t_3 (at 2, 8, 14 and 22 s) are marked with dashed lines in the figure.

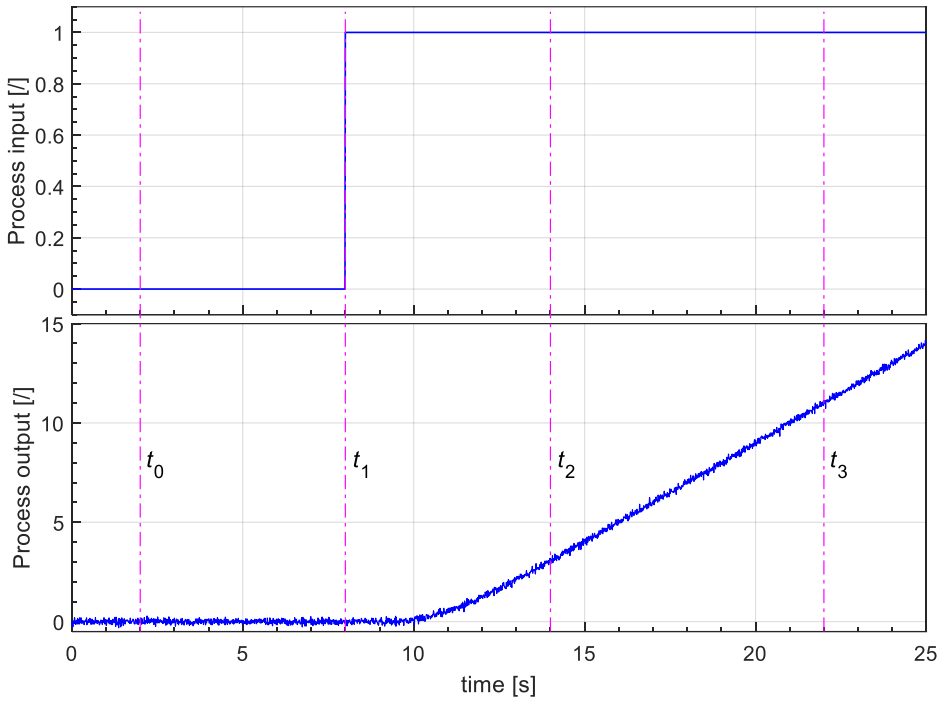

Figure 6.17: The $G_{P1}(s)$ open-loop response with normally distributed random noise with an amplitude level of 0.1.

At time t_1, a step-change was applied to the process input. The process output reached a constant rate of change at time t_2. Therefore, the process signals at time intervals t_0–t_1 and t_2–t_3 were used to obtain the initial and final rates of the process change. The integrations, given in Expressions (2.9), were applied to the process signals at time interval t_1–t_2.

Then, the calculation of the characteristic areas from the process signals with noise was repeated 100 times using Expressions (2.9)–(2.11). The histograms of the calculated areas are shown in Figure 6.18. The blue colour represents the computed areas from the noisy signal (hereafter referred to as *Noise*), and the dashed red lines represent the computed areas without added noise (hereafter referred to as *Without noise, no filtering*). As can be seen from the figure, the noise affects the calculation of the characteristic areas. The phenomenon is more pronounced for higher areas (A_2–A_4) due to the recursive signal integrations. This is confirmed by the standard deviation of the calculated areas shown in Table 6.1.

However, the influence of high-frequency noise on the calculation of the characteristic areas can be reduced by filtering the process input and output signals.

For example, process input and output signals, represented by Figure 6.17, were filtered with the low-pass filter:

$$G_{\mathrm{LP1}} = \frac{1}{1 + T_{\mathrm{F}} s}, \tag{6.11}$$

where

$$T_{\mathrm{F}} = 0.5. \tag{6.12}$$

Subsequently, the calculation of the characteristic areas from the filtered process signals (with the addition of normally distributed random noise) was repeated 100 times. Note that identical time intervals t_0–t_3 were used to calculate the areas. The histograms of the areas calculated from the filtered process time responses (hereafter referred to as *Filtered noise*) are shown in cyan in Figure 6.18. In addition, the dashed black lines represent computed areas from filtered signals without added noise (hereafter referred to as *Without noise, with filtering*). As can be seen from the figure, filtering significantly improves computational precision despite the presence of high-frequency noise. This is confirmed by significantly reduced standard deviation values, which are shown in Table 6.1.

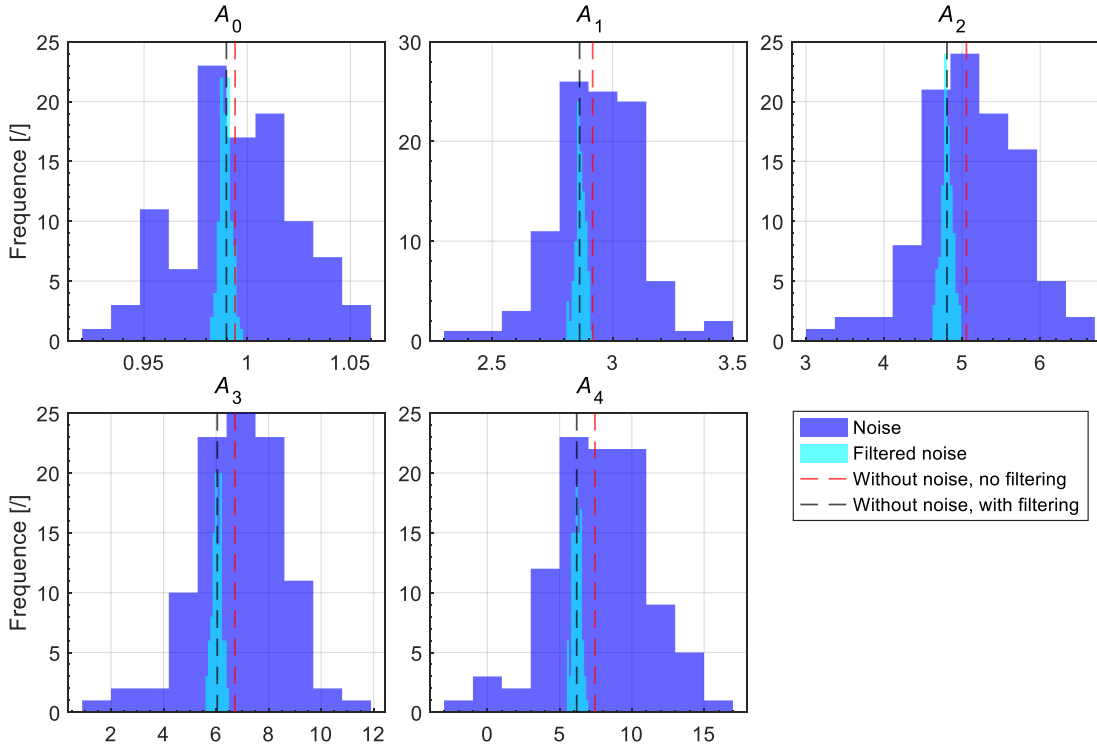

Figure 6.18: Histograms of the calculated characteristic areas for $G_{\mathrm{P1}}(\mathrm{s})$. Normally distributed random noise with an amplitude level of 0.1 was added to the process response.

Table 6.1: Mean and standard deviation of the calculated characteristic areas.

		A_0	A_1	A_2	A_3	A_4
Without noise	no filtering	0.99411	2.9171	5.055	6.7153	7.4451
	with filtering	0.9899	2.8629	4.8059	6.0452	6.1828
Mean	Noise	0.99392	2.93	5.1153	6.8889	7.7874
	Filtered noise	0.98943	2.8651	4.8011	6.0391	6.1817
Standard deviation	Noise	0.027343	0.17445	0.61128	1.7114	3.3378
	Filtered noise	0.0028737	0.020952	0.076274	0.18268	0.30198

Note that the red and black dashed lines (area values calculated without additional noise) do not overlap. The signal filtering introduces a systematic error, i.e., an additional time delay has been added to the process output signal. Since identical time intervals (2, 8, 14 and 22 s) were used for the calculation of both sets of characteristic areas, the filtered process step response was obviously not settled at $t = t_2$.

Next, the effect of high-frequency noise on the tracking and disturbance-rejection performance of the controllers (PI, PID_b and PID_fh) is investigated. The controllers' parameters were calculated using both sets (*Noise* and *Filtered noise*) of the calculated characteristic areas. In addition, for comparison, the controllers' parameters were also computed from "ideal" characteristic areas computed without noise (*Without noise, no filtering*). Note that for the PID_b and PID_fh controllers, the a-priori selected filter time constant TF = 0.01 s was used.

The closed-loop responses of process G_{P1} for the proposed controllers PI $b = 0$, PI $b = 0.5$, PID_b $b = 0.5$, and PID_fh to a reference step change ($r = 1$) and process input step-disturbance ($d = 1$) are shown in Figures 6.19–6.22, respectively.

From the experimental results, it is evident that the high-frequency noise strongly affects the closed-loop performance. However, the detrimental effect of the noise was reduced by filtering the process time-responses before calculating the characteristic areas. Note that the cyan (*Filtered noise*) closed-loop responses do not match the red (*Without noise*) ones. This is due to the systematic error introduced by filtering the process signals when using the same set of times t_0–t_3.

Since the PI controller requires only areas A_0–A_2 for computation of controller parameters, it is more robust to the noise. On the contrary, since the calculation of the reference filter parameters (PID_fh controller) is based on the process model estimated from the characteristic areas (see Chapter 5.4.2), the tracking performance of the PID_fh controller is most affected by the process high-frequency noise.

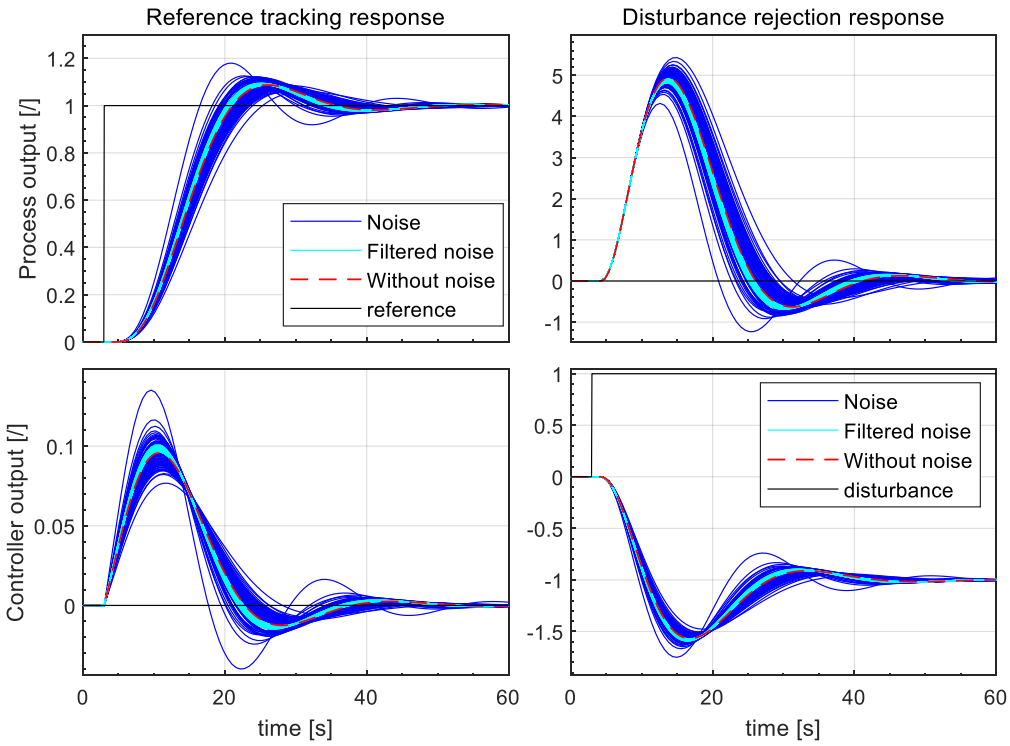

Figure 6.19: The time-domain robustness test for the PI controller with $b = 0$.

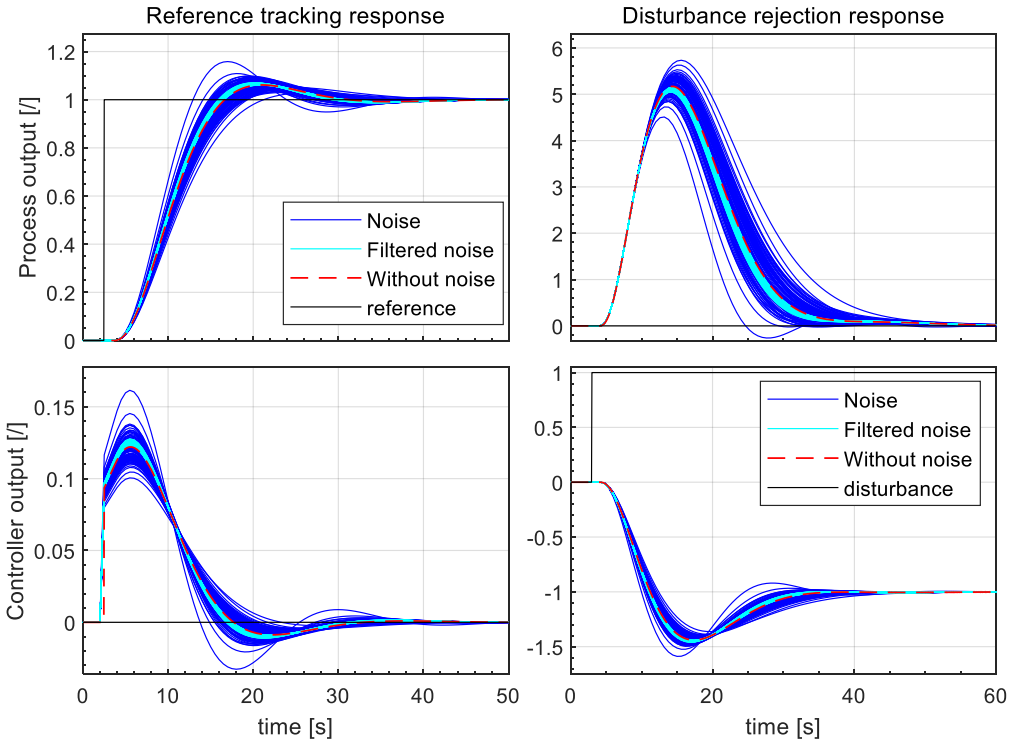

Figure 6.20: The time-domain robustness test for the PI controller with $b = 0.5$.

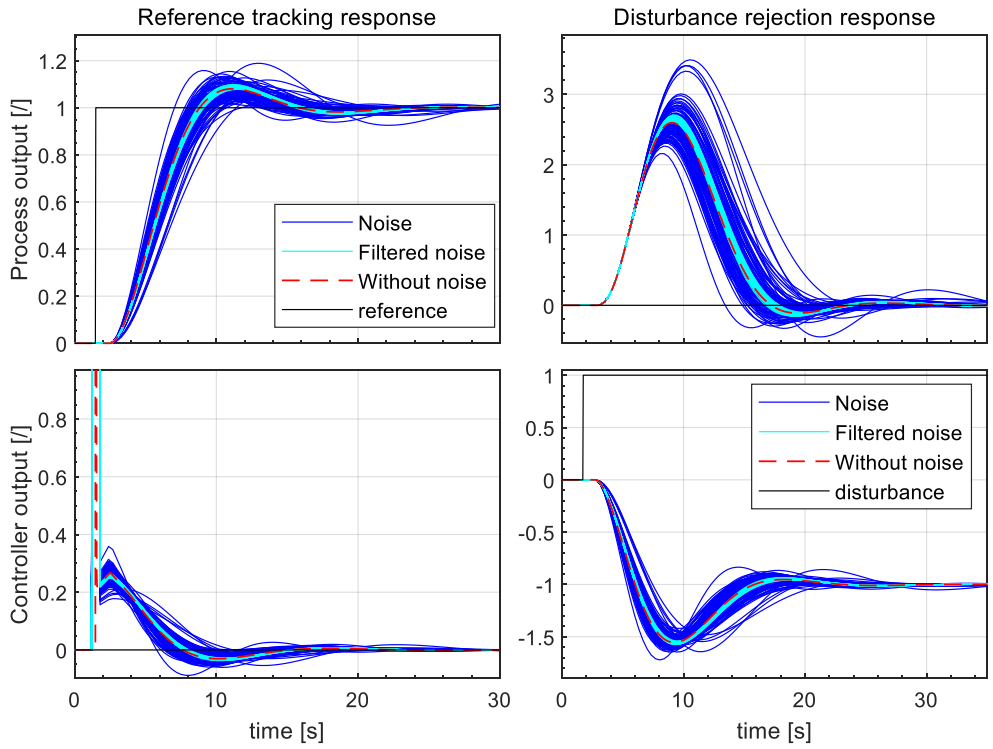

Figure 6.21: The time-domain robustness test for the PID_b controller with $b = 0.5$. Note that, for clarity, the controller output response is zoomed in for the reference step change.

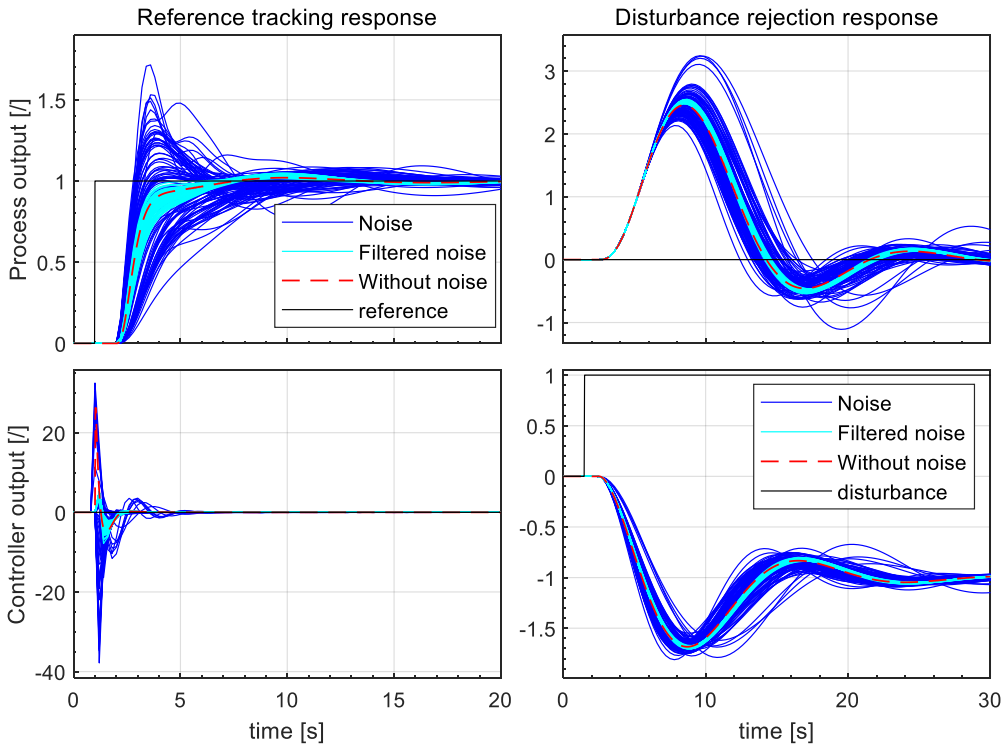

Figure 6.22: The time-domain robustness test for the PID_fh controller.

As the last step, we investigated the influence of the different low-pass filters on the computation of the characteristic areas from the noisy signals. The tests were performed with the first-order filter (6.11) and the second-order filter defined by the next transfer functions:

$$G_{\mathrm{LP2}} = \frac{1}{\left(1 + \frac{T_{\mathrm{F}}}{2} s\right)^2}. \tag{6.13}$$

The following filter time-constants:

$$T_{\mathrm{F1}} = 0.2, T_{\mathrm{F2}} = 0.5, T_{\mathrm{F3}} = 1, \tag{6.14}$$

have been applied to both filters. The calculation of the characteristic areas from the filtered process signals (with the addition of normally distributed noise) was repeated 100 times using filters G_{LP1} and G_{LP2} with all three filter time-constants (6.14).

Histograms of the areas calculated from the filtered process time responses (G_{LP1}) are shown in Figure 6.23. In addition, the areas calculated from the signals without filtering and added noise are indicated with the dashed red lines. As can be seen from the figure, the filter time-constant has a significant effect on the calculated areas, i.e., a higher filter time-constant reduces the standard deviation of the calculated areas. This is also confirmed by calculated standard deviation values presented in Table 6.2 (see the values marked by G_{LP1}). However, the mean values of the areas do not overlap with the dashed red lines. The reason for the systematic error is, as mentioned above, the signal filtering, i.e., the process step responses were not settled at $t = t_2$. This error increases with the value of the filter time-constant. The relative difference between the areas calculated without noise (*Without noise, no filtering*) and the mean values of the areas calculated with applied filter G_{LP1} are shown in Table 6.3.

A similar result is shown in Figure 6.24, which shows the computed areas' histograms when second-order filter G_{LP2} is used. However, as can be seen from the values in the figure, the systematic error becomes smaller.

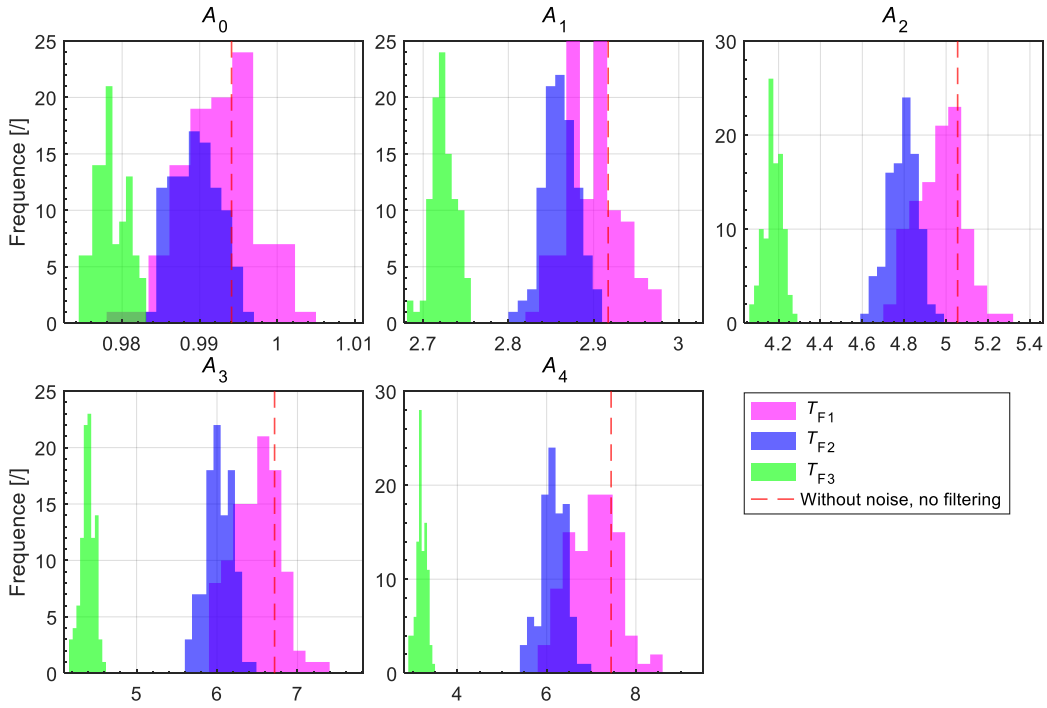

Figure 6.23: Histograms of the calculated characteristic areas for $G_{\mathrm{P1}}(\mathrm{s})$. Process input and output signals were filtered with filter G_{LP1} (6.11) with time constants T_{F1}–T_{F3} (6.14).

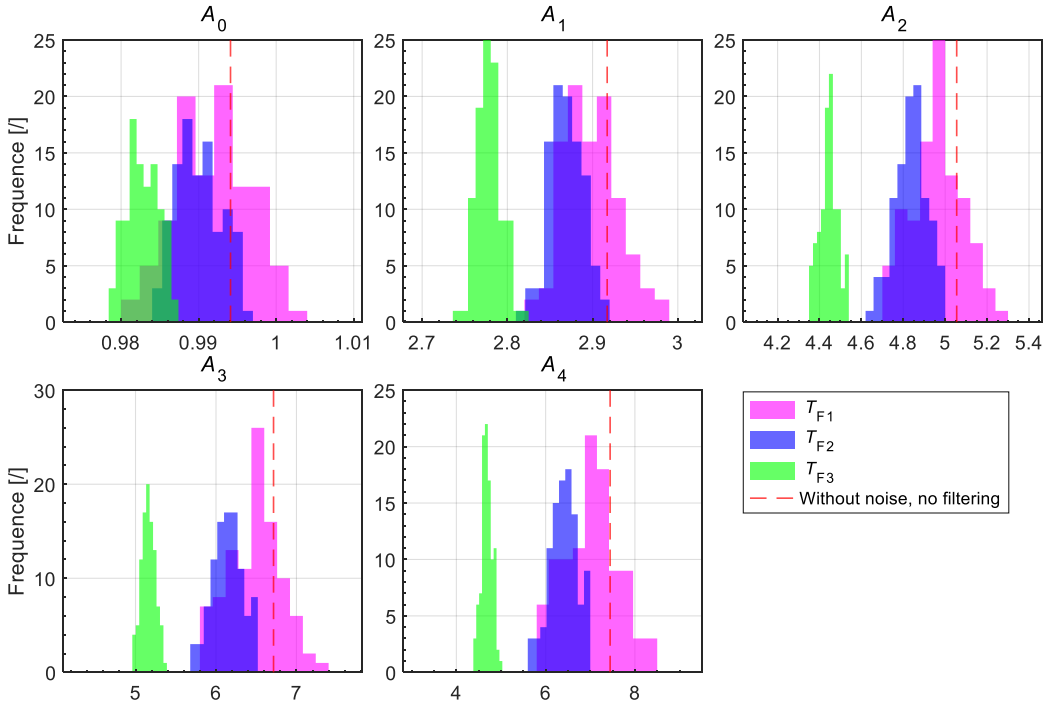

Figure 6.24: Histograms of the calculated characteristic areas for $G_{\mathrm{P1}}(\mathrm{s})$. Process input and output signals were filtered with filter G_{LP2} (6.13) with time constants T_{F1}–T_{F3} (6.14).

Table 6.2: Standard deviation σ of the calculated characteristic areas. Process input and output signals were filtered using different filters with time-constants T_{F1}–T_{F3} (6.14). For the last table entry, times t_2 and t_3, specified for the area calculations, were increased by the value of T_F.

filter	Time-constant	A_0	A_1	A_2	A_3	A_4
	T_{F1}	0.0047439	0.031139	0.11395	0.29679	0.53501
G_{LP1}	T_{F2}	0.0029504	0.019703	0.069948	0.17015	0.28351
	T_{F3}	0.0020695	0.014017	0.04187	0.085768	0.1166
	T_{F1}	0.0047346	0.032319	0.12271	0.32351	0.58707
G_{LP2}	T_{F2}	0.0029413	0.019939	0.074639	0.1836	0.31099
	T_{F3}	0.0020919	0.014479	0.043522	0.088488	0.12606
G_{LP2}	T_{F1}	0.0048971	0.033101	0.12884	0.3478	0.65073
$+ t_{2,3}$	T_{F2}	0.0028449	0.020628	0.081113	0.21598	0.39351
increase	T_{F3}	0.0018689	0.015822	0.05251	0.13347	0.23061

Table 6.3: Relative difference between the areas computed without noise and the mean values of the areas computed from filtered signals. Process input and output signals were filtered using different filters with time-constants T_{F1}–T_{F3} (6.14). For the last table entry, times t_2 and t_3, specified for the area calculations, were increased by the value of T_F.

filter	Time-constant	A_0	A_1	A_2	A_3	A_4
	T_{F1}	-0.0016262	-0.0062182	-0.01697	-0.033441	-0.055198
G_{LP1}	T_{F2}	-0.0046511	-0.019198	-0.051571	-0.10351	-0.17422
	T_{F3}	-0.015665	-0.066235	-0.17398	-0.3455	-0.57088
	T_{F1}	-0.002084	-0.0064669	-0.018077	-0.035123	-0.057306
G_{LP2}	T_{F2}	-0.0041209	-0.016431	-0.043401	-0.085028	-0.13956
	T_{F3}	-0.011356	-0.047285	-0.12084	-0.23165	-0.3705
G_{LP2}	T_{F1}	-0.0003211	0.0003678	-0.00089	-0.001541	-0.001929
$+ t_{2,3}$	T_{F2}	-0.0004725	-0.001056	-0.004394	-0.00968	-0.01794
increase	T_{F3}	-0.001511	-0.006540	-0.022154	-0.052512	-0.10332

Next, as a rule of thumb, times t_2 and t_3 were increased by a value of T_F, where T_F is the time-constant (6.14) of the currently used filter G_{LP2} (6.13). This means that the step response of the filtered process has nearly settled at $t = t_2$. As the integration time increases, larger standard deviations can be expected due to the additional high-frequency noise. However, as mentioned above, the systematic error should decrease.

The calculation of the characteristic areas from the filtered process signals (adding normally distributed random noise) was repeated 100 times for each filter time-constant (6.14). Histograms of the areas calculated from the filtered process time responses are shown in Figure 6.25. The mean values of the calculated areas are now much closer to the dashed red lines. A comparison of the relative standard deviations for all experiments, presented in Table 6.2, shows that the G_{LP2} filter with additional time ($G_{LP2} + t_{2,3}$ increase) is the best compromise between systematic error and dispersion of the calculated areas.

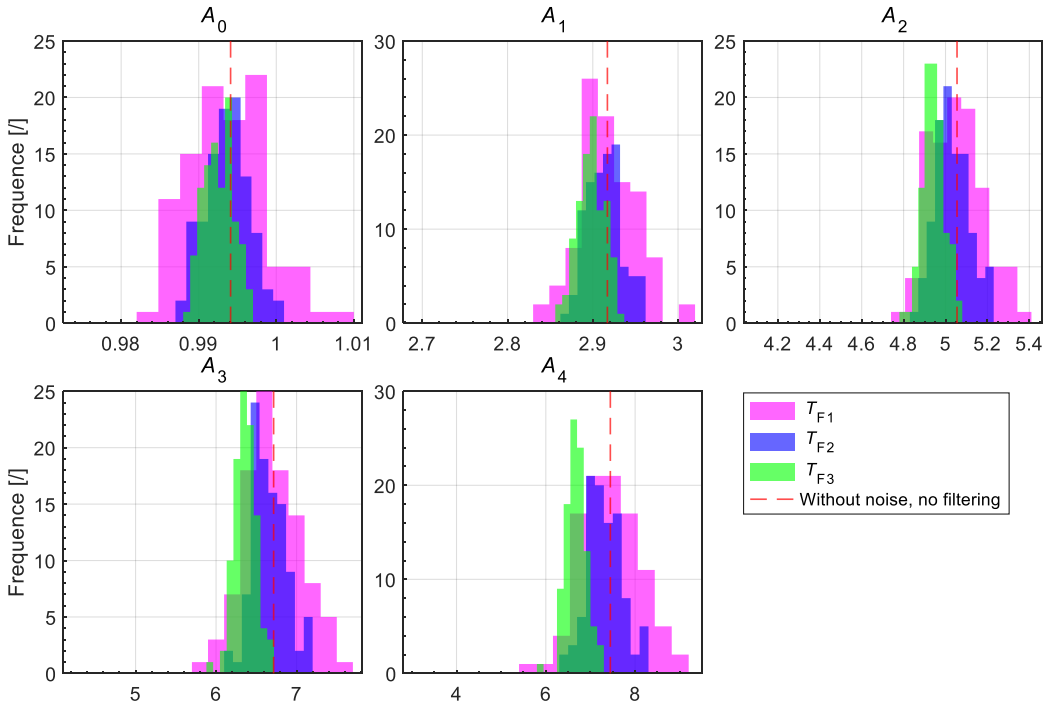

Figure 6.25: Histograms of the calculated characteristic areas for $G_{\mathrm{P1}}(\mathrm{s})$. Process input and output signals were filtered with filter G_{LP2} (6.13) with time constants T_{F1}–T_{F3} (6.14). Times t_2 and t_3, specified for the area calculations, were increased for T_{F} value.

In the end, the influence of the different low-pass filters on the $\mathrm{PID_b}$ closed-loop tracking and disturbance-rejection performance is investigated. The controller parameters were calculated using two sets (G_{LP1} and G_{LP2} + $t_{2,3}$ *increase*) with time constant T_{F2} (0.5). For comparison, the controller parameters were also calculated from the characteristic areas without noise (*Without noise, no filtering*). Note that the a-priori selected PID controller filter time constant $T_{\mathrm{F}} = 0.01$ s was added to the $\mathrm{PID_b}$ controller.

The closed-loop responses of process G_{P1} with the calculated $\mathrm{PID_b}$ $b = 0.5$ controller on a set-point step change ($r = 1$) and the process input step-disturbance ($d = 1$), when applying filters G_{LP1} and G_{LP2} with increased t_2 and t_3 in the calculation of characteristic areas, are shown in Figures 6.26 and 6.27, respectively. It can be seen that in contrast to filter G_{LP1}, the closed-loop responses of filter G_{LP2} (cyan colour) align with the red colour (*Without noise*).

As has been shown, the influence of high-frequency noise on the calculation of characteristic areas can be reduced by filtering the process input and output signals with a low-pass filter. Since the filtering significantly improves the precision of the characteristic area calculation, further tests will be carried out in the future, and the structure and parameters of the low-pass filter will be optimized.

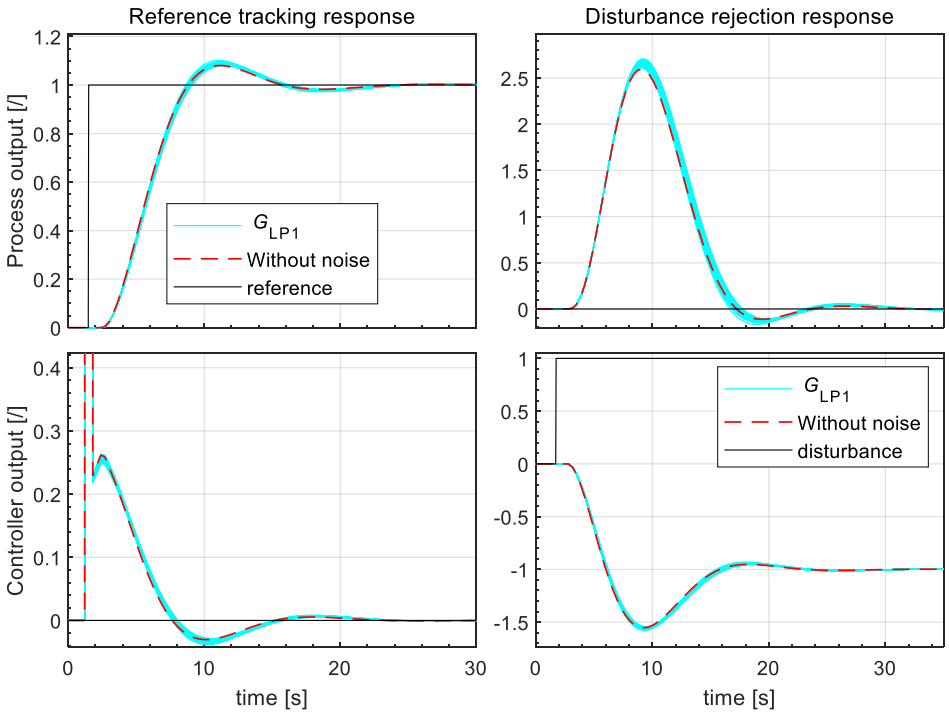

Figure 6.26: The process G_{P1} closed-loop responses for applied filter G_{LP1} with time constant T_{F2} (0.5). Note that, for clarity, the PID$_b$ $b = 0.5$ controller output response is zoomed in for the reference step change.

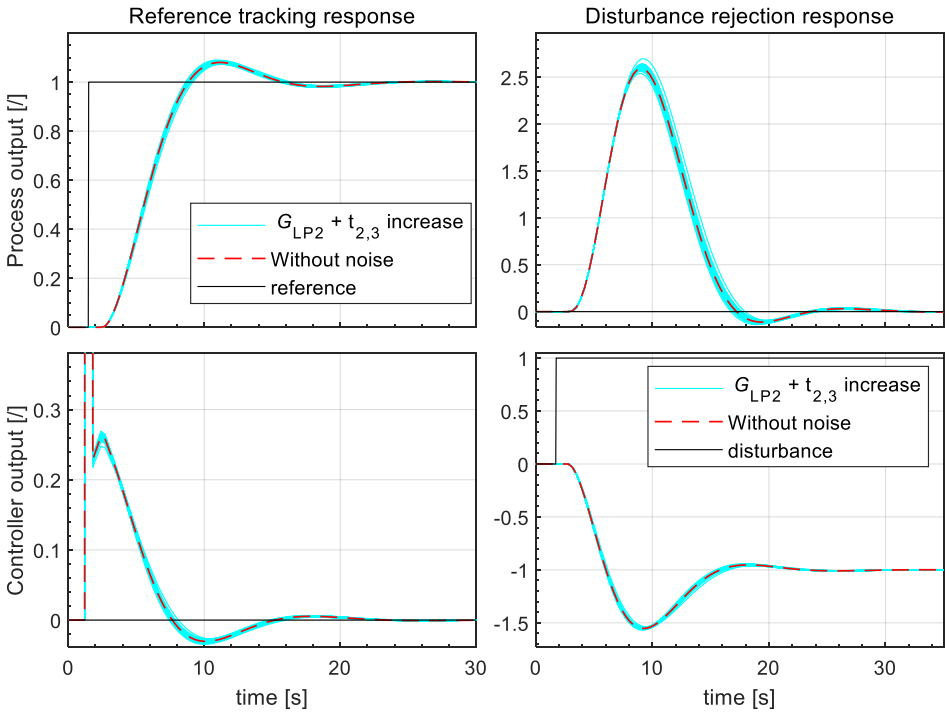

Figure 6.27: The process G_{P1} closed-loop responses for applied filter G_{LP2} with time constant T_{F2} (0.5) and increased times t_2 and t_3. Note that, for clarity, the PID$_b$ $b = 0.5$ controller output response is zoomed in for the reference step change.

Chapter 7

Comparisons With Other Methods

A large part of this chapter was originally published in Kos, T. et al., Applied Sciences (2020), 10: 4, and T. Kos et al., Applied Sciences (2020), 10: 17.

As far as we are aware, no other tuning method for IPs provides tuning based on both the measurement of a simple process open- or closed-loop time response in the time domain and a general process transfer function of arbitrary order with time delay. This means that the proposed tuning method has a significant advantage over alternative tuning methods for PI/PID controllers.

Nevertheless, this chapter compares simulations of different IP models, which are frequently found in the literature, with other PI/PID tuning methods for IPs. It should be noted that the selected tuning methods are not model-free controller tuning methods. Some methods cannot be applied to arbitrary IP models. However, all selected methods provide analytical tuning formulas for calculating the controller parameters.

Reference-tracking ($r = 1$) and disturbance-rejection responses ($d = 1$) were measured for all processes. The following criteria evaluated the tracking and disturbance-rejection performance of the tuning methods:

$$\begin{gathered} \mathrm{IAE} = \int_0^\infty |\mathrm{e}|(t)dt, \\ \mathrm{IAT^2E} = \int_0^\infty t^2 \cdot |\mathrm{e}|(t)dt, \\ \mathrm{RVy} \times \mathrm{IAE}, \end{gathered} \tag{7.1}$$

where RVy is the relative variance of the process output signal:

$$\begin{aligned} \mathrm{RVy(tracking)} &= \frac{\int_0^\infty \left|\frac{dy(t)}{dt}\right| dt}{|y(\infty) - y(0)|}, \\ \mathrm{RVy(disturbance)} &= \frac{\int_0^\infty \left|\frac{dy(t)}{dt}\right| dt}{|y_1 - y(0)| + |y_2 - y_1| + |y(\infty) - y_2)|}, \end{aligned} \tag{7.2}$$

and y_1 and y_2 are the first and second extrema of the process output signal. RVy for tracking becomes 1 for a monotonic process output signal. For any other response (overshoots, undershoots, or oscillations), the value becomes larger. RVy for disturbance becomes 1 for

the process output signal that has only one maximum and one minimum. This is an ideal disturbance-rejection response. Since the RVy measure favours monotonic responses and IAE favours fast responses, the combined measure (RVy × IAE) provides the best tradeoff between speed and monotonicity.

The RVy measures are based on the TV0y and TV2y measures introduced in [81], [225]. Note that the TV0y and TV2y measures are 0 for monotonic responses (or responses with one maximum and one minimum). Since we multiply RVy by IAE, RVy is modified to be 1 instead of 0 under ideal circumstances. Like RVy × IAE, the integral of the squared time absolute error (IAT^2E) measure favours fast and non-oscillatory responses.

Note that the criteria measurements were made after the process output was completely settled, i.e., the simulations were longer than the closed-loop responses shown below.

7.1 Experiments on the PI Controller

Simulations of four different IP models commonly found in the literature are compared with other PI tuning methods for IPs.

The proposed tuning method for the PI controller was compared with three other methods [18], [97], [105]. The first one was the Åström's method [18] for 2-DOF PI controllers. This method is based on the choice of the maximal sensitivity value Ms = 1.4 (hereafter referred to as Åström 1.4) or Ms = 2.0 (hereafter referred to as Åström 2). The second method was that of Taguchi and Araki (hereafter referred to as Taguchi) [105] for 2-DOF PI controllers. This method calculates the controller parameters to optimize the settling time while keeping the overshoot below 20 %. The third method was that of Ali and Majhi (hereafter referred to as Ali–Majhi) [97] for 1-DOF PI controllers. This method optimises the integral-square-error (ISE) criterion and the shape of the Nyquist curve. Note that these methods use different controller structures.

In the proposed tuning method, controller parameter $b = 0.5$ was used in all four cases. This represents a trade-off between tracking and disturbance-rejection performance. The reference-tracking or disturbance-rejection performance of the proposed method can be improved/adjusted by changing parameter b.

The closed-loop tracking ($r = 1$) and disturbance-rejection ($d = 1$) responses were measured on all four process models.

The calculated controller parameters (for all presented tuning methods and the proposed tuning method) for all four IP models can be found in Appendix A.1.

Case 1

The first comparison was performed on the first-order process with a relatively small delay:

$$G_{\mathrm{P1}}(s) = \frac{e^{-0.05s}}{s(1+s)}. \tag{7.3}$$

The closed-loop tracking and the disturbance-rejection responses between the aforementioned tuning rules are compared in Figure 7.1. The criteria values of the tuning rules are shown in Figure 7.2.

According to the IAE criterion, the proposed controller ranked third, and according to the IAT^2E and RVy × IAE criteria, it ranked first in tracking performance. The Åström 2 method showed a somewhat large overshoot, while the Taguchi and Ali–Majhi methods exhibited oscillatory behaviour.

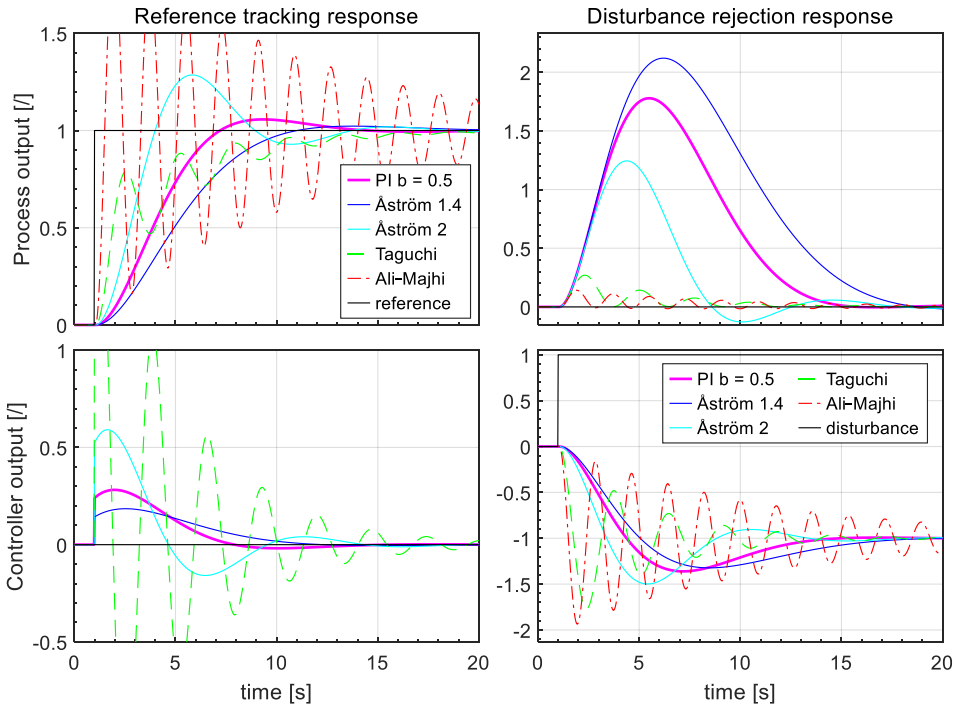

Figure 7.1: The process G_{P1} closed-loop responses. The PI controllers were tuned by the MOMI, Taguchi [105], Ali–Majhi [97], Åström 2, and Åström 1.4 [18] methods. Note that, for clarity, the controller and the process output response is zoomed in for the reference step change, and that for clarity, the Ali–Majhi controller output response is not shown.

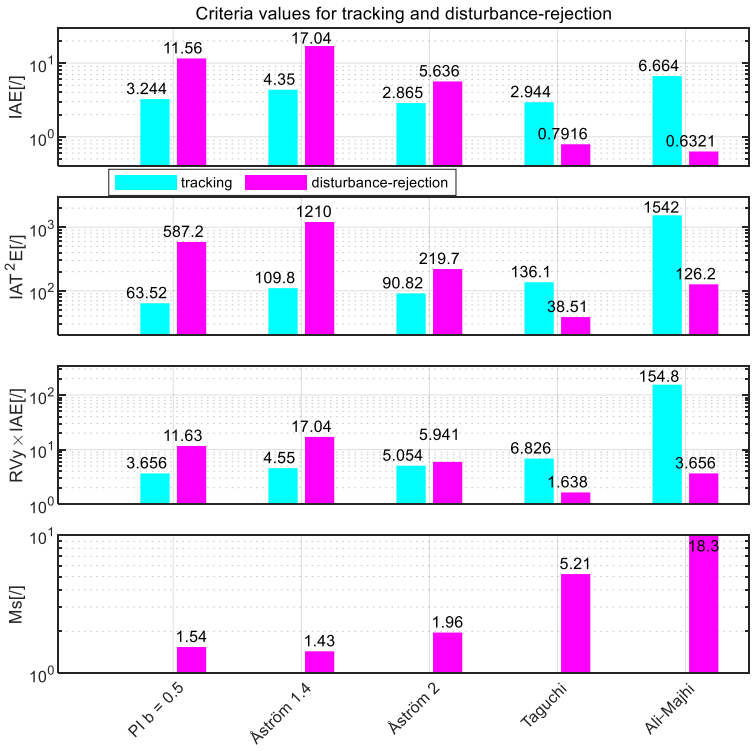

Figure 7.2: Criteria values for process G_{P1}.

The Taguchi method and the Ali–Majhi method obtained the lowest criteria for disturbance-rejection. The proposed tuning method ranked fourth. However, the Taguchi method and the Ali–Majhi method exhibited oscillatory behaviour.

Due to a relatively high degree of oscillation, neither the Taguchi method nor the Ali–Majhi method could be considered the most suitable for the G_{P1} process. This is confirmed by the high Ms values (5.21 and 18.3).

Case 2

The second comparison was performed on the process with pure time delay:

$$G_{\mathrm{P2}}(s) = \frac{e^{-s}}{s}. \tag{7.4}$$

Figure 7.3 compares the tracking and the disturbance-rejection closed-loop responses between the aforementioned tuning rules. The criteria values of the tuning rules are shown in Figure 7.4.

The proposed PI controller received the lowest criteria for tracking. The Åström 2 method ranked second, and the Taguchi method ranked third. The criteria gave significantly higher values to the Åström 1.4 method. The Taguchi method exhibited some undershoot and the Ali-Majhi method some overshoot.

For the disturbance-rejection performance, the criteria favoured the Taguchi method. The Åström 2 method was ranked second, and the proposed method third (close to Åström 2). As for tracking, the Taguchi method exhibited some undershoot.

Concerning sensitivity Ms, the proposed method gave a value of 1.98, while the Taguchi method gave the highest value (2.82). Since the Åström method is based on the Ms values, the expected values were obtained.

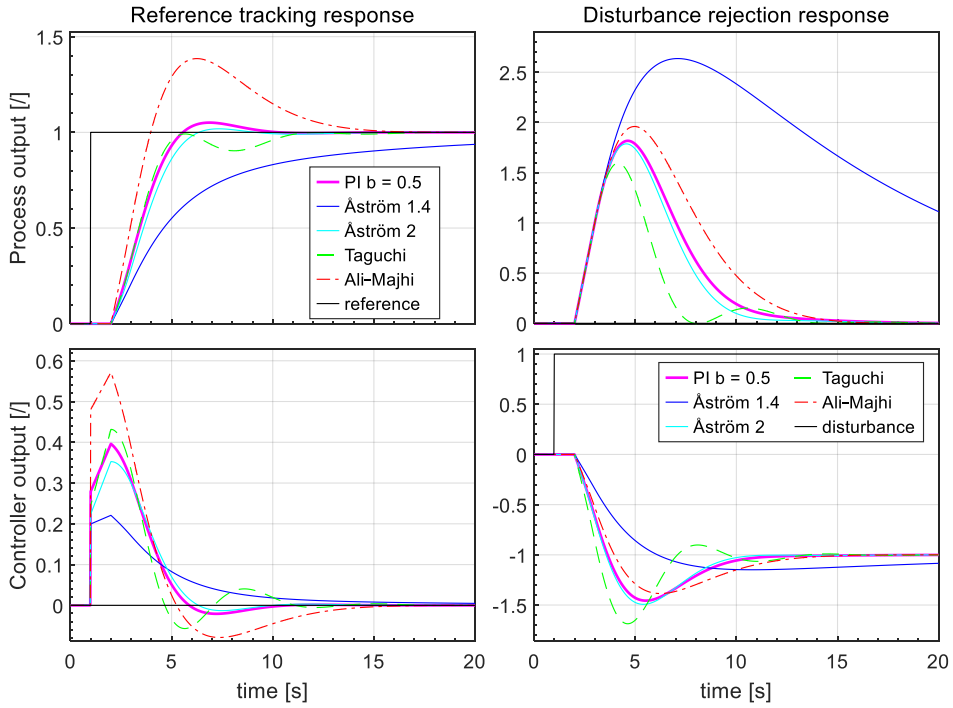

Figure 7.3: The process G_{P2} closed-loop responses. The PI controllers were tuned by the MOMI, Taguchi [105], Ali–Majhi [97], Åström 2, and Åström 1.4 [18] methods.

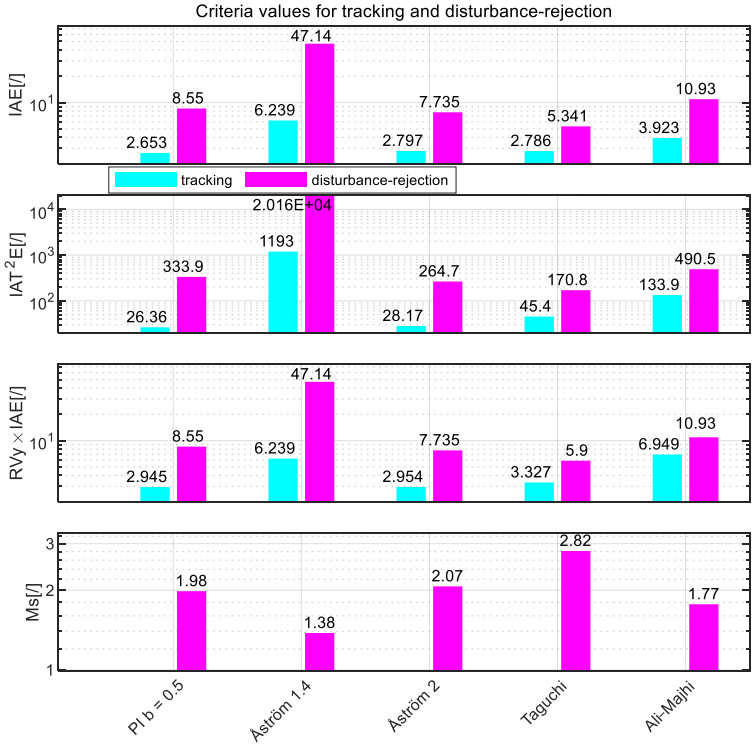

Figure 7.4: Criteria values for process G_{P2}.

Case 3

The third comparison was performed on the second-order process with time delay:

$$G_{\mathrm{P3}}(s) = \frac{e^{-s}}{s(1+s)^2}. \tag{7.5}$$

Figure 7.5 compares the tracking and the disturbance-rejection closed-loop responses between the aforementioned tuning rules. The criteria values of the tuning rules are shown in Figure 7.6. The Ali–Majhi method is missing because it is not suitable for higher-order process models.

The proposed PI controller received the lowest criteria for tracking. The Taguchi method was ranked second, and the Åström 2 method was ranked third. The Taguchi method exhibited some undershoot.

For the disturbance-rejection performance, the criteria favoured the Taguchi method. The proposed method ranked second, and the Åström 2 method ranked third. As for tracking, the Taguchi method exhibited some undershoot.

Concerning sensitivity Ms, the proposed method gave a value of 1.82, and the Taguchi method gave the highest value (2.71). As expected, the Ms values were lower for the Åström method since it is based on Ms values.

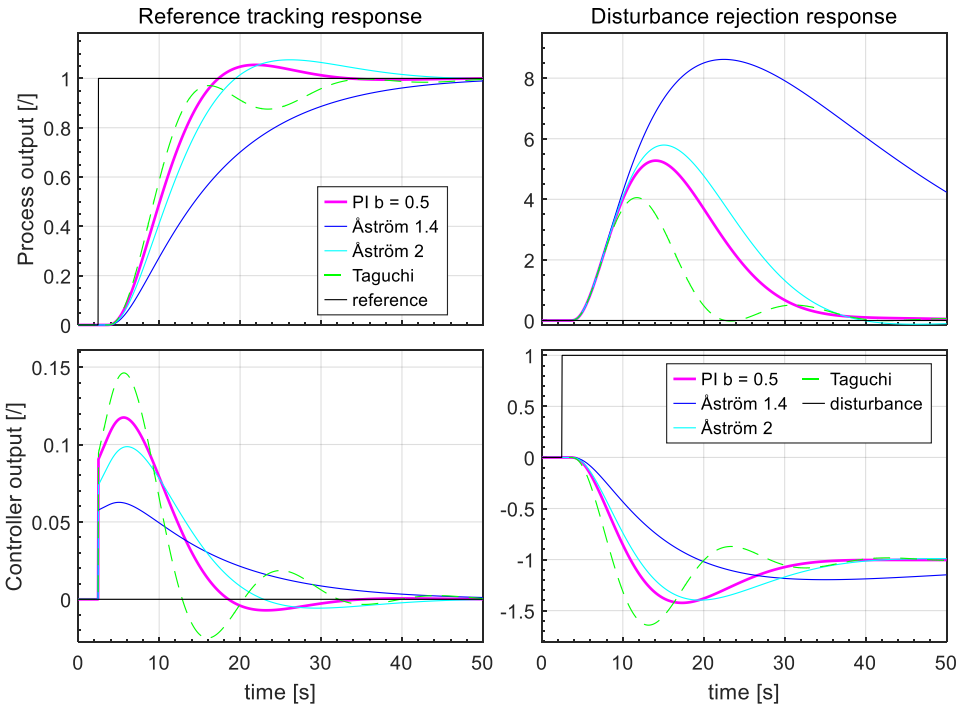

Figure 7.5: The process G_{P3} closed-loop responses. The PI controllers were tuned by the MOMI, Taguchi [105], Åström 2, and Åström 1.4 [18] methods.

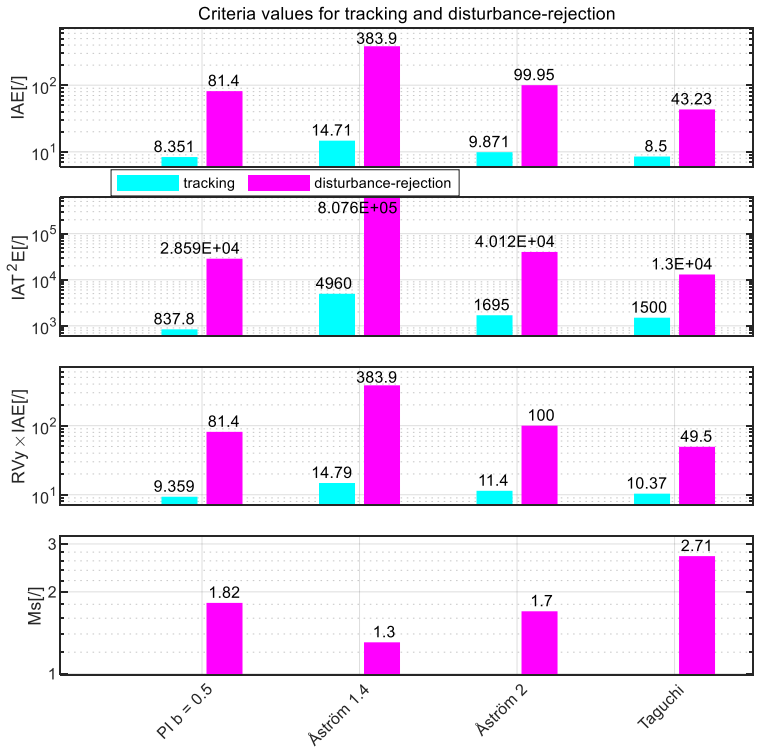

Figure 7.6: Criteria values for process G_{P3}.

Case 4

The last comparison was performed on the high-order process:

$$G_{\mathrm{P4}}(s) = \frac{1}{s(1+0.25s)^8}. \tag{7.6}$$

Figure 7.7 compares the tracking and the disturbance-rejection closed-loop responses between the aforementioned tuning rules. The criteria values of the tuning rules are shown in Figure 7.8.

Only the proposed and Åström methods were suitable for the high-order process. According to the criteria, the proposed controller ranked first in tracking and disturbance-rejection performance.

Concerning sensitivity Ms, the proposed method gave a value of 1.89. As expected, the Ms values were lower for the Åström method since it is based on Ms values.

The experimental results showed that the proposed MOMI method provided excellent closed-loop responses for a wide range of process models compared to some other methods. The disturbance-rejection and tracking responses were relatively fast and stable, with relatively small overshoots. As mentioned earlier, the tracking or disturbance-rejection performance can be further improved by changing controller parameter b accordingly.

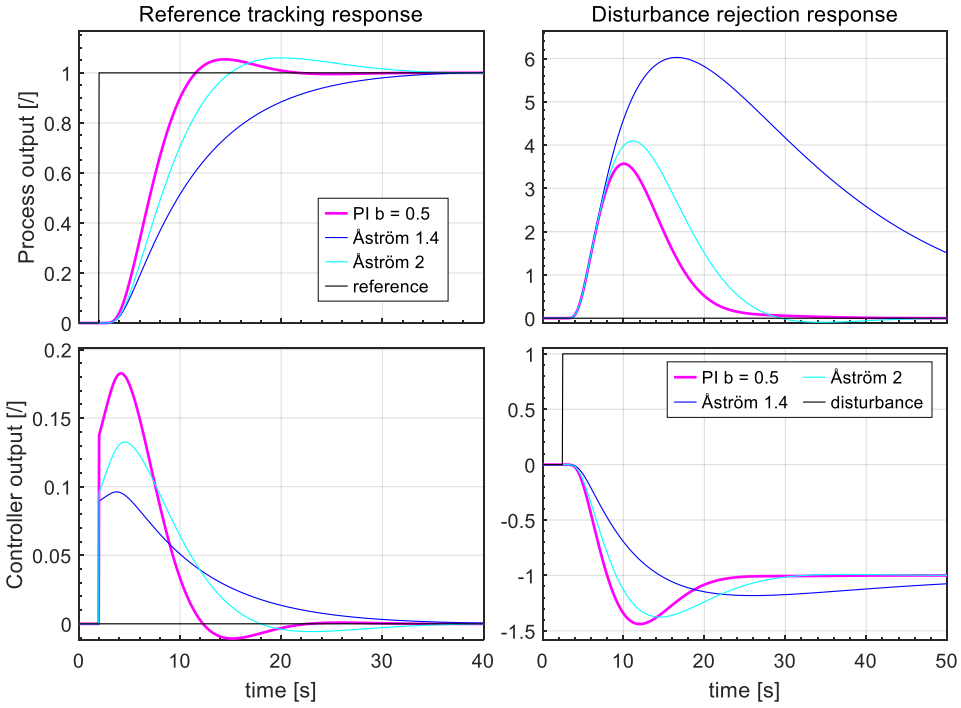

Figure 7.7: The process G_{P4} closed-loop responses. The PI controllers were tuned by the MOMI, Åström 2, and Åström 1.4 [18] methods.

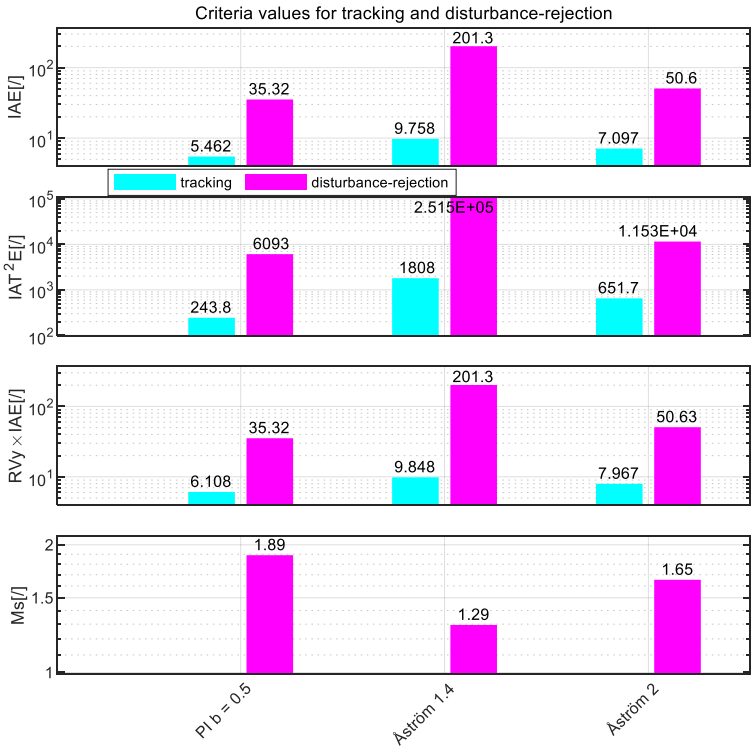

Figure 7.8: Criteria values for process G_{P4}.

7.2 Experiments on the PID Controller

Simulations of five different IP models commonly found in the literature are compared with other PID tuning methods for IPs.

The proposed tuning method for the PID_{f2} and PID_{fh} controllers has been compared with five other methods [25], [97], [104], [105], [116]. The first method is Ali and Majhi's method [97] (hereafter referred to as Ali–Majhi) for 1-DOF PID controllers. This method achieves optimal load disturbance-rejection for IPs with minimisation of the Integral of the Squared Error (ISE) criterion with Nyquist curve constraints, e.g., the slope has a certain slope at the gain crossover frequency. The second method is that of Taguchi and Araki [105] (hereafter referred to as Taguchi) for 2-DOF PID controllers. This method optimises the settling time while keeping the overshoot below 20%. The third is the method of Medarametla and Manimozhi [104] (hereafter referred to as Medarametla), which is based on the loop sensitivity transfer function. This controller consists of a 1-DOF PID controller with a second-order Lead/Lag filter and a fourth-order reference filter that cancels some controller zeros. The fourth method is that of Anil and Padma Sree [116] (hereafter referred to as Anil–Padma), which uses a pole-placement strategy, and the tuning parameter is Ms. The controller consists of a 2-DOF PID controller with a first-order Lead/Lag filter. The last one is the method of Åström and Hägglund [25]. This method is based on selecting a maximal sensitivity value $Ms = 1.4$ (hereafter referred to as Åström 1.4) or $Ms = 2.0$ (hereafter referred to as Åström 2). In this method, a 2-DOF PID controller is used. Note that these methods use different controller structures.

The closed-loop tracking ($r = 1$) and disturbance-rejection ($d = 1$) responses were measured on all five process models. In all cases, the a priori chosen time constant of the

controller filter was $T_F = 0.01$ s, except for the Ali–Majhi method, where the time constant was set to the suggested value $T_F = T_D \times 0.1$.

The calculated controller parameters (for all presented tuning methods and the proposed tuning method) for all five IP models can be found in Appendix A.2.

Case 1

The next pure integrator plus time delay is chosen as

$$G_{P1}(s) = \frac{e^{-s}}{s}. \tag{7.7}$$

Figures 7.9 and 7.10 compare the tracking and the disturbance-rejection closed-loop responses between the aforementioned tuning rules. The criteria values of the tuning rules are shown in Figure 7.11.

According to the IAE criterion, the proposed controllers ranked first, and according to the IAT^{2}E criterion, they ranked first and third in tracking performance. The proposed PID$_{fh}$ controller also ranked first in the RVy $\times$ IAE criterion. The Ali–Majhi method showed a large overshoot, and the Åström 2 method exhibited a somewhat oscillatory behaviour.

The Taguchi method received the lowest criteria for disturbance-rejection. The proposed tuning method was ranked second. However, the Taguchi method exhibited a slightly oscillatory response.

Concerning sensitivity Ms, Anil–Padma and Medarametla suggested Ms = 2 for processes without zero, while the proposed method gave values below 3.3.

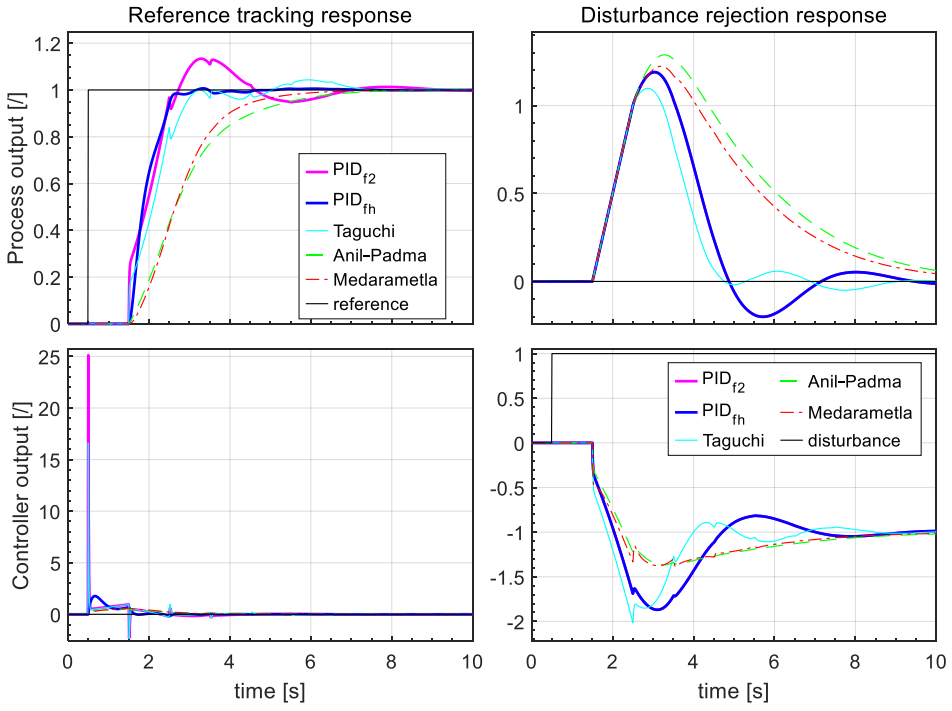

Figure 7.9: The process G_{P1} closed-loop responses. The PID controllers were tuned by the PID$_{f2}$, PID$_{fh}$, Taguchi [105], Anil–Padma [116], and Medarametla [104] methods.

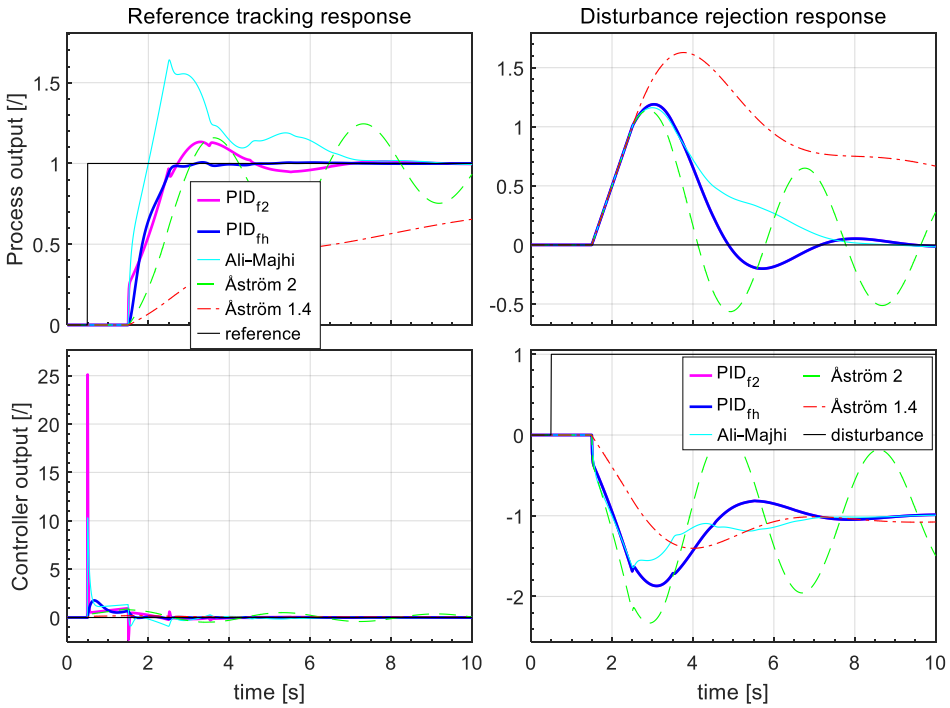

Figure 7.10: The process G_{P1} closed-loop responses. The PID controllers were tuned by the PID_{f2}, PID_{fh}, Ali–Majhi [97], Åström 2, and Åström 1.4 [25] methods.

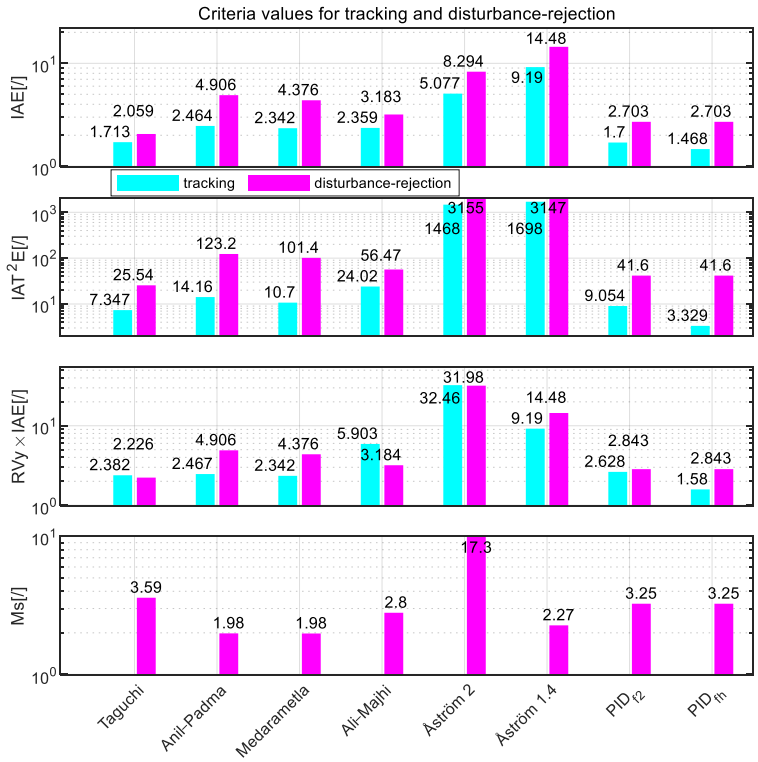

Figure 7.11: Criteria values for process G_{P1}.

Case 2

The following slightly delayed first-order process is chosen:

$$G_{\mathrm{P2}}(s) = \frac{e^{-0.35s}}{s(1+1.35s)}. \tag{7.8}$$

Figures 7.12 and 7.13 compare the closed-loop tracking and disturbance-rejection responses for all the above tuning rules. The criteria values of the aforementioned tuning rules are shown in Figure 7.14.

The proposed $\mathrm{PID_{fh}}$ controller received the lowest criteria for tracking. The Medarametla method ranked second, and the $\mathrm{PID_{f2}}$ ranked third. The Taguchi and the Ali–Majhi methods exhibited somewhat oscillatory behaviour.

For the disturbance-rejection performance, the criteria favoured Medarametla's method. However, the proposed method was ranked second, close to Medarametla. As for tracking, the Taguchi and Ali–Majhi methods also exhibited oscillatory behaviour.

Concerning sensitivity Ms, Anil–Padma and Medarametla suggested $\mathrm{Ms} = 2$ for processes without zero, while the proposed method gave values below 3.

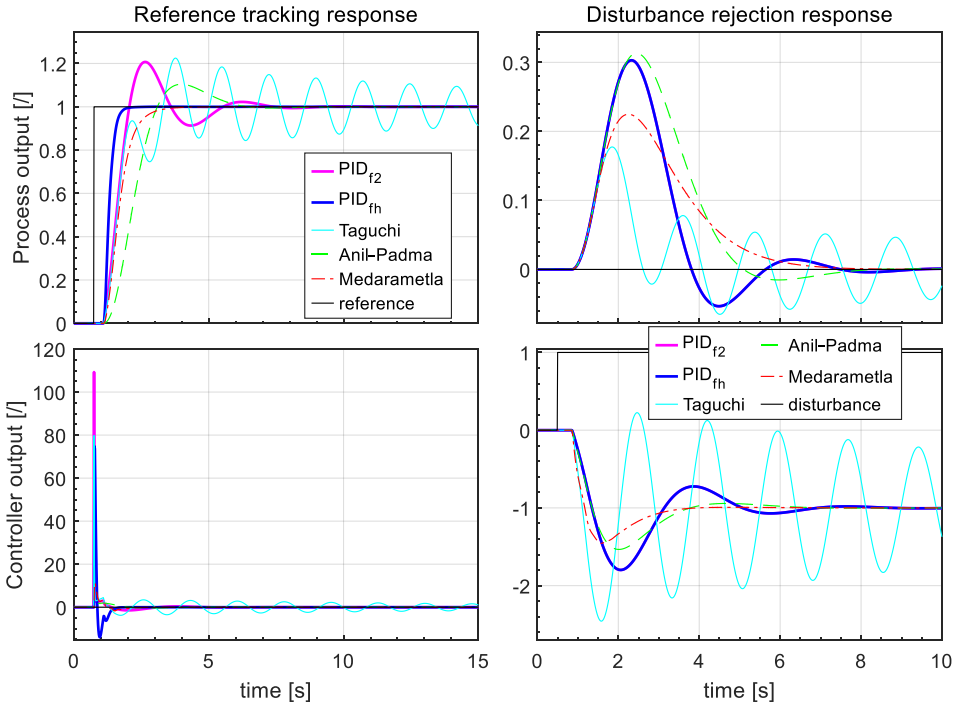

Figure 7.12: The process G_{P2} closed-loop responses. The PID controllers were tuned by the $\mathrm{PID_{f2}}$, $\mathrm{PID_{fh}}$, Taguchi [105], Anil–Padma [116], and Medarametla [104] methods.

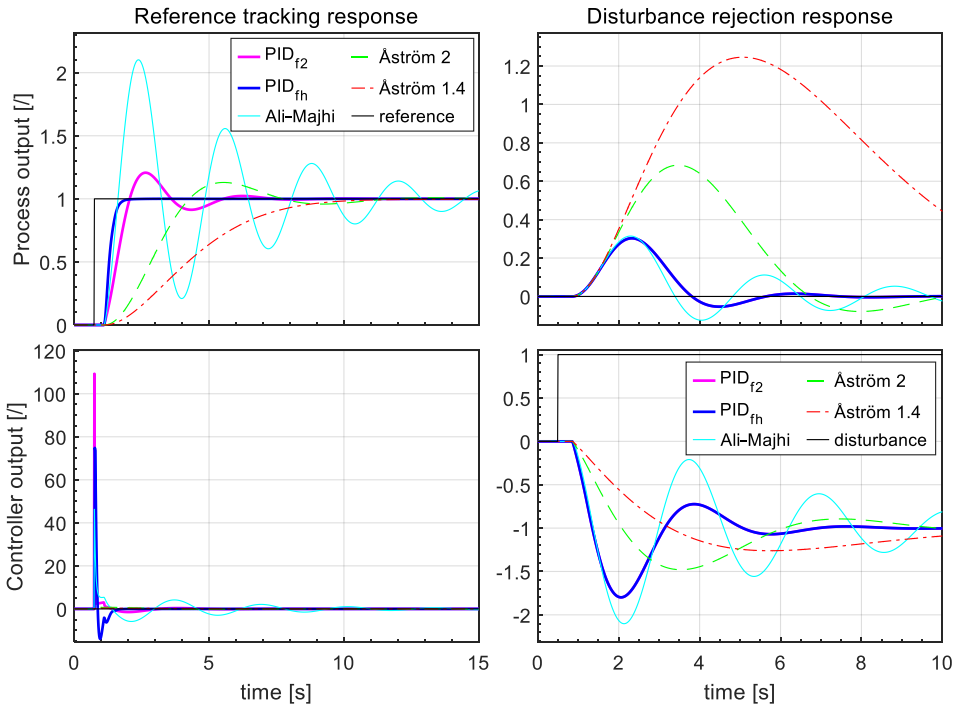

Figure 7.13: The process G_{P2} closed-loop responses. The PID controllers were tuned by the PID_{f2}, PID_{fh}, Ali–Majhi [97], Åström 2, and Åström 1.4 [25] methods.

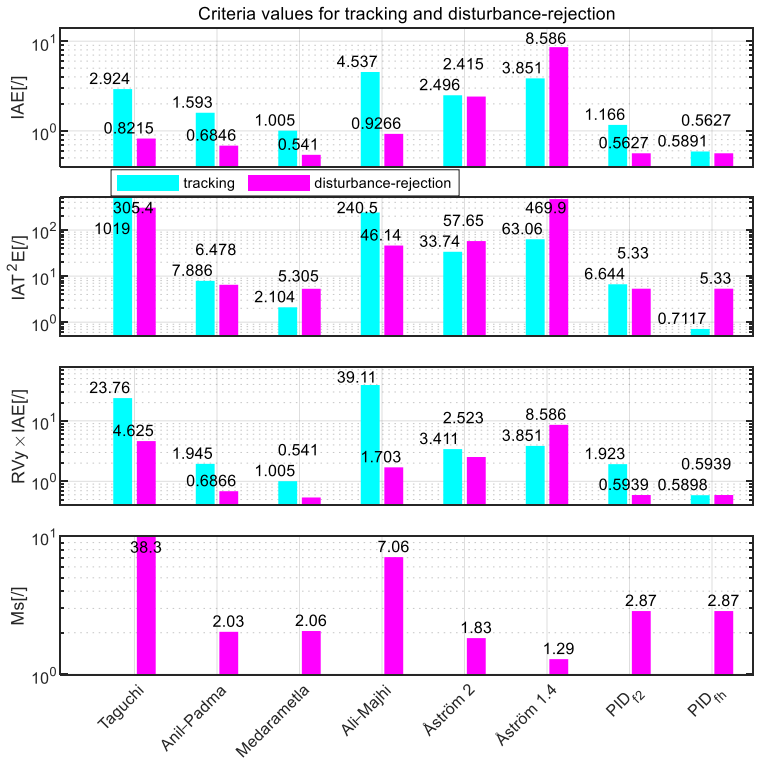

Figure 7.14: Criteria values for process G_{P2}.

Case 3

The next second-order process with time delay is chosen:

$$G_{\mathrm{P3}}(s) = \frac{e^{-s}}{s(1+1.5s)^2}. \tag{7.9}$$

Figure 7.15 compares closed-loop tracking and disturbance-rejection responses between tuning rules. Some methods are missing because they are not suitable for second-order process models. The criteria values of the tested tuning methods are shown in Figure 7.16.

The tracking criteria gave the lowest values for the proposed controllers. The Åström methods ranked second. Again, the Taguchi method exhibited oscillatory behaviour.

The lowest disturbance-rejection criterion was also given for the proposed controllers, closely followed by the Åström 2 method.

Regarding sensitivity Ms, the proposed method gave values lower than 2.5. As expected, the Ms values were lower for the Åström methods since they are based on Ms values.

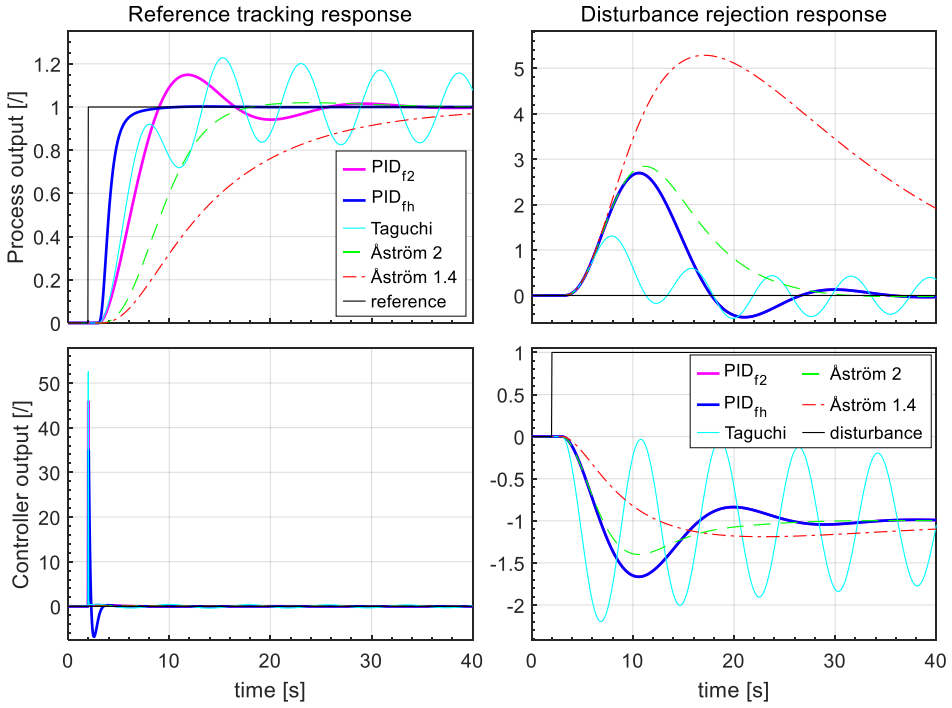

Figure 7.15: The process G_{P3} closed-loop responses. The PID controllers were tuned by the $\mathrm{PID_{f2}}$, $\mathrm{PID_{fh}}$, Taguchi [105], Åström 2, and Åström 1.4 [25] methods.

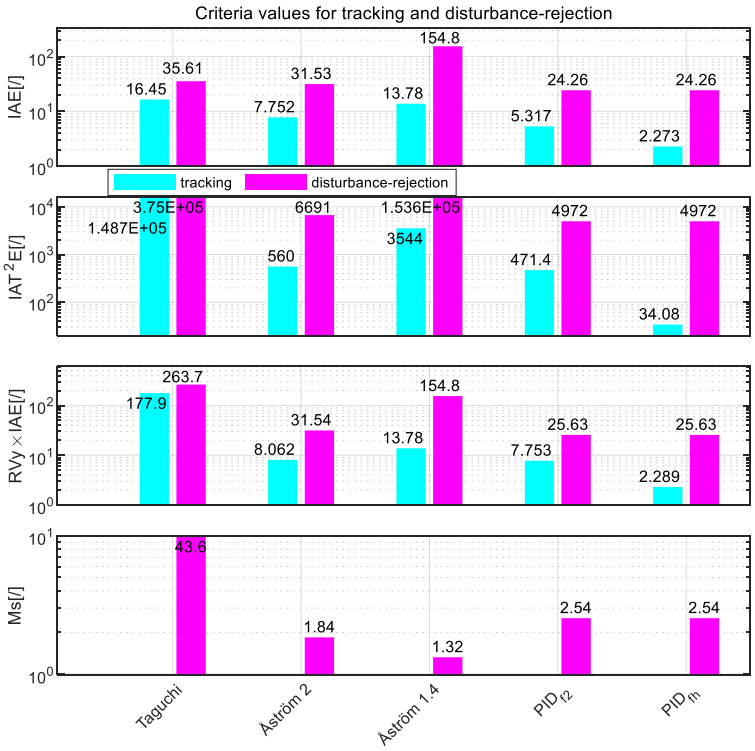

Figure 7.16: Criteria values for process G_{P3}.

Case 4

The following high-order non-minimum phase process is chosen:

$$G_{P4}(s) = \frac{0.5(1-0.5s)e^{-0.7s}}{s(1+0.4s)(1+0.1s)(1+0.5s)}. \tag{7.10}$$

An experiment using this process has already been carried out by Medarametla and Manimozhi [104] (Medarametla) and Anil and Padma Sree [116] (Anil–Padma).

Figures 7.17 and 7.18 compare closed-loop tracking and the disturbance-rejection responses between the aforementioned tuning rules. Some methods are missing because they are not suitable for higher-order process models. The criteria values are shown in Figure 7.19.

The lowest IAE and IAT²E criteria for tracking were obtained with the PID_{fh} controller. The Medarametla method ranked second, and the proposed PID_{f2} controller ranked third. Similarly, the RVy × IAE criterion favoured the proposed PID_{fh} controller, the Anil–Padma method was ranked second, and the Medarametla method was ranked third.

Similar results were obtained for the disturbance-rejection performance. The proposed PID_{f2} and PID_{fh} controllers ranked first, and the Medarametla method ranked second.

Concerning sensitivity Ms, Anil–Padma and Medarametla suggested Ms = 2.81 for this process, while the proposed method gave values below 3.2. As expected, Ms values were lower under the Åström methods because the tuning method is based on Ms values.

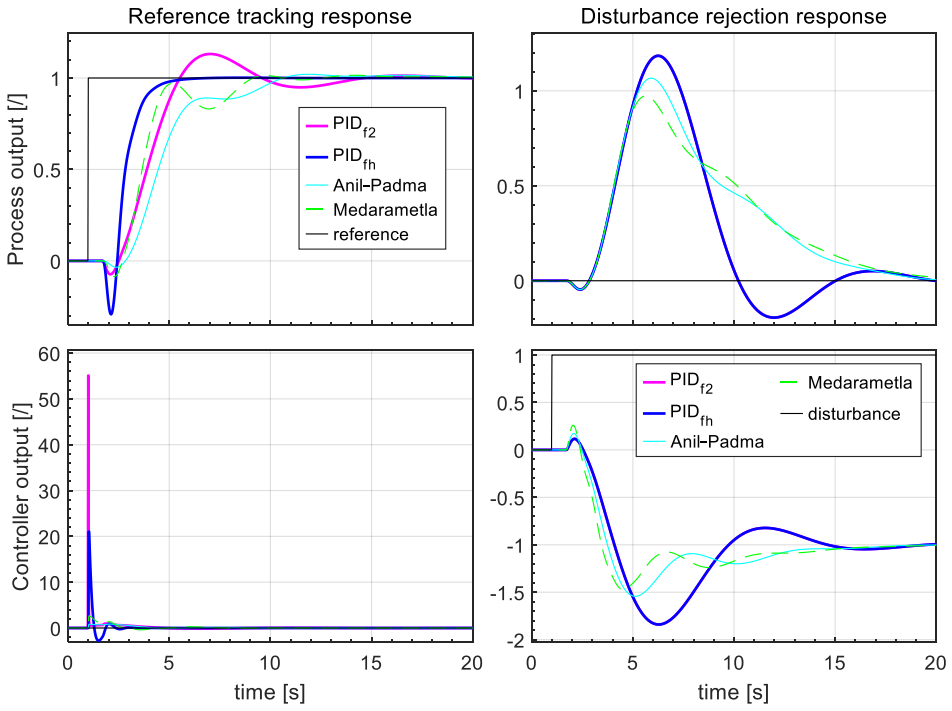

Figure 7.17: The process G_{P4} closed-loop responses. The PID controllers were tuned by the PID_{f2}, PID_{fh}, Anil–Padma [116], and Medarametla [104] methods.

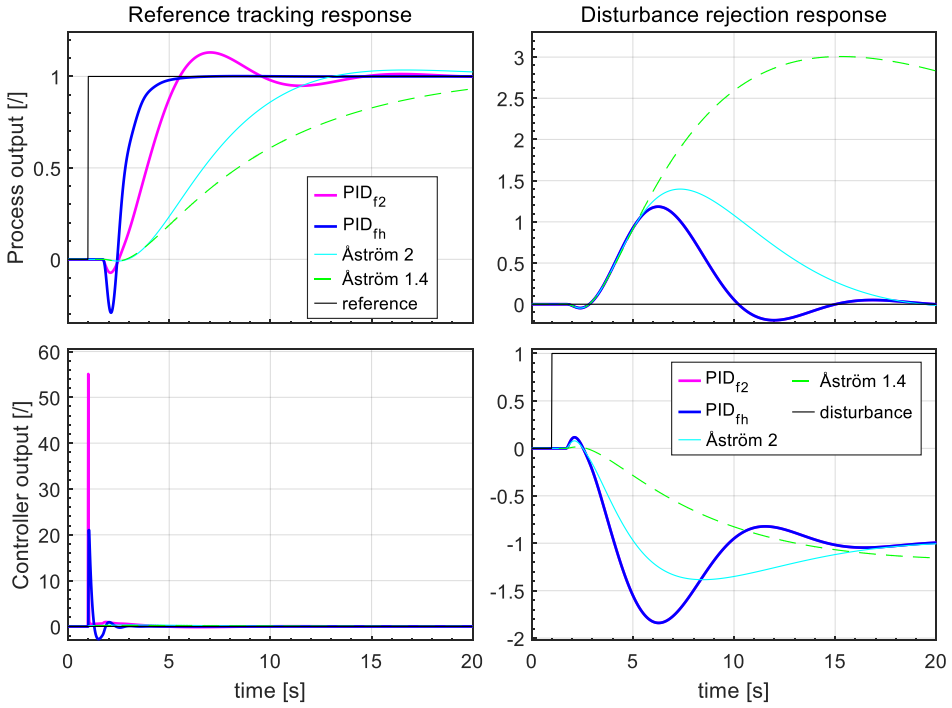

Figure 7.18: The process G_{P4} closed-loop responses. The PID controllers were tuned by the PID_{f2}, PID_{fh}, Åström 2, and Åström 1.4 [25] methods.

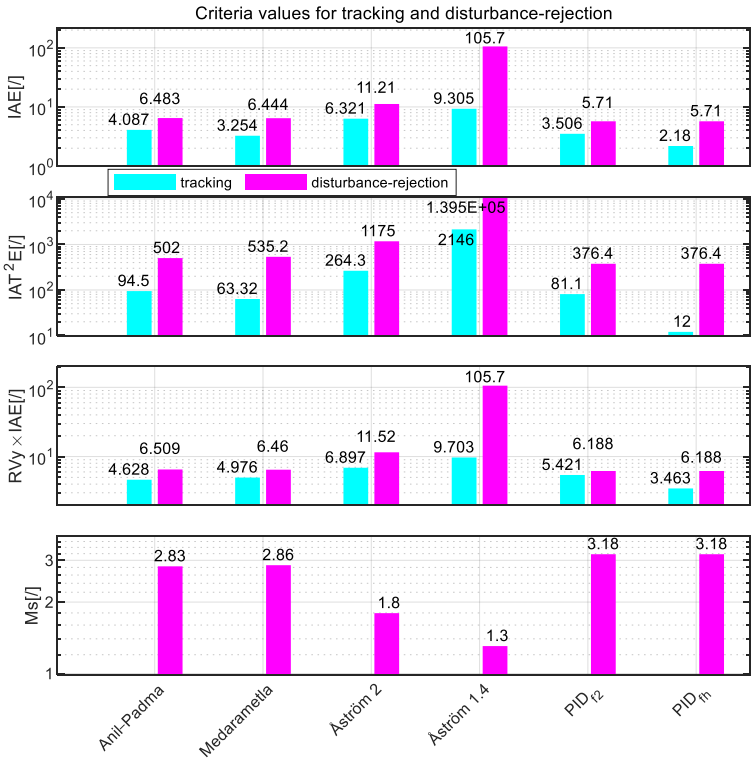

Figure 7.19: Criteria values for process G_{P4}.

Case 5

The next high-order process is chosen:

$$G_{\mathrm{P5}}(s) = \frac{1}{s(1+0.25s)^8}. \tag{7.11}$$

The tracking and the disturbance-rejection closed-loop responses between the chosen tuning rules are compared in Figure 7.20. The criteria values are shown in Figure 7.21.

Only the proposed and Åström methods were suitable for the high-order process. According to the criteria, the proposed controllers ($\mathrm{PID_{f2}}$ and $\mathrm{PID_{fh}}$) ranked first in tracking and disturbance-rejection performance. As expected, the Ms values were lower under the Åström methods because the tuning method is based on the Ms values.

All the experimental results showed that the proposed $\mathrm{PID_{f2}}$ and $\mathrm{PID_{fh}}$ controllers have excellent tracking and disturbance-rejection performance for various process models compared with some other tuning methods based on similar tuning procedures. The proposed controllers ranked first in most cases. The closed-loop responses were stable and fast, with only small overshoots.

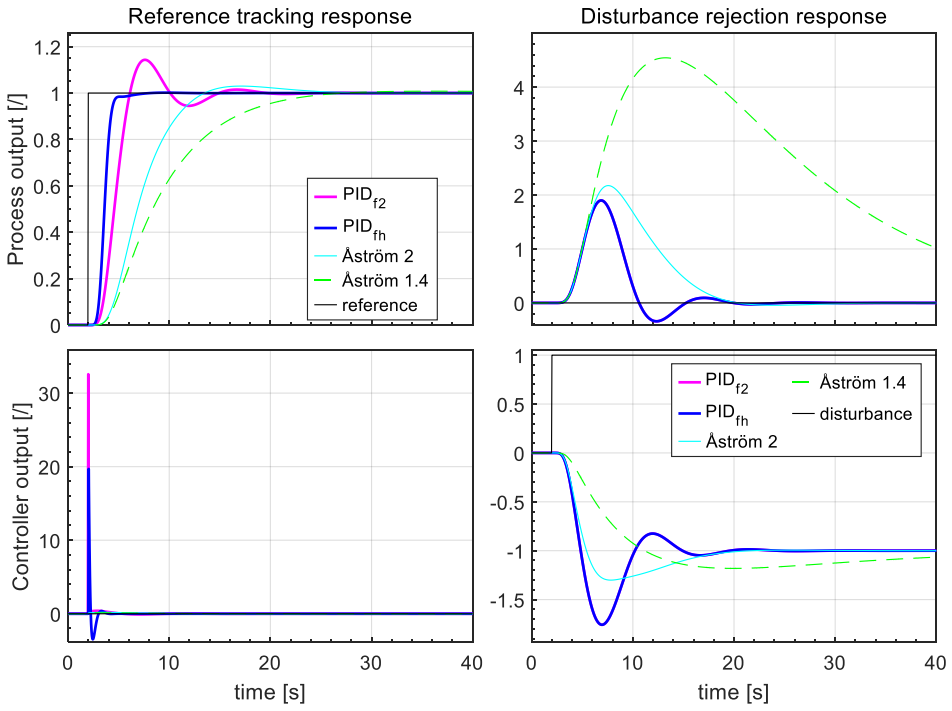

Figure 7.20: The process G_{P5} closed-loop responses. The PID controllers were tuned by the PID_{f2}, PID_{fh}, Åström 2, and Åström 1.4 [25] methods.

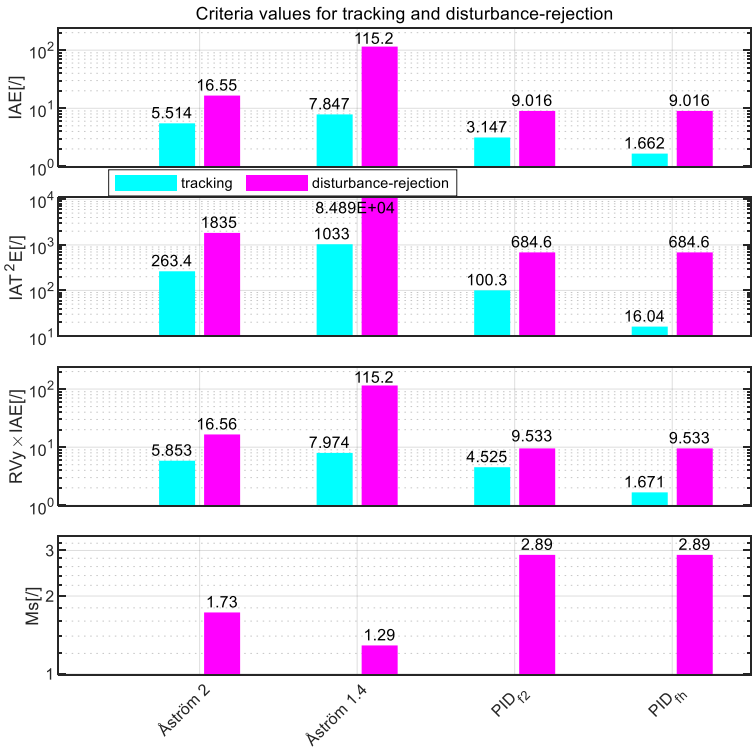

Figure 7.21: Criteria values for process G_{P5}.

Chapter 8

Real-Time Experiments

A large part of this chapter was originally published in Kos, T. et al., Applied Sciences (2020), 10: 4, T. Kos et al., Applied Sciences (2020), 10: 17, and T. Kos et al., AIP Advances (2019), 9: 3.

In this chapter, real-time experiments in the time domain are presented. Some experiments were performed with the PI and some with the PID controller. In order to test as wide a range of processes or practical problems as possible, the chosen real-time systems differ significantly from each other.

8.1 Hydraulic Laboratory Plant

The proposed PI controller's tuning method was tested on a hydraulic laboratory plant, as shown in Figure 8.1. The plant consisted of three water tanks. Figure 8.2 shows a schematic diagram of the setup. The process input was the voltage at pump P_1, and the process output was the level of filtered-water in the first tank (h_1). The valve V_{12} was closed (see Figure 8.2). Since the water flowed from tank T_1 into the main tank, located below the three tanks (valve V_1 was open), the process did not include an integrator. However, since the main time constant was very large, the process could be considered an approximation of an integrating system. Water levels were measured using pressure sensors. A custom-built USB-DAQ card was used for data acquisition, and the closed-loop control was implemented in MATLAB and Simulink software packages. More information on this particular laboratory setup can be found in [226].

The open- and closed-loop experiments were performed on the setup. First, a voltage step-change was applied to pump P_1. The voltage (process input) and the water level in reservoir T_1 (process output) are shown in Figure 8.3. The actual water level (in mm) could be determined by multiplying the measured process output value by 0.5.

From the measured open-loop responses, the following characteristic areas were calculated using Expressions (2.9)–(2.11):

$$A_0 = 0.476, A_1 = 0.994, A_2 = 1.57. \tag{8.1}$$

Expressions (4.6) and (4.4) were used to calculate the next PI controller parameters:

$$K_{\mathrm{P}} = 0.54, K_{\mathrm{I}} = 0.069, \tag{8.2}$$

where, to improve disturbance-rejection performance, factor $b = 0$ was chosen ($b = 0$ corresponds to a 2-DOF controller).

The closed-loop responses to two reference changes and artificially added step-disturbances at process input (d) are shown in Figure 8.4. From the response in Figure 8.4,

it can be seen that the proposed method results in a quite efficient control of the hydraulic plant. The non-linear behaviour of the plant can be seen from the different responses to positive and negative references and the changes in the input step-disturbance.

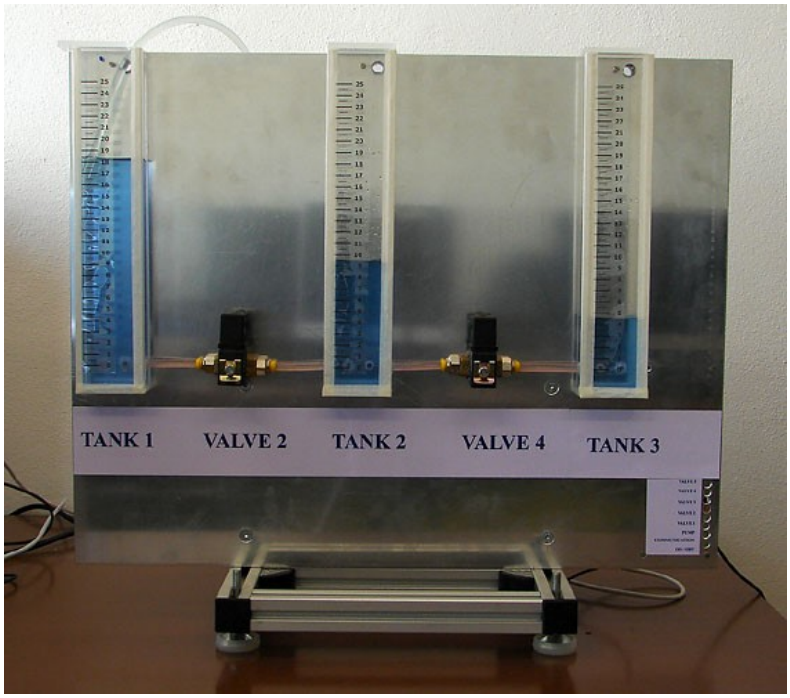

Figure 8.1: Hydraulic laboratory setup.

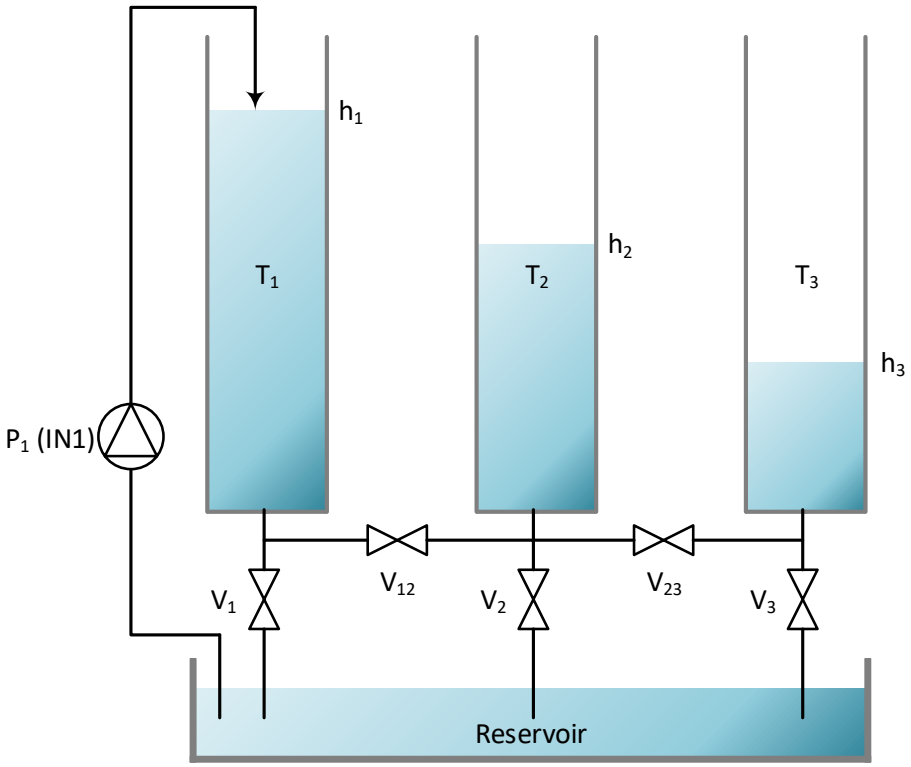

Figure 8.2: Schematic diagram of the hydraulic laboratory setup.

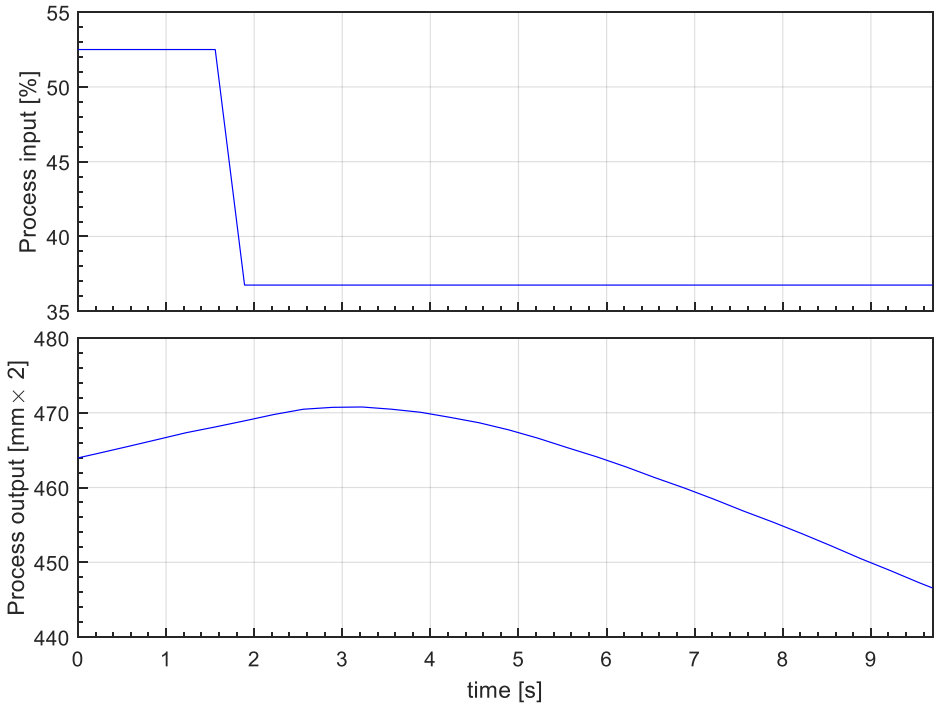

Figure 8.3: Hydraulic process open-loop response. Process input (voltage on the pump in %) and output (water level in mm multiplied by a factor of 2) signals during the experiment.

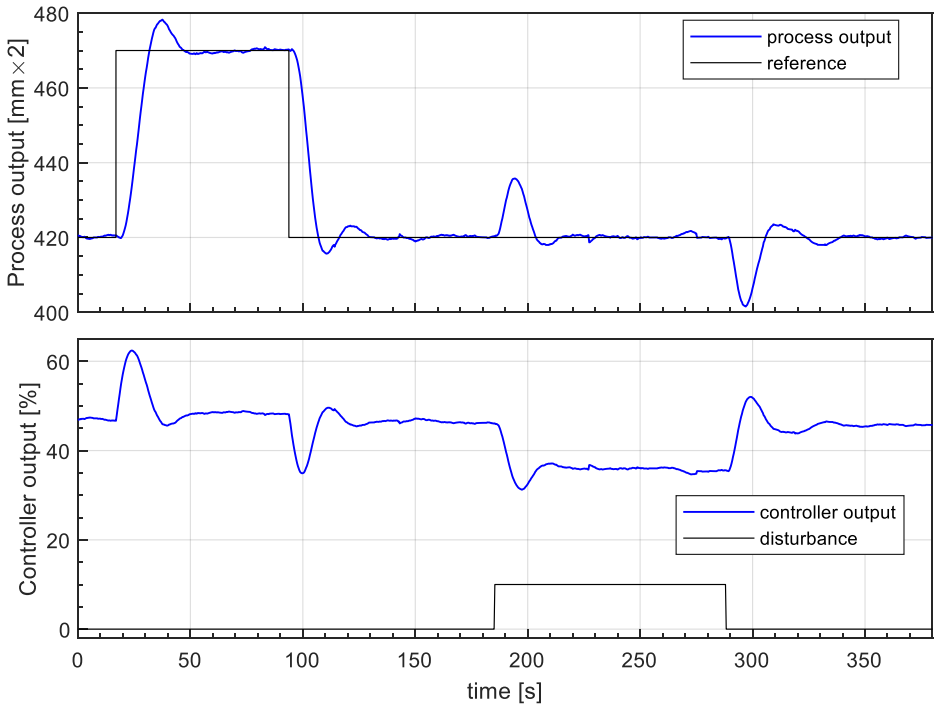

Figure 8.4: Hydraulic process closed-loop response. Process input (voltage on the pump in %) and output (water level in mm multiplied by a factor of 2) signals during the experiment.

8.2 Industrial Autoclave

The proposed PI controller's tuning method was also tested on an industrial autoclave, as shown in Figure 8.5. An autoclave is used for the production of plastics. The process input is the electrical power of the heaters (from 0 to 100%), and the process output is the internal temperature (in °C). The process was supervised by a SCADA system connected to the underlying PLC controllers with a sampling time of 1 s.

Figure 8.5: Industrial autoclave.

The process was self-regulatory with a main time constant of more than one day. However, the desired closed-loop time constant was less than 30 min. On the other hand, in the first few minutes, the process open-loop step-response was similar to the IP with delay (see Figure 8.6). Therefore, only the first part of the process open-loop response was used to calculate the controller parameters.

First, a step-change was applied to the process input (change of electrical power from 0% to 2%). Figure 8.6 shows the process response (temperature). From the measured open-loop responses, using Expressions (2.9)–(2.11), the following characteristic areas were calculated:

$$A_0 = 0.0044, A_1 = 0.3651, A_2 = 17.86. \tag{8.3}$$

Expressions (4.6) and (4.4) were used to calculate the next PI controller parameters:

$$K_{\mathrm{P}} = 1.55, K_{\mathrm{I}} = 0.052, \tag{8.4}$$

where factor $b = 0$ was chosen to improve disturbance-rejection performance.

Since the closed-loop test was performed during plastic production, disturbance-rejection performance could not be tested. Therefore, only the tracking performance was tested. Figure 8.7 shows the closed-loop responses to a reference change. From the obtained closed-loop responses, it can be seen that the proposed method results in a quite efficient temperature control of the autoclave.

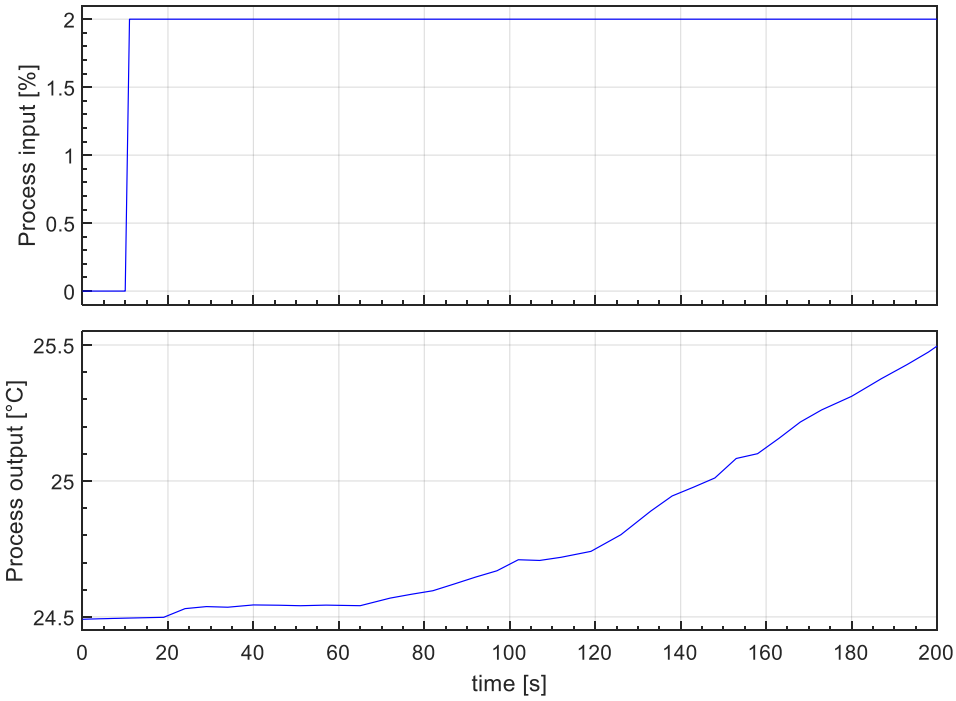

Figure 8.6: Industrial autoclave open-loop response. Process input (electric power in %) and output (temperature in °C) signals during manual experiment within the first 3 minutes.

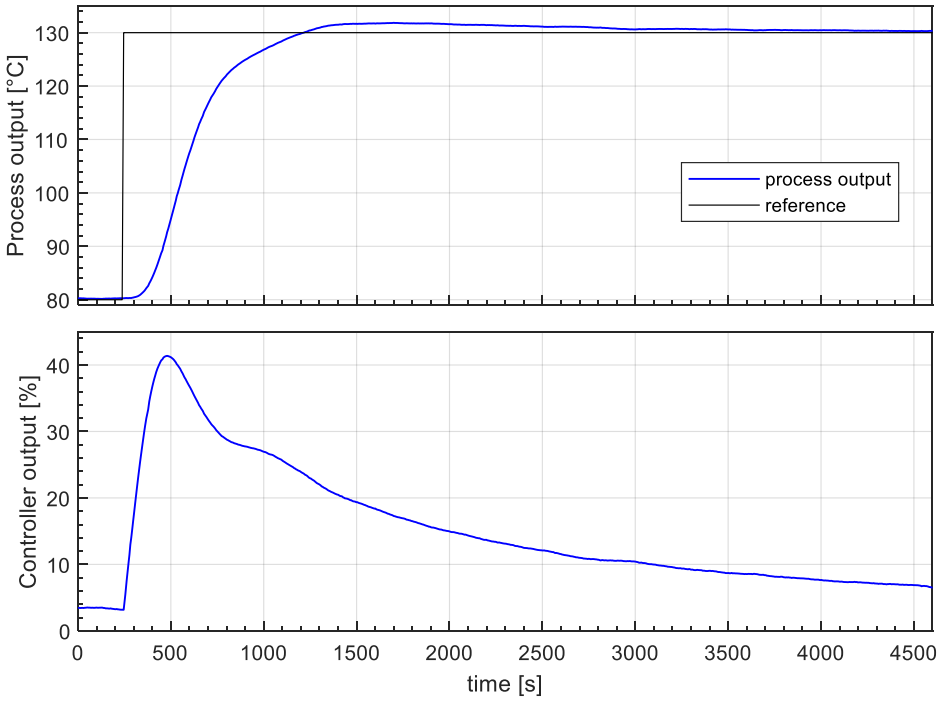

Figure 8.7: Industrial autoclave closed-loop response. Process input (electric power in %) and output (temperature in °C) signals during the experiment.

8.3 Solid-Oxide Fuel Cell

Experimental evaluation was also performed on a solid-oxide fuel cell (SOFC) system shown in Figures 8.8 and 8.9. As explained in [227], "*The system is comprised of two modules: a stack and a balance of plant (BoP). The 80-cell stack is sealed in an insulating housing and connected to the BoP module. The system can generate up to 10 kW of electric power from a single 80-cell SOFC stack. The feasible operating range for the unit in question is defined by the following variables: an airflow rate in the range of 700–1600 l/min and a natural gas flow rate up to 35 l/min, while the maximum operating temperature is 850 °C at the exhausts and 800 °C at the inlets.*"

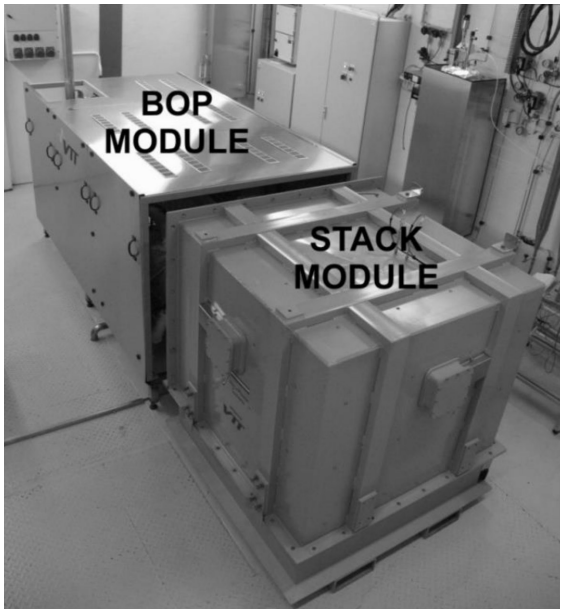

Figure 8.8: The solid-oxide fuel cell (SOFC) power generating unit. The unit is installed at the VTT Technical Research Centre of Finland [227].

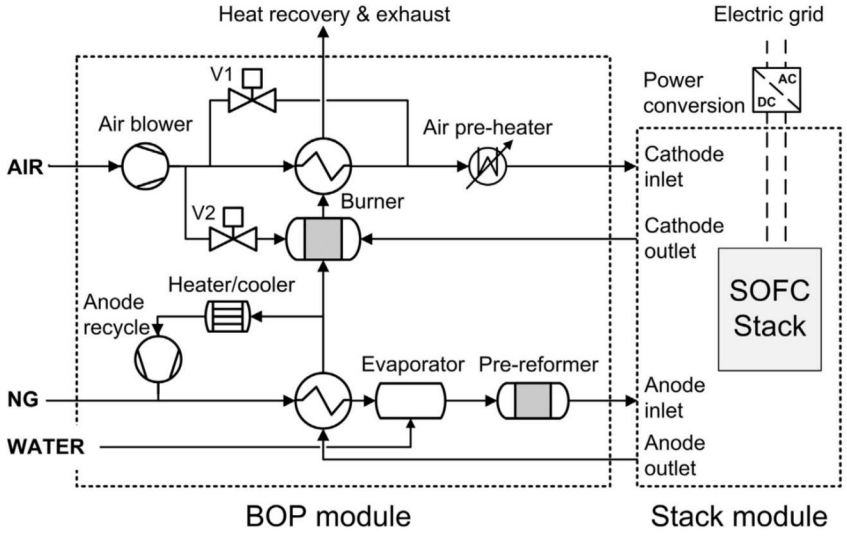

Figure 8.9: Schematic representation of the SOFC power generation unit [227].

The proposed tuning method was tested on the temperature control loop of an air heat exchanger (Air HEX) of a SOFC by using a PI controller. The process input was the flow rate of natural gas (NG) in standard litres per minute. The process output was the temperature of the heat exchanger in degrees Celsius. The control was performed with a Mitsubishi PLC controller [227] with a sampling time of 1 s.

The open-loop measurement is shown in Figure 8.10. The available measurements were not long enough to find a reliable process model. However, since the process resembles the IP with a delay at the beginning of its response (between 0 and 900 s), the controller parameters were calculated using the proposed tuning method for PI controllers.

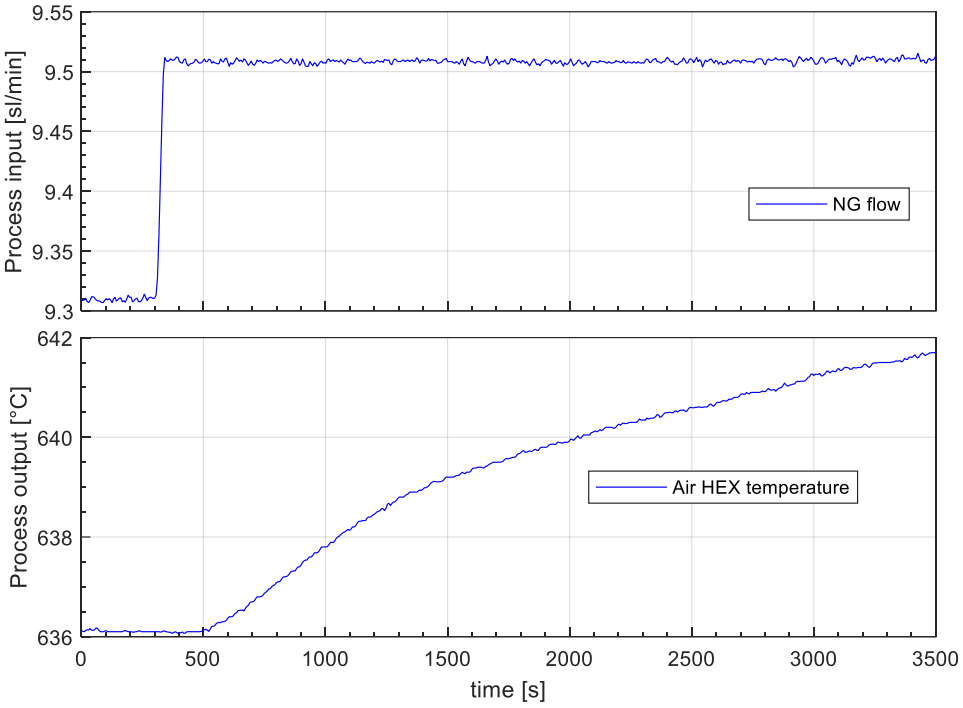

Figure 8.10: Open-loop response of Air HEX control loop.

From the measured open-loop response, using Expressions (2.9)–(2.11), the following characteristic areas were calculated:

$$A_0 = 0.0204, A_1 = 4.667, A_2 = 610.96. \tag{8.5}$$

Using Expressions (4.6) and (4.4), the next PI controller parameters were calculated for $b = 0$:

$$K_{\mathrm{P}} = 0.122, K_{\mathrm{I}} = 1.517 \cdot 10^{-4}, T_{\mathrm{F}} = 804\ s, \tag{8.6}$$

where T_{F} stands for the first-order reference filter time-constant. Here, we were using reference filtering instead of the reference weighting approach, as discussed in Chapter 4.2.

The closed-loop experiment was performed by decreasing the reference temperature of Air HEX from 652 to 642 °C. Figure 8.11 shows the closed-loop responses to a reference change. From the obtained closed-loop responses, it can be seen that the proposed method results in a quite efficient control of the temperature of Air HEX, i.e., the closed-loop response is stable and smooth.

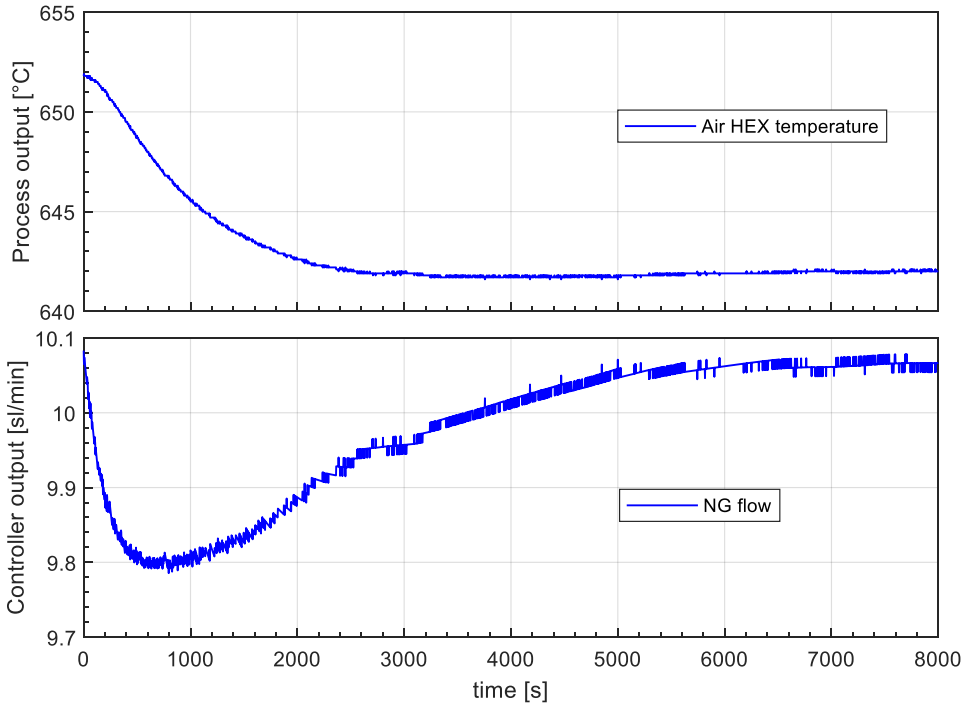

Figure 8.11: Closed-loop response of Air HEX control loop.

8.4 Control System for Charge-Amplifier Drift Compensation

The proposed tuning method was applied to a control system for drift compensation of charge-amplifier. It should be noted that the charge amplifier is intended for low-level electric charge measurements. Therefore, it is a very precise, low-noise instrument with stable characteristics.

The charge amplifier's main drawback is its sensitivity to DC input current, which causes a DC drift until the amplifier saturates due to cumulative summation. This saturation results in the inability to measure the output voltage of the charge amplifier. This problem is particularly severe for long-term DC or quasi-static measurements and for low-frequency periodic measurements [43]–[45], [228].

The studied drift compensation control system was part of a custom-built measurement system for automated low-frequency (1 kHz – 2 mHz) and high-temperature (25 °C – 450 °C) polarisation measurements of dielectric materials (Figure 8.12). Note that this type of setup is frequently used to characterise dielectric and piezoelectric materials because it is inexpensive and allows measurements at low driving frequencies, which allows the assessment of the electrical conductivity of the samples [55], [62]. This system consists of a Stanford Research Systems SR830 lock-in amplifier, a Kistler 5018A commercial charge-amplifier, and a temperature-regulated furnace to heat the measured samples. As an example, we represent the sample impedance Z_S as resistance R and capacitance C in a parallel configuration. Characterization takes place as follows.

A low voltage sinusoidal signal from the lock-in amplifier is applied to the electrodes of the sample. This voltage signal generates an electric field on the sample, and a charge amplifier measures the resulting charge Q of the sample. The output signal of the charge

amplifier is then analyzed with a lock-in amplifier. For more information about this concept of dielectric-material characterization, see [55], [62]. It should be noted that the control system for drift compensation enables measurement in the extended frequency and temperature range. In addition, the signal-to-noise ratio (SNR) is increased, which improves measurement precision.

The control system for drift compensation consists of a PID controller, a supervisory controller, and measurement of the mean value of the charge amplifier output voltage (DC value calculator). The primary task of the supervisory controller is the supervision of all system components. The controller is connected to the existing software for automated dielectric measurement. Depending on the output frequency of the sinusoidal generator, the controller adjusts the sampling frequency of the data acquisition card. It also includes automatic tuning of the controller parameters depending on the properties of the measured samples, the charge amplifier charge-voltage conversion ratio and the measured signal frequency.

The DC drift is compensated by an additional DC component with an opposite value at the charge-amplifier input. Charge amplifier output voltage U_1 is sampled by an analogue-to-digital converter (ADC), whose sampling frequency is a multiple of a sinusoidal generator frequency. The sampled points of one sinusoidal period of output voltage U_1 are then averaged to calculate a mean (DC) value, denoted as y. DC signal is then fed into feedback input y of the PID controller. Since the offset voltages of the operational amplifier and the sinusoidal generator are relatively small (up to a few mV), voltage u of the PID controller output is reduced by the voltage divider (consisting of R_D and the internal resistance R_G of the sinusoidal generator).

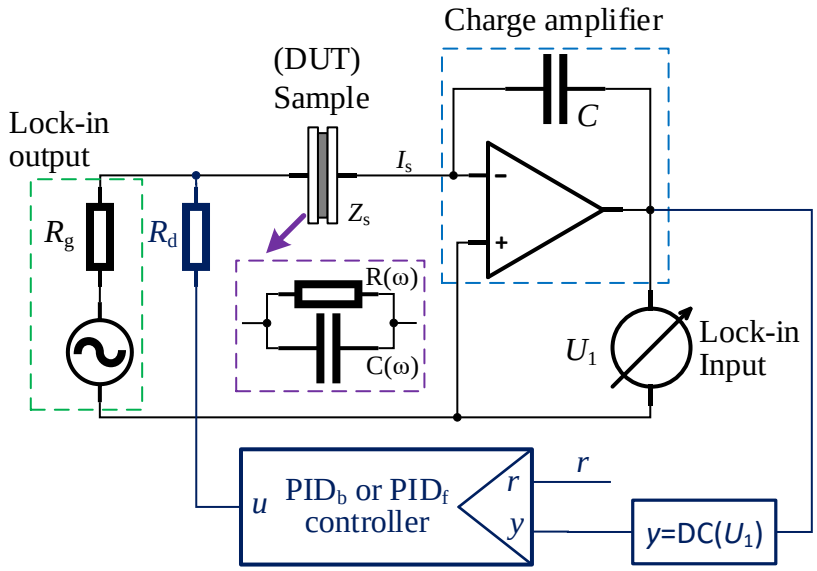

Figure 8.12: Custom-made measurement system for low-frequency and high-temperature polarisation measurements of dielectric materials with a charge-amplifier drift compensation control system. The measurement system is located at the Electronic Ceramics Department at the Jožef Stefan Institute.

The PID$_b$, PID$_{f2}$, and PID$_{fh}$ controllers were implemented using the LabVIEW software package, and data acquisition was performed using a NI USB-6001 card. The process output and input signals were limited between −10 and 10 V. The sampling time of the closed-loop control was 5 ms.

First, a step-change (input voltage signal 0 to −1 V) was applied to the process input. Figure 8.13 shows the open-loop response of the process.

Then, the following characteristic areas (with and without the added PID controller filter time constant, T_{F}) were calculated using Expressions (2.9)–(2.11):

$$\begin{gathered} A_0 = -8.5309, A_1 = -1.0748, A_2 = -0.0880, \\ A_3 = -5.7974 \times 10^{-3}, A_4 = -3.1956 \times 10^{-4}, \end{gathered} \tag{8.7}$$

$$\begin{gathered} T_{\mathrm{F}} = 0.02, A_{0\mathrm{F}} = -8.5309, A_{1\mathrm{F}} = -1.2454, A_{2\mathrm{F}} = -0.11291, \\ A_{3\mathrm{F}} = -8.0556 \times 10^{-3}, A_{4\mathrm{F}} = -4.8067 \times 10^{-4}. \end{gathered} \tag{8.8}$$

Based on the calculated characteristic areas (8.7), and according to Expression (5.34), the following second-order model of the process was calculated [216]:

$$G_{\mathrm{M}}(s) = \frac{-8.5309e^{-0.0179s}}{s(1 + 0.1081s + 0.0035s^2)}. \tag{8.9}$$

The comparison between the model (G_{M}) and the actual process time responses is shown in Figure 8.13.

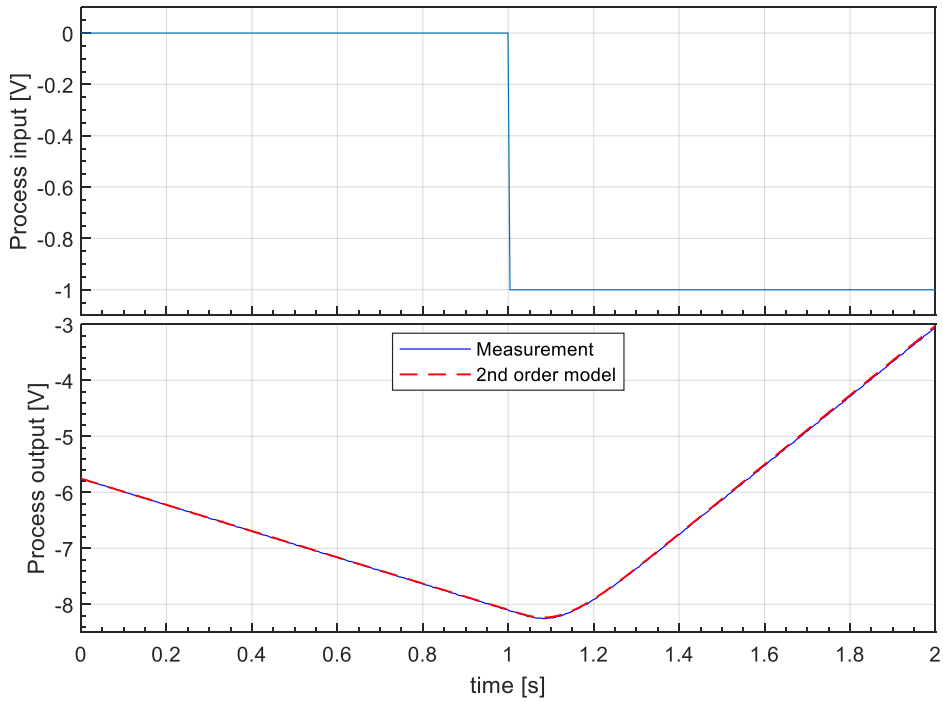

Figure 8.13: The open-loop response of the control system for charge-amplifier drift compensation and its second-order model.

The next $\mathrm{PID_b}$ controller parameters for $b = 0$ and $b = 0.5$ were calculated with Equations (5.10) and (5.13) using the calculated characteristic areas (8.8):

$$b = 0, K_{\mathrm{P}} = -1.1655, K_{\mathrm{I}} = -3.7512, K_{\mathrm{D}} = -0.063854, \tag{8.10}$$

$$b = 0.5, K_{\mathrm{P}} - 1.0688, K_{\mathrm{I}} = -2.8916, K_{\mathrm{D}} = -0.061832. \tag{8.11}$$

Next, using Expressions (5.14) and (5.32)–(5.43), the reference filter parameters for the PID_{fh} controller

$$\begin{gathered} b_{\text{F5}} = 3.8442 \times 10^{-6}, b_{\text{F4}} = 2.1293 \times 10^{-4}, b_{\text{F3}} = 4.1389 \times 10^{-3}, \\ b_{\text{F2}} = 4.5521 \times 10^{-2}, b_{\text{F1}} = 0.30178, \\ T_{\text{dm}} = 1.7874 \times 10^{-2}, K_{\text{CL}} = 1.2, T_{\text{CL}} = 0.1244, n = 2, \end{gathered} \tag{8.12}$$

and for the PID_{f2} controller

$$b_{\text{F2}} = 1.3029 \times 10^{-2}, b_{\text{F1}} = 0.16143, \tag{8.13}$$

were calculated. Note that for the PID_{f2} and PID_{fh} controllers, the PID_{b} controller gains were calculated for $b = 0$ (8.10).

The process closed-loop responses of the calculated PID_{b}, PID_{f2}, and PID_{fh} controllers with a reference step change ($r = 0.5$) and an artificially added process input step-disturbance ($d = 1$) are shown in Figure 8.14. As can be seen, the proposed method results in efficient drift compensation control. The comparison illustrates the superior tracking performance of the PID_{f2} and PID_{fh} controllers. As expected, the disturbance-rejection performance of the PID_{f2} and PID_{fh} controllers is equal to that of the PID_{b} controller with $b = 0$. This is confirmed by the criteria values shown in Figure 8.15. The IAT^2E measure is generally not recommended for noisy measurement signals. However, in our case, the noise of the process output was negligible.

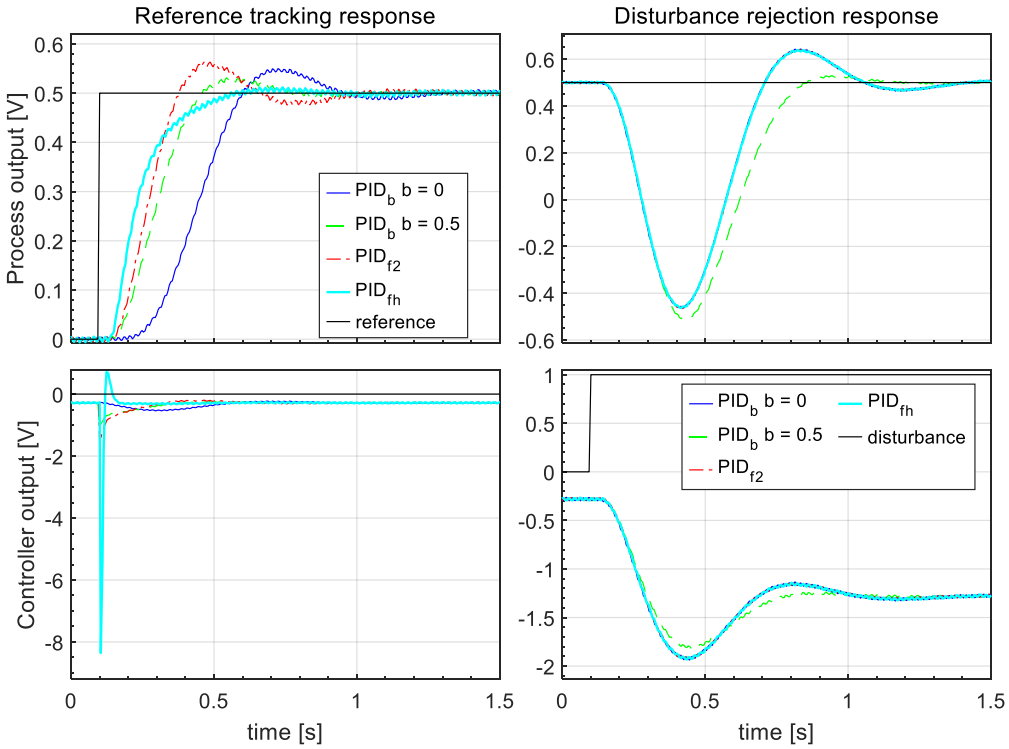

Figure 8.14: The control system for the charge-amplifier drift compensation closed-loop response.

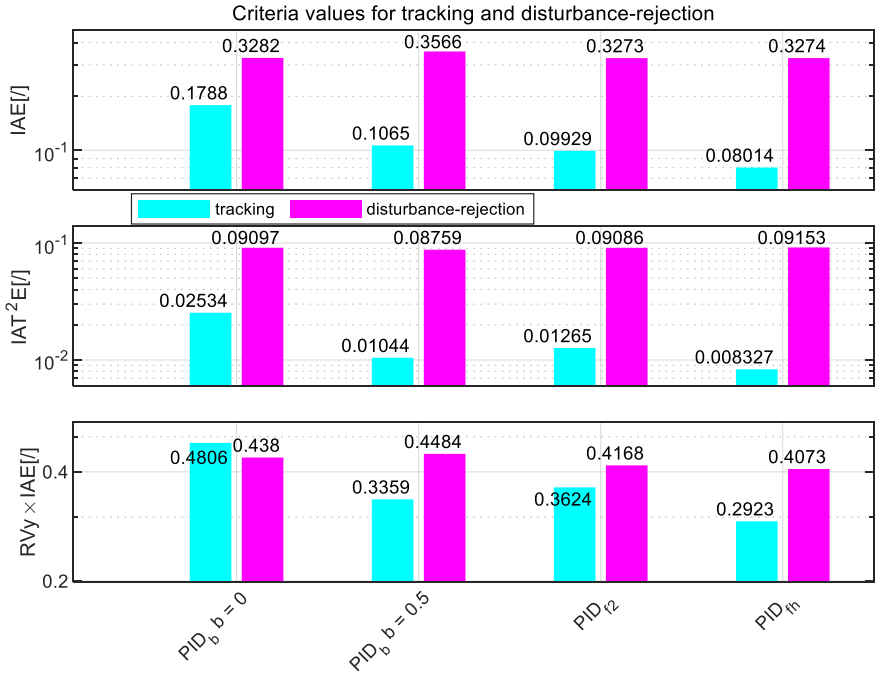

Figure 8.15: Criteria values for the charge-amplifier drift compensation.

Chapter 9

Conclusions and Outlook

The thesis presents a comprehensive study of the MOMI tuning method extension for integrating processes using different 2-DOF PI/PID control structures. The developed method remains nonparametric, i.e., it does not require an explicit process model to compute the controller parameters. This is an attractive approach since an intermediate step to compute the process model, which could be affected by a possible mismatch of the process model, can be eliminated. The controller parameters can be calculated from the characteristic areas, which can be calculated analytically from the time response of the process or from the transfer function of a general order with time delay. Both approaches are equivalent. In addition, two approaches are presented for the realization of a 2-DOF controller, i.e., with reference weighting or reference filtering. The calculation of the controllers' parameters is based on simple algebraic expressions, which makes the proposed method suitable for less demanding hardware, such as slower PLC controllers.

Furthermore, the developed extension of the tuning procedure provides an additional option to emphasize either noise rejection or tracking performance using the reference weighting parameter. In order to achieve the best overall closed-loop performance (optimal tracking and disturbance-rejection performance), two reference filter structures are presented. The main advantage of using a reference filter is that such a filter can significantly improve the tracking performance without degrading the disturbance-rejection performance. The parameters of the reference filter are also calculated using the characteristic areas, so the process model is not needed.

In addition, equations have been proposed to calculate the average closed-loop residence time, i.e., a measure that defines the speed of the control loop. The advantage of this measure is a prediction of the closed-loop tracking and disturbance-rejection speed. Furthermore, an additional parameter was provided to modify the closed-loop speed by changing the average closed-loop residence time. Based on this parameter, the user has the ability to recalculate the controller parameters to speed up or slow down the closed-loop response. For example, if the closed-loop response is too aggressive, the average closed-loop residence time can be increased, and the controller parameters can be recalculated. Thus, the less aggressive controller is obtained. It is worth mentioning that the mentioned additional speed parameter can also be calculated from the characteristic areas.

Furthermore, the thesis investigated the stability of the proposed tuning method and its robustness to changes in the process parameters (gain, time constants and time delay). It was shown that a change in the process gain or the time delay does not degrade the tracking or disturbance-rejection performance. Furthermore, the robustness of the calculated characteristic areas in a noisy environment was investigated, and a new approach to reduce the influence of high-frequency noise on the calculation of the characteristic areas was proposed.

Moreover, this work also proposed a method to identify a lower-order process model directly from the characteristic areas, i.e., from the nonparametric description of the process (in time-domain) or from the general order transfer function with a time delay (in frequency-domain).

The proposed controllers were also compared with other PI/PID tuning methods for integrating processes. The comparison showed superior control performance compared to the other tuning methods currently proposed.

In the last part of the thesis, the proposed tuning method was also tested on the following laboratory and industrial setups: a charge amplifier drift compensation system, a laboratory hydraulic system, an industrial autoclave, and a solid oxide fuel cell temperature control system. The closed-loop responses were fast and sufficiently damped in all experiments.

Numerous topics remained to be addressed. Of them, the following are of the greatest interest:

- Introduction of an optimisation criterion that includes both the average closed-loop residence time (speed of the closed-loop response) and the high-frequency noise attenuation. This criterion can be chosen to find the optimum between the speed of the closed-loop response and the measurement noise attenuation.
- Using higher-order controller filters in order to find the filter that provides the best high-frequency noise attenuation according to the given controller sampling time (T_S).
- Further testing and optimisation of the proposed signal filtering in the calculation of the characteristic areas from the process time responses.

Therefore, we will focus on answering these questions in our future work.

Appendix A

Calculated Controller Parameters

A.1 The PI Controllers' Parameters

This subchapter of the appendix shows all controllers' parameters in Chapter 7.1 (Comparison with other tuning methods for the PI controller).

Table A.1: The controller parameters for Åström's method [18]. The method is denoted as Åström 1.4 and Åström 2. The method employs a two-degrees-of-freedom (2-DOF) PI controller.

	Ms = 1.4			Ms = 2		
Process	K_P	K_I	b	K_P	K_I	b
G_{P1}	0.38606	0.059555	0.3701	0.73299	0.20251	0.7145
G_{P2}	0.33198	0.021211	0.60138	0.57645	0.12928	0.38732
G_{P3}	0.095403	0.0026051	0.60491	0.1539	0.010355	0.47995
G_{P4}	0.13644	0.0049685	0.6559	0.21485	0.02059	0.44584

Table A.2: The controller parameters for Taguchi's and Araki's method [105]. The method is denoted as Taguchi. The method employs a 2-DOF PI controller.

Process	K_P	K_I	b
G_{P1}	5.6676	1.2633	0.34396
G_{P2}	0.7662	0.18729	0.319
G_{P3}	0.29137	0.023165	0.32429
G_{P4}	/	/	/

Table A.3: The controller parameters for Ali's and Majhi's method [97]. The method is denoted as Ali–Majhi. The method employs a one-degree-of-freedom (1-DOF) PI controller.

Process	K_P	K_I	b
G_{P1}	12.6898	2.14342	1
G_{P2}	0.48	0.091603	1
G_{P3}	/	/	/
G_{P4}	/	/	/

Table A.4: The calculated characteristic areas for process models.

Process	A_0	A_1	A_2
G_{P1}	1	1.05	1.0513
G_{P2}	1	1	0.5
G_{P3}	1	3	5.5
G_{P4}	1	2	2.25

Table A.5: The calculated controller parameters for the proposed PI controller.

Process	K_P	K_I	b
G_{P1}	0.48041	0.086549	0.5
G_{P2}	0.55848	0.11696	0.5
G_{P3}	0.181	0.012285	0.5
G_{P4}	0.27477	0.028313	0.5

A.2 The PID Controllers' Parameters

This subchapter of the appendix shows all controllers' parameters in Chapter 7.2 (Comparison with other tuning methods for the PID controller).

Table A.6: The controller parameters for Ali's and Majhi's method [97]. The method is denoted as Ali–Majhi. The method employs a 1-DOF PID controller.

Process	K_P	K_I	K_D	T_F
G_{P1}	1.03	0.32492	0.5047	0.049
G_{P2}	4.6318	2.4992	2.1229	0.045833
G_{P3}	/	/	/	/
G_{P4}	/	/	/	/
G_{P5}	/	/	/	/

Table A.7: The controller parameters for Taguchi's and Araki's method [105]. The method is denoted as Taguchi. The method employs a 2-DOF PID controller.

Process	K_P	K_I	K_D	b	c
G_{P1}	1.253	0.52471	0.51837	0.3358	0.3203
G_{P2}	7.7503	5.5604	4.8194	0.3353	0.16557
G_{P3}	1.0249	0.16716	2.3111	0.3334	0.22731
G_{P4}	/	/	/	/	/
G_{P5}	/	/	/	/	/

Table A.8: The controller parameters for Medarametla's and Manimozhi's method [104]. The method is denoted as Medarametla. The method employs a 1-DOF PID controller with a Lead/Lag filter and reference filter.

Process	K_P	K_I	K_D	Ms	a_1	b_1	b_2	p
G_{P1}	0.8418	0.22851	0.13904	2	0.25	0.13049	/	0.67096
G_{P2}	4.2777	1.8486	2.7609	2	0.062884	0.0029418	0.0875	0.32734
G_{P3}	/	/	/	/	/	/	/	/
G_{P4}	1.0978	0.1576	1.0447	2.81	0.32	0.2941	0.049	0.9
G_{P5}	/	/	/	/	/	/	/	/

Table A.9: The controller parameters for Anil's and Padma Sree's method [116]. The method is denoted as Anil–Padma. The method employs a 2-DOF PID controller with a Lead/Lag filter.

Process	K_P	K_I	K_D	b	c	Ms	α	β
G_{P1}	0.83518	0.20382	0.29696	0.4	0	2	/	/
G_{P2}	3.2276	1.5841	2.169	0.4	0	2	0.21915	0.169
G_{P3}	/	/	/	/	/	/	/	/
G_{P4}	1.003	0.15723	0.65927	0.4	0	2.81	1.1608	0.549
G_{P5}	/	/	/	/	/	/	/	/

Table A.10: The controller parameters for Åström's method [25]. The method is denoted as Åström 1.4 and Åström 2. The method employs a 2-DOF PID controller. Note that c = 0.

	Ms = 1.4				Ms = 2			
Process	K_P	K_I	K_D	b	K_P	K_I	K_D	b
G_{P1}	0.75744	0.069015	0.015814	0.16209	1.5703	0.57756	0.34643	0.20601
G_{P2}	0.71797	0.11646	0.60513	0.37543	1.4744	0.4846	0.93961	0.37464
G_{P3}	0.16477	0.0064618	0.33641	0.45974	0.35767	0.032304	0.72858	0.3435
G_{P4}	0.2779	0.0094486	0.054395	0.71258	0.71432	0.094751	0.55202	0.23398
G_{P5}	0.18428	0.0086819	0.095989	0.64949	0.4441	0.063073	0.43352	0.28467

Table A.11: The calculated characteristic areas for process models.

Process	A_0	A_1	A_2	A_3	A_4
G_{P1}	1	1	0.5	0.16667	0.041667
G_{P2}	1	1.7	2.3563	3.1881	4.3045
G_{P3}	1	4	10.25	21.9167	42.7292
G_{P4}	0.5	1.1	1.2525	1.0333	0.7114
G_{P5}	1	2	2.25	1.875	1.2891

Table A.12: The calculated characteristic areas for process models with additional filter time constant $T_F = 0.01$ s.

Process	A_{0F}	A_{1F}	A_{2F}	A_{3F}	A_{4F}
G_{P1}	1	1.01	0.5101	0.17177	0.043384
G_{P2}	1	1.71	2.3733	3.2118	4.3367
G_{P3}	1	4.01	10.2901	22.0196	42.9494
G_{P4}	0.5	1.105	1.2635	1.046	0.72186
G_{P5}	1	2.01	2.2701	1.8977	1.308

Table A.13: The calculated PID controller parameters for the PID_{f2} and PID_{fh} controllers with filter time constant $T_F = 0.01$ s.

Process	K_P	K_I	K_D
G_{P1}	1.128	0.47494	0.33942
G_{P2}	3.8867	2.3031	2.2796
G_{P3}	0.42189	0.053533	0.66242
G_{P4}	1.1228	0.22574	0.79237
G_{P5}	0.64575	0.1444	0.44386

Table A.14: The intermediate calculated parameters for the reference filters' calculations.

Process	K_{P1}	K_{D1}	K_M	b_{1m}	T_{dm}	a_{1m}	a_{2m}	K_{CL}
G_{P1}	0.74265	0.25007	1	0	1	0.0101	0	3
G_{P2}	1.4017	1.8969	1	0	0.35	1.35	0	3
G_{P3}	0.267362	0.572123	1	0	1	3	2.25	3
G_{P4}	0.72349	0.5989	0.5	-0.50961	0.739	0.95139	0.23772	3
G_{P5}	0.42588	0.35601	1	0	0.8691	1.1309	0.38947	3

Table A.15: The reference filter parameters for the PID_{f2} controller.

Process	b_{F2}	b_{F1}
G_{P1}	0.52881	1.0284
G_{P2}	0.4745	0.97417
G_{P3}	8.5723	4.1406
G_{P4}	2.441	2.2095
G_{P5}	2.2552	2.1238

Table A.16: The reference filter parameters for the PID_{fh} controller.

Process	b_{F5}	b_{F4}	b_{F3}	b_{F2}	b_{F1}	T_{dm}	T_{CL}	n
G_{P1}	0.0036331	0.25639	0.93567	1.716	1.8749	1	0.44884	2
G_{P2}	0.007054	0.12374	0.51052	1.1389	1.5126	0.35	0.23781	2
G_{P3}	26.401	73.2914	60.0364	27.1967	7.38084	1	1.24675	2
G_{P4}	1.1367	6.4463	9.8454	8.2311	4.0948	0.739	0.92147	2
G_{P5}	1.7303	6.8381	9.8559	8.1185	4.0373	0.8691	0.7827	2

References

[1] T. Kos and D. Vrančić, "MATLAB's implementation of Parametric and Nonparametric PI/PID Controller Tuning Method for Integrating Processes based on Magnitude Optimum," 2021. https://doi.org/10.5281/zenodo.4646865 (accessed Mar. 30, 2021).

[2] K. J. K. J. Åström and T. Hägglund, "Automatic tuning of simple regulators with specifications on phase and amplitude margins," *Automatica*, vol. 20, no. 5, pp. 645–651, Sep. 1984, doi: 10.1016/0005-1098(84)90014-1.

[3] W. K. Ho, O. P. Gan, E. B. Tay, and E. L. Ang, "Performance and gain and phase margins of well-known PID tuning formulas," *IEEE Transactions on Control Systems Technology*, vol. 4, no. 4, pp. 473–477, Jul. 1996, doi: 10.1109/87.508897.

[4] R. Vilanova and A. Visioli, *PID Control in the Third Millennium*, 1st ed. London: Springer London, 2012.

[5] A. Visioli, "Time-optimal plug&control for integrating and FOPDT processes," *Journal of Process Control*, vol. 13, no. 3, pp. 195–202, Apr. 2003, doi: 10.1016/S0959-1524(02)00059-8.

[6] L. D. Desborough and R. M. Miller, "Increasing Customer Value of Industrial Control Performance Monitoring— Honeywell Experience," in *AIChE Symposium Series*, Jan. 2001, vol. 98, no. 326, pp. 169–189.

[7] M. Shamsuzzoha and S. Skogestad, "The setpoint overshoot method: A simple and fast closed-loop approach for PID tuning," *Journal of Process Control*, vol. 20, no. 10, pp. 1220–1234, Dec. 2010, doi: 10.1016/J.JPROCONT.2010.08.003.

[8] C. G. Sigurd Skogestad, "Should we forget the Smith Predictor?," *IFAC-PapersOnLine*, vol. 51, no. 4, pp. 769–774, 2018, doi: 10.1016/j.ifacol.2018.06.203.

[9] F. Faccin and J. O. Trierweiler, "A Novel Tool for Multi-Model PID Controller Design," *IFAC Proceedings Volumes*, vol. 37, no. 9, pp. 251–256, Jul. 2004, doi: 10.1016/S1474-6670(17)31820-7.

[10] K. J. Åström and T. Hägglund, "The future of PID control," *Control Engineering Practice*, vol. 9, no. 11, pp. 1163–1175, Nov. 2001, doi: 10.1016/S0967-0661(01)00062-4.

[11] L. R. da Silva, R. C. C. Flesch, and J. E. Normey-Rico, "Controlling industrial dead-time systems: When to use a PID or an advanced controller," *ISA Transactions*, vol. 99, pp. 339–350, Apr. 2020, doi: 10.1016/j.isatra.2019.09.008.

[12] A. Alfi, A. Bakhshi, M. Yousefi, and H. A. Talebi, "Design and Implementation of Robust-Fixed Structure Controller for Telerobotic Systems," *Journal of Intelligent & Robotic Systems*, vol. 83, no. 2, pp. 253–269, Aug. 2016, doi: 10.1007/s10846-016-0335-2.

[13] K. J. Åström and T. Hägglund, *Advanced PID Control*, 1st ed. ISA - The Instrumentation, Systems and Automation Society, 2006.

[14] A. Leva, C. J. Cox, and A. E. Ruano, *Hands-on PID autotuning : a guide to better utilisation*. New York, United States: IFAC Profesional Brief, 2002.

[15] S. Skogestad, "Simple analytic rules for model reduction and PID controller tuning," *Journal of Process Control*, vol. 13, no. 4, pp. 291–309, Jun. 2003, doi: 10.1016/S0959-1524(02)00062-8.

[16] A. O'Dwyer, *Handbook of PI and PID Controller Tuning Rules*, 3rd ed. London, UK: Imperial College Press, 2009.

[17] J. G. Ziegler and N. B. Nichols, "Optimum Settings for Automatic Controllers," *Transactions of the ASME*, vol. 64, pp. 759–768, 1942.

[18] K. J. Åström, H. Panagopoulos, and T. Hägglund, "Design of PI Controllers based on Non-Convex Optimization," *Automatica*, vol. 34, no. 5, pp. 585–601, May 1998, doi: 10.1016/S0005-1098(98)00011-9.

[19] R. Gorez, "A survey of PID auto-tuning methods," *Journal A.*, vol. 38, no. 1, pp. 3–10, 1997.

[20] M. Huba, "Constrained Pole Assignment Control," in *Current Trends in Nonlinear Systems and Control*, L. Menini, L. Zaccarian, and C. T. Abdallah, Eds. Boston, MA: Birkhäuser Boston, 2006, pp. 163–183.

[21] M. Huba, *Theory of Automatic Control 3: Constrained PID Control*. Bratislava: STU, 2006.

[22] T. Sato, I. Hayashi, Y. Horibe, R. Vilanova, and Y. Konishi, "Optimal Robust PID Control for First- and Second-Order Plus Dead-Time Processes," *Applied Sciences*, vol. 9, no. 9, p. 1934, May 2019, doi: 10.3390/app9091934.

[23] H. Meneses, O. Arrieta, F. Padula, R. Vilanova, and A. Visioli, "PI/PID Control Design Based on a Fractional-Order Model for the Process," *IFAC-PapersOnLine*, vol. 52, no. 1, pp. 976–981, 2019, doi: 10.1016/j.ifacol.2019.06.189.

[24] Y. Li, K. H. Ang, and G. C. Y. Chong, "Patents, software, and hardware for PID control: an overview and analysis of the current art," *IEEE Control Systems*, vol. 26, no. 1, pp. 42–54, Feb. 2006, doi: 10.1109/MCS.2006.1580153.

[25] K. J. Åström and T. Hägglund, *PID controllers : theory, design, and tuning*, 2nd ed. Research Triangle Park, N.C.: International Society for Measurement and Control, 1995.

[26] G. M. Van Der Zalm, *Tuning of Pid-type Controllers: Literature Overview*. Eindhoven,The Netherlands: Technische Universiteit Eindhoven, 2004.

[27] D. E. Seborg, D. A. Mellichamp, T. F. Edgar, and F. J. Doyle, *Process Dynamics and Control*, 3rd ed. John Wiley & Sons, 2010.

[28] A. Visioli and Q. Zhong, *Control of Integral Processes with Dead Time*, 1st ed. London: Springer-Verlag London, 2011.

[29] I. L. Chien and P. S. Fruehauf, "Consider IMC tuning to improve controller performance," *Chemistry Engineering Progress*, vol. 86, no. 10, pp. 33–41, 1990.

[30] C. Fuentes and W. L. Luyben, "Control of high-purity distillation columns," *Industrial & Engineering Chemistry Process Design and Development*, vol. 22, no. 3, pp. 361–366, Jul. 1983, doi: 10.1021/i200022a004.

[31] Q.-G. Wang, C. C. Hang, and X.-P. Yang, "Single-loop controller design via IMC principles," *Automatica*, vol. 37, no. 12, pp. 2041–2048, Dec. 2001, doi: 10.1016/S0005-1098(01)00170-4.

[32] R. Srividya and M. Chidambaram, "On-line controllers tuning for integrator plus delay systems," *Process Control and Quality*, vol. 9, no. 1, pp. 59–66, 1997.

[33] B. A. Ogunnaike and W. H. Ray, *Process Dynamics, Modeling, and Control*, 1st ed. New York, United States: Oxford University Press Inc, 1994.

[34] N. M. Filatov, U. Keuchel, and H. Unbehauen, "Dual control for an unstable mechanical plant," *IEEE Control Systems*, vol. 16, no. 4, pp. 31–37, Aug. 1996, doi: 10.1109/37.526913.

[35] T. Liu and F. Gao, *Industrial Process Identification and Control Design: Step-test and Relay-experiment-based Methods*, 1st ed. London: Springer London, 2012.

[36] T.-L. Chia and I. Lefkowitz, "Internal model-based control for integrating processes," *ISA Transactions*, vol. 49, no. 4, pp. 519–527, Oct. 2010, doi: 10.1016/j.isatra.2010.03.012.

[37] B. W. Bequette, *Process Control: Modeling, Design and Simulation*, 1st ed. Upper Saddle River, N.J.: Upper Saddle River, N.J., 2003.

[38] M. Hovd and S. Skogestad, "Pairing Criteria for Decentralized Control of Unstable Plants," *Industrial & Engineering Chemistry Research*, vol. 33, no. 9, pp. 2134–2139, Sep. 1994, doi: 10.1021/ie00033a016.

[39] L. Wang and W. R. Cluett, "Tuning PID controllers for integrating processes," *IEE Proceedings - Control Theory and Applications*, vol. 144, no. 5, pp. 385–392, Sep. 1997, doi: 10.1049/ip-cta:19971435.

[40] N.-S. Pai, S.-C. Chang, and C.-T. Huang, "Tuning PI/PID controllers for integrating processes with deadtime and inverse response by simple calculations," *Journal of Process Control*, vol. 20, no. 6, pp. 726–733, Jul. 2010, doi: 10.1016/j.jprocont.2010.04.003.

[41] W. P. Kistler, "Messverstärker zur Messung von elektrischer Ladung," Schweiz. Patentsch. 267431, 1950.

[42] P. M. Günter, C. Schwarz, and R. Teichmann, *Combustion Engines Development - Comprehensible presentation of the simulation of combustion engine processes*, 1st ed. Berlin, Heidelberg: Springer Berlin Heidelberg, 2012.

[43] G. Gautschi, *Piezoelectric Sensorics*, 1st ed. Berlin, Heidelberg: Springer Berlin Heidelberg, 2002.

[44] J. Fraden, *Handbook of Modern Sensors*, 4th ed. New York, NY: Springer-Verlag New York, 2010.

[45] R. Morrison, "Analog Circuits," in *Grounding and Shielding:Circuits and Interference*, Hoboken, NJ, USA: John Wiley & Sons, Inc., pp. 65–95.

[46] S. Dalle Vacche, Y. Leterrier, V. Michaud, D. Damjanovic, A. B. Aebersold, and J.-A. E. Månson, "Effect of interfacial interactions on the electromechanical response of poly(vinylidene fluoride-trifluoroethylene)/BaTiO3 composites and its time dependence after poling," *Composites Science and Technology*, vol. 114, pp. 103–109, Jun. 2015, doi: 10.1016/j.compscitech.2015.04.012.

[47] A. F. Barzegar, D. Damjanovic, and N. Setter, "The effect of boundary conditions and sample aspect ratio on apparent d/sub 33/ piezoelectric coefficient determined by direct quasistatic method," *IEEE Transactions on Ultrasonics, Ferroelectrics and Frequency Control*, vol. 51, no. 3, pp. 262–270, Mar. 2004, doi: 10.1109/TUFFC.2004.1320781.

[48] E. Lemaire, R. Moser, C. J. Borsa, and D. Briand, "Green paper-based piezoelectronics for sensors and actuators," *Sensors and Actuators A: Physical*, vol. 244, pp. 285–291, Jun. 2016, doi: 10.1016/j.sna.2016.04.024.

[49] H. Birol, D. Damjanovic, and N. Setter, "Preparation and characterization of (K0.5Na0.5)NbO3 ceramics," *Journal of the European Ceramic Society*, vol. 26, no. 6, pp. 861–866, Jan. 2006, doi: 10.1016/j.jeurceramsoc.2004.11.022.

[50] Q. Guo, G. Z. Cao, and I. Y. Shen, "Cost-Effective Measurements of Piezoelectric Coefficient d33 of Thin-Film PZT Using a Mini Force Hammer," in *Volume 7: 5th International Conference on Micro- and Nanosystems; 8th International Conference on Design and Design Education; 21st Reliability, Stress Analysis, and Failure Prevention Conference*, 2011, pp. 269–277, doi: 10.1115/DETC2011-47512.

[51] Q. Guo, G. Z. Cao, and I. Y. Shen, "Measurements of Piezoelectric Coefficient d 33 of Lead Zirconate Titanate Thin Films Using a Mini Force Hammer," *Journal of Vibration and Acoustics*, vol. 135, no. 1, p. 011003, Feb. 2013, doi: 10.1115/1.4006881.

[52] A. Barzegar, D. Damjanovic, N. Ledermann, and P. Muralt, "Piezoelectric response of thin films determined by charge integration technique: Substrate bending effects," *Journal of Applied Physics*, vol. 93, no. 8, pp. 4756–4760, Apr. 2003, doi: 10.1063/1.1558228.

[53] A. J. Bur, "Measurements of the dynamic piezoelectric properties of bone as a function of temperature and humidity," *Journal of Biomechanics*, vol. 9, no. 8, pp. 495–507, Jan. 1976, doi: 10.1016/0021-9290(76)90066-X.

[54] G. Davies *et al.*, "Dielectric and pyroelectric properties of poly[2,3-bis(trifluoromethyl)norbornadiene]," *Polymer*, vol. 36, no. 2, pp. 235–243, Jan. 1995, doi: 10.1016/0032-3861(95)91309-U.

[55] M. I. Morozov and D. Damjanovic, "Hardening-softening transition in Fe-doped Pb(Zr,Ti)O3 ceramics and evolution of the third harmonic of the polarization response," *Journal of Applied Physics*, vol. 104, no. 3, p. 034107, Aug. 2008, doi: 10.1063/1.2963704.

[56] D. V. Taylor, D. Damjanovic, and N. Setter, "Nonlinear contributions to dielectric and piezoelectric properties in lead zirconate titanate thin films," *Ferroelectrics*, vol. 224, no. 1, pp. 299–306, Mar. 1999, doi: 10.1080/00150199908210580.

[57] S. Zhang, M. Xu, X. Liang, and S. Shen, "Shear flexoelectric coefficient μ1211 in polyvinylidene fluoride," *Journal of Applied Physics*, vol. 117, no. 20, p. 204102, May 2015, doi: 10.1063/1.4921444.

[58] Y. Tajitsu *et al.*, "Ferroelectric Behavior in Thin Films of Polyurea-5," *Japanese Journal of Applied Physics*, vol. 35, no. Part 1, No. 9B, pp. 5199–5202, Sep. 1996, doi: 10.1143/JJAP.35.5199.

[59] A. Mazzalai, D. Balma, N. Chidambaram, Li Jin, and P. Muralt, "Simultaneous piezoelectric and ferroelectric characterization of thin films for MEMS actuators," in *2013 Joint IEEE International Symposium on Applications of Ferroelectric and Workshop on Piezoresponse Force Microscopy (ISAF/PFM)*, Jul. 2013, pp. 363–366, doi: 10.1109/ISAF.2013.6748724.

[60] M. Makarovič, J. Walker, E. Khomyakova, A. Bencan, B. Malic, and T. Rojac, "Control of electrical conductivity in 0.7BiFeO3 - 0.3SrTiO3 ferroelectric ceramics via thermal treatment in nitrogen atmosphere and Mn doping," *Informacije MIDEM*, vol. 46, no. 3, pp. 154–159, 2016.

[61] T. Rojac, M. Makarovic, J. Walker, H. Ursic, D. Damjanovic, and T. Kos, "Piezoelectric response of BiFeO3 ceramics at elevated temperatures," *Applied Physics Letters*, vol. 109, no. 4, p. 042904, Jul. 2016, doi: 10.1063/1.4960103.

[62] M. I. Morozov and D. Damjanovic, "Charge migration in Pb(Zr,Ti)O3 ceramics and its relation to ageing, hardening, and softening," *Journal of Applied Physics*, vol. 107, no. 3, pp. 1–10, 2010, doi: 10.1063/1.3284954.

[63] K. H. Baumgärtel, D. Zöllner, and K.-L. Krieger, "Classification and Simulation Method for Piezoelectric PVDF Sensors," *Procedia Technology*, vol. 26, pp. 491–498, 2016, doi: 10.1016/j.protcy.2016.08.062.

[64] R. Igreja and C. J. Dias, "Dielectric response of interdigital chemocapacitors: The role of the sensitive layer thickness," *Sensors and Actuators B: Chemical*, vol. 115, no. 1, pp. 69–78, May 2006, doi: 10.1016/j.snb.2005.08.019.

[65] K. Kim, S. Zhang, G. Salazar, and X. Jiang, "Design, fabrication and characterization of high temperature piezoelectric vibration sensor using YCOB crystals," *Sensors and Actuators A: Physical*, vol. 178, pp. 40–48, May 2012, doi: 10.1016/j.sna.2012.02.003.

[66] Y.-C. Hsu, C.-C. Wu, C.-C. Lee, G. Z. Cao, and I. Y. Shen, "Demonstration and characterization of PZT thin-film sensors and actuators for meso- and micro-structures," *Sensors and Actuators A: Physical*, vol. 116, no. 3, pp. 369–377, Oct. 2004, doi: 10.1016/j.sna.2004.05.024.

[67] M. Huba, K. Žáková, P. Bisták, M. Hypiusová, and P. Ťapák, "Seeking a unique view to control of simple models," *IFAC-PapersOnLine*, vol. 52, no. 9, pp. 91–96, 2019, doi: 10.1016/j.ifacol.2019.08.130.

[68] M. Huba, P. Moura Oliveira, P. Bistak, D. Vrancic, and K. Žáková, "A Set of Active Disturbance Rejection Controllers Based on Integrator Plus Dead-Time Models," *Applied Sciences*, vol. 11, no. 4, p. 1671, Feb. 2021, doi: 10.3390/app11041671.

[69] J. E. Normey-Rico, *Control of Dead-time Processes*, 1st ed. London: Springer London, 2007.

[70] M. Huzmezan, W. A. Gough, G. A. Dumont, and S. Kovac, "Time delay integrating systems: a challenge for process control industries. A practical solution," *Control Engineering Practice*, vol. 10, no. 10, pp. 1153–1161, Oct. 2002, doi: 10.1016/S0967-0661(02)00060-6.

[71] D. B. S. Kumar and R. Padma Sree, "Tuning of IMC based PID controllers for integrating systems with time delay," *ISA Transactions*, vol. 63, pp. 242–255, Jul. 2016, doi: 10.1016/j.isatra.2016.03.020.

[72] M. Huba, "Exploring PID tuning strategies considering noise impact in the IPDT plant control," *IFAC-PapersOnLine*, vol. 52, no. 27, pp. 204–211, 2019, doi: 10.1016/j.ifacol.2019.12.757.

[73] H. Yin, W. Zhang, R. Yao, and S. Lin, "IMC-PID Load Disturbance Rejection Controller with Set-point Filter for The Integrating and Unstable Processes with Time delay," in *2018 37th Chinese Control Conference (CCC)*, Jul. 2018, pp. 142–147, doi: 10.23919/ChiCC.2018.8483151.

[74] F. Peker and I. Kaya, "Integral-Proportional Derivative (I-PD) Controller Tuning for Pure Integrating Processes with Time Delay," in *2019 International Conference on Applied Automation and Industrial Diagnostics (ICAAID)*, Sep. 2019, vol. 1, pp. 1–6, doi: 10.1109/ICAAID.2019.8934961.

[75] M. Huba and D. Vrančić, "Introduction to the Discrete Time PIDmn Control for the IPDT Plant," *IFAC-PapersOnLine*, vol. 51, no. 6, pp. 119–124, 2018, doi: 10.1016/j.ifacol.2018.07.140.

[76] S. Chakraborty, S. Ghosh, and A. Kumar Naskar, "I–PD controller for integrating plus time-delay processes," *IET Control Theory & Applications*, vol. 11, no. 17, pp. 3137–3145, Nov. 2017, doi: 10.1049/iet-cta.2017.0112.

[77] M. Huba, "Model-based higher-order PID control design," Jul. 2020.

[78] C. Grimholt and S. Skogestad, "Optimal PI and PID control of first-order plus delay processes and evaluation of the original and improved SIMC rules," *Journal of Process Control*, vol. 70, pp. 36–46, Oct. 2018, doi: 10.1016/j.jprocont.2018.06.011.

[79] C. Dalen and D. Di Ruscio, "Performance Optimal PI controller Tuning Based on Integrating Plus Time Delay Models," *Algorithms*, vol. 11, no. 6, p. 86, Jun. 2018, doi: 10.3390/a11060086.

[80] H. Takeda and Y. Yamashita, "Process-Identification and Design of Robust PI Controller for a Self-Oscillating Integral Process with Dead Time," *Journal of Chemical Engineering of Japan*, vol. 52, no. 5, pp. 447–454, May 2019, doi: 10.1252/jcej.18we261.

[81] M. Huba, "Performance measures, performance limits and optimal PI control for the IPDT plant," *Journal of Process Control*, vol. 23, no. 4, pp. 500–515, Apr. 2013, doi: 10.1016/j.jprocont.2013.01.002.

[82] M. Vítečková and A. Víteček, "2DOF PI and PID Controllers Tuning," *IFAC Proceedings Volumes*, vol. 43, no. 2, pp. 343–348, 2010, doi: 10.3182/20100607-3-CZ-4010.00061.

[83] U. M. Nath, C. Dey, and R. K. Mudi, "Stabilized IMC-PI controller designing for IPDT processes based on gain and phage margin criteria," *IFAC-PapersOnLine*, vol. 53, no. 1, pp. 129–134, 2020, doi: 10.1016/j.ifacol.2020.06.022.

[84] M. Vítečková and A. Víteček, "Two-degree of freedom controller tuning for integral plus time delay plants," *ICIC Express Letters*, vol. 2, no. 3, pp. 225–229, 2008.

[85] P. Bagheri and H. Nemati, "Novel Tuning Strategy for Two-Degree-of-Freedom PI Controllers," *IFAC Proceedings Volumes*, vol. 44, no. 1, pp. 6757–6762, Jan. 2011, doi: 10.3182/20110828-6-IT-1002.03312.

[86] M. Huba, P. Bisták, Z. Skachová, and K. Žáková, "Predictive antiwindup PI and PID controllers based on I1- and I2 models with dead time," in *The 6th IEEE Mediterranean Conference on Control and Systems*, Jun. 1998, pp. 532–537.

[87] A. Visioli, "Optimal tuning of PID controllers for integral and unstable processes," *IEE Proceedings - Control Theory and Applications*, vol. 148, no. 2, pp. 180–184, Mar. 2001, doi: 10.1049/ip-cta:20010197.

[88] M. Huba, D. Vrancic, and P. Bistak, "PID Control with Higher Order Derivative Degrees for IPDT Plant Models," *IEEE Access*, vol. Accepted, pp. 1–1, Dec. 2020, doi: 10.1109/ACCESS.2020.3047351.

[89] I. Kaya, "Optimal PI–PD Controller Design for Pure Integrating Processes with Time Delay," *Journal of Control, Automation and Electrical Systems*, Feb. 2021, doi: 10.1007/s40313-021-00692-2.

[90] M. A. Siddiqui, S. H. Laskar, M. N. Anwar, and M. Naseem, "A Model-Free PI/PID Controller based on Direct Synthesis Approach to achieve Disturbance Rejection," in *IECON 2019 - 45th Annual Conference of the IEEE Industrial Electronics Society*, Oct. 2019, pp. 207–212, doi: 10.1109/IECON.2019.8926967.

[91] P. Mercader and A. Baños, "A PI tuning rule for integrating plus dead time processes with parametric uncertainty," *ISA Transactions*, vol. 67, pp. 246–255, Mar. 2017, doi: 10.1016/j.isatra.2017.01.025.

[92] A. Raza, N. Pathak, and M. N. Anwar, "A PID controller tuning rule for FOPDT process to achieve better load disturbance rejection based on maximum sensitivity," in *2017 International Conference on Smart grids, Power and Advanced Control Engineering (ICSPACE)*, Aug. 2017, pp. 149–154, doi: 10.1109/ICSPACE.2017.8343421.

[93] M. Shamsuzzoha, S. Skogestad, and I. J. Halvorsen, "A simple approach for on-line PI controller tuning using closed-loop setpoint responses," *Computer Aided Chemical Engineering*, vol. 28, pp. 619–624, Jan. 2010, doi: 10.1016/S1570-7946(10)28104-X.

[94] D. O. Rene Pereira, W. B. Correia, F. G. Nogueira, and B. C. Torrico, "Automatic Tuning Method for PID Controllers Applied to Integrating and Unstable Processes," in *2018 13th IEEE International Conference on Industry Applications (INDUSCON)*, Nov. 2018, pp. 744–749, doi: 10.1109/INDUSCON.2018.8627347.

[95] M. Huba, "Constrained filtered PID Controller for IPDT plants," in *2019 27th Mediterranean Conference on Control and Automation (MED)*, Jul. 2019, no. 3, pp. 636–641, doi: 10.1109/MED.2019.8798590.

[96] B. Vanavil, A. V. N. L. Anusha, M. Perumalsamy, and A. S. Rao, "Enhanced IMC-PID controller design with lead-lag filter for unstable and integrating processes with time delay," *Chemical Engineering Communications*, vol. 201, no. 11, pp. 1468–1496, Nov. 2014, doi: 10.1080/00986445.2013.818983.

[97] A. Ali and S. Majhi, "PID controller tuning for integrating processes," *ISA Transactions*, vol. 49, no. 1, pp. 70–78, Jan. 2010, doi: 10.1016/j.isatra.2009.09.001.

[98] R. Vilanova, O. Arrieta, and P. Ponsa, "Robust PI/PID controllers for load disturbance based on direct synthesis," *ISA Transactions*, vol. 81, pp. 177–196, Oct. 2018, doi: 10.1016/j.isatra.2018.07.040.

[99] S. Atic, E. Cokmez, F. Peker, and I. Kaya, "PID Controller Design for Controlling Integrating Processes with Dead Time using Generalized Stability Boundary Locus," *IFAC-PapersOnLine*, vol. 51, no. 4, pp. 924–929, 2018, doi: 10.1016/j.ifacol.2018.06.104.

[100] M. Irshad and A. Ali, "Optimal tuning rules for PI/PID controllers for inverse response processes," *IFAC-PapersOnLine*, vol. 51, no. 1, pp. 413–418, 2018, doi: 10.1016/j.ifacol.2018.05.063.

[101] R. C. Panda, "Synthesis of PID controller for unstable and integrating processes," *Chemical Engineering Science*, vol. 64, no. 12, pp. 2807–2816, Jun. 2009, doi: 10.1016/j.ces.2009.02.051.

[102] I. Kaya and H. Cengiz, "Optimal tuning of PI/PID controllers for integrating processes with inverse response," in *2017 21st International Conference on System Theory, Control and Computing (ICSTCC)*, Oct. 2017, pp. 717–722, doi: 10.1109/ICSTCC.2017.8107121.

[103] M. Vítečková and A. Víteček, "2DOF PID controller tuning for integrating plants," in *2016 17th International Carpathian Control Conference (ICCC)*, May 2016, pp. 793–797, doi: 10.1109/CarpathianCC.2016.7501204.

[104] P. K. Medarametla and M. Manimozhi, "Novel proportional-integral-derivative controller with second order filter for integrating processes," *Asia-Pacific Journal of Chemical Engineering*, vol. 13, no. 3, p. e2195, May 2018, doi: 10.1002/apj.2195.

[105] H. Taguchi and M. Araki, "Two-Degree-of-Freedom PID Controllers — Their Functions and Optimal Tuning," *IFAC Proceedings Volumes*, vol. 33, no. 4, pp. 91–96, Apr. 2000, doi: 10.1016/S1474-6670(17)38226-5.

[106] W. L. Luyben, "Identification and Tuning of Integrating Processes with Deadtime and Inverse Response," *Industrial & Engineering Chemistry Research*, vol. 42, no. 13, pp. 3030–3035, Jun. 2003, doi: 10.1021/ie020935j.

[107] S. Srivastava and V. S. Pandit, "A 2-Dof LQR based PID controller for integrating processes considering robustness/performance tradeoff," *ISA Transactions*, vol. 71, pp. 426–439, Nov. 2017, doi: 10.1016/j.isatra.2017.09.010.

[108] E. Cokmez, S. Atiç, F. Peker, and I. Kaya, "Fractional-order PI Controller Design for Integrating Processes Based on Gain and Phase Margin Specifications," *IFAC-PapersOnLine*, vol. 51, no. 4, pp. 751–756, 2018, doi: 10.1016/j.ifacol.2018.06.206.

[109] A. Seshagiri Rao, V. S. R. Rao, and M. Chidambaram, "Direct synthesis-based controller design for integrating processes with time delay," *Journal of the Franklin Institute*, vol. 346, no. 1, pp. 38–56, Feb. 2009, doi: 10.1016/j.jfranklin.2008.06.004.

[110] F. Alyoussef and I. Kaya, "A New Analytical Method for Finding the Centroid of Stability Locus for Controlling Integrating Processes," in *2019 International Conference on Applied Automation and Industrial Diagnostics (ICAAID)*, Sep. 2019, pp. 1–6, doi: 10.1109/ICAAID.2019.8934967.

[111] I. Kaya, "Integral-Proportional Derivative tuning for optimal closed loop responses to control integrating processes with inverse response," *Transactions of the Institute of Measurement and Control*, vol. 42, no. 16, pp. 3123–3134, Dec. 2020, doi: 10.1177/0142331220941657.

[112] M. Veronesi and A. Visioli, "Performance assessment and retuning of PID controllers for integral processes," *Journal of Process Control*, vol. 20, no. 3, pp. 261–269, Mar. 2010, doi: 10.1016/j.jprocont.2009.12.007.

[113] P. K. Medarametla and V. L. N. Komanapalli, "Maximum Sensitivity Based New PID Controller Tuning for Integrating Systems Using Polynomial Method," *Chemical Product and Process Modeling*, vol. 12, no. 3, p. 20160070, Jan. 2017, doi: 10.1515/cppm-2016-0070.

[114] P. K. Medarametla and M. Manimozhi, "A New Control Scheme for Integrating Processes with Inverse Response and Time Delay," *Chemical Product and Process Modeling*, vol. 13, no. 4, p. 20170071, Dec. 2018, doi: 10.1515/cppm-2017-0071.

[115] I. Kaya, "I-PD Controller Design for Integrating Time Delay Processes Based on Optimum Analytical Formulas," *IFAC-PapersOnLine*, vol. 51, no. 4, pp. 575–580, 2018, doi: 10.1016/j.ifacol.2018.06.157.

[116] C. Anil and R. Padma Sree, "Tuning of PID controllers for integrating systems using direct synthesis method," *ISA Transactions*, vol. 57, pp. 211–219, Jul. 2015, doi: 10.1016/j.isatra.2015.03.002.

[117] S. Atic and I. Kaya, "Generalized Stability Boundary Locus for PI Controller Design for Controlling Integrating Processes with Dead Time," 2017.

[118] M. M. Ozyetkin, C. Onat, and N. Tan, "PID Tuning Method for Integrating Processes Having Time Delay and Inverse Response," *IFAC-PapersOnLine*, vol. 51, no. 4, pp. 274–279, 2018, doi: 10.1016/j.ifacol.2018.06.077.

[119] R. C. Panda, V. Vijayan, V. Sujatha, P. Deepa, D. Manamali, and A. B. Mandal, "Parameter estimation of integrating and time delay processes using single relay feedback test," *ISA Transactions*, vol. 50, no. 4, pp. 529–537, Oct. 2011, doi: 10.1016/j.isatra.2011.06.004.

[120] L. Eriksson, T. Oksanen, and K. Mikkola, "PID controller tuning rules for integrating processes with varying time-delays," *Journal of the Franklin Institute*, vol. 346, no. 5, pp. 470–487, Jun. 2009, doi: 10.1016/j.jfranklin.2009.01.003.

[121] V. F. Kuzishchin, E. I. Merzlikina, and H. Van Va, "PD and PDD algorithms with integrating object: Tuning on the basis of approach to suboptimal algorithm," in *2017 International Conference on Industrial Engineering, Applications and Manufacturing (ICIEAM)*, May 2017, pp. 1–5, doi: 10.1109/ICIEAM.2017.8076155.

[122] E. C. Goud and A. S. Rao, "Design of Noise Filters for Integrating Time Delay Processes," *Chemical Product and Process Modeling*, vol. 15, no. 2, p. 20190056, Nov. 2019, doi: 10.1515/cppm-2019-0056.

[123] I. Kaya, "Optimum I-PD Controller Design for Integrating Processes with Inverse Response and Time Delay," in *2019 International Conference on Applied Automation and Industrial Diagnostics (ICAAID)*, Sep. 2019, pp. 1–6, doi: 10.1109/ICAAID.2019.8934955.

[124] M. Shamsuzzoha and M. Lee, "PID controller design for integrating processes with time delay," *Korean Journal of Chemical Engineering*, vol. 25, no. 4, pp. 637–645, Jul. 2008, doi: 10.1007/s11814-008-0106-2.

[125] I. Kaya and F. Peker, "Optimal I-PD controller design for setpoint tracking of integrating processes with time delay," *IET Control Theory & Applications*, vol. 14, no. 18, pp. 2814–2824, Dec. 2020, doi: 10.1049/iet-cta.2019.1378.

[126] M. Ajmeri and A. Ali, "Direct synthesis based tuning of the parallel control structure for integrating processes," *International Journal of Systems Science*, vol. 46, no. 13, pp. 2461–2473, Oct. 2015, doi: 10.1080/00207721.2013.871369.

[127] K. Ghousiya Begum, A. Seshagiri Rao, and T. K. Radhakrishnan, "Enhanced IMC based PID controller design for non-minimum phase (NMP) integrating processes with time delays," *ISA Transactions*, vol. 68, pp. 223–234, May 2017, doi: 10.1016/j.isatra.2017.03.005.

[128] M. Irshad and A. Ali, "Optimal Tuning Rules for Integrating Processes for 2-DOF Parallel Control Structure," in *2019 6th International Conference on Control, Decision and Information Technologies (CoDIT)*, Apr. 2019, pp. 256–261, doi: 10.1109/CoDIT.2019.8820508.

[129] M. M. Ozyetkin, C. Onat, and N. Tan, "PI-PD controller design for time delay systems via the weighted geometrical center method," *Asian Journal of Control*, vol. 22, no. 5, pp. 1811–1826, Sep. 2020, doi: 10.1002/asjc.2088.

[130] M. M. Ozyetkin, "A simple tuning method of fractional order PIλ-PDμ controllers for time delay systems," *ISA Transactions*, vol. 74, pp. 77–87, Mar. 2018, doi: 10.1016/j.isatra.2018.01.021.

[131] W. Zhang, Y. Cui, and X. Ding, "An Improved Analytical Tuning Rule of a Robust PID Controller for Integrating Systems with Time Delay Based on the Multiple Dominant Pole-Placement Method," *Symmetry*, vol. 12, no. 9, p. 1449, Sep. 2020, doi: 10.3390/sym12091449.

[132] N. M. Darwish, "PID controller design in the frequency domain for time-delay systems using direct method," *Transactions of the Institute of Measurement and Control*, vol. 40, no. 3, pp. 940–950, Feb. 2018, doi: 10.1177/0142331216675400.

[133] G. Lloyds Raja and A. Ali, "New PI-PD Controller Design Strategy for Industrial Unstable and Integrating Processes with Dead Time and Inverse Response," *Journal of Control, Automation and Electrical Systems*, Jan. 2021, doi: 10.1007/s40313-020-00679-5.

[134] I. Kaya, "Two-degree-of-freedom IMC structure and controller design for integrating processes based on gain and phase-margin specifications," *IEE Proceedings - Control Theory and Applications*, vol. 151, no. 4, pp. 481–487, Jul. 2004, doi: 10.1049/ip-cta:20040658.

[135] P. R. Hemavathy, Y. Mohamed Shuaib, S. Lakshmanaprabu, and A. Raseem Ahamed, "Integer and Non-Integer Filter Design with IMC PD Controller for a First Order Delay Integrating Process," in *2019 2nd International Conference on Intelligent Computing, Instrumentation and Control Technologies (ICICICT)*, Jul. 2019, pp. 1486–1490, doi: 10.1109/ICICICT46008.2019.8993138.

[136] R. Ranganayakulu, A. Seshagiri Rao, and G. Uday Bhaskar Babu, "Improved fractional filter IMC–PID controller design for enhanced performance of integrating plus time delay processes," *Indian Chemical Engineer*, pp. 1–18, Sep. 2019, doi: 10.1080/00194506.2019.1656553.

[137] Q. B. Jin and Q. Liu, "Analytical IMC-PID design in terms of performance/robustness tradeoff for integrating processes: From 2-Dof to 1-Dof," *Journal of Process Control*, vol. 24, no. 3, pp. 22–32, Mar. 2014, doi: 10.1016/j.jprocont.2013.12.011.

[138] H. Najafizadegan, F. Merrikh-Bayat, and A. Jalilvand, "IMC-PID controller design based on loop shaping via LMI approach," *Chemical Engineering Research and Design*, vol. 124, pp. 170–180, Aug. 2017, doi: 10.1016/j.cherd.2017.06.007.

[139] Z. Bingul and O. Karahan, "Comparison of PID and FOPID controllers tuned by PSO and ABC algorithms for unstable and integrating systems with time delay," *Optimal Control Applications and Methods*, vol. 39, no. 4, pp. 1431–1450, Jul. 2018, doi: 10.1002/oca.2419.

[140] A. Raza and N. Anwar, "Control of Integrating Process with Time Delay," *Chemical Product and Process Modeling*, vol. 14, no. 3, p. 20180042, Sep. 2019, doi: 10.1515/cppm-2018-0042.

[141] K. G. Papadopoulos, N. D. Tselepis, and N. I. Margaris, "Type-III closed loop control systems-Digital PID controller design," *Journal of Process Control*, vol. 23, no. 10, pp. 1401–1414, Nov. 2013, doi: 10.1016/j.jprocont.2013.09.001.

[142] T. B. Šekara and M. R. Mataušek, "Classification of dynamic processes and PID controller tuning in a parameter plane," *Journal of Process Control*, vol. 21, no. 4, pp. 620–626, Apr. 2011, doi: 10.1016/j.jprocont.2010.12.004.

[143] S. E. Hamamci and M. Koksal, "Calculation of all stabilizing fractional-order PD controllers for integrating time delay systems," *Computers & Mathematics with Applications*, vol. 59, no. 5, pp. 1621–1629, Mar. 2010, doi: 10.1016/j.camwa.2009.08.049.

[144] K. G. Papadopoulos, *PID Controller Tuning Using the Magnitude Optimum Criterion*, 1st ed. Cham: Springer International Publishing, 2015.

[145] D. C. Meena and A. Devanshu, "Genetic algorithm tuned PID controller for process control," in *2017 International Conference on Inventive Systems and Control (ICISC)*, Jan. 2017, pp. 1–6, doi: 10.1109/ICISC.2017.8068639.

[146] M. A. Siddiqui, M. N. Anwar, and S. H. Laskar, "Tuning of PIDF Controller in Parallel Control Structure for Integrating Process with Time Delay and Inverse Response Characteristic," *Journal of Control, Automation and Electrical Systems*, vol. 31, no. 4, pp. 829–841, Aug. 2020, doi: 10.1007/s40313-020-00603-x.

[147] M. N. Anwar and S. Pan, "A frequency response model matching method for PID controller design for processes with dead-time," *ISA Transactions*, vol. 55, pp. 175–187, Mar. 2015, doi: 10.1016/j.isatra.2014.08.020.

[148] M. R. Mataušek and T. B. Šekara, "PID controller frequency-domain tuning for stable, integrating and unstable processes, including dead-time," *Journal of Process Control*, vol. 21, no. 1, pp. 17–27, Jan. 2011, doi: 10.1016/j.jprocont.2010.09.007.

[149] J.-C. Jeng, "A model-free direct synthesis method for PI/PID controller design based on disturbance rejection," *Chemometrics and Intelligent Laboratory Systems*, vol. 147, pp. 14–29, Oct. 2015, doi: 10.1016/j.chemolab.2015.08.004.

[150] C. Dey, R. K. Mudi, and D. Simhachalam, "A simple nonlinear PD controller for integrating processes," *ISA Transactions*, vol. 53, no. 1, pp. 162–172, Jan. 2014, doi: 10.1016/j.isatra.2013.09.011.

[151] W. Zhang, J. M. Rieber, and D. Gu, "Optimal dead-time compensator design for stable and integrating processes with time delay," *Journal of Process Control*, vol. 18, no. 5, pp. 449–457, Jun. 2008, doi: 10.1016/j.jprocont.2007.09.001.

[152] M. R. Mataušek and A. I. Ribić, "Control of stable, integrating and unstable processes by the Modified Smith Predictor," *Journal of Process Control*, vol. 22, no. 1, pp. 338–343, Jan. 2012, doi: 10.1016/j.jprocont.2011.08.006.

[153] W. D. Zhang and Y. X. Sun, "Modified Smith Predictor for Controlling Integrator/Time Delay Processes," *Industrial & Engineering Chemistry Research*, vol. 35, no. 8, pp. 2769–2772, Jan. 1996, doi: 10.1021/ie950664v.

[154] S. Chakraborty, S. Ghosh, and A. K. Naskar, "All-PD control of pure Integrating Plus Time-Delay processes with gain and phase-margin specifications," *ISA Transactions*, vol. 68, pp. 203–211, May 2017, doi: 10.1016/j.isatra.2017.01.031.

[155] D. G. Padhan and S. Majhi, "An improved parallel cascade control structure for processes with time delay," *Journal of Process Control*, vol. 22, no. 5, pp. 884–898, Jun. 2012, doi: 10.1016/j.jprocont.2012.03.003.

[156] P. García and P. Albertos, "A new dead-time compensator to control stable and integrating processes with long dead-time," *Automatica*, vol. 44, no. 4, pp. 1062–1071, Apr. 2008, doi: 10.1016/j.automatica.2007.08.022.

[157] M. A. Davó and A. Baños, "Reset control of integrating plus dead time processes," *Journal of Process Control*, vol. 38, pp. 22–30, Feb. 2016, doi: 10.1016/j.jprocont.2015.12.001.

[158] M. Huba, "Comparing 2DOF PI and predictive disturbance observer based filtered PI control," *Journal of Process Control*, vol. 23, no. 10, pp. 1379–1400, Nov. 2013, doi: 10.1016/j.jprocont.2013.09.007.

[159] T. Liu and F. Gao, "Enhanced IMC-based Load Disturbance Rejection Design for Integrating Processes with Slow Dynamics," *IFAC Proceedings Volumes*, vol. 43, no. 5, pp. 67–72, 2010, doi: 10.3182/20100705-3-BE-2011.00012.

[160] Q. Jin, X. Sun, Q. Wang, and L. Liu, "A Novel TDF Control Scheme for Integrating and Double Integrating Processes with Time Delay Based on Modified IMC Structure," *Journal of Chemical Engineering of Japan*, vol. 49, no. 2, pp. 166–175, 2016, doi: 10.1252/jcej.15we022.

[161] S. Uma, M. Chidambaram, A. Seshagiri Rao, and C. K. Yoo, "Enhanced control of integrating cascade processes with time delays using modified Smith predictor," *Chemical Engineering Science*, vol. 65, no. 3, pp. 1065–1075, Feb. 2010, doi: 10.1016/j.ces.2009.09.061.

[162] S. Uma, M. Chidambaram, and A. S. Rao, "Set point weighted modified Smith predictor with PID filter controllers for non-minimum-phase (NMP) integrating processes," *Chemical Engineering Research and Design*, vol. 88, no. 5–6, pp. 592–601, May 2010, doi: 10.1016/j.cherd.2009.09.008.

[163] Z. Wang, H. Tian, X. Geng, J. Cui, and T. Liu, "Predictor based 2DOF control design for inverse response processes with time delay," in *2018 33rd Youth Academic Annual Conference of Chinese Association of Automation (YAC)*, May 2018, pp. 65–70, doi: 10.1109/YAC.2018.8406348.

[164] W. Zhang, Y. Wang, Z. Yin, Y. Wang, and W. Zhang, "Optimal control of non-minimum phase integrating processes with time delay using disturbance observer-based control scheme," *International Journal of Systems Science*, vol. 49, no. 8, pp. 1725–1737, Jun. 2018, doi: 10.1080/00207721.2018.1479000.

[165] D. Wang, T. Liu, X. Sun, and C. Zhong, "Discrete-time domain two-degree-of-freedom control design for integrating and unstable processes with time delay," *ISA Transactions*, vol. 63, pp. 121–132, Jul. 2016, doi: 10.1016/j.isatra.2016.03.017.

[166] G. L. Raja and A. Ali, "Modified parallel cascade control strategy for stable, unstable and integrating processes," *ISA Transactions*, vol. 65, pp. 394–406, Nov. 2016, doi: 10.1016/j.isatra.2016.07.008.

[167] G. L. Raja and A. Ali, "Smith predictor based parallel cascade control strategy for unstable and integrating processes with large time delay," *Journal of Process Control*, vol. 52, pp. 57–65, Apr. 2017, doi: 10.1016/j.jprocont.2017.01.007.

[168] S. Pashaei and P. Bagheri, "Parallel cascade control of dead time processes via fractional order controllers based on Smith predictor," *ISA Transactions*, vol. 98, pp. 186–197, Mar. 2020, doi: 10.1016/j.isatra.2019.08.047.

[169] S. Uma and A. S. Rao, "Enhanced modified Smith predictor for second-order non-minimum phase unstable processes," *International Journal of Systems Science*, vol. 47, no. 4, pp. 966–981, Mar. 2016, doi: 10.1080/00207721.2014.911385.

[170] G. L. Raja and A. Ali, "Modified series cascade control strategy for integrating processes," in *2018 Indian Control Conference (ICC)*, Jan. 2018, pp. 252–257, doi: 10.1109/INDIANCC.2018.8307987.

[171] G. L. Raja and A. Ali, "Enhanced tuning of Smith predictor based series cascaded control structure for integrating processes," *ISA Transactions*, Dec. 2020, doi: 10.1016/j.isatra.2020.12.045.

[172] C. Rodríguez, J. L. Guzman, M. Berenguel, and J. E. Normey-Rico, "Optimal feedforward compensators for integrating plants," *IFAC Proceedings Volumes*, vol. 47, no. 3, pp. 170–175, 2014, doi: 10.3182/20140824-6-ZA-1003.01917.

[173] D. G. Padhan and S. Majhi, "Enhanced cascade control for a class of integrating processes with time delay," *ISA Transactions*, vol. 52, no. 1, pp. 45–55, Jan. 2013, doi: 10.1016/j.isatra.2012.08.004.

[174] Q.-C. Zhong and J. E. Normey-Rico, "Control of integral processes with dead-time. Part 1: Disturbance observer-based 2DOF control scheme," *IEE Proceedings - Control Theory and Applications*, vol. 149, no. 4, pp. 285–290, Jul. 2002, doi: 10.1049/ip-cta:20020438.

[175] R. C. Oldenbourg and H. Saratorius, "A Uniform Approach to the Optimum Adjustment of Control Loops," *Transactions of the ASME*, vol. 76, no. 8, pp. 1265–1279, 1954.

[176] D. Vrančić, S. Strmčnik, and Đ. Juričić, "A magnitude optimum multiple integration tuning method for filtered PID controller," *Automatica*, vol. 37, no. 9, pp. 1473–1479, Sep. 2001, doi: 10.1016/S0005-1098(01)00088-7.

[177] A. L. Whiteley, "Theory of servo systems, with particular reference to stabilization," *Journal of the Institution of Electrical Engineers - Part II: Power Engineering*, vol. 93, no. 34, pp. 353–367, Aug. 1946, doi: 10.1049/ji-2.1946.0083.

[178] D. Vrančić, "Magnitude Optimum Techniques for PID Controllers," in *Introduction to PID Controllers - Theory, Tuning and Application to Frontier Areas*, 1st ed., vol. 37, no. 9, R. C. Panda, Ed. Rijeka: InTech, 2012, pp. 75–102.

[179] D. Vrančić, Y. Peng, and C. Danz, "A comparison between different PI controller tuning methods - Report DP-7286," 1995. http://www-e2.ijs.si/Damir.Vrancic/Files/dp7286.pdf (accessed Feb. 18, 2020).

[180] D. Vrančić, Y. Peng, and S. Strmčnik, "A new PID controller tuning method based on multiple integrations," *Control Engineering Practice*, vol. 7, no. 5, pp. 623–633, May 1999, doi: 10.1016/S0967-0661(98)00198-1.

[181] D. Vrancic and S. Strmcnik, "Practical guidelines for tuning PID controllers by using MOMI method," in *ISIE '99. Proceedings of the IEEE International Symposium on Industrial Electronics (Cat. No.99TH8465)*, Jul. 1999, vol. 3, pp. 1130–1134, doi: 10.1109/ISIE.1999.796854.

[182] G. Prando, "Non-Parametric Bayesian Methods for Linear System Identification," University of Padova, 2016.

[183] H. Rake, "Identification: Transient- and Frequency-Response Methods," in *Concise Encyclopedia of Modelling & Simulation*, D. P. Atherton and P. Borne, Eds. Elsevier, 1992, pp. 204–209.

[184] K. Dharmalingam and T. Thangavelu, "Parameter estimation using relay feedback," *Reviews in Chemical Engineering*, vol. 35, no. 4, pp. 505–529, Apr. 2019, doi: 10.1515/revce-2017-0099.

[185] T. Liu, Q.-G. Wang, and H.-P. Huang, "A tutorial review on process identification from step or relay feedback test," *Journal of Process Control*, vol. 23, no. 10, pp. 1597–1623, Nov. 2013, doi: 10.1016/j.jprocont.2013.08.003.

[186] T. Liu and F. Gao, "A frequency domain step response identification method for continuous-time processes with time delay," *Journal of Process Control*, vol. 20, no. 7, pp. 800–809, Aug. 2010, doi: 10.1016/j.jprocont.2010.04.007.

[187] T. Liu and F. Gao, *Industrial Process Identification and Control Design*, 1st ed. London: Springer London, 2012.

[188] Q.-G. Wang, T. H. Lee, and C. Lin, *Relay Feedback*, 1st ed. London: Springer London, 2003.

[189] M. Hofreiter, "Biased-Relay Feedback Identification for Time Delay Systems," *IFAC-PapersOnLine*, vol. 50, no. 1, pp. 14620–14625, Jul. 2017, doi: 10.1016/j.ifacol.2017.08.1740.

[190] M. Hofreiter, "Alternative Identification Method using Biased Relay Feedback," *IFAC-PapersOnLine*, vol. 51, no. 11, pp. 891–896, 2018, doi: 10.1016/j.ifacol.2018.08.491.

[191] M. Hofreiter and A. Hornychová, "Process Identification Using Relay Shifting Method for Auto Tuning of PID Controller," *MATEC Web of Conferences*, vol. 292, p. 01015, Sep. 2019, doi: 10.1051/matecconf/201929201015.

[192] J. Lee, S. W. Sung, F. Y. Lee, M. Baldea, and T. F. Edgar, "Full Closed-Loop Tests for the Relay Feedback Autotuning of Stable, Integrating, and Unstable Processes," *ACS Omega*, vol. 4, no. 20, pp. 18760–18770, Nov. 2019, doi: 10.1021/acsomega.9b02732.

[193] T. Liu and F. Gao, "Identification of integrating and unstable processes from relay feedback," *Computers & Chemical Engineering*, vol. 32, no. 12, pp. 3038–3056, Dec. 2008, doi: 10.1016/j.compchemeng.2008.04.006.

[194] A. Hornychova and M. Hofreiter, "Relay Feedback Identification Method for PID Controller Tuning," in *2020 21th International Carpathian Control Conference (ICCC)*, Oct. 2020, pp. 1–6, doi: 10.1109/ICCC49264.2020.9257286.

[195] C. C. Hang, K. J. Astrom, and Q. G. Wang, "Relay feedback auto-tuning of process controllers — a tutorial review," *Journal of Process Control*, vol. 12, no. 1, pp. 143–162, Jan. 2002, doi: 10.1016/S0959-1524(01)00025-7.

[196] I. Kaya, "Relay feedback identification and model based controller design," University of Sussex, 1999.

[197] I. Kaya and D. P. Atherton, "Parameter estimation from relay autotuning with asymmetric limit cycle data," *Journal of Process Control*, vol. 11, no. 4, pp. 429–439, Aug. 2001, doi: 10.1016/S0959-1524(99)00073-6.

[198] İ. Kaya, "Parameter Estimation for Integrating Processes Using Relay Feedback Control under Static Load Disturbances," *Industrial & Engineering Chemistry Research*, vol. 45, no. 13, pp. 4726–4731, Jun. 2006, doi: 10.1021/ie060270b.

[199] T. B. Šekara and M. R. Mataušek, "Relay-based critical point estimation of a process with the PID controller in the loop," *Automatica*, vol. 47, no. 5, pp. 1084–1088, May 2011, doi: 10.1016/j.automatica.2011.02.010.

[200] S.-H. Shen, J.-S. Wu, and C.-C. Yu, "Use of biased-relay feedback for system identification," *AIChE Journal*, vol. 42, no. 4, pp. 1174–1180, Apr. 1996, doi: 10.1002/aic.690420431.

[201] J. Berner, T. Hagglund, and K. J. Astrom, "Improved relay autotuning using normalized time delay," in *2016 American Control Conference (ACC)*, Jul. 2016, pp. 1869–1875, doi: 10.1109/ACC.2016.7525191.

[202] M. Hofreiter, "Shifting Method for Relay Feedback Identification," *IFAC-PapersOnLine*, vol. 49, no. 12, pp. 1933–1938, 2016, doi: 10.1016/j.ifacol.2016.07.913.

[203] H. Rake, "Step response and frequency response methods," *Automatica*, vol. 16, no. 5, pp. 519–526, Sep. 1980, doi: 10.1016/0005-1098(80)90075-8.

[204] T. Marlin, *Process Control: Designing Processes and Control Systems for Dynamic Performance*, 2nd ed. New York, NY: McGraw-Hill, 2000.

[205] C. T. Huang and W. C. Clements, "Parameter estimation for the second-order-plus-dead-time model," *Industrial & Engineering Chemistry Process Design and Development*, vol. 21, no. 4, pp. 601–603, Oct. 1982, doi: 10.1021/i200019a011.

[206] G. P. Rangaiah and P. R. Krishnaswamy, "Estimating second-order dead time parameters from underdamped process transients," *Chemical Engineering Science*, vol. 51, no. 7, pp. 1149–1155, Apr. 1996, doi: 10.1016/S0009-2509(96)80013-3.

[207] G. P. Rangaiah and P. R. Krishnaswamy, "Estimating Second-Order plus Dead Time Model Parameters," *Industrial & Engineering Chemistry Research*, vol. 33, no. 7, pp. 1867–1871, Jul. 1994, doi: 10.1021/ie00031a029.

[208] H.-P. Huang, M.-W. Lee, and C.-L. Chen, "A System of Procedures for Identification of Simple Models Using Transient Step Response," *Industrial & Engineering Chemistry Research*, vol. 40, no. 8, pp. 1903–1915, Apr. 2001, doi: 10.1021/ie0005001.

[209] J. Mikleš and M. Fikar, *Process Modelling, Identification, and Control*, 1st ed. Berlin, Heidelberg: Springer Berlin Heidelberg, 2007.

[210] Tao Liu, Ke Yao, and Furong Gao, "Identification and Autotuning of Temperature-Control System With Application to Injection Molding," *IEEE Transactions on Control Systems Technology*, vol. 17, no. 6, pp. 1282–1294, Nov. 2009, doi: 10.1109/TCST.2008.2006746.

[211] Q.-G. Wang, X. Guo, and Y. Zhang, "Direct identification of continuous time delay systems from step responses," *Journal of Process Control*, vol. 11, no. 5, pp. 531–542, Oct. 2001, doi: 10.1016/S0959-1524(00)00031-7.

[212] Q. Bi, W.-J. Cai, E.-L. Lee, Q.-G. Wang, C.-C. Hang, and Y. Zhang, "Robust identification of first-order plus dead-time model from step response," *Control Engineering Practice*, vol. 7, no. 1, pp. 71–77, Jan. 1999, doi: 10.1016/S0967-0661(98)00166-X.

[213] H. Rake, "Identification: Transient- and Frequency-Response Methods," in *Systems & Control Encyclopedia: Theory, Technology, Applications*, 1st ed., M. G. Singh, Ed. New York, NY: Pergamon Press, 1987.

[214] V. Strejc, "Auswertung der dynamischen Eigenschaften von Regelstrecken bei gemessenen Ein- und Ausgangssignalen allgemeiner Art," *Z. Messen, Steuern, Regeln*, vol. 3, pp. 7–11, 1960.

[215] H.-P. Preuß, "Prozeßmodellfreier PID-Regler- Entwurf nach dem Betragsoptimum / Model-free PID-controller design by means of the method of gain Optimum," *at - Automatisierungstechnik*, vol. 39, no. 1–12, Jan. 1991, doi: 10.1524/auto.1991.39.112.15.

[216] D. Vrečko, D. Vrančić, Đ. Juričić, and S. Strmčnik, "A new modified Smith predictor: the concept, design and tuning," *ISA Transactions*, vol. 40, no. 2, pp. 111–121, Apr. 2001, doi: 10.1016/S0019-0578(00)00039-2.

[217] D. Vrančić and S. Strmčnik, "Design of 2-DOF PI controller for integrating processes," in *2011 8th Asian Control Conference (ASCC)*, 2011, pp. 1135–1140.

[218] D. Vrančić, S. Strmčnik, J. Kocijan, and P. B. de Moura Oliveira, "Improving disturbance rejection of PID controllers by means of the magnitude optimum method," *ISA Transactions*, vol. 49, no. 1, pp. 47–56, Jan. 2010, doi: 10.1016/j.isatra.2009.08.002.

[219] C. C. Hang, K. J. Åström, and W. K. Ho, "Refinements of the Ziegler–Nichols tuning formula," *IEE Proceedings D Control Theory and Applications*, vol. 138, no. 2, p. 111, 1991, doi: 10.1049/ip-d.1991.0015.

[220] J. Deur, "Design of reduced-order feedforward controller," in *UKACC International Conference on Control (CONTROL '98)*, Sep. 1998, vol. 1998, pp. 207–212, doi: 10.1049/cp:19980228.

[221] J. L. Schiff, *The Laplace Transform: Theory and Applications*. New York, NY: Springer New York, 1999.

[222] D. Vrančić, M. Huba, and P. M. Oliveira, "PID controller tuning for integrating processes," *IFAC-PapersOnLine*, vol. 51, no. 4, pp. 586–591, 2018, doi: 10.1016/j.ifacol.2018.06.159.

[223] T. Kos, M. Huba, and D. Vrančić, "Parametric and Nonparametric PI Controller Tuning Method for Integrating Processes Based on Magnitude Optimum," *Applied Sciences*, vol. 10, no. 4, p. 1443, Feb. 2020, doi: 10.3390/app10041443.

[224] R. Vilanova, V. M. Alfaro, and O. Arrieta, "Robustness in PID Control," in *PID Control in the Third Millennium: Lessons Learned and New Approaches*, 1st ed., R. Vilanova and A. Visioli, Eds. London: Springer London, 2012, pp. 113–145.

[225] M. Huba, "Filtered PIDA Controller for the Double Integrator Plus Dead Time," *IFAC-PapersOnLine*, vol. 52, no. 27, pp. 106–113, 2019, doi: 10.1016/j.ifacol.2019.12.741.

[226] M. Huba, "Školská hydraulická sústava uDAQ28/3H," 2008. https://www.eas.sk/mod/product/show.php?ID=52 (accessed Feb. 04, 2020).

[227] B. Dolenc, P. Boškoski, M. Stepančič, A. Pohjoranta, and Đ. Juričić, "State of health estimation and remaining useful life prediction of solid oxide fuel cell stack," *Energy Conversion and Management*, vol. 148, pp. 993–1002, Sep. 2017, doi: 10.1016/j.enconman.2017.06.041.

[228] P. Horowitz and W. Hill, *The Art of Electronics*, 3rd ed. Cambridge, United Kingdom: Cambridge University Press, 2015.

Bibliography

Publications Related to the Thesis

Journal Articles

[1] T. Kos, M. Huba, and D. Vrančić, "Parametric and Nonparametric PI Controller Tuning Method for Integrating Processes Based on Magnitude Optimum," Applied Sciences, vol. 10, no. 4, p. 1443, Feb. 2020, doi: 10.3390/app10041443.

[2] T. Kos, M. Huba, and D. Vrančić, "Parametric and Nonparametric PID Controller Tuning Method for Integrating Processes Based on Magnitude Optimum," Applied Sciences, vol. 10, no. 17, p. 6012, Aug. 2020, doi: 10.3390/app10176012.

[3] T. Kos, T. Rojac, J. Petrovčič, and D. Vrančić, "Control system for automated drift compensation of the stand-alone charge amplifier used for low-frequency measurement," AIP Advances, vol. 9, no. 3, p. 035133, Mar. 2019, doi: 10.1063/1.5064631.

Other Publications

Journal Articles

[4] M. Otoničar, A. Bradeško, L. Fulanović, T. Kos, H. Uršič Nemevšek, A. Benčan, M. Cabral, A. Henriques, J.L. Jones, L. Riemer, D. Damjanović, G. Dražić, B. Malič, and T. Rojac, "Connecting the Multiscale Structure with Macroscopic Response of Relaxor Ferroelectrics," Advanced Functional Materials, vol. 30, no. 52, p. 2006823, Dec. 2020, doi: 10.1002/adfm.202006823.

[5] T. Kos, J. Petrovčič, Z. Šaponia, B. Musizza, G. Podržaj, S. Strajnar, and D. Vrančić, "Razvoj in preizkus delovanja inteligentnega diferenčnega tlačnega pogona s sistemom za odpravo nihanj iSET = Development and testing of the intelligent differential pressure drive with anti-oscillation system iSET," Ventil : revija za fluidno tehniko in avtomatizacijo, vol. 25, no. 2, pp. 140–146, 2019.

[6] J. Walker, T.J.M. Bayer, M. Makarovic, T. Kos, S. Trolier-McKinstry, B. Malic, and T. Rojac, "Cobalt doping to influence the electrical conductivity of (Bi 0.91 Dy 0.09)FeO 3 ceramics," Materials Letters, vol. 225, pp. 126–129, Aug. 2018, doi: 10.1016/j.matlet.2018.04.125.

[7] D. Kuščer, T. Rojac, D. Belavič, M.S. Zarnik, A. Bradeško, T. Kos, B. Malič, M. Boerrigter, D.M. Martin, and M. Faccini, "Integrated piezoelectric vibration system for fouling mitigation in ceramic filtration membranes," Journal of Membrane Science, vol. 540, pp. 277–284, Oct. 2017, doi: 10.1016/j.memsci.2017.06.054.

[8] D. Belavič, A. Bradeško, T. Kos, and T. Rojac, "Design and integration of a piezoelectric vibrating device in an LTCC structure," Microelectronics International, vol. 34, no. 3, pp. 121–126, Aug. 2017, doi: 10.1108/MI-02-2017-0008.

[9] T. Rojac, M. Makarovic, J. Walker, H. Ursic, D. Damjanovic, and T. Kos, "Piezoelectric response of BiFeO3 ceramics at elevated temperatures," Applied Physics Letters, vol. 109, no. 4, p. 042904, Jul. 2016, doi: 10.1063/1.4960103.

Published Scientific Conference Contribution

[10] T. Kos, J. Petrovčič, Z. Šaponia, B. Musizza, G. Podržaj, S. Strajnar, and D. Vrančić, "Inteligentni diferenčni tlačni pogon s sistemom za odpravo nihanj iSET (ang. Intelligent differential pressure drive with anti-oscillation system iSET)," in AIG'19 - Avtomatizacija v industriji in gospodarstvu 11, 2019, pp. 110–116.

[11] D. Belavic, G. Muscalu, K. Vojisavljevic, M. Hodnik, D. Kuscer, T. Kos, T. Pecnik, S. Drnovsek, J. Zajac, B. Malic, and A. Anghelescu, "Ceramic packaging of PiezoMEMS devices," in 2017 21st European Microelectronics and Packaging Conference (EMPC) & Exhibition, Sep. 2017, pp. 1–4, doi: 10.23919/EMPC.2017.8346888.

Published Professional Conference Contribution

[12] B. Dolenc, G. Nusev, T. Kos, P. Boškoski, D. Vrečko, D. Vrančić, and Đ. Juričić, "Novi koncept vodenja sklada trdno-oksidnih gorivnih celic na podlagi stanja naprave (ang. The new concept of the solid-oxide fuel cells stack control based on device status)," in AIG'17 - Avtomatizacija v industriji in gospodarstvu 10, 2017, pp. 151–158.

Published Scientific Conference Contribution Abstract (invited lecture)

[13] T. Rojac, A. Benčan, G. Dražić, M. Makarovič, M. Otoničar, A. Bradeško, T. Kos, L. Fulanović, J.L. Jones, H. Uršič Nemevšek, D. Damjanović, and B. Malič, "Complex interactions between domain walls and pinning centers : implications to piezoelectric nonlinearity and hysteresis," Jun. 2019.

[14] T. Rojac, A. Benčan, G. Dražić, M. Makarovič, M. Otoničar, A. Bradeško, T. Kos, L. Fulanović, J.L. Jones, H. Uršič Nemevšek, D. Damjanović, and B. Malič, "Ferroelectric domain walls and their dynamic interactions with pinning centers," in 2019 IEEE International Symposium on Applications of Ferroelectrics, Jul. 2019, p. 484.

[15] D. Belavič, K. Makarovič, A. Bradeško, M. Santo-Zarnik, T. Kos, M. Hodnik, H. Uršič, A. Benčan, D. Kuščer, and T. Rojac, "LTCC-based MEMS and microfluidic devices," in 40th International Microelectronics and Packaging IMAPS Poland Conference, 2016, pp. 12–13.

Published Scientific Conference Contribution Abstract

[16] M. Otoničar, A. Bradeško, L. Fulanović, T. Kos, S. Drnovšek, H. Uršič Nemevšek, M. Cabral, A. Henriques, J.L. Jones, D. Damjanović, B. Malič, and T. Rojac, "Contributions to the electromechanical response in polycrystalline relaxor ferroelectrics," in 2019 IEEE International Symposium on Applications of Ferroelectrics, Jul. 2019, p. 22.

[17] D. Belavič, A. Bradeško, T. Kos, S. Drnovšek, M. Hodnik, and T. Rojac, “Integration of piezoelectric vibration device into the LTCC structure,” in 40th International Microelectronics and Packaging IMAPS Poland Conference, 2016, pp. 47–48.

Biography

Tomaž Kos was born on 21 August 1988 in Novo mesto, Slovenia. After completing the Secondary School of Electronics at the Novo mesto School Center in 2007, he enrolled at the Faculty of Electrical Engineering, University of Ljubljana. He obtained an Engineer's degree in 2014 (thesis entitled: Microcontroller supervised power supply) and a Master's degree in 2016 in Electrical Engineering (thesis entitled: Measurement system for automated low-frequency and high-temperature characterization of dielectric materials). During his studies, he did several part-time jobs in various fields of electrical engineering, such as Control Engineering, Electronics, and Power Engineering. In addition, he was involved in scientific research in various research projects at the Jožef Stefan Institute in the period 2013-2016.

In 2016, he was accepted into the Young Researchers Program of the Slovenian Research Agency under the supervision of Asst. Prof. Damir Vrančić and enrolled in the PhD program at the Jožef Stefan International Postgraduate School. During his studies, his research focused on advanced system control with embedded electronic systems and the development of new control techniques. In addition, he has also been involved in the study and development of the measurement systems and techniques for dielectric and piezoelectric electrical and electromechanical characterization.

During his studies, he was involved in various research and industrial development projects and visited several institutions abroad. In 2017-2018 he was involved in the development of the new Danfoss district heating products. In 2019, he visited the group of Ferroelectrics and Functional Materials, *École Polytechnique Fédérale de Lausanne*, Switzerland, where he developed a drift compensation solution for the charge amplifier used for piezoelectric measurements. In 2019, he participated in the Erasmus Traineeship Exchange Programme at the Materials Science Ceramics Group at the *Technische Universität Darmstadt*, Germany, where he developed a custom measurement system for impedance spectroscopy of high-power piezoelectric ceramics at high-voltage DC bias.

Awards:

- Dean's Award for exemplary completed academic requirements in the 2nd year of the postgraduate (Master's) programme, Ljubljana, 2016.
- Prešeren award for students for Master's Thesis, Ljubljana, 2016.
- Award of the Technology Network Process Control Technology (PCT) for the best Master's thesis, Maribor, 2017.